

BUPT

MULTI-WALL CARBON NANOTUBES-BASED COMPOSITE ELECTRODES FOR ELECTROANALYSIS APPLICATIONS

Teză destinată obținerii
titlului științific de doctor
la

Universitatea "Politehnica" din Timișoara
în domeniul INGINERIE CHIMICĂ
de către

Biolog Adriana Ileana REMEȘ

Conducător științific:

Referenți științifici:

prof.univ.dr.ing Georgeta BURTICA

prof.univ.dr.dr. h.c. Joop SCHOONMAN

prof.univ.dr.ing. Stephen J. PICKEN

conf.univ.dr.ing. Florica MANEA

Ziua susținerii tezei: 27 Ianuarie 2012

Seriile Teze de doctorat ale UPT sunt:

BUPT

- | | |
|------------------------|---|
| 1. Automatică | 7. Inginerie Electronică și Telecomunicații |
| 2. Chimie | 8. Inginerie Industrială |
| 3. Energetică | 9. Inginerie Mecanică |
| 4. Ingineria Chimică | 10. Știința Calculatoarelor |
| 5. Inginerie Civilă | 11. Știința și Ingineria Materialelor |
| 6. Inginerie Electrică | |

Universitatea „Politehnica” din Timișoara a inițiat seriile de mai sus în scopul diseminării expertizei, cunoștințelor și rezultatelor cercetărilor întreprinse în cadrul școlii doctorale a universității. Seriile conțin, potrivit H.B.Ex.S Nr. 14 / 14.07.2006, tezele de doctorat susținute în universitate începând cu 1 octombrie 2006.

Copyright © Editura Politehnica – Timișoara, 2006

Această publicație este supusă prevederilor legii dreptului de autor. Multiplicarea acestei publicații, în mod integral sau în parte, traducerea, tipărirea, reutilizarea ilustrațiilor, expunerea, radiodifuzarea, reproducerea pe microfilme sau în orice altă formă este permisă numai cu respectarea prevederilor Legii române a dreptului de autor în vigoare și permisiunea pentru utilizare obținută în scris din partea Universității „Politehnica” din Timișoara. Toate încălcările acestor drepturi vor fi penalizate potrivit Legii române a drepturilor de autor.

România, 300159 Timișoara, Bd. Republicii 9,
tel. 0256 403823, fax. 0256 403221
e-mail: editura@edipol.upt.ro

ACKNOWLEDGEMENTS

BUPT

The work described in the present thesis was not a solitary effort. In fact, it is the culmination of many fruitful discussions, interactions and collaborations with people of the Politehnica University of Timisoara, Romania and Delft University of Technology, The Netherlands.

First of all, I would like to thanks to my promotor, Professor Georgeta Burtica for her help and kindness. Also, I would like to express my profound gratitude to my supervisor **Associate Professor Florica Manea** for her constant supervision and availability, her useful comments and her constructive critics, her positive attitude and help, as well as for the numerous (non-)scientific discussions. Florica, your contribution to this thesis has simply been huge. It has been a pleasure to work with you. I really hope that we will keep in touch in the future.

I acknowledge my thesis committee, **Prof.Dr.dr.h.c. Joop Schoonman**, **Prof.Dr. Stephen J. Picken**, for finding time to read through the manuscript of the present thesis, and for their valuable and precious comments and suggestions, not only during the revision of my thesis, but also all along to my second year of my Ph.D.

This research would not have been possible without the financial support of the Romanian National Research Programs – PNII: STEDIWAT, no. 32-125/2008, NANO-ZEOREZID, no.72-156/2008, PNII: 165/2011, and partially supported by the strategic grant POSDRU/6/1.5/S/13, Project ID6998 (2008), co-financed by the European Social Fund-Investing in People, within the Sectoral Operational Programme Human Resources Development 2007-2013.

During my Ph.D. study, I have had the great chance to interact with several researchers from TUDelft. Krishna Kowlgi, Alberto Martinez-Joaristi, Plamen Malchev, Anika Embrechts, Telma Leitao thank for your friendship and hospitality.

Thank you very much to my colleagues, namely Sorina Motoc, Anamaria Baci, Aniela Pop, for their patience, good mood and their contributions to this thesis. Working with you has been extremely motivating, rewarding and pleasant.

Now to my best friend Iuliana, thank you for your friendship, help, support and being present!

My deepest gratitude goes to my family for encouragement, support and assistance throughout the three years of my project.

Mihai, you know that this last quote is pre-eminently for you. You are fantastic! Thanks for always being there by my side and for all your love and support through these years.

Remes Adriana Ileana

Multi-Wall Carbon Nanotubes-Based Composite Electrodes for Electroanalysis Applications

BUPT

Teze de doctorat ale UPT, Seria 4, Nr. 58, Editura Politehnica, 2012, 166 pagini, 73 figuri, 17 tabele.

ISSN: 1842-8223

ISBN: 978-606-554-437-6

Keywords: Carbon Nanotubes, Electrochemical sensors and biosensors, Pentachlorophenol, Salicylic acid, Acetylsalicylic acid, Glucose, Raman spectroscopy, Electrical conductivity

Summary

Chapter 1 is a general introduction in nanotechnology and carbon nanotubes. The enormous potential impact of nanomaterials for new technologies has been highlighted.

Chapter 2 presents a general overview of the history of nanotubes, their structures, properties, synthesis techniques, and applications with a primary focus on advances in electrochemical sensors and biosensors based on carbon nanotubes. The challenges related to the use of carbon nanotubes to enhance the performance of electrochemical sensors and biosensors are discussed. This chapter also highlights the importance of selecting and developing suitable routes for the synthesis of carbon nanotubes, in order to effectively exploit their properties for electrochemical sensors and biosensors.

Chapter 3 deals with the use of voltammetric techniques in analytical chemistry. These methods are highly appealing to the analytical chemist owing to their high sensitivity, low cost, simplicity of instrumentation, and ease of implementation. Furthermore, voltammetric techniques offer the possibility to determine the analyte concentration directly in the sample without pretreatment or chemical separation, as well as to analyze colored materials and samples with dispersed solid particles.

Chapter 4 introduces the scope and objectives that have motivated this work.

Chapter 5 presents details related to the experimental part of the thesis including protocols and devices used. Firstly, a list of materials and reagents is described. Secondly, the importance of the processing conditions and the characteristics of the composite electrodes are presented in detail, starting from the dispersion of CNTs in the polymer matrix, and finishing with the electrical measurements. Finally, the aim of this chapter is to supply a complete protocol that can be reproduced and therefore be used in practice for future research.

Chapter 6 focuses on the applications and integrations of modified/unmodified MWCNT-Epoxy composite electrodes as chemical sensors. The electrochemical detection of pentachlorophenol (PCP), salicylic acid (SA), acetylsalicylic acid (ASA), and glucose are described.

Finally, *chapter 7* presents the main conclusions related to this thesis giving at the same time some recommendations for future research in the field of CNTs-based composite electrodes for electroanalysis applications.

TABLE OF CONTENTS

Abbreviations	8
Abstract	10
List of tables	11
List of figures	12
Chapter 1. Introduction in nanotechnology and carbon nanotubes	18
Chapter 2. Carbon nanotubes-based electrodes applied in electrochemical sensors and bisensors	20
2.1 Carbon nanotubes	20
2.1.1 History of nanotubes	20
2.1.2 Structure of nanotubes	21
2.1.3 Synthesis, purification, and functionalization	22
2.1.4 Processing of CNT-polymer composites	24
2.1.4.1 Solution processing	24
2.1.4.2 Bulk mixing	25
2.1.4.3 Melt processing	26
2.1.4.4 In-situ polymerization	26
2.1.5 Properties	27
2.1.6 Applications	27
2.1.6.1 Applications in sensors	30
2.1.6.2 Applications in biosensors	31
2.2 Health and environmental impacts	32
2.3 Conclusions	34
2.4 References	34
Chapter 3. Electrochemical techniques in sensor applications	38
3.1 Cyclic voltammetry (CV)	38
3.1.1 Reversible System	40
3.1.2 Irreversible and Quasi-reversible System	42
3.2 Differential-Pulse Voltammetry (DPV)	42
3.3 Square-Wave Voltammetry (SWV)	44
3.4 Chronoamperometry (CA)	44
3.5 Pulsed amperometric detection (PAD)	45
3.6 References	46
Chapter 4. Scope and thesis objectives	47
Chapter 5. Preparation and characterization of modified/unmodified MWCNT-Epoxy composite electrodes	50
5.1 Introduction	50
5.2 Experimental section	51
5.2.1 Materials and reagents	51
5.2.2 Preparation of the composites	57
5.2.3 Characterization of the composites	58
5.3 Results and discussion	59
5.3.1 Dispersion quality	59

5.3.2 Morphological and structural characterization	62
5.3.2.1 Scanning Electron Microscopy (SEM)	62
5.3.2.2 Raman spectroscopy	66
5.3.2.3 Electrical conductivity	68
5.4 Conclusions	71
5.5 References	71
Chapter 6. Applications of modified/unmodified MWCNT-Epoxy composite electrodes	74
6.1 MWCNT-Epoxy (MWCNT-EP) composite electrode for pentachlorophenol (PCP) detection	74
6.1.1 Pentachlorophenol (PCP)	74
6.1.2 Experimental	76
6.1.3 Results and discussion	77
6.1.3.1 Electrochemical characterization of MWCNT-EP composite electrode using potassium ferricyanide	77
6.3.1.2 Cyclic voltammetry measurements	79
6.3.1.3 Pulsed-voltammetric measurements	83
6.1.4 Conclusions	93
6.2 MWCNT-Epoxy composite electrode for salicylic acid (SA) and acetylsalicylic acid (ASA) detection	94
6.2.1 Salicylic acid (SA)	94
6.2.2 Experimental	95
6.2.3 Results and discussion	95
6.2.3.1 Electrochemical detection of salicylic acid in 0.1 M Na ₂ SO ₄ supporting electrolyte	96
6.2.3.2 Electrochemical detection of salicylic acid in 0.1 M NaOH supporting electrolyte	107
6.2.3.3 Application of the MWCNT-Epoxy composite electrode for salicylic acid detection without supporting electrolyte	122
6.2.4 Acetylsalicylic acid (ASA)	130
6.2.5 Conclusions	139
6.3 MWCNT-HKUST-Epoxy composite electrode for glucose detection	140
6.3.1 Glucose	140
6.3.2 Experimental	140
6.3.3 Results and discussions	141
6.3.3.1 Electrochemical characterization of MWCNT-HKUST-Epoxy composite electrode using potassium ferricyanide	141
6.3.3.2 Cyclic voltammetry measurements	143
6.3.4 Conclusions	153
6.4 References	154
Chapter 7. General conclusions and future perspectives	156
7.1 General conclusions	156
7.2 Future perspectives	159
List of publications and conferences presentations	160
Publications – ISI Web of Knowledge	162
Curriculum Vitae	163

Abbreviations

AA	ascorbic acid
AD	arc discharge
ADH	alcohol dehydrogenase
ASA	acetylsalicylic acid
CA	chronoamperometry
CE	counter electrode
CEA	carcinoembryonic antigen
CNTs	carbon nanotubes
CNT-EC	carbon nanotubes-based electrochemical sensors
Co	cobalt
CV	cyclic voltammetry
CVD	chemical vapor deposition
DA	dopamine
DDAB	didodecyldimethylammonium bromide
DMF	dymethylformamide
DNA	deoxyribonucleic acid
EC	electrochemical sensors
DPV	differential-pulse voltammetry
E_{pa}/E_{pc}	anodic/cathodic peak potential
EMI	electromagnetic interference
ESD	electrostatic discharge
F	frequency
Fe	iron
FED	field-emission displays
GCE	glassy carbon electrode
GOx	glucose oxidase
GNp	gold nanoparticles
HiPCO	high pressure Co conversion
HOPG	highly ordered pyrolytic graphite
HRP	horseradish peroxidase
I_{pa}/I_{pc}	anodic/cathodic peak current
LA	laser ablation
LOD	limit of detection
LQ	limit of quantification
Ma	modulation amplitude
MB	Meldola's blue
MOF	metal-organic framework
MPA	multiple-pulse amperometry
MWCNTs	multi-wall carbon nanotubes
MWCNT-EP	multi-wall carbon nanotubes-epoxy composite electrode
NADH	nicotinamide adenine dinucleotide
NiTsPc	nickel tetrasulfonated metallophthalocyanine
PAD	pulsed amperometric detection
PAMAM	polyamidoamine
PCP	pentachlorophenol
PMMA	poly(methyl methacrylate)
PDDA	poly(diallyldimethylammonium) chloride
POx	putrescine oxidase

PFT	polymerization filling technique
PS	polystyrene
PSA-ACT	prostate-specific antigen- α_1 -antichymotrypsin
PU	polyurethane
PVA	poly (vinyl alcohol)
Pt	platinum
R²	correlation coefficient
RE	reference electrode
RSD	relative standard deviation
RuO₂	rutherfordium oxide
SA	salicylic acid
SEM	scanning electron microscopy
Sp	step potential
SWV	square-wave voltammetry
SWCNTs	single-wall carbon nanotubes
THF	tetrahydrofuran
UA	uric acid
Y	yttrium
WE	working electrode

ABSTRACT

Chapter 1 is a general introduction in nanotechnology and carbon nanotubes. The enormous potential impact of nanomaterials for new technologies has been highlighted.

Chapter 2 presents a general overview of the history of nanotubes, their structures, properties, synthesis techniques, and applications with a primary focus on advances in electrochemical sensors and biosensors based on carbon nanotubes. The challenges related to the use of carbon nanotubes to enhance the performance of electrochemical sensors and biosensors are discussed. This chapter also highlights the importance of selecting and developing suitable routes for the synthesis of carbon nanotubes, in order to effectively exploit their properties for electrochemical sensors and biosensors.

Chapter 3 deals with the use of voltammetric techniques in analytical chemistry. These methods are highly appealing to the analytical chemist owing to their high sensitivity, low cost, simplicity of instrumentation, and ease of implementation. Furthermore, voltammetric techniques offer the possibility to determine the analyte concentration directly in the sample without pretreatment or chemical separation, as well as to analyze colored materials and samples with dispersed solid particles.

Chapter 4 introduces the scope and objectives that have motivated this work.

Chapter 5 presents details related to the experimental part of the thesis including protocols and devices used. Firstly, a list of materials and reagents is described. Secondly, the importance of the processing conditions and the characteristics of the composite electrodes are presented in detail, starting from the dispersion of CNTs in the polymer matrix, and finishing with the electrical measurements. Finally, the aim of this chapter is to supply a complete protocol that can be reproduced and therefore be used in practice for future research.

Chapter 6 focuses on the applications and integrations of modified/unmodified MWCNT-Epoxy composite electrodes as chemical sensors. The electrochemical detection of pentachlorophenol (PCP), salicylic acid (SA), acetylsalicylic acid (ASA), and glucose are described.

Finally, *chapter 7* presents the main conclusions related to this thesis giving at the same time some recommendations for future research in the field of CNTs-based composite electrodes for electroanalysis applications.

List of tables

Table 2.1	Comparison between SWNTs and MWNTs.
Table 2.2	Summary and comparison of the most important synthesis methods for CNTs.
Table 5.1	Raman data analysis results.
Table 5.2	Electrical conductivity of the electrode materials containing 25 wt% MWCNTs.
Table 6.1	Physical and chemical properties of PCP.
Table 6.2	The electrochemical parameters of the redox system (ferri/ferrocyanide) determined from the anodic branches of CVs.
Table 6.3	The electrochemical parameters of the redox system (ferri/ferrocyanide) determined from the cathodic branches of CVs.
Table 6.4	Apparent diffusion coefficient and the electroactive surface area of MWCNT-Epoxy composite electrode.
Table 6.5	Electroanalytical performance of the MWCNT-Epoxy composite electrode for the detection of PCP in 0.1M Na ₂ SO ₄ supporting electrolyte.
Table 6.6	The electroanalytical performance of the MWCNT-Epoxy composite electrode for the voltammetric detection of SA in 0.1 M Na ₂ SO ₄ supporting electrolyte.
Table 6.7	The electroanalytical performance of the MWCNT-Epoxy composite electrode for the voltammetric detection of SA in 0.1 M NaOH supporting electrolyte.
Table 6.8	The electroanalytical parameters for SA direct detection of the MWCNT-Epoxy composite electrode in Bega River and the tap water, without supporting electrolyte.
Table 6.9	The electroanalytical parameters for direct detection of ASA of the MWCNT-Epoxy composite electrode in 0.1 M Na ₂ SO ₄ and 0.1 M NaOH supporting electrolytes.
Table 6.10	The electrochemical parameters of the redox system (ferri/ferrocyanide) determined from the anodic branches of CVs.
Table 6.11	The electrochemical parameters of the redox system (ferri/ferrocyanide) determined from the cathodic branches of CVs.
Table 6.12	Apparent diffusion coefficient and the electroactive surface area of MWCNT-HKUST-Epoxy composite electrode.
Table 6.13	The electroanalytical parameters for glucose direct detection of the MWCNT-HKUST-Epoxy composite electrode in 0.1 M NaOH supporting electrolyte.

List of figures

- Figure 2.1** Schematic diagrams of an individual (a) SWCNTs and (b) MWCNTs.
- Figure 2.2** Schematic diagrams of showing how a hexagonal sheet of graphite is rolled to form a CNT.
- Figure 2.3** Projected markets for nanotubes 2006-2015.
- Figure 2.4** Market applications of carbon nanotubes.
- Figure 2.5** Exponential increases in the number of CNT publications. The number of publications listed in the ISI Web of Science database identified with the keyword 'carbon nanotubes' (grey bars) and 'carbon nanotubes toxicity' (black bars) are depicted per year.
- Figure 3.1** CV potential waveform with switching potentials (left), and the expected response of a reversible redox couple during a single-potential cycle (right), connected with the experimental CV set-up: counter electrode (CE) working electrode (WE) and reference electrode (RE) in an electrochemical cell.
- Figure 3.2** Qualitative diagrams showing concentration-distance profile at various stages of the cyclic voltammogram the solid lines correspond to the reducing species and the dotted lines to the oxidizing species.
- Figure 3.3** Potential diagram for DPV.
- Figure 3.4** Square-wave form showing the amplitude of SWV.
- Figure 3.5** Schematic of the PAD waveform.
- Figure 5.1** SEM images of (a-b) as-received MWCNTs, showing that nanotube bundles are highly entangled and (c) TEM image of as-received MWCNTs.
- Figure 5.2** Synthesis of HKUST and view along the 100 direction of the cubic cell (picture from Sigma-Aldrich).
- Figure 5.3** N₂ sorption of the HKUST synthesized by electrochemical methods.
- Figure 5.4** XRD analysis of electrochemical HKUST.
- Figure 5.5** SEM image of the prepared HKUST (Cu-BTC) material.
- Figure 5.6** Schematic diagram of MWCNT-Epoxy composites preparation.
- Figure 5.7** The optical images of MWCNTs dispersed in different types of solvents.
- Figure 5.8** Number and intensity distribution of MWCNTs before/after dispersion in: (a-b) DMF and (c-d) THF.
- Figure 5.9** (a-c) SEM images of MWCNT-Epoxy composite electrode at different magnifications.
- Figure 5.10** (a-c) SEM images of MWCNT-Cu-BTC-epoxy composite electrode at different magnifications.
- Figure 5.11** Raman spectra of: (a) as received MWCNTs and (b) MWCNT-Epoxy.
- Figure 5.12** Four-point electrical conductivity as a function of MWCNTs weight content.
- Figure 5.13** Plot of $\log(\sigma_{DC})$ vs. $\log(\rho - \rho_c)$. Solid line represents the best-fitted value according to Eq. 5.1
- Figure 6.1** (a) Potentiostat/galvanostat PGSTAT 302 (EcoChemie); (b) Metrohm cell with three electrodes configuration.
- Figure 6.2** (a) CVs of the MWCNT-EP composite electrode in 4 mM K₃[Fe(CN)₆] in 0.1 M KNO₃ supporting electrolyte at different scan rates: 1) 0.025, 2) 0.05, 3) 0.1, 4) 0.2, 5) 0.3 Vs⁻¹. (b) Calibration plots of the oxidative and reductive peak currents vs. square root of scan rate.

Figure 6.3 (a) CVs of the MWCNT-EP composite electrode recorded at a potential scan rate 0.05 Vs^{-1} and a potential range between -0.5 V and $+1.25 \text{ V/SCE}$ in $0.1 \text{ M Na}_2\text{SO}_4$ supporting electrolyte (curve 1) and in the presence of different PCP concentrations: 2) $2 \mu\text{M}$, 3) $4 \mu\text{M}$, 4) $6 \mu\text{M}$, 5) $8 \mu\text{M}$, 6) $10 \mu\text{M}$. (b) Calibration plot of the anodic currents recorded at $E = +0.97 \text{ V/SCE}$ vs. PCP concentration.

Figure 6.4 (a) CVs of $8 \mu\text{M}$ PCP at MWCNT-EP composite electrode in $0.1 \text{ M Na}_2\text{SO}_4$ supporting electrolyte (1) with different scan rates: $0.01, 0.02, 0.03, 0.04, 0.05, 0.07, 0.09, 0.1, 0.2 \text{ Vs}^{-1}$; potential range: -0.5 and $+1.2 \text{ V/SCE}$. (b) The anodic peak current vs. square root of scan rate; (c) The peak potential E_p vs. $\log(v)$.

Figure 6.5 (a) DPVs of the MWCNT-EP composite electrode at modulation amplitude 0.2 V , step potential 0.02 V and potential scan rate of 0.05 Vs^{-1} , potential range between $+0.5 \text{ V}$ and $+1.0 \text{ V}$ vs. SCE in $0.1 \text{ M Na}_2\text{SO}_4$ supporting electrolyte (curve 1) and in the presence of different PCP concentrations: 2) $2 \mu\text{M}$, 3) $4 \mu\text{M}$, 4) $6 \mu\text{M}$, 5) $8 \mu\text{M}$, 6) $10 \mu\text{M}$, 7) $12 \mu\text{M}$. (b) Calibration plot of the anodic currents recorded at $E = +0.80 \text{ V/SCE}$ vs. PCP concentration.

Figure 6.6 (a) SWVs of the MWCNT-EP composite electrode, modulation amplitude 0.1 V , step potential 0.01 V and frequency 10Hz ; potential range between $+0.6 \text{ V}$ and $+1.2 \text{ V/SCE}$ in $0.1 \text{ M Na}_2\text{SO}_4$ supporting electrolyte (curve 1) and in the presence of different PCP concentrations: 2) $2 \mu\text{M}$, 3) $4 \mu\text{M}$, 4) $6 \mu\text{M}$, 5) $8 \mu\text{M}$, 6) $10 \mu\text{M}$, 7) $12 \mu\text{M}$. (b) Calibration plot of the anodic currents recorded at $E = +0.90 \text{ V/SCE}$ vs. PCP concentration.

Figure 6.7 (a) DPVs recorded on MWCNT-EP composite electrode (modulation amplitude 0.2 V , step potential 0.02 V), potential scan rate 0.05 Vs^{-1} in potential range between $+0.5 \text{ V}$ and $+1.2 \text{ V}$ vs. SCE in $0.1 \text{ M Na}_2\text{SO}_4$ supporting electrolyte (curve 1) and in the presence of $8 \mu\text{M}$ PCP concentration after different accumulation times: 2) 0 min , 3) 5 min , 4) 10 min , 5) 20 min , 6) 30 min , 7) 40 min , 8) 50 min . (b) Peak current responses and enhancement factor for the detection of $8 \mu\text{M}$ PCP at MWCNT-EP composite electrode as a function of the accumulation time recorded at $E = +0.83 \text{ V/SCE}$.

Figure 6.8 (a) SWVs recorded on MWCNT-EP composite electrode, accumulation time of 40 minutes (modulation amplitude 0.1 V , step potential 0.01 V and frequency 10Hz), potential range $+0.5$ to $+1.2 \text{ V}$ vs. SCE in $0.1 \text{ M Na}_2\text{SO}_4$ supporting electrolyte (1) and in the presence of different PCP concentrations: 2) $0.02 \mu\text{M}$, 3) $0.04 \mu\text{M}$, 4) $0.06 \mu\text{M}$, 5) $0.08 \mu\text{M}$, 6) $0.2 \mu\text{M}$, 7) $0.4 \mu\text{M}$. (b) Calibration plot of the anodic currents recorded at $E = +0.95 \text{ V/SCE}$ vs. PCP concentration: $0.02, 0.04, 0.06, 0.08 \mu\text{M}$. (c) Calibration plot of the anodic currents recorded at $E = +0.95 \text{ V/SCE}$ vs. PCP concentration: $0.08, 0.2, 0.4 \mu\text{M}$. (d) Calibration plot of the anodic currents recorded at $E = +0.95 \text{ V/SCE}$ vs. PCP concentration: $0.02, 0.04, 0.06, 0.08, 0.2, 0.4 \mu\text{M}$.

Figure 6.9 (a) CAs recorded on MWCNT-EP composite electrode in $0.1 \text{ M Na}_2\text{SO}_4$ supporting electrolyte (curve 1) and in the presence of different PCP concentrations (curves 2-6): $2, 4, 6, 8, 10 \mu\text{M}$ recorded at $E = +0.97 \text{ V}$. (b) Calibration plot of the anodic currents recorded at $E = +0.97 \text{ V}$ vs. PCP concentration.

Figure 6.10 (a) MPAs recorded at MWCNT-EP electrode in $0.1 \text{ M Na}_2\text{SO}_4$ supporting electrolyte and in the present of different PCP concentrations: $2, 4, 6, 8, 10, 12 \mu\text{M}$ recorded at 1) $E = +1.25 \text{ V}$; 2) $E = +0.97 \text{ V}$ and 3) $E = -0.1 \text{ V}$ vs. SCE. (b) The calibration plots of the currents recorded at 1) $E = +0.97\text{V}$; 2) $E = +1.25\text{V}$; 3) $E = -0.1 \text{ V/SCE}$ vs. PCP concentration.

Figure 6.11 Chemical formula of salicylic acid (SA).

Figure 6.12 CVs of the MWCNT-EP composite electrode in 0.1 M Na₂SO₄ supporting electrolyte (1) and in the presence of 0.6 mM SA (3), and in 0.1 M NaOH supporting electrolyte (2) and in the presence of 0.6 mM SA (4).

Figure 6.13 (a) CVs of the MWCNT-EP composite electrode in 0.1 M Na₂SO₄ supporting electrolyte (curve 1) and in the presence of: 0.02, 0.04, 0.06, 0.08, 0.1, 0.12, 0.14, 0.16, 0.18, 0.2, 0.4, 0.6, 0.8, 1, 1.2 mM SA; scan rate 0.05 Vs⁻¹. (b) Calibration plots of anodic peak currents recorded at E= +0.6 V/SCE vs. SA concentration.

Figure 6.14 The possible scheme of oxidation of SA.

Figure 6.15 (a) DPVs of the MWCNT-EP composite electrode in 0.1M Na₂SO₄ supporting electrolyte (curve 1) (modulation amplitude 0.1 V, step potential 0.01 V), potential scan rate of 0.05 Vs⁻¹ and in the presence of: 0.02, 0.04, 0.06, 0.08, 0.1, 0.12, 0.14, 0.16, 0.18, 0.2, 0.4, 0.6, 0.8, 1, 1.2 mM SA concentrations, (b) Calibration plots of the anodic currents recorded at E=+0.52 V vs. SA concentration in the concentration range: b) 0.02 -1.2 mM SA, c) 0.02-0.2mM SA and d) 0.2-1.2 mM SA.

Figure 6.16 (a) DPVs of the MWCNT-EP composite electrode (modulation amplitude 0.1 V, step potential 0.01 V), potential scan rate of 0.05 Vs⁻¹ in 0.1M Na₂SO₄ supporting electrolyte and 0.4 mM SA after different accumulation times: 0 min; 10 min; 20 min; 30 min; 40 min. (b) Peak current responses and enhancement factor for the detection of 0.4 mM PCP at MWCNT-EP composite electrode as a function of the accumulation time recorded at E= +0.46 V/SCE.

Figure 6.17 (a) DPVs of the MWCNT-EP composite electrode (modulation amplitude 0.1 V, step potential 0.01 V), potential scan rate of 0.05 Vs⁻¹ in 0.1M Na₂SO₄ supporting electrolyte and different SA concentrations: 0.02, 0.04, 0.06, 0.08, 1 mM SA after 30 min of accumulation time at E= +0.46 V/SCE. (b) Calibration plot of anodic peak currents recorded at E= +0.46 V/SCE vs. SA concentration.

Figure 6.18 (a) SWVs of the MWCNT-EP composite electrode in 0.1M Na₂SO₄ supporting electrolyte (curve 1) (modulation amplitude 0.05 V, step potential 0.005 V, frequency of 50 Hz), and in the presence of: 0.02, 0.04, 0.06, 0.08, 0.1, 0.12, 0.14, 0.16, 0.18, 0.2, 0.4, 0.6, 0.8, 1, 1.2 mM SA concentrations. (b) Calibration plot of the anodic currents recorded at E=+0.46 V vs. SA concentration.

Figure 6.19 (a) CVs of the MWCNTs-EP electrode recorded at a potential scan rate 0.05 Vs⁻¹ and a potential range between -0.2 V and +0.8 V/SCE in 0.1 M NaOH supporting electrolyte (curve 1) and in the presence of different SA concentrations: 2) 0.6 mM, 3) 1.2 mM, 4) 1.8 mM, 5) 2.4 mM, 6) 3 mM, 7) 3.6 mM. (b) Calibration plot of the anodic currents recorded at E= +0.50 V/SCE vs. SA concentration.

Figure 6.20 (a) DPVs of the MWCNT-EP electrode at (modulation amplitude 0.1 V, step potential 0.01 V) a potential scan rate of 0.05 Vs⁻¹ and the potential range between +0.2 V and +0.8 V vs. SCE in 0.1 M NaOH supporting electrolyte (curve 1) and in the presence of different PCP concentration: 2) 0.02 mM, 3) 0.04 mM, 4) 0.06 mM, 5) 0.08 mM, 6) 0.1 mM, 7) 0.12 mM, 8) 0.14 mM, 9) 0.16 mM, 10) 0.18 mM, 11) 0.2 mM, 12) 0.4 mM, 13) 0.6 mM, 14) 0.8 mM, 15) 1mM, 16) 1.2 mM. (b) Calibration plot of the anodic currents recorded at E=+0.41 V/SCE vs. SA concentration.

Figure 6.21 (a) DPVs of the MWCNT-EP composite electrode (modulation amplitude 0.1 V, step potential 0.01 V), potential scan rate of 0.05 Vs⁻¹ in 0.1M NaOH supporting electrolyte and different SA concentrations: 0.02, 0.04, 0.06, 0.08, 0.1 mM SA after 30 min of accumulation time at E= +0.41 V/SCE. (b)

Calibration plot of the anodic currents recorded at $E=+0.41$ V/SCE vs. SA concentration.

Figure 6.22 SWVs on MWCNT-EP composite electrode (step potential= 0.03 V, modulation amplitude= 0.005 V), potential range $+0.2$ to $+0.7$ V vs. SCE in 0.1 M NaOH and the corresponding signal to SA oxidation in the concentration range 0.2 - 1.2 mM SA at different frequencies: a) $f=10$ Hz, b) $f=20$ Hz, c) $f=30$ Hz, d) $f=40$ Hz, e) $f=50$ Hz and f) $f=100$ Hz.

Figure 6.23 Calibration plots of the anodic current recorded at $E=+0.46$ V/SCE vs. SA concentration at different frequencies: a) $f=10$ Hz, b) $f=20$ Hz, c) $f=30$ Hz, d) $f=40$ Hz, e) $f=50$ Hz and f) $f=100$ Hz.

Figure 6.24 SWVs on MWCNT-EP composite electrode (frequency= 50 Hz, modulation amplitude= 0.03 V), potential range $+0.2$ to $+0.7$ V vs. SCE in 0.1 M NaOH and in the concentration range 0.2 - 1.2 mM SA at different step potentials: a) $Sp=0.005$ V and b) $Sp=0.0025$ V. (c and d) Calibration plots of the anodic current recorded at $E=+0.46$ V/SCE vs. SA concentration.

Figure 6.25 SWVs on MWCNT-EP composite electrode (frequency= 50 Hz, step potential= 0.005 V), potential range $+0.2$ to $+0.7$ V vs. SCE in 0.1 M NaOH and in the concentration range 0.2 - 1.2 mM SA at different modulation amplitude: a) $Ma=0.003$ V, b) $Ma=0.005$ V and c) $Ma=0.1$ V

Figure 6.26 Calibration plots of the anodic current recorded at $E=+0.46$ V/SCE vs. SA concentration at different modulation amplitude: a) $Ma=0.03$ V, b) $Ma=0.05$ V and c) $Ma=0.1$ V.

Figure 6.27 3D Optimization SWV parameters.

Figure 6.28 (a) Chronoamperometric responses of the MWCNT-EP composite electrode recorded at $+0.5$ V/SCE to successive adding of 0.2 mM SA. b) The calibration plot of useful current vs. SA concentration.

Figure 6.29 (a) Amperometric response (BIA) of the MWCNT-EP composite electrode for the successive and continuous addition of 0.2 mM SA. Applied potential: $+0.50$ V vs. SCE. (b) The calibration plot of useful signal vs. SA concentration.

Figure 6.30 CVs recorded at MWCNT-EP composite electrode at a potential scan rate 0.05 Vs⁻¹ and a potential range between -0.2 V and $+0.8$ V/SCE in Bega River, without supporting electrolyte (curve 1) and in 0.1 M Na₂SO₄ supporting electrolyte (curve 2).

Figure 6.31 (a) CVs recorded at the MWCNTs-EP composite at a potential scan rate 0.05 Vs⁻¹ and a potential range between -0.2 V and $+0.8$ V/SCE in Bega River, without supporting electrolyte (curve 1) and in the presence of different SA concentrations: 2) 0.2 mM; 3) 0.4 mM; 4) 0.6 mM; 5) 0.8 mM; 6) 1 mM; 7) 1.2 mM.

Figure 6.32 (a) DPVs of the MWCNT-Epoxy composite electrode in Bega River without supporting electrolyte (black curve) (modulation amplitude 0.1 V, step potential 0.01 V), potential scan rate of 0.05 Vs⁻¹ and in the presence of: 0.2 , 0.4 , 0.6 , 0.8 , 0.1 , 0.12 mM SA concentrations. (b) Calibration plot of the anodic current recorded at $E=+0.52$ V vs. SA concentration.

Figure 6.33 (a) SWVs of the MWCNT-EP composite electrode in Bega River without supporting electrolyte (blue curve) (step potential of 0.005 V, the modulation amplitude of 0.05 V and the frequency of 50 Hz), and in the presence of: 0.2 , 0.4 , 0.6 , 0.8 , 1 , 1.2 mM SA concentrations. (b) Calibration plot of the anodic currents recorded at $E=+0.56$ V vs. SA concentration.

Figure 6.34 (a) DPVs of the MWCNT-EP composite electrode in tap water without

supporting electrolyte (black curve) (modulation amplitude 0.1 V, step potential 0.01 V), potential scan rate of 0.05 Vs⁻¹ and in the presence of: 0.06, 0.08, 0.1, 0.12, 0.14, 0.16, 0.18, 0.2 mM SA concentrations. (b) Calibration plot of the anodic currents recorded at E= +0.65V vs. SA concentration.

Figure 6.35 (a) DPVs of the MWCNT-EP composite electrode in tap water without supporting electrolyte (curve 1) (modulation amplitude 0.1 V, step potential 0.01 V), and in the presence of: 0.2, 0.4, 0.6, 0.8, 1, 1.2 mM SA concentrations. (b) Calibration plot of the anodic currents recorded at E= +0.52 V vs. SA concentration.

Figure 6.36 (a) CVs of the MWCNT-EP composite electrode in 0.1 M Na₂SO₄ supporting electrolyte (curve 1) and in the presence of: 0.02, 0.04, 0.06, 0.08, 0.1, 0.12, 0.14, 0.16, 0.18, 0.2 mM ASA; scan rate 0.05 Vs⁻¹. (b) Calibration plot of the anodic currents at E= +0.60 V/SCE vs. ASA concentration.

Figure 6.37 (a) CVs of the MWCNT-EP composite electrode in 0.1 M Na₂SO₄ supporting electrolyte (curve 1) and in the presence of: 0.2, 0.4, 0.6, 0.8, 1, 1.2 mM ASA; scan rate 0.05 Vs⁻¹. (b) Calibration plot of the anodic currents recorded at E= +0.60 V/SCE vs. ASA concentration.

Figure 6.38 (a) DPVs of the MWCNT-EP composite electrode in 0.1 M Na₂SO₄ supporting electrolyte (curve 1) (modulation amplitude 0.1 V, step potential 0.01 V), potential scan rate 0.05 Vs⁻¹ and in the presence of: 0.02, 0.04, 0.06, 0.08, 0.1, 0.12, 0.14, 0.16, 0.18, 0.2 mM ASA concentrations. (b) Calibration plot of the anodic currents recorded at E= +0.50 V vs. ASA concentration.

Figure 6.39 (a) DPVs of the MWCNT-EP composite electrode in 0.1 M Na₂SO₄ supporting electrolyte (curve 1) (modulation amplitude 0.1 V, step potential 0.01 V), potential scan rate 0.05 Vs⁻¹ and in the presence of: 0.2, 0.4, 0.6, 0.8, 1, 1.2 mM ASA concentrations. (b) Calibration plot of the anodic currents recorded at E= +0.50 V vs. ASA concentration.

Figure 6.40 (a) Detail of CVs of the MWCNT-EP composite electrode in 0.1 M NaOH supporting electrolyte (black curve) and in the presence of: 0.02, 0.04, 0.06, 0.08, 0.1, 0.12, 0.14, 0.16, 0.18, 0.2 mM ASA; scan rate 0.05 Vs⁻¹. (b) Calibration plot of the anodic currents recorded at E= +0.55 V/SCE vs. ASA concentration.

Figure 6.41 (a) DPVs of the MWCNT-EP composite electrode in 0.1 M NaOH supporting electrolyte (curve 1) (modulation amplitude 0.1 V, step potential 0.01 V), potential scan rate 0.05 Vs⁻¹ and in the presence of: 0.02, 0.04, 0.06, 0.08, 0.1, 0.12, 0.14, 0.16, 0.18, 0.2 mM ASA concentrations. (b) Calibration plot of the anodic currents recorded at E=+0.42 V vs. ASA concentration.

Figure 6.42 (a) DPVs of the MWCNT-EP composite electrode in 0.1 M NaOH supporting electrolyte (curve 1) (modulation amplitude 0.1 V, step potential 0.01 V), potential scan rate 0.05 Vs⁻¹ and in the presence of: 0.02, 0.04, 0.06, 0.08, 0.1, 0.12, 0.14, 0.16, 0.18, 0.2 mM ASA concentrations. (b) Calibration plot of the anodic currents recorded at E=+0.42V vs. ASA concentration.

Figure 6.43 (a) CVs of the MWCNT-HKUST-Epoxy composite electrode in 4 mM K₃[Fe(CN)₆] in 0.1 M KNO₃ supporting electrolyte at different scan rates: 1) 0.025, 2) 0.05, 3) 0.1, 4) 0.2, 5) 0.3 Vs⁻¹. (b) Calibration plots of the oxidative and reductive peak currents vs. the square root of the scan rate.

Figure 6.44 (a) CVs of the MWCNT-HKUST-Epoxy composite electrode recorded at a potential scan rate of 0.05 Vs⁻¹ and a potential range between 0 V and + 1.2 V/SCE in 0.1 M NaOH supporting electrolyte (black curve) and in the presence of different glucose concentrations: 1-10 mM (curves 2-11). (b) Calibration plot of the anodic currents recorded at E= +0.6 V/SCE vs. glucose concentration.

Figure 6.45 (a) LSVs of the MWCNT-HKUST-Epoxy composite electrode recorded at a potential scan rate of 0.05 Vs⁻¹ and a potential range between 0 V and + 1.0

V/SCE in 0.1 M NaOH supporting electrolyte (curve 1) and in the presence of different glucose concentrations: 1-10 mM (curves 2-11). (b) Calibration plot of the anodic currents recorded at $E = +0.60$ V/SCE vs. glucose concentration.

Figure 6.46 (a) LSVs recorded on MWCNT-HKUST-Epoxy composite electrode at a potential scan rate of 0.05 Vs^{-1} in potential range between +0.2 V and + 1.0 V vs. SCE in 0.1 M NaOH supporting electrolyte (curve 1) and in the presence of 1 mM glucose concentration after different accumulation times: 2) 0 min, 3) 5 min, 4) 10 min, 5) 20 min, 6) 30 min, 7) 40 min, 8) 50 min. (b) Peak current responses and enhancement factors for the detection of 4 mM glucose at MWCNT-HKUST-Epoxy composite electrode as a function of the accumulation time recorded at $E = +0.60$ V/SCE.

Figure 6.47 (a) LSVs recorded on MWCNT-HKUST-Epoxy composite electrode, accumulation time of 30 minutes, potential range 0 to + 1.0 V vs. SCE in 0.1 M NaOH supporting electrolyte (1) and in the presence of different glucose concentrations: 2) 0.2 mM, 3) 0.4 mM, 4) 0.6 mM, 5) 0.8 mM, 6) 1mM. (b) Calibration plot of the anodic currents recorded at $E = +0.60$ V/SCE vs. glucose concentration.

Figure 6.48 (a) Detail of the DPVs of the MWCNT-HKUST-Epoxy composite electrode at (modulation amplitude 0.002 V, step potential 0.01 V) and potential scan rate of 0.05 Vs^{-1} , potential range between +0.1 V to + 0.6 V vs. SCE in 0.1 M NaOH supporting electrolyte (curve 1) and in the presence of different glucose concentrations: 2) 1 mM, 3) 2 mM, 4) 3 mM, 5) 4 mM, 6) 5 mM, 7) 6 mM. (b) Calibration plot of the anodic currents recorded at $E = +0.27$ V/SCE vs. glucose concentration.

Figure 6.49 (a) Amperometric response (BSA) of the MWCNT-HKUST-Epoxy composite electrode for the successive and continuous addition of 1 mM glucose. Applied potential: +0.6 V vs. SCE. b) The calibration plot of useful signal vs. glucose concentration.

Figure 6.50 DPVs on MWCNT-HKUST-Epoxy composite electrode in (1) supporting electrolyte (0.1 M NaOH); (2) 0.1/50 dilution of *glucose serum stock* solution in supporting electrolyte; (3) 0.2/50 dilution of *glucose serum stock* solution in supporting electrolyte ; (4) 0.3/50 dilution of *glucose serum stock* solution in supporting electrolyte; (5) 0.4/50 dilution of *glucose serum stock* solution in supporting electrolyte ; (6) 0.5/50 dilution of *glucose serum stock* solution in supporting electrolyte; (7) 0.6/50 dilution of *glucose serum stock* solution in supporting electrolyte.

CHAPTER 1

INTRODUCTION IN NANOTECHNOLOGY AND CARBON NANOTUBES

"You very rarely see chaos and nanotechnology mentioned together, but it's nice to know that chaos is not just something that happens on the large scale".
(Arvind Raman)

Nanoscience and nanotechnology primarily deal with the synthesis, characterization, exploration, and exploitation of nanostructured materials. Nanoscience and nanotechnologies are widely seen as having huge potential to bring benefits in areas as diverse as drug development, devices for conversion and storage of sustainable energy, water decontamination, information and communication technologies, and the production of stronger, lighter materials. They are attracting rapidly increasing investments from governments and from businesses in many parts of the world; it has been estimated that the total global investment in nanotechnologies is currently around €5 billion.

Nanotechnology is one of the most active research areas over the last two decades. The term "nanotechnology" was first used by Taniguchi in the paper, "On the Basic Concept of Nanotechnology", presented in 1974, in Japan, as follows: "Nanotechnology mainly consists of the processing of separation, consolidation, and deformation of materials by one atom or one molecule" [1.1]. Later on in the 1980's the basic idea of this definition was explored in much more depth by Drexler, who promoted the technological significance of nanoscale phenomena and devices through the book *Engines of Creation: The Coming Era of Nanotechnology and Nanosystems* [1.2]. Nowadays, the term nanotechnology is a collective term for a set of technologies, techniques and processes – effectively a new way of thinking – rather than a specific area of science or engineering.

Nanotechnology deals with materials and systems having the following key properties [1.3]:

- they have at least one dimension in the range 1–100 nm,
- they are designed through processes that exhibit fundamental control over the physical and chemical attributes of molecular-scale structures,
- they can be combined to form larger structures, for example, nanostructured materials.

Our society requires new materials for a sustainable future, and carbon nanotubes (CNTs) are among the important advanced materials. Advanced materials are a prerequisite for all major research and development areas and for all key technologies ranging from information and communication, health and medicine, energy and environment, to transport and space exploration. Sophisticated materials and material systems with novel properties and unheard of performance will have to be conceived and designed in the decades to come. In natural and man-made environments, nanotechnology will help to solve problems like soil and groundwater remediation, conversion and storage of sustainable energy, air purification, pollution detection and sensing.

The development of the materials of tomorrow will make increased use of new nanoscience concepts, i.e., the design of artificial material structures within the ultimate limit – atom control. New nanofunctions will be created by the control of

size and shape of the nanoparticles as well as by the controlled interactions between them across tailored interfaces. In this way, future materials research will open up a new dimension in the periodic table allowing new material functions beyond the properties tagged by nature to the elements. These future visions of nanomaterials science are bearing on the virtually infinite possible materials combinations and on the resulting emergent phenomena have been anticipated by Richard Feynman's "*There is plenty of room at the bottom*" and Phil W. Anderson's "*More is different*".

It is expected that new nanomaterials will find their way into almost all future technologies: new nanoparticle-reinforced and light-weight materials will be used for transport technologies; new storage media based on nanolayers and quantum dots will revolutionise information technology; new materials based on nanoparticles will be employed in catalytic reactors; new pharmaceutical nanomaterials will serve in drug delivery, and new charge separation materials will enhance the performance of future batteries and fuel cells, to name but a few examples of advanced applications.

Future nanotechnology will be enabled by enhancing fundamental research in the critical areas of nanomaterials synthesis, nanomaterials analysis, and nanomaterials modelling. In all these areas there are major challenges to be met and barriers to be overcome. More specifically, it is necessary that we:

- achieve a much better control of the size and shape of the primary nanoparticles in order to exploit their full potential,
- develop a new level of analytical capability for the in-situ and destruction-free characterization of nanomaterials and nanodevices under the relevant operating conditions as well as with the highest resolution and sensitivity,
- develop a detailed microscopic understanding of how a given artificial nanoarchitecture and its properties are related.

The real progress in nanotechnology started with the discoveries of fullerenes in 1985 and of carbon nanotubes in 1991 which had opened a completely different perspective from that of carbon materials based on graphite-like hexagonal layers. Carbon nanotubes (CNTs) are not only excellent tools for studying one dimensional phenomena, but they are also among the most important and promising nanomaterials and nanostructures. Nowadays, the research in nanotubes has attracted the attention of many scientists in the wide field of materials science and technology. In addition, research has been directed to basic science, with the target to modify structure and chemically modify the surface of CNTs. This has later allowed thinning their properties and possible uses, opening up new applications in chemistry, physics, medicine, materials science, and engineering.

References

- [1.1] N. Taniguchi, On the basic concept of nanotechnology. Proc. ICPB, Tokyo, part II, Japan Society of Precision Engineering 1974.
- [1.2] K.E. Drexler, New York: Anchor Press/Doubleday: 1986.
- [1.3] M.C. Rocco, National Science Foundation, Official who oversees the nanotechnology initiative, Scientific American 285 (2001) 3.

CHAPTER 2

CARBON NANOTUBE-BASED ELECTRODES APPLIED FOR ELECTROCHEMICAL SENSORS AND BIOSENSORS

"It would be possible to describe everything scientifically, but it would make no sense; it would be without meaning, as if you described a Beethoven symphony as a variation of wave pressure". (Albert Einstein)

Summary

This chapter presents a general overview of the history of nanotubes, their structures, properties, synthesis techniques, and applications with a primary focus on advances in electrochemical sensors and biosensors based on carbon nanotubes. The challenges related to the use of carbon nanotubes to enhance the performance of electrochemical sensors and biosensors are discussed. This chapter also highlights the importance of selecting and developing suitable routes for the synthesis of carbon nanotubes, in order to effectively exploit their properties for electrochemical sensors and biosensors.

2.1 Carbon nanotubes

2.1.1 History of nanotubes

Carbon nanotubes (CNTs) have been known since 1976 [2.1], but the Japanese electron microscopist Sumio Iijima reported in *Nature*, 1991 for the first time the observation of "helical microtubules of graphitic carbon" by electron microscopy [2.2]. The synthesis in 1993 of single-wall carbon nanotubes (SWCNTs) was a major event in the development of CNTs [2.3], [2.4]. Even if the discovery of CNTs was an accidental event, it opened up the way to a new research area and inspired scientific activities worldwide, crossing several disciplines.

These structures consist of a single layer of carbon atom arranged in a graphite lattice and rolled into tubes that may be capped on one or both ends. These tubes have extremely small diameters, in the order of a few nanometers, and have been of great scientific interest and study in many fields, such as field-emission materials [2.5]-[2.12] batteries [2.13], tips for scanning probe microscopy [2.14]-[2.20], transistors [2.21], [2.22], diodes [2.23], components for composite materials [2.24], due to their amazing electrical, mechanical and thermal properties. CNTs may be classified into: (a) single-wall carbon nanotubes (SWCNTs) which possess the fundamental cylindrical structure, and (b) multi-wall carbon nanotubes (MWCNTs) (Figure. 2.1) (consist of two or more coaxial cylinders, each rolled out of single sheets, separated by approximately the interlayer spacing in graphite).

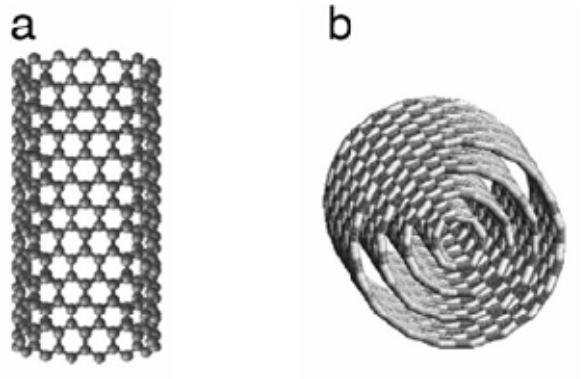


Figure 2.1 Schematic diagram of an individual (a) SWNTs and (b) MWNTs. [2.25]

The following table presents the differences between SWCNTs and MWCNTs.

Table 2.1 Comparison between SWNTs and MWNTs

SWCNT	MWCNT
<ul style="list-style-type: none"> • Single layer of graphene • Catalyst is required for synthesis • Bulk synthesis is difficult as it requires proper control over growth and atmospheric condition • Poor purity • A chance of defect is more during functionalization • Easy characterization and evaluation • It can be easily twisted and is more pliable 	<ul style="list-style-type: none"> • Multiple layers of graphene • Can be produced without catalyst • Bulk synthesis is easy • High purity • A chance of defect is less but once occurred it is difficult to improve • Very complex structure • It cannot be easily twisted

2.1.2 Structure of nanotubes

The primary symmetry classification of CNTs divides them into achiral or chiral [2.26]. An achiral nanotube is defined by a nanotube whose mirror image has an indistinguishable structure to the original one. There are only two cases of achiral nanotubes: armchair and zig-zag nanotubes. The simplest way of specifying the structure of an individual tube is in terms of a vector, the chiral vector (C_h) joining two equivalent points on the original graphene lattice. The cylinder is produced by rolling up the sheet such that the two end-points of the vector are superimposed (Figure 2.2). The chiral vector can be defined in terms of the lattice translational indices (n, m) and the basic vectors a_1 and a_2 of the hexagonal lattice and corresponds to a section of the nanotube perpendicular to the nanotube axis, i.e.

$$C_h = na_1 + ma_2 \quad (n, m \text{ are integers, } 0 \leq |m| \leq n) \quad (2.1)$$

The chiral angle, θ , is defined as the angle between the vectors C_h and a_1 , with values of θ in the range $0^\circ \leq |\theta| \leq 30^\circ$, due to the hexagonal symmetry of the honeycomb lattice, see Eq. (2.2)

$$\cos \theta = \frac{C_h a_1}{|C_h| |a_1|} = \frac{2n + m}{2\sqrt{n^2 + m^2 + nm}} \quad (2.2)$$

The chiral angle θ denotes the tilt angle of the hexagons with respect to the nanotube axis, and the angle θ specifies the spiral symmetry. The two limiting cases, corresponding to the achiral nanotubes, exist where the chiral angle is at 0° (zig-zag) and 30° (armchair). The diameter of the CNTs (d_t) is given by L/π in which L is the circumferential length of the CNTs,

$$d_t = L/\pi \quad (2.3)$$

$$L = |C_h| = \sqrt{C_h C_h} = a\sqrt{n^2 + m^2 + nm} \quad (2.4)$$

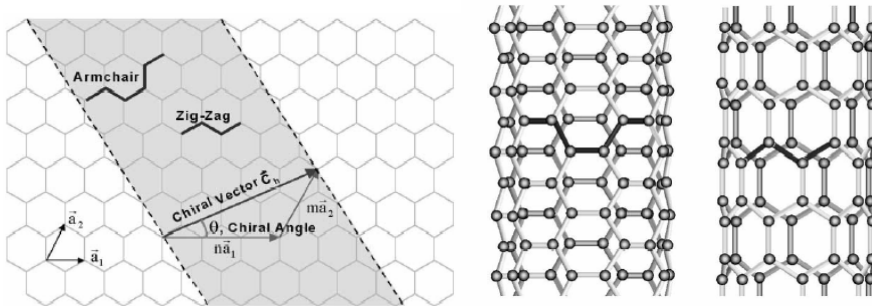


Figure 2.2 Schematic diagrams showing how a hexagonal sheet of graphite is “rolled” to form a CNT [2.27]

Based on theoretical predictions, SWCNTs can be either metallic or semiconducting, depending on their diameters and helical arrangement (n, m). For $n = m$, the tubes are metallic and for other values of $n - m$, the tubes behave as semiconductors with different bandgaps and, therefore, they differ in properties.

2.1.3 Synthesis, purification, and functionalization

Advances have been made in the areas of CNTs synthesis [2.28], [2.29]. Arc discharge (AD) [2.30], which implies the arc evaporation of pure or metal-doped carbon electrodes, laser ablation (LA) [2.31], and chemical vapor deposition (CVD) [2.32], which is based on the decomposition of carbon-containing precursors such as ethane, methane, and carbon monoxide on supported metal catalysts, are the three main methods employed for the CNTs synthesis. Among all the CVD methods

reported, the so-called High-Pressure Carbon Oxide (HiPCO) process [2.33] is particularly successful and used to produce high-quality SWCNTs of small diameters and narrow diameter distributions with rather high yields.

In Table 2.2 a summary and comparison of the above-mentioned methods is presented.

Table 2.2 Summary and comparison of the most important synthesis methods for CNTs.

Synthesis method	Summary	Yield	Strength	Weakness	SWCNTs Or MWCNTs
Arc Discharge (AD)	Graphite evaporated by a plasma via high current	30%	SWCNTs and MWCNTs with few structural defects	Tubes tend to be short and entangled	Both
Chemical Vapor Deposition (CVD)	Decomposition of carbon-based gas precursors	20-100%	Easiest to scale up to industrial production	Typically MWCNTs with a high density of defects	Both
Laser Ablation (LA)	Graphite blasted with intense laser pulses	Up to 75%	Diameter control via reaction temperature	More expensive than other methods	SWCNTs
High Pressure CO Conversion (HiPCO)	Metal catalysts nucleate SWCNTs at high temperature and pressure	95%	Excellent structural integrity for CVD process	Production rates still relatively low	SWCNTs

However, their large-scale synthesis and mass production are prerequisites for a wide range of applications. The production must be environmentally friendly, controllable in quality, low-cost, ideally without the requirement for complicated purification treatments. Summarizing these prerequisites, one may conclude that CVD is still the most widely used synthesis technique for producing large amounts of high-quality CNTs. Despite the high cost of CNTs, at present this method is used by several suppliers, such as NanoLab, Sigma-Aldrich, and Nanocyl.

Current production capacity for CNTs is estimated to be around 100 tonnes per year. The actual production output remains commercially confidential, but is expected to be lower. Most of the capacity is estimated to be multi-walled tubes, with single-wall tubes accounting for about 9 tonnes of capacity.

All synthesis techniques make use of transition metal catalysts such as nickel (Ni), cobalt (Co), iron (Fe), or yttrium (Y) [2.34], which usually remain in the

yield. The metal and the particle size determine the diameter of the CNT growing on their surface. SWCNTs grow on small catalyst particles in the nanometer range, whereas larger particles tend to produce MWCNTs [2.35].

To date, a lot of research is conducted to improve the purity and structural quality of the CNTs. As mentioned before, all the CNT synthesis methods are not equivalent and lead to the production of CNTs with different characteristics, as well as different kinds and levels of impurities, e.g. amorphous carbon, nanographitic structures, and carbon encapsulated catalytic metal nanoparticles [2.36]. These impurities often interfere with the desired properties of CNTs. Therefore, the main concern is how to separate them from the worthless soot and how to purify the tubes. For this purpose, various post-growth treatment methods to purify the nanotubes and eliminate the defects in the tubes have been developed.

The most commonly used purification methods include filtration [2.37]-[2.41] and centrifugation [2.42], which are not very efficient for the removal of impurities, oxidation in the presence of an acid [2.43], or a gas [2.44], and chromatographic separation [2.45]-[2.47]. Less common methods include capillary electrophoresis [2.48] and ultrasonication in the presence of inorganic nanoparticles [2.49]. Hydrothermal treatment has also been found to be effective in the purification of SWNTs [2.50].

CNTs are hydrophobic and, therefore, not soluble in water and, unlike closed cages such as C_{60} , most forms of CNTs are also insoluble in organic solvents [2.45]. Preparation of a homogeneous dispersion of CNTs is of great importance for many potential applications such as in polymer composites and electrochemical sensors. In order to make them soluble, CNTs are usually chemically modified by functionalisation, where submolecular structural units are covalently or noncovalently attached to the surface of CNTs [2.51].

There are two major approaches to nanotube functionalization, i.e., covalent functionalization, which can be achieved by either direct addition reactions of reagents to the surfaces of nanotubes or modification of appropriate surface-bound functional groups (e.g., carboxylic acid) on the nanotubes [2.52]-[2.54], and non-covalent functionalization, which involves van der Waals, $\pi-\pi$, $CH-\pi$, or electrostatic interactions between polymer molecules and CNT surfaces [2.55]-[2.57]. The advantage of non-covalent functionalization is that it does not alter the structure of the nanotubes and, therefore, both electrical and mechanical properties should remain unchanged. There are several non-covalent approaches for nanotube functionalization such as surfactant-assisted dispersion, polymer wrapping, plasma polymerization-treatment, and polymerization filling technique (PFT) [2.58].

2.1.4 Processing of CNT-polymer composites

2.1.4.1 Solution processing

Perhaps the most common method for preparing CNT-polymer composites has been from solution, since it facilitates nanotube dispersion. The general protocol includes the dispersion of CNT powder in a solvent via energetic agitation (magnetic or mechanic stirring, reflux or sonication), mixing the CNT dispersion with a polymer solution and controlled evaporation of the solvent with or without vacuum conditions.

Regarding thermosetting epoxy matrices, an early example of solution-based composite formation was described by Ajayan et al. [2.59]. MWCNTs were

dispersed in ethanol by sonication and mechanically mixed with a mixture of epoxy monomer and curing agent. After evaporation of the volatile solvent, the CNT-epoxy mixture was poured into capsular molds and then cured.

Concerning the fabrication of CNT-based composites with thermoplastic matrices, Jin et al. [2.60] have reported a similar method consisting of solution mixing, casting and drying. The polyhydroxyaminoether polymer was dissolved in the arc discharge-grown CNTs in chloroform under sonication. The suspension was then poured into a Teflon mold and dried under ambient conditions for a certain time. Mechanical stretching of thin strips of the composite at 100°C was found to cause orientation of tubes in the axis of tension. Shaffer and Windle [2.61] dispersed chemically oxidized catalytic MWCNTs in water. The material was carefully blended with solutions of poly (vinyl alcohol) (PVA) in water to give composite dispersions which could be drop-cast to form films with up to 60 wt% nanotubes.

Zhou and co-workers [2.62] utilized a roll-casting technique to prepare composite films of poly(ethylenoxide) embedded with fluorinated CNTs. In order to succeed rapid evaporation of solvent during the suspension casting process, Safadi et al. [2.63] have used the spin coating technique.

Since the casting/evaporation process results in the reagglomeration of CNTs within the composite film, Winey and co-workers [2.64] proposed an alternative approach for fabricating composites with individually dispersed CNTs, the so called coagulation. After the solution mixing step, a CNT/PMMA poly(methyl methacrylate) suspension was dripped into a large excess of poor solvent (water) in order to induce instant precipitation of the polymer chains. The precipitating chains entrapped the carbon nanostructures and prevented them from bundling again. After filtration and drying in vacuum, nanocomposites were obtained with homogeneously distributed CNTs.

2.1.4.2 Bulk mixing

Milling is a mechanical process that leads to local generation of high pressure as a result of collisions throughout the grinding media. Concerning applications in CNT nanotechnology, this method has been used to shorten the lengths of carbon nanostructures [2.65]. A solid-state mechanochemical pulverization process was used to prepare a CNT/polypropylene composite powder [2.66]. This powder was subsequently melt-mixed with a twin-roll masticator to obtain a homogeneous composite. The length of the CNTs was reduced from a few micrometers to ~ 500 nm.

Similarly, ball milling was utilized to incorporate CNTs into polymer matrices [2.67]. In this way, a satisfactory level of dispersion of CNTs into the polymer matrix was obtained, resulting in an improvement of the physical properties of the samples.

2.1.4.3 Melt processing

While solution processing is a valuable technique for both nanotube dispersion and composite formation, it is less suitable for industrial scale processes, where melt processing is preferred because of its speed and simplicity. In addition, the method is suitable for polymers that cannot be processed with solution techniques due to their insolubility in common solvents.

Normally, melt processing involves mixing of CNTs with the molten polymer by shear mixing. Bulk composites can then be prepared by compression molding, injection molding, or extrusion. Advantages of melt processing are its speed and simplicity and easy integration into standard industrial facilities (e.g., extruders, blow-molding machines). Although under high temperatures, this approach can sometimes result in unexpected polymer degradation and oxidation.

Goh and co-workers [2.68] have melt-blended MWCNTs and PMMA in a laboratory mixing molder at a speed of 120 rpm. The mixed samples were then compressed under pressure at 210°C using a hydraulic press to yield composite films. Electron microscopy images showed that the nanotubes are well dispersed in the polymer matrix.

Pötschke and co-workers [2.69], [2.70] thoroughly investigated MWCNTs/polycarbonate composites prepared by melt extrusion and compression molding. By carefully controlling the mixing conditions, they obtained a percolation threshold of about 1 wt%.

2.1.4.4 In-situ polymerization

In-situ polymerisation has been extensively studied for the preparation of functional composites, its main advantage being the creation of a covalent bond between the tube and the matrix. The presence of a polymeric chain onto the tubes surface facilitates their dispersion providing a strong interface at the same time. This technique allows the preparation of composites with high a CNT weight fraction, which could be then diluted by other techniques. For the thermosets such as epoxies or unsaturated polyesters, a curing agent or peroxide is added to initiate the polymerisation. For thermoplastics, the polymerisation can be initiated either by the addition of an initiator or by an increase of temperature.

Jia and other research groups have studied the in-situ radical polymerization of pyrrole [2.71] and phenylacetylene [2.72] in the presence of CNT material. Concerning the processability, the resulting composites exhibited enhanced dispersability in various organic solvents, whereas the electrical, magnetic, and thermal properties of the CNTs were modified by the conducting polymer chains [2.71].

As an alternative approach, efficient doping of CNT sidewalls by conducting polymers has been studied by in-situ electrochemical means [2.73], [2.74]. Microscopy images showed a remarkably uniform polymer coating on individual CNTs, which paves the way for controlled modification of the outer surface of CNTs with selected functionalities. Moreover, the observation of joining individual CNTs by the conducting polymer chains in the composite film was suggested to have great potential in applications such as CNT-based optoelectronic devices.

Kimura et al. [2.75] have mixed styrene monomer with nanotubes and subjected the suspension to a constant magnetic field. By polymerizing the mixture, the nanotubes were found to be kept aligned within the polymer matrix. Analogous

experiments with an epoxy thermoset as a matrix showed that the thermal and electrical properties of the composites were significantly enhanced by magnetic alignment during processing [2.76]. In an analogous work, Bauhofer and co-workers [2.77] dispersed MWCNTs in an epoxy system based on a bisphenol-A resin and an amine hardener. The application of both AC and DC electric fields during nanocomposite curing was used to induce the formation of aligned conductive nanotube networks between the electrodes. The network structure formed in AC fields was found to be more uniform and more aligned compared to that in DC fields.

Concerning the fabrication of CNT-based silicone elastomer composites, Liu et al. [2.78] dispersed the graphitic nanostructures into a viscous mixture of monomers by mechanical grinding of the components. Most probably, the thermal energy given by the grinding process caused the efficient condensation of the precursor substances. The thermal conductivities were found to increase with the CNT amount. There was a 65% enhancement with 3.8 wt% CNT loading.

Similarly, Gojny et al. [2.79] studied the dispersion of CNTs into viscous epoxy monomers via a common shear mixing technique, called calendaring. In a first step, the nanoparticles were manually mixed into the resin while in the following step they were homogeneously dispersed using of a three-roll calendaring.

2.1.5 Properties

What are the properties that make carbon nanotubes so interesting? In fact, it is not just one property that makes carbon nanotubes so extraordinary, but the combination of exceptional properties all combined in one material. These properties range from structural to chemical and from electrical to optical. A short, non-exhaustive summary of carbon nanotube properties follows below.

Structurally, CNTs are probably the strongest and stiffest materials on earth: they have record-high tensile strength in combination with an extremely high elastic modulus. This means that, in theory, they can be made into the strongest fibers possible, stronger than steel or spider silk.

Chemically, a carbon nanotube is very inert and, therefore, highly stable. This is related to the stability of the sp^2 -bonded carbon network. Also CNTs possess very high specific surface and $\sigma - \pi$ (re)hybridization facilitates molecular adsorption, doping, and charge transfer on nanotubes, which, in turn, modulates electronic properties.

Nanotubes display very high thermal conductivity, therefore, it is expected that nanotube reinforcements in a polymeric matrix may also significantly improve the thermal and thermomechanical properties of such composites.

2.1.6 Applications

Over the past years, CNTs have evolved into one of the most intensively studied materials and in demand for various applications, including both large volume applications (e.g., as components in conductive, electromagnetic, microwave absorbing, high-strength composites, supercapacitors, or battery electrodes, battery electronic additives, fuel cell catalysts, transparent conducting films, field-emission displays (FED), and photovoltaic devices) and limited-volume

applications (e.g., as scanning probe tips, drug delivery systems, electronic devices, thermal management systems, sensors, and biosensors). As a novel advanced functional material, CNTs have been considered for use in energy-saving chemistry, green catalytic processes, and advanced energy conversion and storage devices, and so have attracted the attention of multidisciplinary scientists for use in developing a sustainable society.

Main markets at present for nanotubes are aerospace, automotive, defense, electronics, and data storage. The electronics and data storage markets are likely to see the biggest penetration to 2015, with the performance enhancing properties of carbon nanotubes allowing electronics manufacturers to meet demanding market needs across a variety of applications.

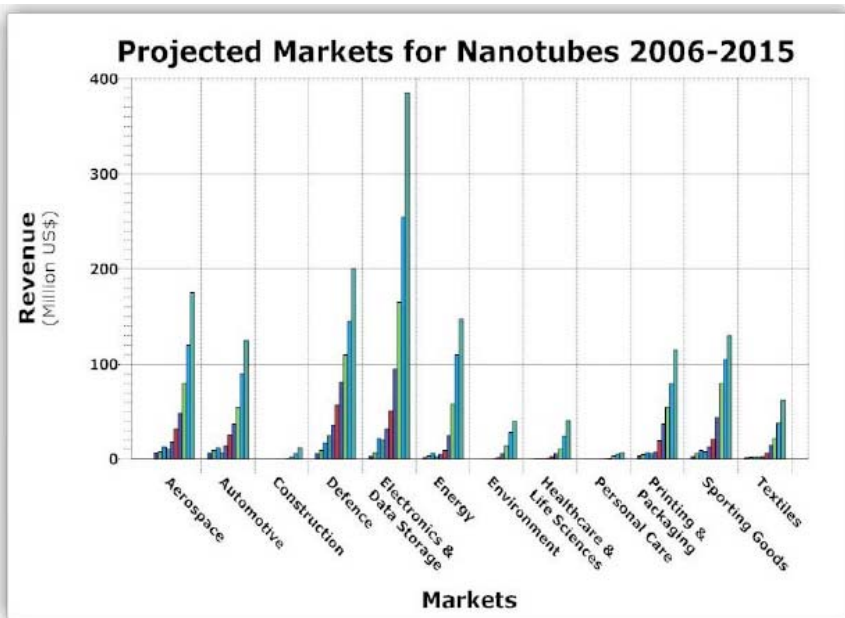


Figure 2.3 Projected markets for nanotubes 2006-2015 (Source: Nanoposts.com)

In aerospace, nanotubes already find application as additives for electrostatic discharge (ESD) and electromagnetic interference (EMI) shielding as electrostatic coatings and component reinforcement additives in the automotive sector, in various defense applications, and as conductive polymer-based composites for field-emission displays (FED). This represents the first generation of nanotubes products; the next generation will be based on controlled fabrications leading to multi-functional and sensory capabilities.

Market Applications of Carbon Nanotubes

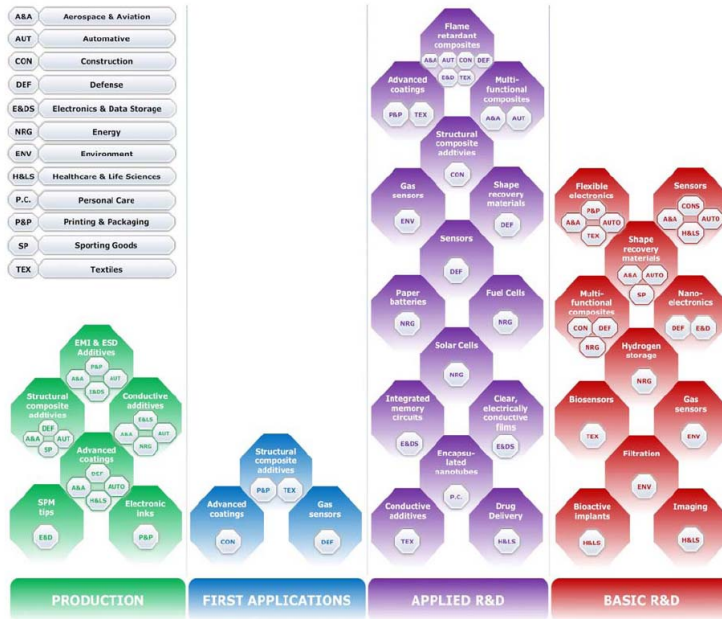


Figure 2.4 Market applications of carbon nanotubes (Source: Nanoposts.com)

There are over 85 companies in the carbon nanotubes market, making it extremely competitive. Several major players are building commercial levels of capacity and bringing prices down significantly. Major market players are Hyperion Catalysis, Arkema, Thomas Swan, Bayer Material Science, and Showa Denko.

Furthermore, the properties due to small dimensions, functional surfaces, good conductivity, excellent biocompatibility, modifiable sidewalls, and high reactivity make CNTs ideal candidates for constructing sensors with high performances. As an example, CNTs have been extensively employed in constructing various electrochemical sensors (EC). Compared with the conventional scale materials and other types of nanomaterials, CNTs have some overwhelming advantages in fabricating electrochemical sensors, including:

- large specific areas and, therefore, improved sensitivity,
- good biocompatibility, that is suitable for constructing electrochemical biosensors, especially for facilitating the electron transfer of redox proteins and enzymes,
- modifiable ends and sidewalls providing a chance for fabricating multifunctional electrochemical sensors via the construction of functional nanostructures,
- possibility of achieving miniaturization.

Electrochemical sensing has been proven as an inexpensive and simple analytical method with remarkable detection sensitivity, reproducibility, and ease of

miniaturization. Numerous advantages of CNTs as electrode materials have been attested for analysis of diversified chemicals of food quality, clinical, and environmental interest.

Carbon nanotubes have been used extensively for electrochemical sensing due to the unique mechanical, chemical, and electrical properties. These properties have fuelled an exponential increase in the number of reports and review [2.80]-[2.85] involving sensors based on CNTs (either single or multi-wall) over the last decade. The first application of carbon nanotubes in the preparation of a sensor was reported by Britto et al. in 1996 [2.86]. Using a carbon nanotube paste electrode with bromoform as the binder, the electrochemical oxidation of dopamine (DA) was explored. The concept of a carbon nanotube paste electrode was later readapted by Valentini et al. [2.87]. However the explosion of interest in CNTs in the early 21st century for use in electroanalysis can be traced back to the work pioneered by Prof. Wang and co-workers who observed the low potential stable of nicotinamide adenine dinucleotide (NADH) detection at a carbon-nanotube-modified glassy carbon electrode [2.88].

Carbon nanotube-based electrochemical sensors (CNT-EC) exhibit a low limit of detection (LOD) and fast response due to the signal enhancement provided by a high surface area, low overvoltage, and fast electrode kinetics. Also an important part of the impressive success of the use of CNT-EC is most probably due to the ability to promote electron transfer in electrochemical reactions. The electrocatalytic effect of CNTs has been attributed to the activity of edge-plane like-graphite sites at the CNTs ends [2.89].

Recent studies demonstrate the excellent electrocatalytic abilities and antifouling properties of carbon nanotubes in electrochemical devices. Electrodes modified with CNTs have been used for electrocatalytic oxidation of NADH [2.88], norepinephrine [2.90], 3,4-dihydroxy phenyl acetic acid [2.91], 4-amino phenol [2.92], 6-mercaptopurine [2.93], ascorbic acid [2.94], nitric oxide [2.95], cytochrome c [2.96], thymine [2.97], L-cysteine [2.98], hydrazine [2.99], glucose [2.100], dopamine [2.101], 2,4,6-trinitrotoluene, [2.102], and uric acid [2.103].

2.1.6.1 Applications in sensors

A new kind of NADH sensor based on a Meldola's blue (MB) functionalized carbon nanotubes nanocomposite-film (MB/CNTs) modified glassy carbon electrode (GCE) has been reported [2.104]. Most of the CNTs-based electrodes for NADH detection are based on physical adsorption of CNTs onto electrode surfaces, usually glassy carbon. However, it is important to note that CNTs have also been dispersed inside an epoxy resin [2.105].

Rubianes and Rivas [2.106] demonstrated the advantages of a composite material prepared by mixing MWCNTs and mineral oil on the electrochemical behavior of different biomolecules. The voltammetric signal for dopamine (DA), ascorbic acid (AA), dopac, and uric acid (UA) largely improved at the composite electrode containing CNTs. Another example of a nanostructured electroactive film to detect DA in the presence of AA has been studied by Siqueira et al. [2.107]. In this study they have fabricated layer-by-layer films of polyamidoamine (PAMAM) incorporating MWCNTs (PAMAM-NT) alternated with nickel tetrasulfonated metallophthalocyanine (NiTsPc), in which the incorporation of CNTs enhanced the NiTsPc redox process and its electrocatalytic properties to detect DA.

Li et al. [2.90] reported the electrocatalytic oxidation of norepinephrine at a glassy carbon electrode (GCE) modified with SWCNTs. The electrode showed a very good reproducibility and stability. The electrocatalytic activity of the SWCNTs-modified glassy carbon electrode was also demonstrated with dopamine, epinephrine, and ascorbic acid. Another approach to determine epinephrine was proposed by Compton et al. [2.108]. They used MWCNTs abrasively attached to the basal plane of pyrolytic graphite.

A fructose sensor was simply prepared by immobilizing fructose dehydrogenase onto a MWCNT modified Pt electrode [2.109]. Galactose sensing can be realized by covalent immobilization of galactose oxidase on chemically crosslinked SWCNT-chitosan [2.110].

A SWCNTs-DDAB (Didodecyldimethylammonium bromide) film modified glassy carbon electrode was used to study the electrochemical behavior of hemoglobin [2.111]. Another interesting application includes the use of CNTs in the detection of blood cholesterol that is of great clinical significance. Roy et al. [2.112] reported the fabrication of vertically aligned CNTs bioprobes on silicon substrates for enzymatic assay of cholesterol. A MWCNT modified electrode using ferrocenedicarboxylic acid as a mediator is capable of detecting folic acid [2.113]. This sensor exhibits efficient electrocatalytic activity towards the oxidation of folic acid at pH 9.0.

2.1.6.2 Applications in biosensors

In the area of medical diagnostics and environmental applications, CNTs-based electrochemical biosensors could be used, for example, to replace more costly and tedious laboratory methods for monitoring a patient's blood for proteins, chemicals, and pathogens, and also for monitoring pollutants in the environment.

The rapid and accurate monitoring of blood glucose level is required for the control of diabetes. Glucose sensors are, therefore, a highly active area of sensor research, and accordingly they account for approximately 85% of the biosensor industry. Here, we report a few publications but there are several reviews of enzymatic electrochemical glucose sensors, published by Heller and Feldman [2.114] and by Wang [2.115]. Multi-wall carbon nanotubes (MWCNTs) have been widely used in glucose sensors for glucose oxidase (GOx) immobilization [2.116]. Some of the recently reported MWCNT matrices for GOx immobilization are ionic liquid n-octylpyridinium hexafluorophosphate dispersed MWCNT [2.117], MWCNT/gold nanoparticles-Teflon composites [2.118], Chitosan-dispersed MWCNT [2.119], gold nanoparticles/ thiol group functionalized MWCNT/Chitosan-ionic liquid [2.120], cobalt hexacyanoferrate nanoparticles/gold nanoparticles (seed)/ MWCNT composites [2.121], crystalline gold nanoparticles modified MWCNT [2.122], platinum nanoparticle/MWCNT composites [2.123], nitrogen doped MWCNT [2.124], and polymerized ionic liquid-wrapped MWCNT [2.125]. Gao et al. have also reported glucose biosensors based on aligned CNTs coated with a conducting polymer [2.126].

An example of an amperometric ethanol biosensor was constructed by Tsai et al. [2.127] using alcohol dehydrogenase (ADH) physically immobilized within poly (vinyl alcohol) PVA-MWCNTs composite obtained by a freezing-thawing process.

The use of CNTs as a novel platform for deoxyribonucleic acid (DNA) immobilization has recently attracted substantial research. CNTs have a dual amplification role, i.e., recognition and transduction events. Therefore, they behave

as carriers for enzyme tags and for accumulating the product of an enzymatic reaction. Kerman et al. [2.128], Drummond et al. [2.129], Wang [2.130], and Gooding [2.131] summarized the state-of-the-art and recent trends in electrochemical DNA biosensor technology.

Ruthenium oxide (RuO_2) can be electrodeposited onto a CNT layer and used as an insulin sensor [2.132]. The sensor retains 97% activity after 60 min stirring of 2 μM insulin solution. Of also interest is the development of a nanocomposite electrode composed of CNTs, and cobalt hexacyanoferrate nanoparticles for detecting bovine insulin [2.133]. Toluidine blue and hemoglobin can be incorporated into a MWCNT-chitosan modified glassy carbon electrode, followed by the deposition of an gold nanoparticles film by electrostatic adsorption and the attachment of anti-human chorionic gonadotrophin (anti-hCG) for selective detection of human chorionic gonadotrophin [2.134].

A CNT-field effect transistor-based procedure, involving the use of various linkers-to spacer ratios can be used for real-time detection of the prostate specific antigen- α_1 -antichymotrypsin (PSA-ACT) complex, a prostate cancer marker [2.135].

Highly precise and sensitive detection of carcinoembryonic antigen in saliva and serum is feasible by using a MWCNT screen-printed electrode and ferrocene liposomes [2.136].

SWCNT and glutathione protected gold nanoparticles (GSH-AuNPs) can be used to detect interleukin-6, a human cancer biomarker [2.137].

Putrescine, a potential biomarker for various cancer diseases, can be detected with high sensitivity by binding putrescine oxidase (POx) to 3-aminopropyltriethoxysilane solubilized MWCNTs [2.138]. PDDA or poly(diallyldimethylammonium) chloride is also used to disperse MWCNTs and a mediatorless putrescine biosensor is constructed employing POx-MWCNT-GCE [2.139].

Putrescine can be detected at negative potentials without any interference from endogenous AA and UA. Putrescine in the plasma of cancerous mice is detected very quickly without any previous purification.

2.2 Health and environmental impacts

Although many advantages are associated with the proposed industrial revolution of nanotechnology [2.140], concerns have been raised about the potential adverse effects that may result from the inevitable interactions between humans and the constituents of nanotechnology [2.141] known as nanomaterials. Examples of such a paradox are carbon nanotubes. Although the number of published scientific papers currently totals over 60 000, only around 550 papers focus on potential health effects (Figure 2.5).

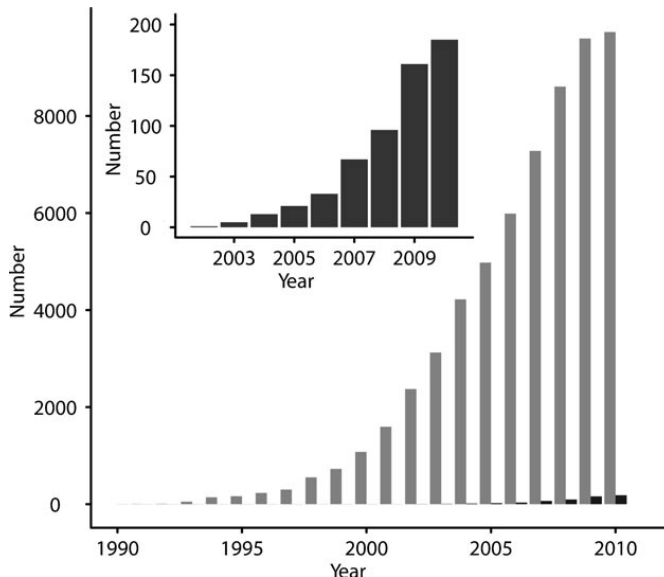


Figure 2.5 Exponential increase of the number of CNT publications. The number of publications listed in the ISI Web of Science database identified with the keyword 'carbon nanotubes' (grey bars) and 'carbon nanotubes toxicity' (black bars) are depicted per year.

The pioneering study that investigated the potential for CNTs to be inhaled was performed by Maynard and colleagues [2.142]. Also numerous papers reported investigations on the potential adverse effects of CNTs on various biological systems, using a variety of exposure methods both in vivo and in vitro [2.143]. Much important knowledge is missing regarding the half-life of CNTs in the body, their accumulation, degradation, elimination, and bio persistency. However, there is an expectation that CNTs accumulate quite significantly in fatty tissues and are very persistent due to the difficulty of modifying them even in laboratories.

Despite this increased quantity of papers on health-related aspects of CNTs since 2003, only a number of landmark papers can be highlighted as providing the basis for the known, or unknown, interactions of CNTs with biological systems. The toxicity of pure CNTs has not been well researched. Until a clear toxicity appraisal is available, CNTs should be handled as toxic material. Nevertheless it is important that precautions are taken in the workplace in manufacturing and research laboratories to manage this potential risk by limiting exposure. However, any harmful effects CNTs may present are greatly reduced when they are embedded in a polymer to create composite materials.

Little is known about the influence of CNT on the environment because very few environmental studies have been conducted. Especially studies of the long term effects of CNTs' presence in nature are lacking, such as effects on the food chain or reproduction. Furthermore the laboratory studies have so far not taken into account realistic biological settings, which are especially important, as the physical and chemical influences on the CNTs change in the environment.

Considering that many nanomaterials are currently manufactured on a small scale, but have potential for market growth, it is necessary to know how much and where particles are used in industry in order to assess the life cycle effects properly.

2.3 Conclusions

This chapter presented an extensive overview of CNTs-based electrodes applied in electrochemical sensors and biosensors. The most relevant properties of CNTs have been listed together with their applications. The current strategies developed over the last ten years to incorporate CNTs into a polymer matrix have also been discussed in the present chapter.

2.4 References

- [2.1] A. Oberlin, M. Endo, T. Koyama, *J. Cryst. Growth* 32 (1976) 335.
- [2.2] S. Iijima, *Nature* 354 (1991) 56.
- [2.3] S. Iijima, T. Ichihashi, *Nature* 363 (1993) 603.
- [2.4] D.S. Bethune, C.H. Klang, M.S. de Vries, G. Gorman, R. Savoy, J. Vazquez, R. Beyers, *Nature* 363 (1993) 605.
- [2.5] S.J. Tans, A.R.M. Verschueren, C. Dekker, *Nature* 393 (1998) 49.
- [2.6] M. Torriones, *Annu. Rev. Mater. Res.* 33 (2003) 33.
- [2.7] R.P. Raffaele, B.J. Landi, J.D. Harris, S.G. Bailey, A.F. Hepp, *Mater. Sci. Eng. B: Solid State Mater. Adv. Technol.* 116 (2005) 233.
- [2.8] T. Feng, J.H. Zhang, X. Wang, X.H. Liu, S.C. Zou, Q. Li, J.F. Xu, *Surf. Rev. Lett.* 12 (2005) 733.
- [2.9] C.M. Hsu, C.H. Lin, H.L. Chang, C.T. Kuo, *Thin Solid Films* 420 (2002) 225.
- [2.10] M.H. Moon, D.J. Kang, J.H. Jung, J.M. Kim, *J. Sep. Sci.* 27 (2004) 710.
- [2.11] O.A. Nerushev, M. Sveningsson, L.K.L. Falk, F. Rohmund, *J. Mater. Chem.* 11 (2001) 1122.
- [2.12] J.J. Zhao, *Curr. Nanosci.* 1 (2005) 169.
- [2.13] B. Gao, C. Bower, J.D. Lorentzen, L. Fleming, A. Kleinhammes, X.P. Tang, L.E. McNeil, Y. Wu, O. Zhou, *Chem. Phys. Lett.* 327 (2000) 69.
- [2.14] E.S. Snow, P.M. Campbell, J.P. Novak, *J. Vac. Sci. Technol. B* 20 (2002) 822.
- [2.15] E.S. Snow, P.M. Campbell, J.P. Novak, *Appl. Phys. Lett.* 80 (2002) 2002.
- [2.16] S.S. Wong, E. Joselevich, A.T. Woolley, C.L. Cheung, C.M. Lieber, *Nature* 394 (1998) 52.
- [2.17] S. Carnally, K. Barrow, M.R. Alexander, C.J. Hayes, S. Stolnik, S.J.B. Tendler, P.M. Williams, C.J. Roberts, *Langmuir* 23 (2007) 3906.
- [2.18] W.P. Huang, H.H. Cheng, S.R. Jian, D.S. Chuu, J.Y. Hsieh, C.M. Lin, M.S. Chiang, *Nanotechnology* 17 (2006) 3838.
- [2.19] J. Martinez, T.D. Yuzvinsky, A.M. Fennimore, A. Zettl, R. Garcia, C. Bustamante, *Nanotechnology* 16 (2005) 2493.
- [2.20] A.J. Austin, C.V. Nguyen, Q. Ngo, *J. Appl. Phys.* 99 (2006) 114304.
- [2.21] C.W. Zhou, J. Kong, H.J. Dai, *Appl. Phys. Lett.* 76 (2000) 1597.
- [2.22] P. Vichchulada, M.D. Lay, *Appl. Phys. Lett.* (2008), Submitted.
- [2.23] J.U. Lee, *Appl. Phys. Lett.* 87 (2005) 3.
- [2.24] M.S. Shaffer, X. Fan, A.-H. Windle, *Carbon* 36 (1998) 1603.
- [2.25] M.S. Dresselhaus, Y.M. Lin, O. Rabin A. Jorio, A.G. Souza Filho, M.A. Pimenta, R. Saito, Ge.G. Samsonidze, G. Dresselhaus, *Mater. Sci. Eng. C* 23 (2003) 129.
- [2.26] R. Saito, G. Dresselhaus, M.S. Dresselhaus, Imperial College Press, London, 1998.
- [2.27] E.T. Thostenson, Z. Ren, T.-W. Chou, *Compos. Sci. Technol.* 61 (2001) 1899.
- [2.28] C.T. Kingston, B. Simard, *Anal. Lett.* 36 (2003) 3119.
- [2.29] M. Terrones, *Int. Mater. Rev.* 49 (2004) 325.
- [2.30] C. Journet, W.K. Maser, P. Berinier, A. Loiseau, M. Lamy de la Chapelle, A. Lefrant P. Deniard, R. Lee, J.E. Fischer, *Nature* 388 (1997) 756.
- [2.31] M. Endo K. Takeuci, K. Kobori H.W. Kroto, A. Sarkar, *Carbon* 33 (1995) 873.
- [2.32] A.G. Rinzler, J. Liu, H. Dai, P. Nikolaev, C.B. Huffman, F.J. Rodriguez-Macias, P.J. Boul, A.H. Lu, D. Heymann, D.T. Colbert, R.S. Lee, J.E. Fischer, A.M. Rao, P.C. Eklund, R.E. Smalley, *Appl. Phys. A* 67 (1998) 29.

- [2.33] P. Nikolaev, M.J. Bronikowski, R.K. Bradley, F. Rohmund, D.T. Colbert, K.A. Smith, R.E. Smalley, *Chem. Phys. Lett.* 313 (1999) 91.
- [2.34] K. Donaldson, R. Aitken, L. Tran, V. Stone, R. Duffin, G. Forrester, et al. *Tox Sciences*, 92 1 (2006) 5.
- [2.35] J. Giles, *Nature*, 441 (2006) 26.
- [2.36] A. Moisala, A.G. Nasibulin, E.I. Kauppinen, *J Phys: Condens. Matter.* 15 (2003) 3011.
- [2.37] B. Shelimov, R.O. Esenaliev, A.G. Rinzler, *Chem Phys Lett.* 282 5 (1998) 429.
- [2.38] H. Shimoda, L. Fleming, K. Horton, *Physica B* 323 1-4 (2002) 135.
- [2.39] M. Yudasaka, M. Zhang, C. Jabs, *Appl Phys A* 71 4 (2000) 449.
- [2.40] M. Holzinger, A. Hirsch, P. Bernier, *Appl Phys A* 70 5 (2000) 599.
- [2.41] T. Abatemarco, J. Stickel, J. Belfort, *J Phys Chem B* 103 18 (1999) 3534.
- [2.42] Y. Sato, T. Ogawa, K. Motomiya, *J Phys Chem B* 105 (2001) 3387.
- [2.43] D. Chattopadhyay, I.Galeska, F. Papadimitrakopoulos, *Carbon* 40 (2002) 985.
- [2.44] I.W. Chiang, B.E. Brinson, R.E. Smalley, J.L. Margrave, H.R. Hauge, *J. Phys. Chem. B.* 105 (2001) 1157.
- [2.45] S. Niyogi, H. Hu, M.A. Hamon, P. Bhowmik, B. Zhao, S.M. Rozenshak, J. Chen, M.E. Itkis, M.S. Meier, R.C. Haddon, *J. Am. Chem. Soc.* 123 (2001) 733.
- [2.46] B. Zhao, H. Hu, S. Niyogi, M.E. Itkis, M.A. Hamon, P. Bhowmik, M.S. Meier, R.C.Haddon, *J. Am. Chem. Soc.* 123 (2001) 11673.
- [2.47] G.S. Duesberg, M. Burghard, J. Munster, G. Philip, S. Roth, *Chem. Commun.* (1998) 435.
- [2.48] S.K. Doorn, R.E. Fields III, H. Hu, M.A. Hamon, R.C. Haddon, J.P. Selegue, V. Majidi, *J. Am. Chem. Soc.* 124 (2002) 3169.
- [2.49] L. Thien-Nga, K. Hernadi, E. Ljubovic, S. Garaj, L. Forro, *Nano Lett.* 2 (2002) 1349.
- [2.50] G.S. Duesberg, S. Roth, P. Downes, A. Minett, R. Graupner, L. Ley, N. Nicoloso, *Chem. Mater.* 15 (2003) 3314.
- [2.51] F. Rancan, S. Rosan, F. Boehm, A. Cantrell, M. Brellreich, H. Schoenberger, et al., *J Photoch Photobio. B* 67 3 (2002) 157.
- [2.52] J. N. Coleman, U. Khan, W. J. Blau, Y. K. Gun'ko, *Carbon* 44 (2006) 1624.
- [2.53] J. N. Coleman, U. Khan, Y. K. Gun'ko, *Adv. Mater.* 18 (2006) 689.
- [2.54] P. Singh, S. Campidelli, S. Giordani, D. Bonifazi, A. Bianco, M. Prato, *Chem. Soc. Rev.* 38 (2009) 2214.
- [2.55] P. Liu, *Eur. Polym. J.* 41 (2005) 2693.
- [2.56] D. Baskaran, J. W. Mays, M. S. Bratcher, *Chem. Mater.* 17 (2005) 3389.
- [2.57] A. Hirsch, *Angew. Chem. Int. Ed.* 41 (2002) 1853.
- [2.58] S. Bredeau, S. Peeterbroeck, D. Bonduel, M. Alexandre, P. Dubois, *Polym.Int.* 57 (2008) 547.
- [2.59] P.M. Ajayan, O. Stephan, C. Colliex, D. Trauth, *Science* 265 (1994) 1212.
- [2.60] L. Jin, C. Bower, O. Zhou, *Appl Phys Lett* 73 (1998) 1197.
- [2.61] M.S.P. Shaffer, A.H. Windle, *Adv Mater* 11 (1999) 937.
- [2.62] H. Geng, R. Rosen, B. Zheng, H. Shimoda, L. Fleming, J. Liu et al., *Adv. Mater.* 14 (2002) 1387.
- [2.63] B. Safadi, R. Andrews, E.A. Grulke, *J Appl .Polym. Sci.* 84 (2002) 2660.
- [2.64] F. Du, J.E. Fischer, K.I. Winey, *J Polym. Sci. B.* 41 (2003) 3333.
- [2.65] N. Pierard, A. Fonseca, Z. Konya, I. Willems, G. van Tendeloo, J.B. Nagy, *Chem. Phys. Lett.* 335 (2001) 1.
- [2.66] H. Xia, Q. Wang, K. Li, G.H. Hu, *J Appl .Polym. Sci.* 93 (2004) 378.
- [2.67] S.Ghose, K.A. Watson, K.J. Sun, J.M. Criss, E.J. Siochi, J.W. Connell, *Compos. Sci. Technol.* 66 (2006) 1995.
- [2.68] Z. Jin, K.P. Pramoda, G. Xu, S.H. Goh, *Chem. Phys. Lett.* 337 (2001) 43.
- [2.69] P. Pötschke, S. Dudkin, I. Alig, *Polymer* 44 (2003) 5023.
- [2.70] P. Pötschke, M. Abdel-Goad, I. Alig, S. Dudkin, D. Lellinger, *Polymer* 45 (2004) 8863.
- [2.71] J. Fan, M. Wan, D. Zhu, B. Chang, Z. Pan, S. Xie, *J Appl. Polym. Sci.* 74 (1999) 2605.
- [2.72] B.Z. Tang, H. Xu, *Macromolecules* 32 (1999) 2569.
- [2.73] C. Downs, J. Nugent, P.M. Ajayan, D.J. Duquette, K.S.V. Santhanam, *Adv. Mater* 11 (1999) 1028.

- [2.74] G.Z. Chen, M.S.P. Shaffer, D. Coleby, G. Dixon, W. Zhou, D.J. Fray DJ, et al. *Adv. Mater.* 12 (2000) 522.
- [2.75] T. Kimura, H. Ago, M. Tobita, S. Ohshima, M. Kyotani, M. Yumura, *Adv. Mater.* 14 (2002) 1380.
- [2.76] E.S. Choi, J.S. Brooks, D.L. Eaton, M.S. Al-Haik, M.Y. Hussaini, H. Garmestani et al. *J. App. Phys.* 94 (2003) 6034.
- [2.77] C.A. Martin, J. Sandler, A.H. Windle, M. Schwarz, W. Bauhofer, K. Schulte et al. *Polymer* 46 (2005) 877.
- [2.78] C.H. Liu, H. Huang, Y. Wu, S.S. Fan, *Appl. Phys. Lett.* 84 (2004) 4248.
- [2.79] F.H. Gojny, M. Wichmann, U. Kopke, B. Fiedler, K. Schulte, *Compos. Sci. Technol.* 64 (2004) 2363.
- [2.80] L. Aguil, P. Yanez-Sedeno, J.M. Pingarron, *Anal. Chim. Acta.* 622 (2008) 11.
- [2.81] C.B. Jacobs, M.J. Peairs, B.J. Venton, *Anal. Chim. Acta.* 662 (2010) 105.
- [2.82] J.H.T. Luong, K.B. Male, S. Hrapovic, *Recent Adv. Biotechnol.* 1 (2007) 181.
- [2.83] A. Merkoci, *Microchim. Acta.* 74 (2006) 152.
- [2.84] G.A. Rivas, M.D. Rubianes, M.C. Rodríguez, N.F. Ferreyra, G.L. Luque, M.L. Pedano, et al., *Talanta* 74 (2007) 291.
- [2.85] M. Trojanowicz, *Trends Anal. Chem.* 25 (2006) 480.
- [2.86] P.J. Britto, K.S.V. Santhanam, P.M. Ajayan, *Bioelectrochem. Bioenerg.* 41 (1996) 121.
- [2.87] F. Valentini, A. Amine, S. Orlanducci, M.L. Terranova, G. Palleschi, *Anal. Chem.* 75 (2003) 5413.
- [2.88] M. Musameh, J. Wang, A. Merkoci, Y. Lin, *Electrochem. Commun.* 4 (2002) 743.
- [2.89] G. Liu, S.L. Riechers, M.C. Mellen, Y. Lin, *Electrochem. Commun.* 7 (2005) 1163.
- [2.90] J. Wang, M. Li, Z. Shi, N. Li, Z. Gu, *Electroanalysis* 14 (2002) 225.
- [2.91] J. Wang, M. Li, Z. Shi, N. Li, Z. Gu, *Electrochim. Acta* 47 (2001) 651.
- [2.92] W. Huang, W. Hu, J. Song, *Talanta* 61 (2003) 411.
- [2.93] X.N. Cao, L. Lin, Y.Y. Zhou, G.Y. Shi, W. Zhang, K. Yamamoto, L.T. Jin, *Talanta* 60 (2003) 106.
- [2.94] H. Luo, Z. Shi, N. Li, Z. Gu, Q. Zhuang, *Anal. Chem.* 73 (2001) 915.
- [2.95] F.H. Wu, G.C. Zhao, X.W. Wei, *Electrochem. Commun.* 4 (2002) 690.
- [2.96] J. Wang, M. Li, Z. Shi, N. Li, Z. Gu, *Anal. Chem.* 74 (2002) 1993.
- [2.97] Z. Wang, Y. Wang, G. Luo, *Electroanalysis* 15 (2003) 1129.
- [2.98] Y.D. Zhao, W.D. Zhang, H. Chen, Q.M. Luo, *Sens. Actuators B* 92 (2003) 279.
- [2.99] Y.D. Zhao, W.D. Zhang, H. Chen, Q.M. Luo, *Talanta* 58 (2002) 529.
- [2.100] J.S. Ye, Y. Wen, W.D. Zhang, L.M. Gan, G.Q. Xu, F.S. Sheu, *Electrochem. Commun.* 6 (2004) 66.
- [2.101] J. Liang, Y. wang, G. Luo, Z. Wang, *J. Electroanal. Chem.* 540 (2003) 129.
- [2.102] J. Wang, S.B. Hocevar, B. Ogorevc, *Electrochem. Commun.* 6 (2004) 176.
- [2.103] J. Wang, M. Li, Z. Shi, N. Li, Z. Gu, *Microchem. J.* 73 (2002) 325.
- [2.104] L. Zhu, J. Zhai, R. Yang, C. Tian, L. Guo, *Biosens. Bioelectron.* 22 (2007) 2768.
- [2.105] M. Pumera, A. Merkoci, S. Alegret, *Sensors and Actuators B* 113 (2006) 617.
- [2.106] M.D. Rubianes, G.A. Rivas, *Electrochem. Comm.* 5 (2003) 689.
- [2.107] J.R. Siqueira, L.H.S. Gasparotto, O.N. Oliviera, V. Zucolotto, *J. Phys. Chem. C.* 112 (2008) 9050.
- [2.108] A. Salimi, C.E. Banks, R.G. Compton, *Analyst* 129 (2004) 225.
- [2.109] M. Tominaga, S. Nomura, I. Taniguchi, *Biosens. Bioelectron.* 24 (2009) 1184.
- [2.110] J. Tkac, J.W. Whittaker, T. Ruzgas, *Biosens. Bioelectron.* 22 (2007) 1820.
- [2.111] P. Yang, Q. Zhao, Z. Gu, Q. Zhuang, *Electroanal.* 16 (2004) 97.
- [2.112] S. Roy, H. Vedala, W. Choi, *Nanotech.* 17 (2006) S14.
- [2.113] A.A. Ensafi, H. Karimi-Maleh, *J. Electroanal. Chem.* 640 (2010) 75.
- [2.114] A. Heller, B. Feldman, *Chem Rev.* 108 (2008) 2482.
- [2.115] J. Wang, *Chem. Rev.* 108 (2008) 814.
- [2.116] R.T. Kachosangi, M.M. Musameh, I.A. Yousef, J.M. Yousef, S.M. Kanan, L. Xiao, S.G. Davies, A. Russell, R.G. Compton, *Anal. Chem.* 81 (2009) 435.
- [2.117] B. Wu, G. Zhang, Y. Zhang, S. Shuang, M.M.F. Choi, *Anal. Biochem.* 340 (2005) 181.
- [2.118] V. Serafin, L. Agui, P.Y. Sedeno, J.M. Pingarron, *Electroanalysis* 21 (2009) 1527.
- [2.119] B. Wu, S. Hou, M. Yu, X. Qin, S. Li, Q. Chen, *Mater. Sci. Eng. C* 29 (2009) 346.
- [2.120] D. Ragupathy, A.I. Gopalan, K. Lee, *Electrochem. Commun.* 11 (2009) 397.

-
- [2.121] S. Wang, L. Lu, M. Yang, Y. Lei, G. Shen, R. Yu, *Anal. Chim. Acta* 651 (2009) 220.
 - [2.122] R.B. Rakhi, K. Sethupathi, S. Ramaprabhu, *J. Phys. Chem. B* 113 (2009) 3190.
 - [2.123] D. Wen, X. Zou, Y. Liu, L. Shang, S. Dong, *Talanta* 79 (2009) 1233.
 - [2.124] S. Deng, G. Jian, J. Lei, Z. Hub, H. Ju, *Biosens. Bioelectron.* 25 (2009) 373.
 - [2.125] C. Xiao, X. Chu, B. Wu, H. Pang, X. Zhang, J. Chen, *Talanta* 80 (2010) 1719.
 - [2.126] M. Gao, L. M. Dai, G. G. Wallace, *Electroanalysis* 15 (2003) 1089.
 - [2.127] Y.C. Tsai, J.-D. Huang, C.-C. Chiu, *Biosens. Bioelectron.* 22 (2007) 3051.
 - [2.128] K. Kerman, M. Kobayashi, E. Tamiya, *Meas. Sci. Technol.* 15 2 (2004) R1.
 - [2.129] T.G. Drummond, M.G. Hill, J.K. Barton, *Nat. Biotechnol.* 21 10 (2003) 1192.
 - [2.130] J. Wang, *Anal. Chim. Acta.* 469 1 (2002) 63.
 - [2.131] J.J. Gooding, *Electroanalysis*, 14 17 (2002) 1149.
 - [2.132] J. Wang, T. Tangkuaram, S. Loyprasert, T. Vazquez-Alvarez, W. Veerasai, P. Kanatharana et al., *Anal. Chim. Acta* 581 (2007) 1.
 - [2.133] F. Qu, M. Yang, Y. Lu, G. Shen, R. Yu, *Anal. Bioanal. Chem.* 386 (2006) 228.
 - [2.134] N. Li, R. Yuan, Y. Chai, S. Chen, H. An, *Bioprocess Biosyst Eng.* 31 (2008) 551.
 - [2.135] J.P. Kim, B.Y. Lee, J. Lee, S. Hong, S.J. Sim, *Biosens. Bioelectron.* 24 (2009) 3372.
 - [2.136] S. Viswanathan, C. Rani, A.V. Anand, J.A.A. Ho, *Biosens. Bioelectron.* 24 (2009) 1984.
 - [2.137] B.S. Munge, C.E. Krause, R. Malhotra, V. Patel, J.S. Gutkind, J.F. Rusling, *Electrochem. Commun.* 11 (2009) 1009.
 - [2.138] J.H.T. Luong, S. Hrapovic, D.S. Wang, *Electroanalytical* 17 (2005) 47.
 - [2.139] J.F. Rochette, E. Sacher, M. Meunier, J.H.T. Luong, *Anal. Biochem.* 336 (2005) 305.
 - [2.140] A. D. Maynard, *Ann. Occup. Hyg.* 51 (2007) 1.
 - [2.141] A. D. Maynard, R. J. Aitken, T. Butz, V. Colvin, K. Donaldson, G. Oberdorster, M. A. Philbert, J. Ryan, A. Seaton, V. Stone, S. S. Tinkle, L. Tran, N. J. Walker, D. B. Warheit, *Nature* 444 (2006) 267.
 - [2.142] A. D. Maynard, P. A. Baron, M. Foley, A. A. Shvedova, E. R. Kisin, V. Castranova, J. Toxicol. Environ. Health A 67 (2004) 87.
 - [2.143] H. J. Johnston, G. R. Hutchison, F. M. Christensen, S. Peters, S. Hankin, K. Aschberger, V. Stone, *Nanotoxicology* 4 (2010) 207.

CHAPTER 3

ELECTROCHEMICAL TECHNIQUES IN SENSOR APPLICATIONS

'The more we know, the faster we can know more'. (Mickio Kaku)

Summary

This chapter discusses the use of voltammetric techniques in analytical chemistry. These methods are highly appealing to the analytical chemist owing to their high sensitivity, low cost, simplicity of instrumentation, and ease of implementation. Furthermore, voltammetric techniques offer the possibility to determine the analyte concentration directly in the sample without pretreatment or chemical separation, as well as to analyze colored materials and samples with dispersed solid particles [3.1-3.3].

3.1 Cyclic voltammetry (CV)

Cyclic voltammetry (CV) is a very versatile electrochemical technique which allows probing the mechanics of redox and transport properties of a system in solution. This technique provides rapid information on the thermodynamic redox processes, on the kinetics of heterogeneous electron-transfer reactions, and on coupled chemical reactions or adsorption processes. This is accomplished with a three-electrode arrangement whereby the potential relative to some reference electrode is scanned at a working electrode, while the resulting current flowing through a counter (or auxiliary) electrode is monitored in a supporting electrolyte. The technique is ideally suited for a quick search of redox couples present in a system, and once located a redox couple may be characterized by more careful analysis of the cyclic voltammogram. More precisely, the controlling electronics is designed such that the potential between the reference and the working electrode can be adjusted, but the big impedance between these two electrodes effectively forces any resulting current to flow through the counter electrode. Usually the potential is scanned back and forth linearly with time between two extreme values using a triangular potential waveform (Figure 3.1.). When the potential of the working electrode is more positive than that of a redox couple present in the solution, the corresponding species may be oxidized (i.e. electrons going from the solution to the electrode) and produce an anodic current. Similarly, on the return scan, as the electrode potential of the working electrode is more positive than that of a redox couple, reduction (i.e. electrons flowing away from the electrode) may occur to cause a cathodic current. By 'International Union of Pure and Applied Chemistry' (IUPAC) convention, anodic currents are positive and cathodic currents negative [3.4].

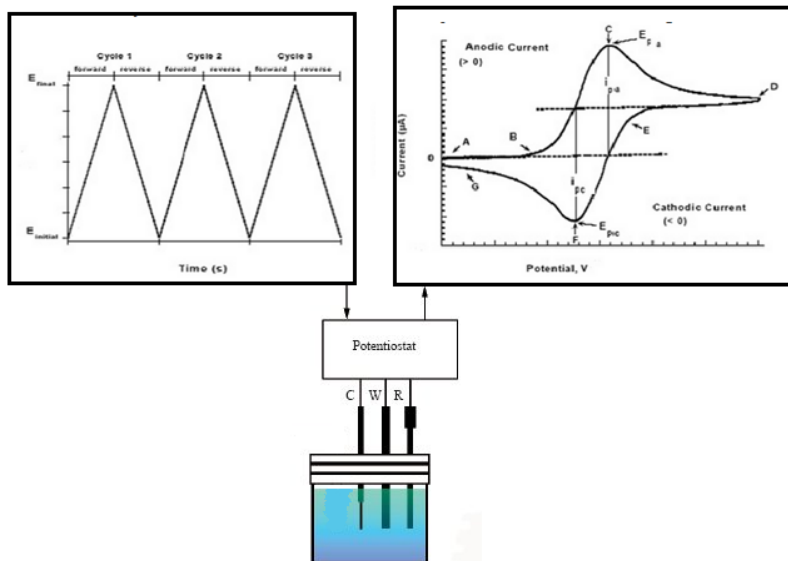


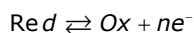
Figure 3.1 CV potential waveform with switching potentials (left), and the expected response of a reversible redox couple during a single-potential cycle (right), connected with the experimental CV set-up: counter electrode (CE), working electrode (WE), and reference electrode (RE) in an electrochemical cell.

The magnitude of the observed faradaic current can provide information on the overall rates of the many processes occurring at the working electrode surface. As is the case for any multi-step process, the overall rate is determined by the slowest step.

For a redox reaction induced at a working electrode, the rate determining step may be any one of the following individual steps depending on the system, i.e.,

- rate of mass transport of the electro-active species
- rate of adsorption or de-sorption at the electrode surface
- rate of the electron transfer between the electro-active species and the electrode, or rates of the individual chemical reactions which are part of the overall reaction scheme.

For the oxidation reaction involving n electrons:



The Nernst Equation gives the relationship between the potential and the concentrations of the oxidized and reduced forms of the redox couple at equilibrium (at 298 K)

$$E = E^{0'} + \frac{0.059}{n} \log_{10} \frac{[\text{Ox}]}{[\text{Red}]} \quad (3.1)$$

Where E is the applied potential, $E^{o'}$ is the formal reduction potential, O_x and Red are the surface concentrations at the electrode/aqueous electrolyte interface, and n is the number of electrons involved in the redox reaction.

Note that the Nernst equation may or may not be valid depending on the system or on the experimental conditions.

A typical voltammogram is shown in Figure 3.1. The scan shown starts at a slightly negative potential, (A) up to some positive switching value, (D) at which the scan is reversed back to the starting potential. The current is first observed to the peak at E_{pa} (with value i_{pa}) indicating that an oxidation is taking place and then drops due to depletion of the reducing species from the diffusion layer. During the return scan the processes are reversed (reduction is now occurring) and a peak current is observed at E_{pc} (corresponding value, i_{pc}).

3.1.1 Reversible System

Providing that the charge-transfer reaction is reversible, and that there is no surface interaction between the electrode and the reagents, and that the redox products are stable (at least in the time frame of the experiment) the ratio of the reverse and the forward current $i_{pr} / i_{pf} = 1.0$ (in Figure 3.1 $i_{pa} = i_{pf}$ and $i_{pc} = i_{pr}$). In addition, for such a system it can be shown that

- the corresponding peak potentials E_{pa} and E_{pc} are independent of scan rate and concentration
- the formal reduction potential for a reversible couple $E^{o'}$ is centered between anodic and cathodic peak potentials, i.e.,

$$E^{o'} = \frac{E_{pa} + E_{pc}}{2} \quad (3.2)$$

- the peak separation ΔE_p for a reversible couple is given by

$$\Delta E_p = E_{pa} - E_{pc} = \frac{0.059}{n} \quad (3.3)$$

at all scan rates. However, the measured value for a reversible process is generally higher due to uncompensated solution resistance and non-linear diffusion. Larger values of ΔE_p , which increase with increasing scan rate, are characteristic of slow electron transfer kinetics.

To distinguish between reversible (diffusion-controlled) and irreversible (charge-transfer controlled) kinetics of an electrode process the potential scan-rate is used as a diagnostic tool – the rate of reagent transport is proportional to the square root of the scan-rate. Thus in one experimental set a shift in reversibility might be executed and analysis of ΔE_p vs. $v^{1/2}$ gives information on reversibility and applicability of further calculations.

In simple terms, the working electrode may be regarded as a "reagent" of adjustable oxidizing or reducing strength. However, this is a purely conceptual image. In fact, the electrochemical processes are occurring at the interface of two different phases, the electrode and the electro-active species in solution. In other words, the processes under studies are heterogeneous in nature.

For the electron transfer to occur, the molecules in solution have to approach the electrode. In a cyclic voltammetry experiment, the solution is kept unstirred and in this situation, mass transport can occur only by diffusion due to concentration gradients created around the electrode surface. Such concentration-distance profiles at different steps of a cyclic voltammogram scan are illustrated in Figure 3.2. The magnitude of the observed signal will be very much a function of the diffusion properties of the system. Intuitively, the current intensity (i.e. the flow of electrons) is expected to depend on the surface area of the working electrode and the concentration of the electro-active species. Also, one can expect the voltage scanning rate to affect the concentration profile around the electrode which itself directly affects the rate of charge transport, and for this matter the diffusion coefficient appears explicitly. The expression of the peak current (A) for the forward sweep in a reversible system at 298 K is given by the Randles-Sevcik equation,

$$I_{pf} = (2.69 \times 10^5) n^{3/2} A D^{1/2} C^* \nu^{1/2} \quad (3.4)$$

Where n is the number of electrons involved in the redox process, A is the active area of the working electrode (cm^2), D is the diffusion coefficient ($\text{cm}^2 \text{s}^{-1}$), C^* is the bulk concentration of the electroactive species (mol cm^{-3}), and ν is the potential scan rate (V s^{-1}).

In the present experiment, the dependence of I_{pf} on scan rate and concentration will be examined.

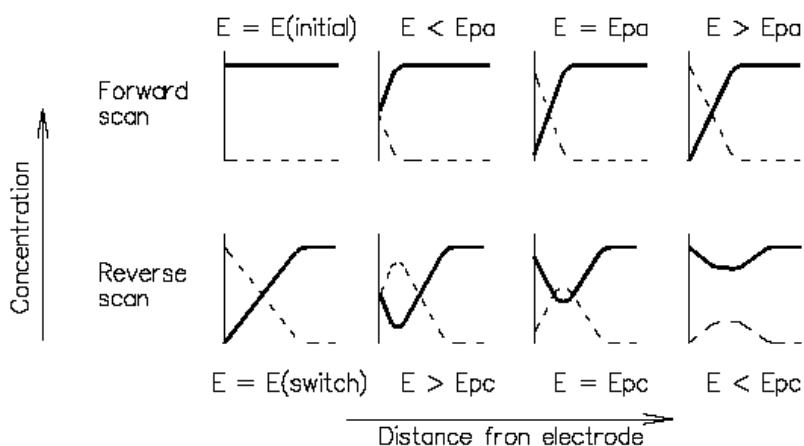


Figure 3.2 Qualitative diagrams showing concentration-distance profiles at various stages of the cyclic voltammograms. The solid lines correspond to the reducing species and the dotted lines to the oxidizing species.

A similar indicator of reversible electron transfer is called the current function, whose value is given by $(i_p/\nu^{1/2})$. The current function should be constant for all scan rates for which the electron transfer is fast enough to maintain the equilibrium ratio between the reduced and the oxidized forms of the redox couple predicted by the Nernst equation.

At this point, it is instructive to note that when describing electrochemical reversibility, it is important to consider not only the value of k° (standard rate constant), but the scan rate for which Nernstian equilibrium cannot be maintained at the electrode surface. At these scan rates, the observed voltammetry will display characteristics of quasireversible or irreversible behavior, such as the spreading out of voltammetric peaks over wider potential ranges, decreased peak currents, and increased values for ΔE_p^2 .

3.1.2 Irreversible and Quasi-reversible Systems

For irreversible processes (those with sluggish electron exchange), the individual peaks are reduced in size and are widely separated. Totally irreversible systems are characterized by a shift of the peak potential with the scan rate [3.4]

$$E_p = E^\circ - \frac{RT}{\alpha n_a F} \left[0.78 - \ln \frac{k^\circ}{D^{1/2}} + \ln \left(\frac{\alpha n_a F v}{RT} \right)^{1/2} \right] \quad (3.5)$$

Where α is the transfer coefficient, and n_a is the number of electrons involved in the charge-transfer step. Thus, E_p occurs at potentials higher than E° , with the overpotential related to k° (standard rate constant) and α . Independent of the value k° , such peak displacement can be compensated by an appropriate change of the scan rate. The peak potential and the half-peak potential (at 25°C) will differ by $48/\alpha n$ mV. Hence, the voltammogram becomes more drawn-out as αn decreases.

The peak current, given by [3.4]

$$i_p = (2.99 \times 10^5) n (\alpha n_a)^{1/2} A C^* D^{1/2} v^{1/2} \quad (3.6)$$

is still proportional to the bulk concentration, but will be lower in height (depending upon the value of v). Assuming a value of 0.5, the ratio of the reversible-to-irreversible current peaks is 1.27 (i.e. the peak current for the irreversible process is about 80% of the peak for a reversible one). For quasi-reversible systems the current is controlled by both the charge transfer and mass transport. The shape of the cyclic voltammogram is a function of $k^\circ / \sqrt{\pi a D}$ (where $a = nFv / RT$). As $k^\circ / \sqrt{\pi a D}$ increases, the process approaches the reversible case. For small values of it, the system exhibits an irreversible behavior. Overall, the voltammograms of a quasi-reversible system are more drawn out and exhibit a larger separation in peak potentials compared to a reversible system.

3.2 Differential-Pulse Voltammetry (DPV)

Differential-pulse voltammetry is a very important technique in chemical analysis and is based on its superior elimination of the capacitive/background current. This is achieved by sampling the current twice: once before pulse

application and then at the end of the pulse. The current sampling is indicated by filled circles in Figure 3.3.

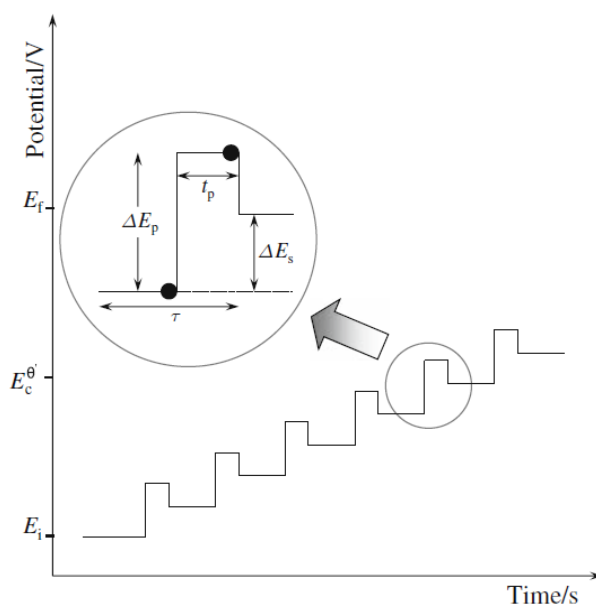


Figure 3.3 Potential diagram for DPV

The system of this measurement is usually the same as that of standard voltammetry. The potential between the working electrode and the reference electrode is changed as a pulse from an initial potential to an interlevel potential and remains at the interlevel potential for about 5 to 100 milliseconds; then it changes to the final potential, which is different from the initial potential. The pulse is repeated, changing the final potential and a constant difference is kept between the initial and the interlevel potential. The values of the currents between the working electrode and auxiliary electrode before and after the pulse are sampled and their differences are plotted versus potential.

The DPV technique can be used to study the redox properties of extremely small amounts of chemicals because of the following features,

- the effect of the charging current can be minimized, so high sensitivity is achieved
- Faradaic current is extracted, so electrode reactions can be analyzed more precisely.

The main characteristics of DPV are

- reversible reactions show symmetrical peaks and irreversible reactions show asymmetrical peaks
- the detection limit is about 10^{-8} M.

3.3 Square-Wave Voltammetry (SWV)

Square-wave voltammetry (SWV) is one of the fastest pulse techniques that can be applied in both electrokinetic and analytic measurements. In square-wave voltammetry, a square-wave is superimposed on the potential staircase sweep. Oxidation or reduction of species is registered as a peak or trough in the current signal at the potential at which the species begins to be oxidized or reduced. In staircase voltammetry the potential sweep is a series of stair steps (Figure 3.4). The current is measured at the end of each potential change, right before the next, so that the contribution to the current signal from the capacitive charging current is minimized. The differential current is then plotted as a function of potential, and the reduction or oxidation of species is measured as a peak or trough. Due to the lesser contribution of capacitive charging currents the detection limits for SWV are on the order of nanomolar concentrations. The major advantage of the square-wave voltammetry is its speed.

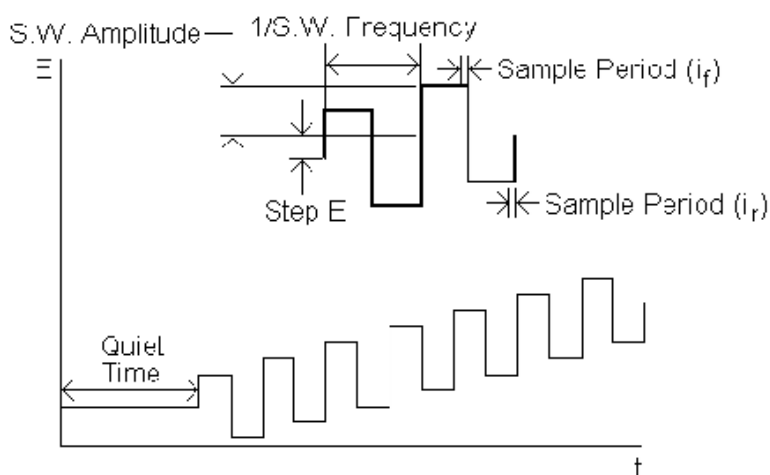


Figure 3.4 Square-wave form showing the amplitude of SWV

3.4 Chronoamperometry (CA)

Chronoamperometry (CA) is an electrochemical technique in which the potential of the working electrode is stepped and the resulting current from Faradic processes occurring at the electrode (caused by the potential step) is monitored as a function of time. A stationary working electrode and unstirred solution are used. The resulting current-time dependence is monitored.

Chronoamperometry is often used for measuring the diffusion coefficient of electroactive species or the surface area of the working electrode. It can also be applied to study the mechanisms of the electrode processes.

3.5 Pulsed amperometric detection (PAD)

Johnson and coworkers [3.5, 3.6] were the first to introduce pulsed amperometric detection as an electroanalytical technique (PAD) using platinum electrodes. They used it for the detection of alcohols, formic acid, and cyanide in flow-injection systems [3.7]. Later, Johnson and other researchers also developed PAD methods for amino acids, aldehydes, carbohydrates, sulfite, and sulfide [3.8-3.10]. Following the first reports [3.5, 3.6], a number of interesting and important articles appeared in the literature discussing different aspects and applications of the triple-pulse waveform or pulsed amperometric detection (PAD) [3.11-3.19].

Pulsed amperometric detection (PAD) is an excellent method for quantitative detection of numerous organic compounds that adsorb at noble metal electrodes but cannot be detected satisfactorily by conventional amperometry at constant applied (dc) potential. PAD relies on repeated applications of a multiple-pulse (mostly triple pulse) waveform consisting of regeneration/ detection, oxidation and reduction potentials. The last two of those three steps are designed for electrode cleaning. The first of the three steps usually combines regeneration of the electrode surface with a short period of signal acquisition by integration of currents resulting from the detection enabling electrode reaction. The second step should remove all reaction products and the third step restores the oxidation state of the electrode surface for the detection enabling electrode reaction of analytes of interest. Many different waveforms have been reported for the detection with platinum electrodes.

Figure 3.5 presents a schematic diagram of PAD waveform.

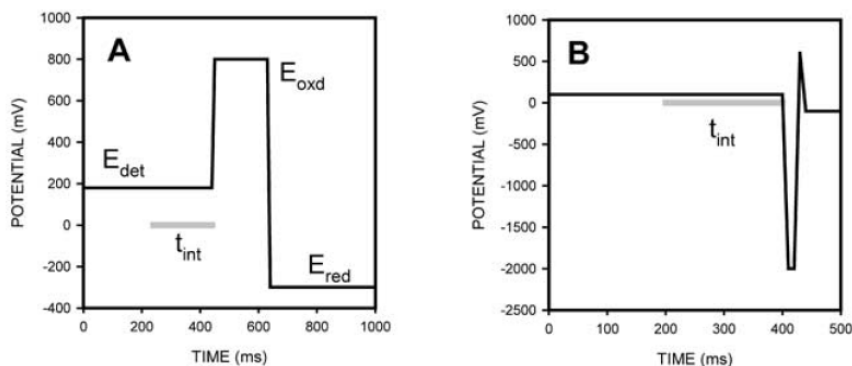


Figure 3.5 Schematic of the PAD waveform

3.6 References

- [3.1] L. Codognoto, S.A.S. Machado, L.A. Avaca, *Diam. Relat. Mater.* 11 (2002) 1670.
- [3.2] V.A. Pedrosa, L. Codognoto, L.A. Avaca, *Quim. Nova* 26 (2003) 844.
- [3.3] D. Souza, S.A.S. Machado, L.A. Avaca, *Quim. Nova* 26 (2003) 81.
- [3.4] J. Wang, *Analytical Electrochemistry*, Third Edition, Wiley-VCH, 2006, pp 29-35.
- [3.5] S. Hughes, P. L. Meschi, D. C. Johnson, *Anal. Chim. Acta* 132 (1981) 1.
- [3.6] S. Hughes, D. C. Johnson, *Anal. Chim. Acta* 132 (1981) 11.
- [3.7] J.A. Polta, D.C. Johnson, *Anal. Chem.* 57 (1985) 1373.
- [3.8] D.S. Austin, J.A. Polta, T.Z. Polta, A.P.-C. Tang, T.D. Cabelka, D.C. Johnson, *J. Electroanal. Chem.* 168 (1984) 227.
- [3.9] D.C. Johnson, D. Dobberpuhl, R. Roberts, P. Vandeberg, *J. Chromatogr.* 640 (1993) 79.
- [3.10] J. Cheng, P. Jandik, X. Liu, C. Pohl, *J. Electroanal. Chem.* 608 (2007) 117.
- [3.11] S. Hughes, D. C. Johnson, *J. Agric. Food Chem.* 30 (1982) 712.
- [3.12] S. Hughes, D. C. Johnson, *Anal. Chim. Acta* 149 (1983) 1.
- [3.13] G. G. Neuburger, D. C. Johnson, *Anal. Chem.* 59 (1987) 150.
- [3.14] W. R. LaCourse, W. R., Johnson, D. C., *Carbohydr. Res.* 215 (1991) 159.
- [3.15] D. C. Johnson, W. R. LaCourse, *Electroanalysis* 4 (1992) 367.
- [3.16] R. E. Roberts, D. C. Johnson, *Electroanalysis* 6 (1994) 269.
- [3.17] R. D. Rocklin, T. R. Tullsen, M. G. Marucco, *J. Chromatogr. A.* 671 (1994) 109.
- [3.18] R. E. Roberts, D. C. Johnson, *Electroanalysis* 7 (1995) 1015.
- [3.19] J. Wen, R. M. Cassidy, A. S. Baranski, *J. Chromatogr. A* 811 (1998) 181.

CHAPTER 4

SCOPE AND THESIS OBJECTIVES

"The scientist is not a person who gives the right answers, he's one who asks the right questions". (Claude Levi-Strauss)

Given the importance of the improvement of the quality of life, which is associated with the state of environment, health and food safety control, the most research and numerous organizations are considering the potential application of nanoscience and green nanotechnologies to solve technical challenges associated with environment and health monitoring. Technology developers and others claim that these nanomaterials and nanotechnologies offer more effective, efficient, durable, and affordable approaches to build smart sensors characterized by multiple applications, i.e., environment, life and health.

In this context, the electroanalysis and its applications have experienced a large extent and development in recent years. The development of electroanalysis application is dependent direct on both the electrode materials and the fundamental aspects regarding the use of classical electroanalytical techniques, and elaboration of new techniques.

Suitable technologies for achieving elaboration and characterization of certain electrode materials that represent the electroanalytical performance key are being required. Widespread attention has been focused on the aspects regarding electrode composition and structure, selectivity, sensitivity, feasibility, lifetime. Moreover, these technologies have to be able to miniaturize sensor for batch and flow injection detection experiments, and in-situ detection.

Based on our previous research results regarding the electroanalysis using zeolite modified/unmodified carbon-based composite electrodes and taking into account the superior properties of multi-walled carbon nanotubes, i.e., surface area, capacity of analyte storage, electrocatalytic activity for a wide range of compounds, possibility of electrodes miniaturization, and ultrasensitive microelectrode arrays behavior, the general objective of this study is to elaborate new and nano-structured carbon-based composite electrodes with enhanced electroanalytical performance. In addition, a new class of highly porous materials referred to as metal-organic framework (MOF) materials which offer many application potentials especially in sensing and catalysis, will be used for electrode modification to improve its electrochemical and electrocatalytic properties. This research aims to the development of new composite electrodes-based on multi-walled carbon nanotubes characterized by microelectrodes array behavior for detection of trace analytes of interest in environmental monitoring, and also, with applications in other fields, i.e., medical, pharmaceutical, and food.

The main objectives of this research have been the following:

- Elaboration of some composite electrode materials based on multi-walled carbon nanotubes and modified with metal-organic framework (MOF) materials, characterized by useful properties for the quantitative evaluation of selected organic compounds,
- Structural, morphological, and electrical characterization of the composite materials,

- Evaluation of the electrochemical behavior of the electrode materials in the presence of target analytes,
- The evaluation of the electrode materials behavior in different supporting electrolytes and in the presence of the target analytes, which allows to establish the relationships between obtained electrode material and oxidation reaction type of organics (direct, indirect, electrochemical mediated oxidation),
- Detection experiments performance, which provides information regarding amperometric/voltammetric detection, detection potential value, concentration ranges, electrode sensitivity, stability, reproducibility and lifetime, detection limits, calibration,
- Testing of the composite electrodes for selective / simultaneous detection of analytes in aqueous solutions,
- Assessment of the electrochemical detection methods accuracy by their comparison with the conventional methods,
- Testing of noninvasive detection methods in clinical, pharmaceutical and food products analysis.

Two types of composite electrodes were synthesized and characterized with focus on their use for detection of the analytes, i.e.

-multi-walled carbon nanotube-epoxy composite electrodes with an optimum multi-wall carbon nanotubes loading synthesized by a two-roll mill method

- Copper benzene tricarboxylate (metal-organic framework-MOF)-modified-multi-walled carbon nanotubes-epoxy composite-electrode were synthesized, also by the two-roll mill method.

To achieve the general objectives, several specific objectives have been considered:

- Assessment of dispersion degree of multi-walled carbon nanotubes in different types of solvents and epoxy matrix,
- Synthesis of new multi-walled carbon nanotubes-epoxy composites
- Synthesis of new composites multi-walled carbon nanotubes modified with metal-organic framework (copper benzene tricarboxylate, called HKUST) in epoxy matrix,
- Structural and morphological characterization of composites by SEM/EDAX, Raman spectroscopy,
- DC electrical characterization of composite materials by the four-point probe method,
- Composition optimization of the composite materials,
- Obtaining of new electrodes based on the selected composites,
- Comparative electrochemical characterization of electrode materials in different supporting electrolytes and in the presence of target analytes by cyclic voltammetry (CV),
- Identification and selection of optimal conditions for composite electrode material types with microelectrodes array behavior,
- Achievement of individual amperometric / voltammetric detection experiments by using cyclic voltammetry (CV), differential-pulse voltammetry (DPV), square-wave voltammetry (SWV), chronoamperometry (CA), and multiple-pulsed amperometry (MPA),
- Preconcentration / detection scheme development based on the sorption property of the composite electrode to improve the electroanalytical performance,
- Multiple- pulse amperometry characteristics exploitation to enhance also the detection of the electroanalytical performances,

- Exploitation of the microelectrodes array advantage for analyte detection in the absence of supporting electrolyte,
- Assessment of the selective and / or simultaneous detection for certain analytes. Establishing of the electroanalytical performances detection,
- Testing of obtained sensors for non-invasive quantitative evaluation of some compounds of interest in medicine, pharmacy, and food products.

Several target analytes have been selected for the assessment of the electroanalytical performance of the new synthesized composite electrodes, i.e.,

Pentachlorophenol (PCP) has been included in the list of Persistent Organic Pollutants (POPs) and is the most toxic representative of the chlorophenols and also an important organic chemical for environmental studies because of its widespread application in industry, agriculture, and commercial product formation and preservation. Pentachlorophenol is found in all environmental media (air, soil, and water) as a result of its past widespread use. PCP concentrations in drinking water are usually in the range of 0.01–0.1 µg/L (World Health Organization, 1987).

Salicylic acid (SA) is of one of the drugs most widely used in the world as a pain reliever and anti-inflammatory medicine, but banned from veterinary therapeutic treatment. Salicylic acid is, therefore, monitored in the urine and blood of animals to be slaughtered.

Acetylsalicylic acid (ASA) known as aspirin, is a pharmaceutical product with anti-inflammatory, analgesic, and antipyretic qualities. ASA is widely used in curing fever and headache caused by cold and is also to some extent effective in Alzheimer's disease, cardiovascular disease, and cancer.

The determination of **glucose** concentration is extremely important clinically in the diagnosis and treatment of diabetes, but also is important in areas such as biotechnology and food industry.

In their complexity, current performances and potential applications are very promising, opened both to fundamental research, technology, and application synchronous with acute and major contemporary issues, including the preparation and processing of last generation materials, i.e., carbon nanotubes and metal-organic framework materials. More detailed knowledge about the correlations between materials parameters, i.e., their chemical composition and dimension, and behavior of electrode materials as amperometric/voltammetric sensor can pave the way to the optimization and to establish a new dimension of both the electrochemical techniques and the environmental life and health quality control. No doubt, the field of electroanalysis using modified nano-structured carbon based-electrodes will experience a development beyond pioneer applications, and a better understanding of the fundamentals associated with the electrochemical oxidation processes and detections will be achieved. Also, these fundamental electrochemical aspects represent the basis for the development of a new class of nano-structured carbon-based composite sensors with multiple applications, i.e., environment, life, health.

CHAPTER 5

PREPARATION AND CHARACTERIZATION OF MODIFIED/UNMODIFIED MWCNT-EPOXY COMPOSITE ELECTRODES

„A pretty experiment is in itself often more valuable than twenty formulae extracted from our minds. (Albert Einstein)

Summary

This chapter presents details related to the experimental part of the thesis including protocols and devices used. Firstly, a list of materials and reagents is described. Secondly, the preparation and characterization of the electrodes is presented in detail, starting from the dispersion of CNTs, processing technique, and finishing with the electrical measurements. Finally, the aim of this chapter is to supply a complete protocol that can be reproduced and therefore be used in practice for future research.

5.1 Introduction

Epoxy resin-based CNT composites have been extensively investigated due to the potential that these materials have in a number of industrial/technological applications. Effective utilization of nanotubes in epoxy resin composites with regard to enhancement of mechanical properties and electrical conductivity depends primarily on the ability to disperse the nanotubes homogeneously throughout the polymer matrix and tailor the interfacial interactions between the components of the composite. However, homogeneous dispersion of CNTs is difficult due to the intermolecular van der Waals interactions between the nanotubes, thus resulting in the formation of aggregates. This problem presents a major challenge in the field of CNT composites.

CNTs are usually supplied in highly entangled bundles, making handling and dispersion during composite processing a formidable hurdle. To optimize CNT composites, one must maintain high CNT aspect ratios, orient the CNTs, enhance interfacial interactions between nanotubes and epoxy resin, and eliminate slippage between the CNTs in ropes or between the nanotubes and epoxy resin.

N,N-dimethylformamide (DMF) is the most extensively used polar solvent and more than half of the papers deal with CNT-based electrochemical sensors using DMF as the dispersing solvent [5.1]-[5.14]. There are also some other solvents used to prepare CNT suspensions, including water [5.15]-[5.21], acetone [5.22]-[5.26], ethanol [5.27]-[5.29] and even toluene [5.30], [5.31]. However, compared with these solvents, DMF has some overwhelming advantages for dispersing CNTs, for example, much higher stability and exfoliation efficiency.

For CNT-epoxy resin composites, the high-power dispersion methods, such as ultrasonication and high-speed shearing, are the simplest and most convenient to improve the dispersion of CNTs in a polymer matrix. By taking advantage of the

multi-effects of ultrasound, the aggregates and entanglements of CNTs can be effectively broken down. For example, Li et al. [5.32] used a simple solution-precipitation technique to improve the dispersion of CNTs in a polycarbonate solution by sonication at a frequency of 20 kHz for 10 min. They showed that the CNTs were uniformly dispersed in a polycarbonate matrix. In this case, the ultrasonic wave as well as mechanically stirring played important roles in the formation of the composites with a uniform distribution.

Qian et al. [5.33] also used a simple solution-evaporation method assisted by high-energy sonication to prepare polystyrene (PS)/MWCNT composite films, in which MWCNTs were dispersed homogeneously in the PS matrix. Similarly, Sandler et al. [5.34] dispersed CNTs in epoxy under high-speed stirring (2000 rpm) for 1 h, and proved that intense stirring was an effective process to achieve dispersed CNTs uniformly in epoxy. More recently Cho and co-workers successfully prepared polyurethane PU/MWNTs composites with better dispersion of CNTs up to 20 wt% in PU [5.35].

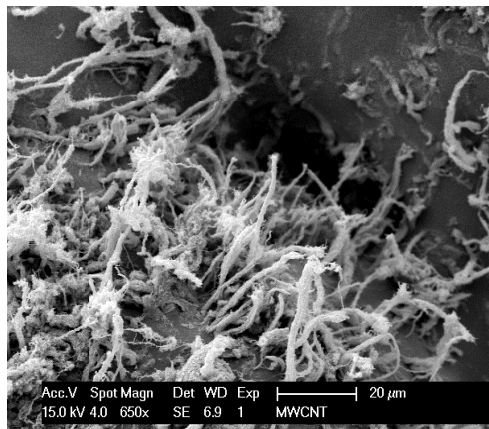
However, it is very important to note the fact that if the sonication treatment is too intensive and/or lasts too long, it can lead to local damage of the CNT walls, if not to CNT shortening [5.36], [5.37]. Local damage deteriorates both electrical and mechanical properties.

5.2 Experimental section

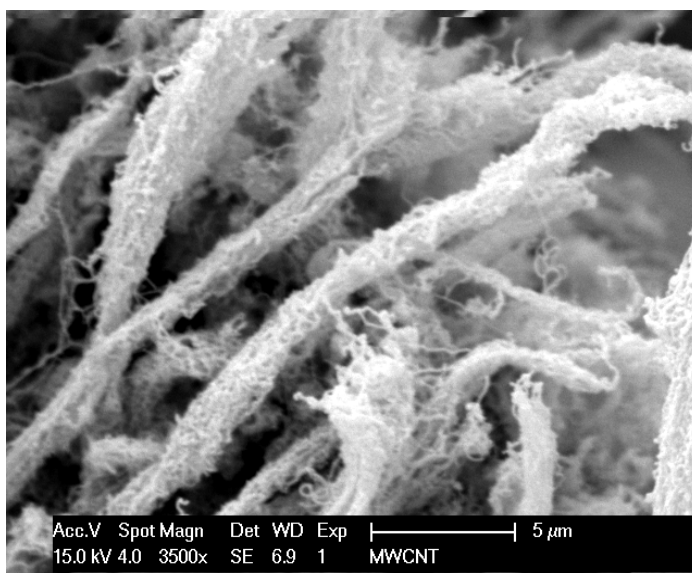
5.2.1 Materials and reagents

Multiwall carbon nanotubes (NC7000 with 90% purity; length 1.5 μm ; average diameter 9.5 nm and surface area around 250- 300 m^2/g , produced by catalytic carbon vapor deposition method (CCVD)) were supplied by Nanocyl, Belgium (Figure 5.1 a, b and c). The matrix system used was the epoxy resin Araldite®LY5052 and the curing agent Aradur®5052 manufactured by Huntsman Advanced Materials, Switzerland. The epoxy resin Araldite®LY5052 has relatively lower viscosity ($\eta_{25} = 1000\text{--}1500$ mPas).

a)



b)



c)

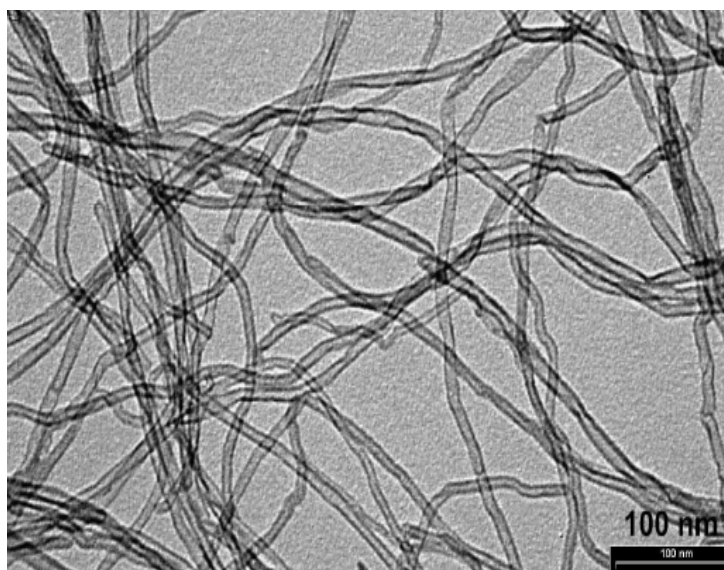


Figure 5.1 SEM images of (a-b) as-received MWCNTs, showing that nanotube bundles are highly entangled and (c) TEM image of as-received MWCNTs.

N,N-dimethylformamide or DMF ($\text{HCON}(\text{CH}_3)_2$, 99.8%), tetrahydrofuran or THF ($\text{C}_4\text{H}_8\text{O}$, 99.9%), ethanol ($\text{CH}_3\text{CH}_2\text{OH}$, 99.5%), toluene ($\text{C}_6\text{H}_5\text{CH}_3$, 99.8%),

acetone (CH_3COCH_3 , 99.9%), chloroform (CHCl_3 , 99%), were all purchased from Sigma-Aldrich BV and were used as solvents. The MWCNTs and all the reagents were used as received.

Synthetic crystalline micro and mesoporous materials, e.g. zeolites, have become one of the major areas of research during the last few decades. They find applications in many different fields such as catalysis, adsorption/separation/storage, electronics, health, semiconductor and food industry, detergents [5.38]. Several unique aspects of these structured materials are responsible for their success: they have a very high adsorption capacity, active sites of different strengths; the size of their channels and cavities is in the range of that of many molecules of interest, and many of them present excellent ion exchange capabilities and exciting electronic properties.

Metal Organic Frameworks (MOFs) are among the most sophisticated nano-structured solids. The combination of organic and inorganic building blocks offers an almost infinite number of combinations, enormous flexibility in pore size, shape and structure. They possess a wide range of pore size and pore volumes, and their chemical environment can be fine-tuned by selecting the appropriate building blocks [5.39]. Their porosity is much higher than that of their inorganic counterpart zeolites (up to 90%), justifying the designation 'framework'. Their thermostability is sometimes unexpectedly high, reaching temperatures above 400 °C. All these features make MOFs a special class of solids with the potential of transcending many common limitations in different technological disciplines, such as ferromagnetism [5.40], semiconductivity and gas separation [5.41], storage [5.42], sensing [5.43], catalysis [5.44], drug delivery [5.45] or proton conductivity [5.46].

Copper benzene tricarboxylate [$\text{Cu}_3(\text{BTC})_2$, BTC=1,3,5-benzenetricarboxylate] was one of the first reported MOF in 1999 and named HKUST-1 [5.47]. Since then, it has become one of the most studied MOFs. It is commonly prepared under hydrothermal conditions with a copper salt (usually nitrate) and 1,3,5-benzenetricarboxylic acid (BTC). The precursors are dissolved and mixed in mixtures ethanol (EtOH) and water, and finally heated up [5.47], [5.48], although synthesis at room temperature is possible. It was also the first MOF synthesized electrochemically [5.49].

This polymer forms face-centered-cubic crystals that contain an intersecting three-dimensional (3D) system of large square-shaped pores (9 Å by 9 Å). The pores themselves can contain up to 10 additional water molecules per formula unit. The material has a reasonable degree of thermal stability (up to 240°C) and a capacity for chemical functionalization of the channel linings. A view down the [100] direction of the cubic cell of HKUST-1 reveals 1-nm-size channels with fourfold symmetry (Figure 5.2). The nanochannels intersect to provide a 3D connected network of pores. A view through the cell body diagonal [111] reveals a honeycomb arrangement of large hexagonal-shaped windows of 18.6 Å diameters.

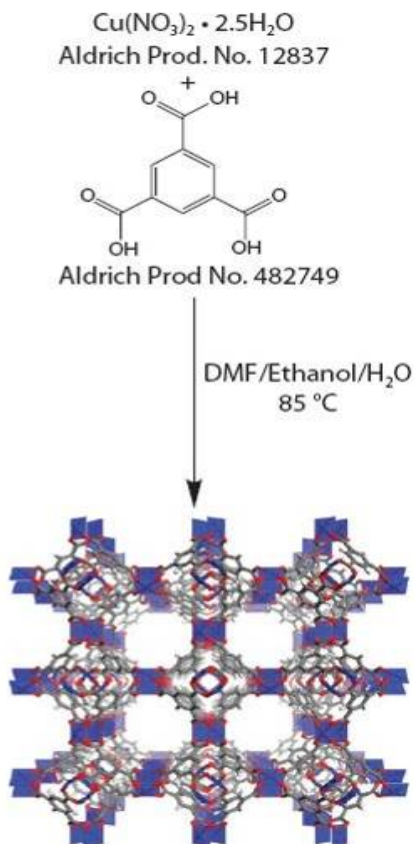


Figure 5.2 Synthesis of HKUST and view along the 100 direction of the cubic cell (picture from Sigma-Aldrich) [5.50]

The HKUST used in this study was synthesized by electrochemical methods [5.51]. 15 mmol (3.15g) of 1,3,5-benzenetricarboxylic acid (trimesic acid, BTC) and 33 mmol (1.038 g) Tributylmethylammonium methyl sulphate (MTBS) are dissolved in 100 mL 96 vol% ethanol (78.5g). The mixture is heated up to the 40 °C in an electrochemical cell with 2 copper electrodes at a distance of at least 3 cm. When the temperature is reached and with vigorously agitation, a current intensity of 5 mA /cm² is applied to the electrodes for 1 hour. The produced material is filtered off and cleaned with ethanol at room temperature overnight, then filtered again and dried at 100 °C.

The material obtained is analyzed by nitrogen (N₂) sorption analysis in order to obtain more information about their pore structure. N₂ sorption analysis was carried out in a Quantachrome Autosorb-6B. BET surface area is calculated over the range of relative pressures between 0.005 and 0.05. The pore volume is calculated as the uptake (cm³/g) at a relative pressure of 0.5. The sample was pretreated before measurement. It was outgassed under vacuum at a temperature of 473 K for 16 h. The analysis result can be observed in Figure 5.3. The isotherm is a type I, isotherm [5.52] typical for microporous materials. The calculated BET surface area

is 1600 m²/g (calculated between 0.02 and 0.10 P/P0), and a pore volume of 0.72 cm³/g (calculated at P/P0=0.5), which coincides with data reported in literature and theoretical calculations.

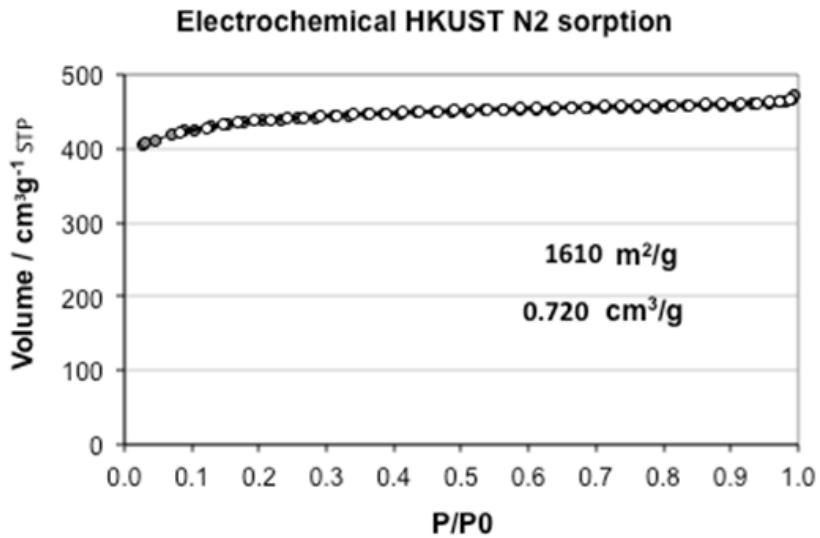


Figure 5.3 N2 sorption of the HKUST synthesized by electrochemical methods.

XRD analyses confirm the crystalline structure (Figure 5.4). The XRD analysis confirms a good fitting with the calculated XRD structure. Although it looks like there is a preferential growth in the direction 111 ($2\theta=13.5$), because of the lower intensity diffraction at directions 002 111 ($2\theta=7.8$) and 022 ($2\theta=11.0$).

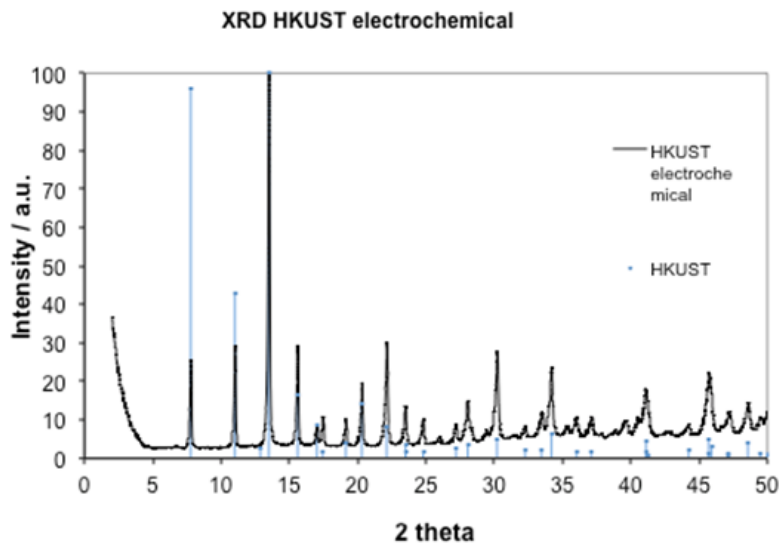


Figure 5.4 XRD analysis of electrochemical HKUST.

Nevertheless, SEM picture (Figure 5.5) show bipyramidal crystals with a broad size distribution, from cca. 500 nm up to several μm , with no preferential orientation.

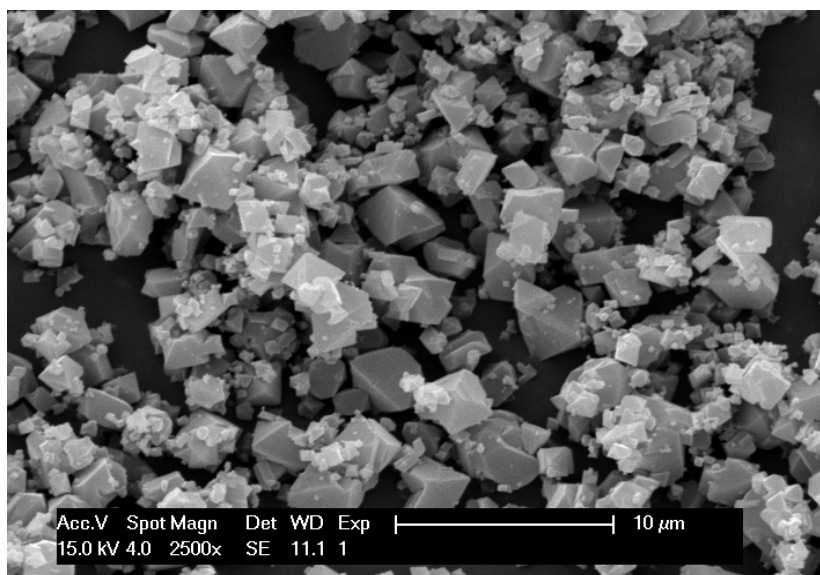


Figure 5.5 SEM image of the prepared HKUST (Cu-BTC) material.

5.2.2 Preparation of the composites

The MWCNT-Epoxy and the MWCNT-HKUST-Epoxy composite electrodes were obtained by an effective two-roll mill procedure (TRM). The ratios of the two electrodes were chosen to reach 25 wt% content of MWCNTs and 75 wt% content of epoxy resin for MWCNT-epoxy composite electrode, and 25 wt% content of MWCNTs, 25 wt% content of HKUST, and 50 wt% content of epoxy resin for MWCNT-HKUST-epoxy composite electrode, respectively.

In the first step MWCNTs without any further treatment were dispersed into THF by ultrasonication using a Cole-Parmer® 750-Watt Ultrasonic Processor for a specific period of time (10 min) to spread out the nanotubes. The second step in achieving a high level of dispersion was to mix the suspension and the liquid epoxy resin (without hardener). The mixture was left overnight in a vacuum oven at 60°C in order to evaporate the solvent. In the processing step the MWCNT-HKUST-Epoxy composite electrode was obtained by mixing the HKUST particles with the MWCNTs, and the batch was two-roll milled for several times on a laboratory scale two-row mill (Collin) at constant temperature of 70 °C and also at different times and shear intensities. Then the hardener was added and mixing was continued for an additional 10 min to ensure a uniform homogeneity. Finally, the resulting paste was poured into cylindrical PVC tubes, electrical contact was completed using a copper wire and these electrodes were cured in an oven at 80°C for 24 h, and subsequently left to cool down at room temperature for 24 hrs. The same procedure was applied for the MWCNT-Epoxy composite electrodes.

Figure 5.6 shows the schematic diagram for the MWCNT-epoxy composite preparation.

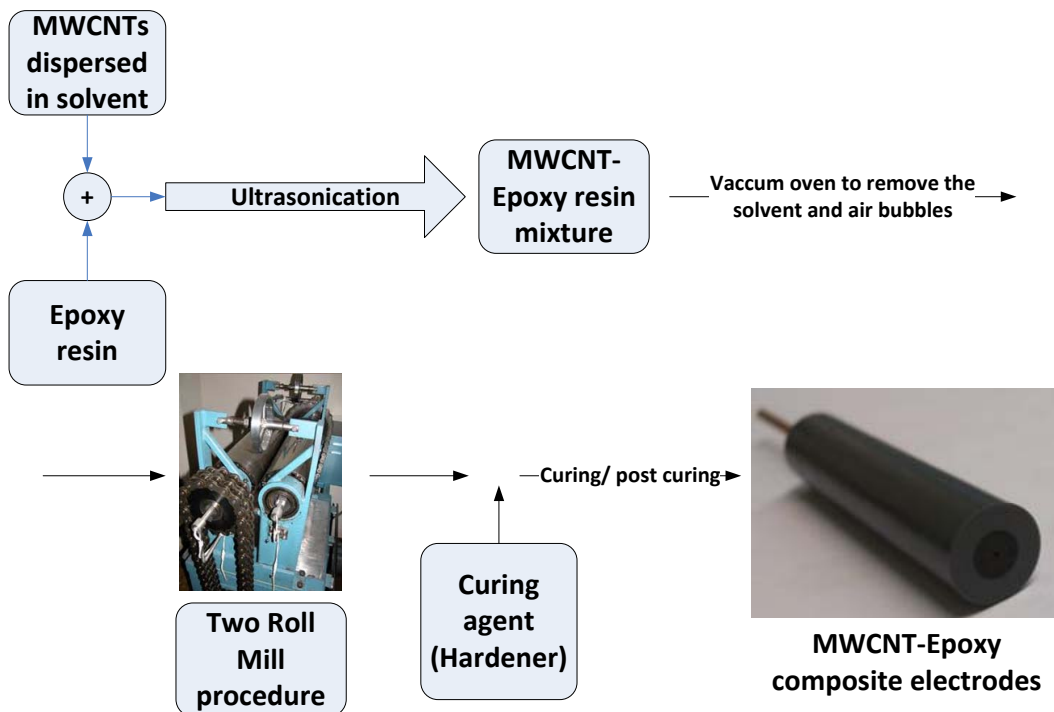


Figure 5.6 Schematic diagram of MWCNT-Epoxy composite electrodes preparation.

5.2.3 Characterization of the composites

Dispersion

Dynamic Light Scattering (DLS) and zetasizing measurements were performed on a Zetasizer Nano ZS from Malvern Instruments Limited, using the 173° angle non-invasive back-scatter mode and the M3-phase analysis light scattering mode, respectively. The instrument has a red 4.0 mW 633 He-Ne laser. The multiple peak high-resolution fitting procedure was used to obtain the particle size distribution from the auto-correlation function.

Scanning Electron Microscopy (SEM)

The SEM images were obtained using an XL20, Philips Scanning Electron Microscope, with an acceleration voltage of 15 kV. The samples could be investigated without gold-sputtering because of their good electrical conductivity.

Raman Spectroscopy

The Raman spectra were obtained using a Renishaw Raman Imaging Microscope, system 2000. The green ($\lambda=514$ nm) polarized radiation of an argon ion laser beam of 20 mW was used for excitation. A Leica DMLM optical microscope

with a Leica PL Floutar L500x/5 objective lens was used to determine the analyzed part of the sample. The focus (maximum opening at 100%) and power (10%) were carefully optimized in order to not alter the sample during the measurement.

The spectral resolution of the system was 2cm^{-1} , with an exposure time of 120 s.

Electrical conductivity

The electrical conductivity of MWCNTs-epoxy composites was determined by four-point probe contact (DC) conductivity measurements. All measurements were performed using a digital multimeter DMM2000 and a current source 6221 DC, both provided by Keithley. Silver paste was used as electrical contacts.

5.3 Results and discussion

5.3.1 Dispersion quality

Dynamic Light Scattering (DLS), also known as Photon Correlation Spectroscopy, is one of the most popular methods used to determine the length of CNTs in dispersion. Compared to microscopy techniques, DLS can use samples in solution, and provides an average measurement over a large number of CNTs. These types of measurements are very useful for the identification of the best solvent to process the composites, because they give a good indication of the level of aggregate dispersion of nanotubes in solution. However, the degree of dispersion in solution may not reflect the final dispersion within the polymer matrix.

To directly compare the dispersion stability of MWCNTs, Figure 5.7 presents photographs of MWCNTs (0.5 mg) solutions prepared in different types of solvents after 10 minutes of sonication.

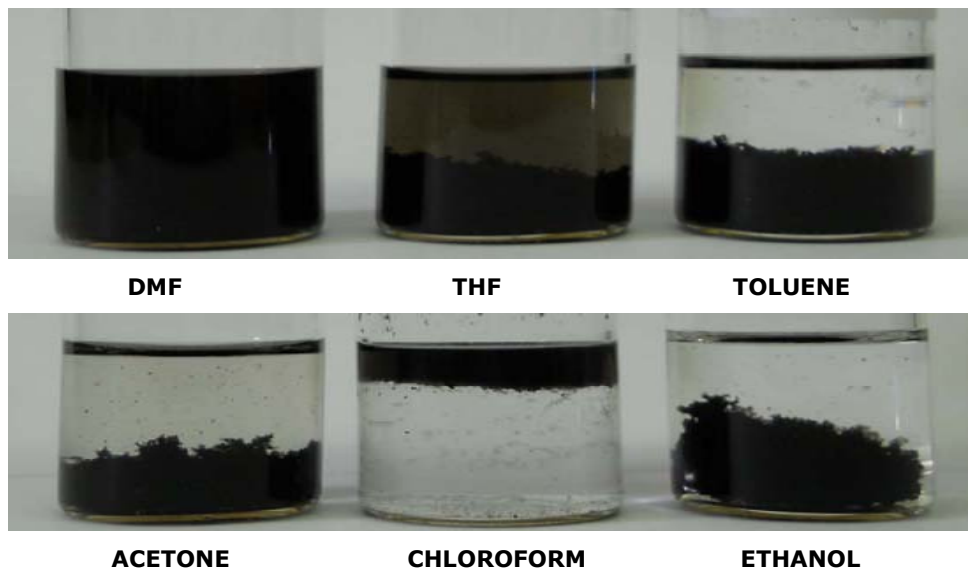


Figure 5.7 The optical images of MWCNTs dispersed in different types of solvents.

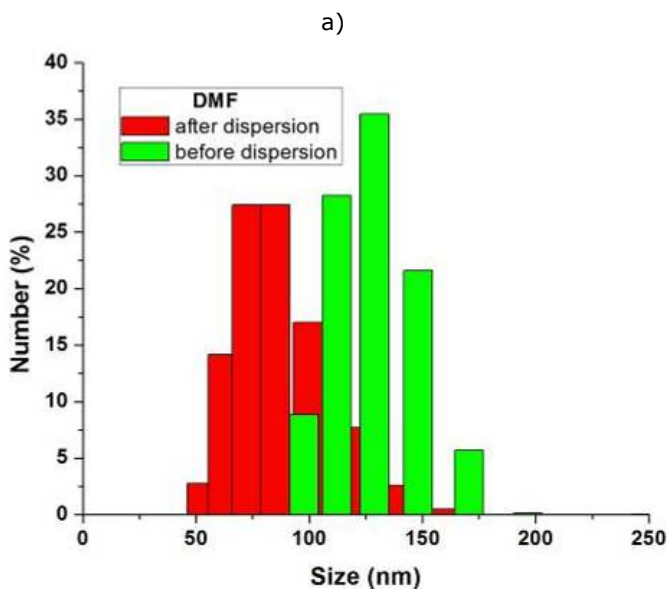
We have found that the MWCNTs dispersed in DMF were completely dispersed and there was no sediment observed at the bottom of the glass beaker. This can be explained by the presence of carboxyl groups, which are supposed to be directly attached to the walls of CNTs and also might contribute to improvement of the interfacial interaction, and the dispersion state. In the case of THF, MWCNTs were partially dispersed and a small amount of sediment is observed at the bottom of the glass beaker.

On the other hand, it can clearly be seen that the ultrasonication of MWNTs in toluene, acetone, chloroform and ethanol resulted in a poor degree of dispersion. The large MWCNT agglomerates indicate that the tightly entangled MWCNTs in the powder form have not been separated and they remained in the state of entanglements, moreover, most of the nanotubes are sedimenting.

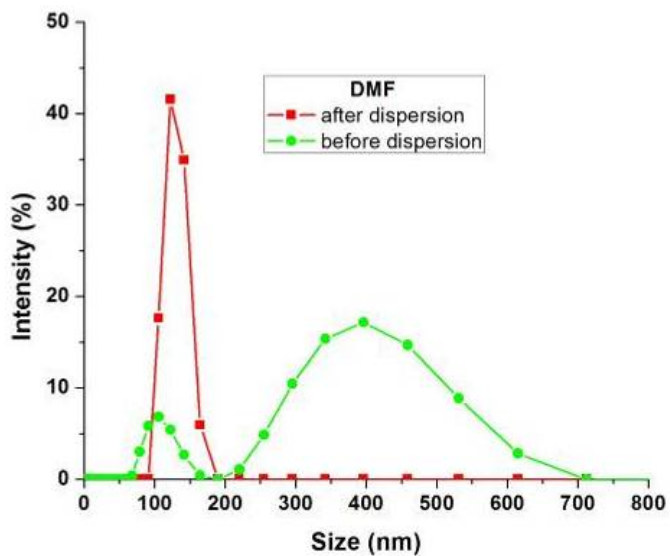
Considering that the boiling points of acetone, chloroform, THF, ethanol, toluene, and DMF are 56, 61.2, 66, 78, 110.6 and 130°C, respectively, it is reasonable that the easier the solvent can evaporate in the evaporation step, the less the solvent will remain to affect the curing reaction in processing step.

Even if MWCNTs are well dispersed in DMF, some problems will encounter in the evaporation process because of the high boiling point. Based on the above considerations, THF appeared to be better in this case, so it was decided to use only THF as solvent for nanotube dispersion for electrodes composite preparation.

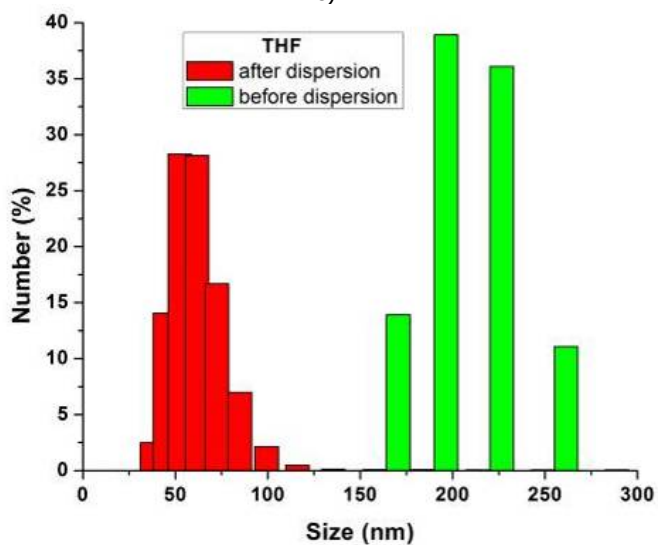
Figure 5.8 shows the histograms of MWCNTs agglomerate sizes measured by the particle size analyzer. The agglomerate size was measured before and after dispersion in DMF and THF solvents.



b)



c)



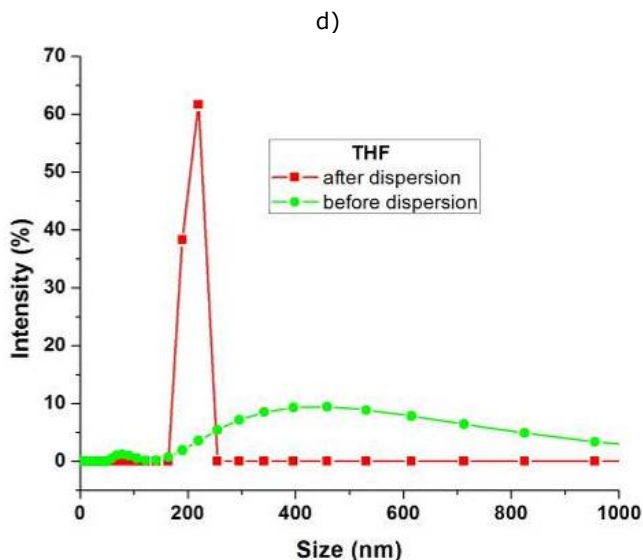


Figure 5.8 Number and intensity distribution of MWCNTs before/after dispersion in: (a-b) DMF and (c-d) THF.

When comparing the MWCNTs agglomerates before dispersion in DMF to those before dispersion in THF, the mean particle size is in the range 100-200 nm in DMF, and 150-250 nm in THF. After dispersion, the mean particle size showed more than 50% decrease in agglomeration of CNTs for both solvents, suggesting a uniform dispersion of CNTs by ultrasonication (Figure 5.8 (a and c)).

Also, from the intensity distribution graphs (Figure 5.8 (b and d)), it can be seen that the intensity lines are shifting to the left in comparison with non-dispersed CNTs, for which the intensity are higher for a wide size range (from 200 to 600 nm). These results prove that the average particle sizes were decreased by dispersion and MWCNTs agglomeration is avoided. The measurements did not show any good results for the dispersion of MWCNTs in acetone, toluene, ethanol, and chloroform.

In conclusion, two types of solvents were able to disperse MWCNTs, i.e., DMF and THF. Toluene, acetone, chloroform, and ethanol, were not suitable for MWCNTs dispersion, as they cause the particles to agglomerate just in a few minutes after the sonication process.

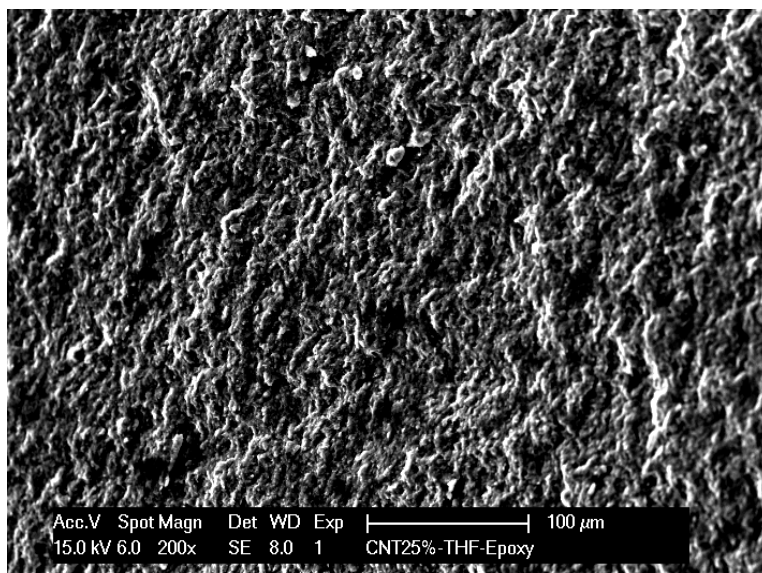
5.3.2 Morphological and structural characterization

5.3.2.1 Scanning Electron Microscopy (SEM)

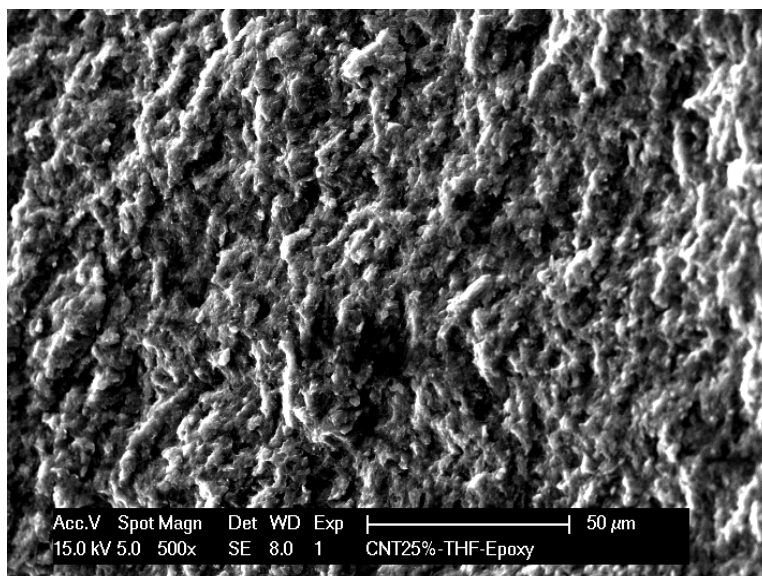
Morphological analyses are very important for the evaluation of the dispersion state, morphology, and structure of carbon nanotubes in the epoxy matrix. Figure 5.9 (a-c) shows a typical set of SEM micrographs of the MWCNT-Epoxy composite, while Figure 5.10 (a-c) shows a typical set of SEM micrographs of

the MWCNT-HKUST-Epoxy composite at different magnifications, showing the overall distribution of nanotubes and HKUST particles in the epoxy matrix.

a)



b)



c)

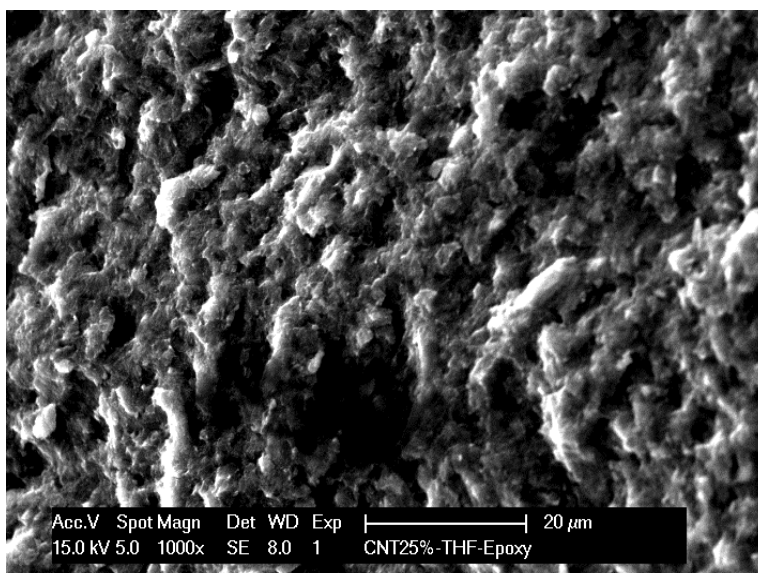
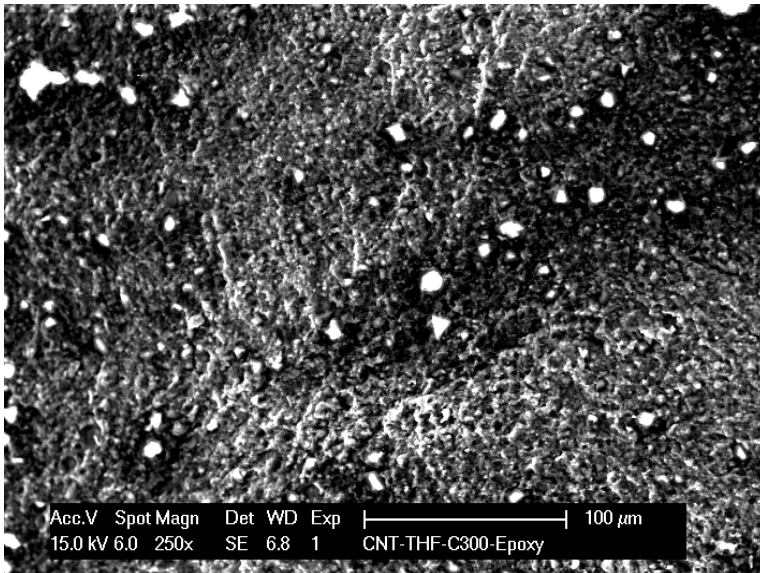


Figure 5.9 (a-c) SEM images of MWCNT-Epoxy composite electrode at different magnifications.

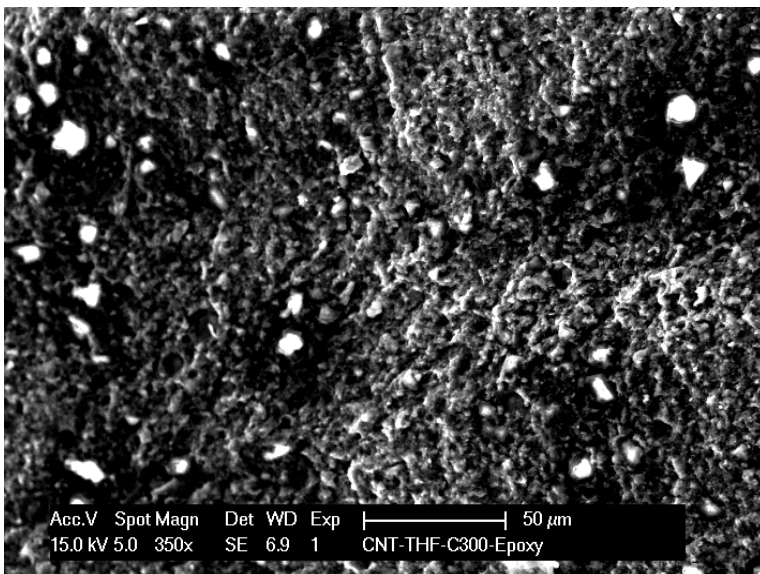
The SEM micrographs Figure 5.9 (a-c) of the MWCNT-Epoxy composite indicate that nanotubes are homogeneously dispersed and distributed within the polymer matrix without any signs of agglomeration. Furthermore, no CNT bundles are present.

The morphology of the MWCNT-HKUST-Epoxy composite is depicted in Figure 5.10 (a-c). It can be seen that the HKUST particles are coated almost homogeneously on the walls of carbon nanotubes. Loading of HKUST particles on MWCNT will provide a larger surface area for electrocatalytic reaction.

a)



b)



c)

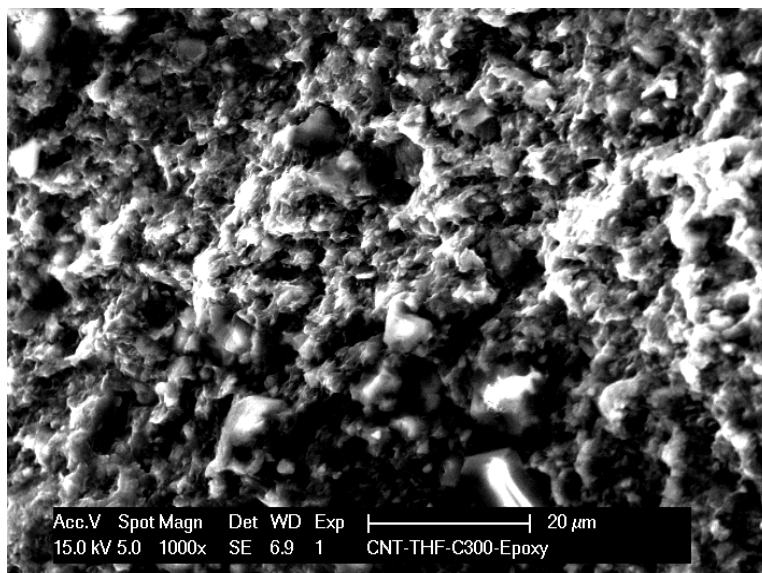


Figure 5.10 (a-c) SEM images of MWCNT-HKUST-Epoxy composite electrode at different magnifications.

5.3.2.2 Raman spectroscopy

Raman spectroscopy has been proved to be one of the most important techniques for the characterization of MWCNTs. For instance, this analytical technique may provide information on their diameter distribution [5.53]-[5.56], the state of aggregation of the CNTs [5.57], [5.58], or even their orientation [5.59]-[5.61]. In this study, Raman spectroscopy was used to further investigate the MWCNTs alignment and defects within the epoxy matrix.

Raman spectra of CNTs typically display four main characteristic features. The radial mode band (RMB 100–400 cm^{-1}), which is a unique characteristic of SWCNTs [5.62] and not generally observed for MWCNTs. Two other Raman bands are the *D* band (disorder band) located between 1300–1370 cm^{-1} , and the *G* band (graphite band or TM-tangential mode), which appears in the region around 1580–1600 cm^{-1} . As shown in Figure 5.11, the *D* band at around 1345 cm^{-1} and the *G* band at around 1582 cm^{-1} were clearly observed for both as-received MWCNT and MWCNT-Epoxy. The *D* band originates from the sp^2 hybridized (graphite-like carbon atoms) disorder in the graphitic structure, and is the most sensitive Raman peak to the nanotube alignment. The *G* band, assigned to the in-plane vibration of the graphitic wall, is less sensitive to orientation [5.63]. Another Raman band in the spectrum of CNTs, is the *D*^{*}-band, which represents the overtone of the disorder and it is located at $\sim 2600 \text{ cm}^{-1}$.

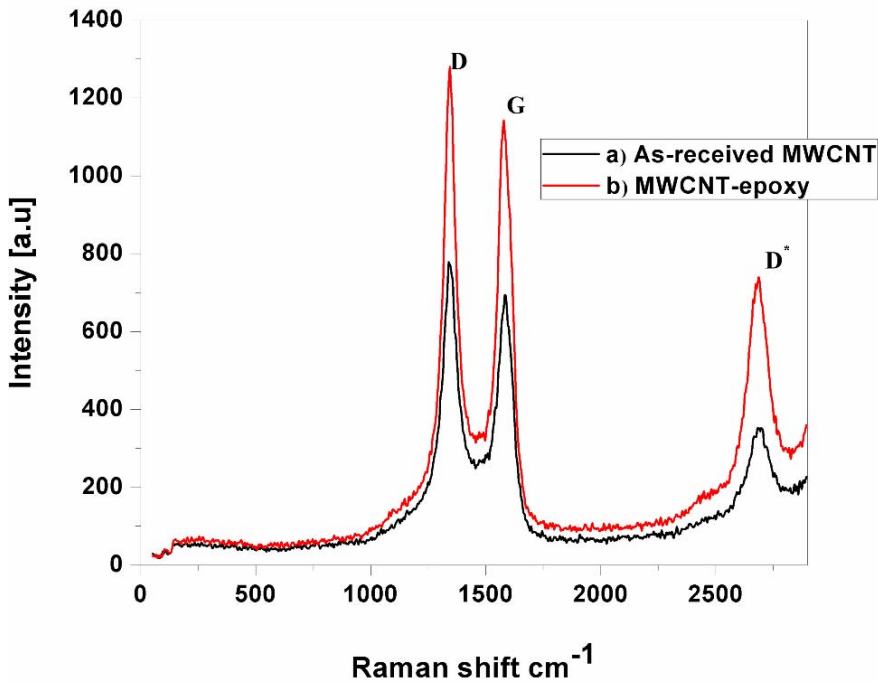


Figure 5.11 Raman spectra of: (a) as received MWCNTs and (b) MWCNT-Epoxy.

Comparing the spectra of as-received MWCNT and MWCNT-Epoxy, we found that the shapes and intensities of the D and G bands, respectively, are not different. Therefore, epoxy resin has no effect on the nanotube alignment.

Furthermore, the value of the intensity ratios of the D and G bands (I_D/I_G) is indicative of the degree of disorder of the MWCNTs structure. The degree of disorder of the MWCNTs can also be expressed by the intensity ratio of the D* and G bands. An increase in I_D/I_G or decrease in I_{D^*}/I_G indicates higher defect concentrations, or a higher degree of disorder. The Raman data analysis results are presented in Table 5.1

Table 5.1 Raman data analysis results

Samples	I_D/I_G	I_{D^*}/I_G
As-received MWCNTs	1.12	0.50
MWCNT-epoxy	1.11	0.64

It was found that for as-received MWCNTs the I_D/I_G ratio value is 1.12 and for MWCNT-Epoxy the I_D/I_G ratio value is 1.11, indicating that there is no significant increase of defects or breakage cause by the sonication process in nanotubes structure.

5.3.2.3 Electrical conductivity

The electrical conductivity of a composite is strongly dependent on the filler loading and there is often a percolation threshold concentration beyond which electrical conductivity occurs. At low filler concentrations, the conductivity remains very close to the conductivity of the pure, electrically insulating polymer matrix since the fillers are dispersed individually or are present as small clusters in the matrix. Above the percolation threshold concentration, independent fillers tend to link together to form conductive networks. This leads to a significant increase in the electrical conductivity of the composite.

Several parameters, such as the choice of polymer, the aspect ratio of the filler [5.64], [5.65], the matrix/filler and the filler/filler interaction [5.66], the degree of orientation of the filler [5.67], [5.68] all affect the percolation threshold. In addition, the processing technique [5.69], mixing stresses applied during preparation, as well as the shaping procedure play very important roles. Very diverse percolation thresholds for CNT-based composites have been reported by various research groups—from 0.0025 wt% for CNT/epoxy composites up to 11 wt% for SWNT/poly(3-octylthiophene) composites [5.70].

The percolation threshold is a basic characteristic of a conductive composite, and describes the behavior of conductive polymer composites. Their σ_{DC} at and beyond the percolation threshold (p_c) are generally described by a power law relationship, Eq.1 [5.71], [5.72]

$$\sigma_{DC} = \sigma_0(p - p_c)^t, \text{ for } p > p_c \quad (5.1)$$

Where σ_{DC} is the electrical conductivity of the composites, σ_0 is the electrical conductivity of the MWCNTs itself, p is the volume fraction of filler, p_c is the percolation threshold, i.e., the critical volume fraction to form a conductive network, t is the conductivity exponent, which generally reflects the dimensionality of the system, and $p - p_c$ is known as the reduced mass.

This power law is supposed to be universal [5.73], implying that the value of the critical exponent t primarily depends on the dimensionality of the percolating system and not on the details of the geometric structure of the interaction. For a three-dimensional filler network, t is theoretically equal to 2 [5.73], [5.74]-[5.77]. Even if a power law is very often evidenced in experimental results, t values found for conductive fibers such as carbon black or CNTs dispersed in polymers are most of the time different from this expected value of 2 [5.71], [5.78]-[5.81]. Several reasons can account for such a divergence between theoretical and experimental results and between experimental results themselves. The first possible sources of divergence are purely practical, and linked to the way of analysis of the experimental data [5.82]. In this way, the choice of the critical region above the experimental threshold, inside which the power law is expected to hold, differs from one experimental series of experiments to another one. It has even been suggested [5.82] that this region is so narrow that the t values experimentally determined have actually no reason to fit the universal value. Secondly, most of the theoretical models based on percolation theory mainly emphasize the geometrical effects of the filler network formation, hardly taking into consideration the morphology and the type of fillers, as well as thermodynamic effects, such as possible interactions between fillers, or between fillers and matrix [5.66], [5.77]. In particular, most

theoretical models are based on the assumption that the arrangement of conductive filler particles in the matrix is perfectly random and homogeneous, which is rarely the case in 'real' systems. Thirdly, the presence of a thin polymer layer of finite conductance between the filler particles, which prevents direct contact between them, generates an inter-particle distance distribution that is specific for the conditions of preparation of the composite [5.77], [5.83]-[5.84]. This interparticle polymer layer plays a role in determining the transport mechanism taking place in the composite. In classical percolation theory, the global connectivity of the network presupposes simultaneous geometrical and electrical connectivity associated with the bonding of "adjacent" elements of the system. In the case of nearest range hopping or tunneling, the main contribution of the electron transfer is the one occurring between "nearest" neighbors, implying that geometrical and electrical connectivities are concomitant [5.83]. Experimental values of 0.7–3.1 for t have been reported [5.81].

Figure 5.12 shows the dependence of electrical conductivity versus MWCNT weight percent. To investigate the electrical properties of the MWCNT-Epoxy composite electrode, the percolation curve was constructed by varying the MWCNT loading.

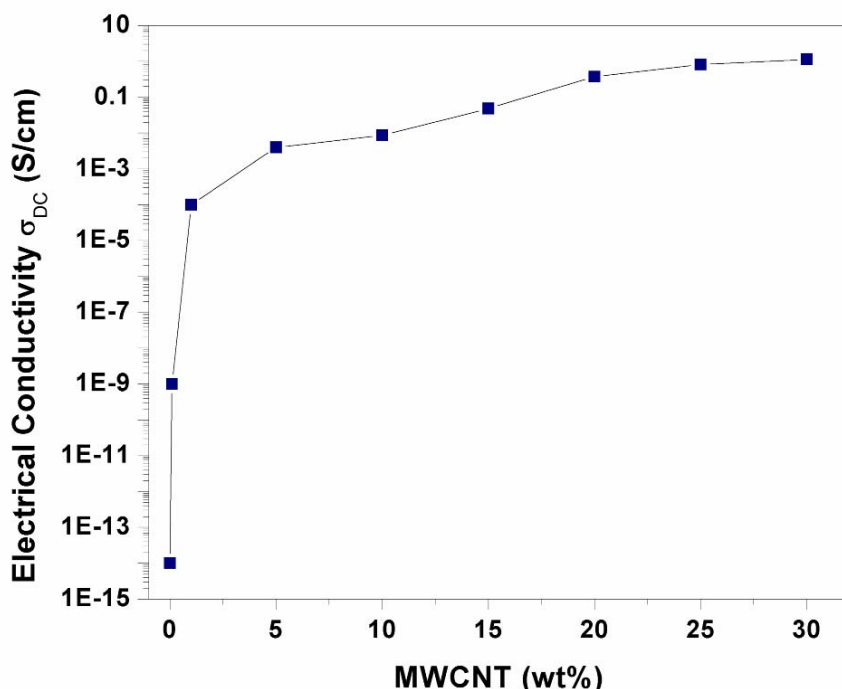


Figure 5.12 Four-point electrical conductivity as a function of MWCNTs weight content.

At low MWCNTs loadings, as long as no conductive CNT network is formed in the epoxy matrix, the conductivity of the composite remains very close to the one of the pure insulating epoxy matrix. When a sufficient amount of CNT filler is loaded, at the so-called percolation threshold, the filler particles form a network, resulting in

the formation of an initial conductive path throughout the entire material. At this critical concentration, i.e., between 0.1 and 1 wt% of MWCNT, the conductivity drastically increases by many orders of magnitude, from 10^{-9} S/cm to 10^{-4} S/cm. At higher MWCNTs content, e.g. about 5 wt%, the conductivity level is about 4×10^{-3} S/cm, and beyond this concentration the conductivity increase eventually reaches a plateau. This is typical of the percolation behavior usually observed for composites based on conductive fillers, and can be referred to as an ideal percolation behavior.

As evident from the graph, the conductivity increases in a classical percolating way. A log-log plot of conductivity as a function of the $(p - p_c)$ is presented in Figure 5.13. A linear relationship can be clearly seen. Using Eq. (5.1), the best fitted values are for $p_c = 5.5$ wt%, and $t = 3.06$.

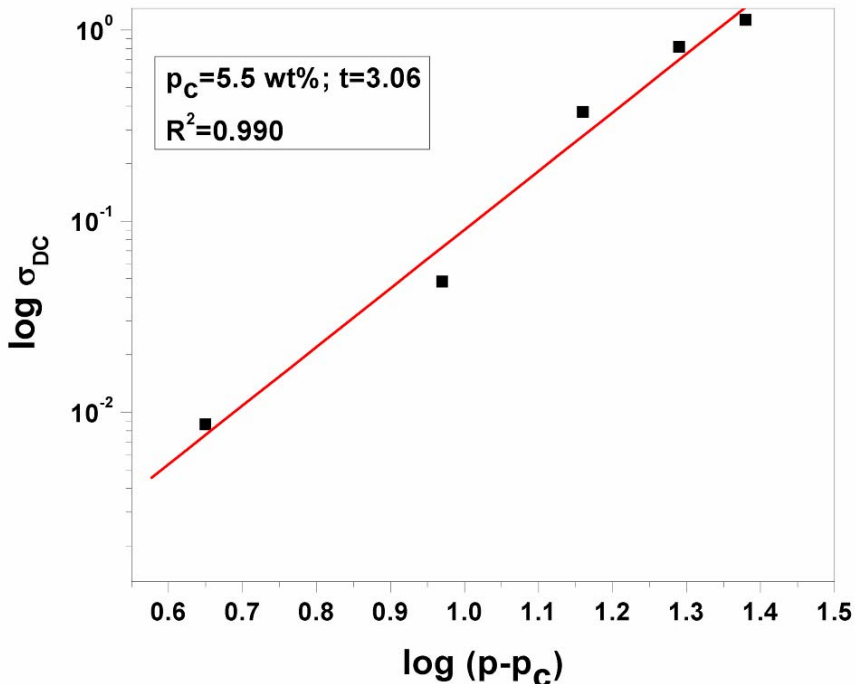


Figure 5.13 Plot of $\log(\sigma_{DC})$ vs. $\log(p - p_c)$. Solid line represent the best-fitted value according to Eq. 5.1

As mentioned above, the conductivity exponent t generally reflects the dimensionality of the system with values typically around 1.3 and 2.0 for two and three-dimensions, respectively. Here the conductivity critical exponent's value is equal to 3.06 close to the universal value for three-dimensional percolation systems.

The composite electrode containing 25 %, wt MWCNTs was selected as optimal composition for further composite preparations based on the correlation between morphology and electrical conductivity. The results obtained by four-point probe resistance measurements (FPP) for electrical characterization of the CNT composite electrodes are presented in Table 5.2.

Table 5.2 Electrical conductivity of the electrode materials containing 25 wt% MWCNTs

Electrode type	Electrical conductivity σ_{DC} (S/cm)
MWCNT-Epoxy	0.373
MWCNT-HKUST-Epoxy	0.605

An improvement of the electrical conductivity of the MWCNT-HKUST-Epoxy composite electrode is ascribed to the presence of Cu.

5.4 Conclusions

Two types of MWCNT-Epoxy and MWCNT-HKUST-Epoxy composite electrodes were prepared, both by using the same two-roll mill method.

The technique presented in this chapter and based on pre-dispersion of CNTs in a solvent, followed by mixing with epoxy resin, has been proven to be the easiest, least laborious, and very effective way to achieve relatively uniform CNT dispersions in composites, and has proven its efficiency.

The length and diameter distributions of MWCNTs in different types of solvent have been successfully determined by dynamic light scattering technique.

The electrical properties of MWCNT-Epoxy and MWCNT-HKUST-Epoxy composite electrodes strongly depend on the homogeneity of distribution of CNTs in the epoxy matrix. Furthermore, the critical factors determining the percolation threshold of MWCNT-Epoxy composites include: the aspect ratio of CNTs, disentanglement of CNT agglomerates on the nanoscale, and as presented before the uniform distribution of the CNTs.

The electrical measurements at room temperature clearly indicate an electrical percolation threshold at \sim about 5.5 wt% MWCNTs at which DC conductivity values increase by several orders of magnitude.

SEM micrographs showed that the MWCNTs distributions were quite homogeneous in the epoxy matrix. Also HKUST particles were almost homogeneously distributed on the walls of CNTs.

The Raman Spectroscopy results indicated that no significant increase of defects or breakage in nanotubes structure was caused by the sonication process.

5.5 References

- [5.1] H. Luo, Z. Shi, N. Li, Z. Gu, Q. Zhuang, *Analytical Chemistry* 73 (2001) 915.
- [5.2] K. Yamamoto, G. Shi, T. Zhou, et al., *Analyst*, 128 (2003) 249.
- [5.3] X.-X. Yan, D.-W. Pang, Z.-X. Lu, J.-Q. Lu, H. Tong, *J. Electroanal. Chem* 569 (2004) 47.
- [5.4] Z. Xu, X. Chen, X. Qu, J. Jia, S. Dong, *Biosensors and Bioelectronics* 20 (2004) 579.
- [5.5] Q. Zhao, Z.-N. Gu, Q.-K. Zhuang, *Electrochem. Commun.* 6 (2004) 83.
- [5.6] J. Wang, S. B. Hocevar, B. Ogorevc, *Electrochem. Commun.* 6 (2004) 176.
- [5.7] L. Wang, J. Wang, F. Zhou, *Electroanalysis*, 16 (2004) 627.
- [5.8] Z.-H. Gan, Q. Zhao, Z.-N. Gu, Q.-K. Zhuang, *Anal. Chim. Acta* 511 (2004) 239.
- [5.9] N. S. Lawrence, R. P. Deo, J. Wang, *Anal. Chim. Acta* 517 (2004) 131.
- [5.10] Y.-P. Ding, W.-L. Liu, Q.-S. Wu, X.-G. Wang, *J. Electroanal. Chem.* 575 (2005) 275.

72-Preparation and characterization of modified/unmod. MWCNT-Epoxy electrodes 5

- [5.11] L. Jiang, R.Wang, X. Li, L. Jiang, G. Lu, *Electrochem. Commun.* 7 (2005) 597.
- [5.12] X. Jiang, Z. Zhang, H. Bai, et al. *Spectrochimica Acta Part A* 61 (2005) 943.
- [5.13] Q. Zhao, L. Guan, Z. Gu, Q. Zhuang, *Electroanalysis* 17 (2005) 85.
- [5.14] K. A. Joshi, J. Tang, R. Haddon, J. Wang, W. Chen, A. Mulchandani, *Electroanalysis* 17 (2005) 54.
- [5.15] W. Zhang, F. Wan, W. Zhu, et al., *Journal of Chromatography B* 818 (2005) 227.
- [5.16] G.Wang, J.-J. Xu, H.-Y. Chen, *Electrochem. Commun.* 4 (2002) 506.
- [5.17] M. Guo, J. Chen, L. Nie, S. Yao, *Electrochimica Acta* 49 (2004) 2637.
- [5.18] M.Guo, J. Chen, D. Liu, L. Nie, S. Yao, *Bioelectrochemistry* 62 (2004) 29.
- [5.19] J. Chen and C. X. Cai, *Chinese Chemical Letters* 15 (2004) 813.
- [5.20] Y. Zhang, Y. Wen, Y. Liu, D. Li, J. Li, *Electrochem. Commun.* 6 (2004) 1180.
- [5.21] M. Guo, J. Chen, J. Li, B. Tao, S. Yao, *Anal. Chim. Acta* 532 (2005) 71.
- [5.22] F.-H. Wu, G.-C. Zhao, X.-W. Wei, *Electrochem. Commun.* 4 (2002) 690.
- [5.23] G.-C. Zhao, L. Zhang, X.-W. Wei, Z.-S. Yang, *Electrochem. Commun.* 5 (2003) 825.
- [5.24] F.-H. Wu, G.-C. Zhao, X.-W. Wei, Z.-S. Yang, *Microchimica Acta* 144 (2004) 243.
- [5.25] G.-C. Zhao, L. Zhang, X.-W. Wei, *Analytical Biochemistry* 329 (2004) 160.
- [5.26] G.-C. Zhao, Z.-Z. Yin, L. Zhang, X.-W. Wei, *Electrochem. Commun.* 7 (2005) 256.
- [5.27] C. Hu, W. L. Wang, S. X.Wang, W. Zhu, Y. Li, *Diamond and Related Materials* 12 (2003) 1295.
- [5.28] J. Qu, Y. Shen, X. Qu, S. Dong, *Chemical Communications* 1 (2004) 34.
- [5.29] N. Jia, L. Wang, L. Liu, Q. Zhou, Z. Jiang, *Electrochem. Commun.* 7 (2005) 349.
- [5.30] S. Lefrant, M. Baibarac, I. Baltog, J. Y.Mevellec, L.Mihut, O. Chauvet, *Synthetic Metals* 144 (2004) 133.
- [5.31] S. H. Lim, J. Wei, J. Lin, Q. Li, J. KuaYou, *Biosensors and Bioelectronics* 20 (2005) 2341.
- [5.32] C. Li, X.J. Pang, M.Z. Qu, Q.T. Zhang, B. Wang, B.L. Zhang et al., *Compos Part A* 37 (2005) 1485.
- [5.33] D. Qian, E.C. Dickey, R. Andrews, T. Rantell, *Appl. Phys. Lett.* , 76 (2000) 2868.
- [5.34] J. Sandler, M.S.P. Shaffer, T. Prasse, W. Bauhofer, K. Schulte, A.H. Windle, *Polymer*, 40 (1999) 5967.
- [5.35] N.G. Sahoo, Y.C. Jung, H.J. Yoo, J.W. Cho, *Macromol Chem Phys*, 207 (2006) 1773.
- [5.36] M. Cinke, J. Li, B. Chen, A. Cassell, L. Delzeit, J. Han, M. Meyyappan, *Chem. Phys. Lett.* 365 (2002) 69.
- [5.37] A. Peigney, C. Laurent, E. Flahaut, R.R. Bacsa, A. Rousset, *Carbon* 39 (2001) 507.
- [5.38] F. Schüth, W. Schmidt, *Advanced Materials* 14 (2002) 629.
- [5.39] H. Li, M. Eddaoudi, M. O'Keeffe, O.M. Yaghi, *Nature* 402 (1999) 276.
- [5.40] M. Kurmoo, *Chemical Society Reviews* 38 (2009) 1353.
- [5.41] C. Gucuyener, J. van den Bergh, J. Gascon, F. Kapteijn, *Journal of the American Chemical Society* 132 (2010) 17704.
- [5.42] L.J. Murray, M. Dinca, J.R. Long, *Chemical Society Reviews* 38 (2009) 1294.
- [5.43] J.R. Li, R.J. Kuppler, H.C. Zhou, *Chemical Society Reviews* 38 (2009) 1477.
- [5.44] D. Farrusseng, S. Aguado, C. Pinel, *Angewandte Chemie International Edition* 48 (2009) 7502.
- [5.45] P. Horcajada, T. Chalati, C. Serre, B. Gillet, C. Sebrie, T. Baati, J.F. Eubank, D. Heurtaux, P. Clayette, C. Kreuz, J.S. Chang, Y.K. Hwang, V. Marsaud, P.N. Bories, L. Cynober, S. Gil, G. Ferey, P. Couvreur, R. Gref, *Nature Materials* 9 (2010) 172.
- [5.46] J.A. Hurd, R. Vaidhyanathan, V. Thangadurai, C.I. Ratcliffe, I.L. Moudrakovski, G.K.H. Shimizu, *Nat Chem* 1 (2009) 705.
- [5.47] S.S.Y. Chui, S.M.F. Lo, J.P.H. Charmant, A.G. Orpen, I.D. Williams, *Science* 283 (1999) 1148.
- [5.48] K. Schlichte, T. Kratzke, S. Kaskel, *Microporous and Mesoporous Materials* 73 (2004) 81.
- [5.49] a) U. Mueller, M. Schubert, F. Teich, H. Puetter, K. Schierle-Arndt and J. Pastre, *Journal of Materials Chemistry* 16 (2006) 626-636. b) U. Mueller, H. Puetter, M. Hesse, H. Wessel, M. Schubert, J. Huff, M. Guzmann, U. Muller, H. Putter, J. Huf and M. Gutzmann in *Electrochemical preparation of crystalline, porous, organometallic framework materials, useful e.g. for storage of gases, such as methane for use in fuel cells, with generation of*

- metal ions from an anode in the preparation medium, Vol. Basf Ag (Badi) Basf Se (Badi), 2005.
- [5.50] <http://www.sigmaaldrich.com/technical-documents/articles/material-matters/selected-applications.html>.
- [5.51] Martinez et al. Chemistry of Materials, 2012, submitted
- [5.52] K.S.W. Sing, Reporting physisorption data for gas/solid systems with special reference to the determination of surface area and porosity, Pure Appl. Chem. 57 (1985) 603-619.
- [5.53] S.M. Bachilo, M.S. Strano, C. Kittrell, R.H. Hauge, R.E. Smalley, R.B. Weisman, Science 298 (2002) 2361.
- [5.54] M.S. Dresselhaus, P.C. Eklund, Adv. Phys. 49 (2000) 705.
- [5.55] M. Sugano, A. Kasuya, K. Tohji, Y. Saito, Y. Nishima, Chem. Phys. Lett. 292 (1998) 575.
- [5.56] O. Jost, A.A. Gorbunov, W. Pompe, T. Pichler, R. Friedlein, M. Knupfer, M. Reibold, H.-D. Bauer, L. Dunsch, M.S. Golden, J. Fink, Appl. Phys. Lett. 75 (1999) 2217.
- [5.57] D.A. Heller, P.W. Barone, J.P. Swanson, R.M. Mayrhofer, M.S. Strano, J. Phys. Chem. B. 108 (2004) 6905.
- [5.58] M.J. O'Connell, S. Sivaram, S.K. Doorn, Phys. Rev. B. 69 (2004) 235415.
- [5.59] A.M. Rao, A. Jorio, M.A. Pimenta, M.S.S. Dantas, R. Saito, G. Dresselhaus, M.S. Dresselhaus, Phys. Rev. B. 84 (2000) 1820.
- [5.60] R. Haggemueller, H.H. Gommans, A.G. Rinzler, J.E. Fischer, K.I. Winey, Chem. Phys. Lett. 330 (2000) 219.
- [5.61] J.E. Fischer, W. Zhou, J. Vavro, M.C. Llaguno, C. Guthy, R. Haggemueller, M.J. Casavant, D.E. Walters, R.E. Smalley, J. Appl. Phys. 93 (2003) 2157.
- [5.62] J.M. Jehng, W.C. Tung, C.H. Kuo, J. Porous. Mater. 15 (2008) 43.
- [5.63] A. Jorio G. Dresselhaus, M.S. Dresselhaus In: illustrated, editor. Carbon nanotubes: advanced topics in the synthesis, structure, properties and applications. Springer; 2008.
- [5.64] J.Y. Yi, G.M. Choi, J. Electroceram. 3 (1999) 361.
- [5.65] D. Hecht, L. Hu, G. Grüner, Appl. Phys. Lett. 89 (2006) 133112.
- [5.66] K. Miyasaka, K. Watanabe, E. Jojima, H. Aida, M. Sumita, K.J. Ishikawa, Mater. Sci. 17 (1982) 1610.
- [5.67] S.H. Munson- McGee, Phys. Rev. B. 43 (1991) 3331.
- [5.68] F. Du, J.E. Fischer, K.I. Winey, Phys. Rev. B. 72 (2005) 121404(R).
- [5.69] F.C. Dalmas, C. Gauthier, L. Chazeau, R. Dendievel, Comp. Sci. Technol. 67 (2007) 829.
- [5.70] W. Bauhofer, J.Z. Kovacs, Compos Sci Technol 69 (2009) 1486.
- [5.71] Y.J. Kim, T.S. Shin, H.D. Choi, J.H. Kwon, Y.-C. Chung, H.G. Yon, Carbon 43 (2005) 23.
- [5.72] G. Hu, C. Zhao, S. Zhang, M. Yang, Z. Wang, Polymer 47 (2006) 480
- [5.73] I. Balberg, S. Bozowski, Solid State Commun. 44 (1982) 551.
- [5.74] S. Kirkpatrick, Rev. Mod. Phys. 45 (1973) 574.
- [5.75] D. Stauffer, A. Aharony, Introduction to percolation theory. Taylor&Francis: 1992.
- [5.76] I. Balberg, Phys. Rev. Lett. 59 (1987) 1305.
- [5.77] W.Y. Hsu, W.G. Holtje, J.R. Barkley, J. Mater. Sci. Lett. 7 (1988) 459.
- [5.78] M.B. Bryning, M.F. Islam, J.M. Kikkawa, A.C. Yodth, Adv. Mater. 17 (2005) 1186.
- [5.79] J.K.W. Sandler, J.E. Kirk, M.S.P. Shaffer, A.H. Windle, Polymer 44 (2003) 5893.
- [5.80] B.E. Kilbride, J.N. Coleman, J. Fraysse, P. Fournet, M. Cadek, A. Drury, S. Hutzler, S. Roth, W.J. Blau, J. Appl. Phys. 92 (2002) 4024.
- [5.81] S. Barrau, A. Demont, C. Laurent, C. Lacabanne, Macromolecules 36 (2003) 5187.
- [5.82] F. Carmona, J. Ravier, Carbon 40 (2002) 151.
- [5.83] I. Balberg, D. Azulay, D. Toker, O. Millo, Int. J. Mod. Phys. B 18 (2004) 2091.
- [5.84] J.Z. Kovacs, B.S. Velagala, K. Schulte, W. Bauhofer, Compos. Sci. Technol. 67 (2007) 922.

CHAPTER 6

APPLICATIONS OF MODIFIED/UNMODIFIED MWCNT-EPOXY COMPOSITE ELECTRODES

"Nothing in life is to be feared, it is only to be understood. Now is the time to understand more, so that we may fear less". (Marie Curie)

Summary

This chapter presents the applications and integrations of modified/unmodified MWCNT-Epoxy composite electrodes as chemical sensors. The electrochemical detection of pentachlorophenol (PCP), salicylic acid (SA), acetylsalicylic acid (ASA), and glucose are described in the following sections.

6.1 MWCNT-Epoxy (MWCNT-EP) composite electrode for pentachlorophenol (PCP) detection

6.1.1 Pentachlorophenol (PCP)

Chlorophenols are a major group of pollutants of environmental concern. Due to the widespread and toxicological properties, several chlorinated phenols, such as pentachlorophenol (PCP), 2-chlorophenol, 2,4- dichlorophenol, 2,4,6-trichlorophenol (2,4,6- TCP) have been classified by the US Environmental Protection Agency (EPA) as priority pollutants (US EPA, 1979).

Pentachlorophenol (PCP) is a synthetic substance, made from other chemicals, and does not occur naturally in the environment. PCP has been included in the list of Persistent Organic Pollutants (POPs), and is the most toxic representative of the chlorophenols. It is also an important organic chemical for environmental studies because of its widespread application in industry, agriculture, and commercial product formation and preservation [6.1]. Pentachlorophenol is found in all environmental media (air, soil, and water) as a result of its past widespread use. PCP concentrations in drinking-water are usually in the range of 0.01–0.1 µg/L (World Health Organization, 1987) [6.2].

Information regarding the physical and chemical properties of pentachlorophenol is presented in Table 6.1.

6.1. MWCNT-Epoxy composite electrode for pentachlorophenol (PCP) detection- 75

Table 6.1 Physical and chemical properties of PCP

Properties	Pentachlorophenol
Molecular weight	266.35
Color	Colorless or white (pure); dark gray to brown (crude product)
Physical state	Crystalline solid (pure); pellets or powder (crude product)
Melting point	191°C
Boiling point	310°C (decomposition)
Density	1.978 g/cm ³
Odor	Phenolic; very pungent
Solubility Water Organic solvents	14 mg/L at 20°C Very soluble in alcohol and ether; soluble in benzene; slightly soluble in cold petroleum ether.

Humans may be exposed to PCP in occupational settings through inhalation of contaminated workplace air and dermal contact with the compound or with wood products treated with the compound. General population exposure may occur through contact with contaminated environmental media, particularly in the vicinity of wood treatment facilities and hazardous waste sites. Important routes of exposure appear to be inhalation of contaminated air, inhalation exposure to PCP that has volatilized from treated wood surfaces, ingestion of contaminated groundwater used as a source of drinking water, ingestion of contaminated food, and dermal contact with contaminated soils or wood products treated with the compound.

Adverse health effects have been observed in humans and in experiments with animals following short- and long-term exposure to PCP by the inhalation, oral, and dermal exposure routes. The liver, thyroid, immune system, reproductive system, and the developing organism are the primary targets of PCP toxicity. Case reports of individuals acutely exposed to PCP via inhalation and dermal contact and longer-term occupational exposure via inhalation and/or dermal contact identify a number of adverse health effects. The observed effects include symptoms associated with uncoupling of oxidative phosphorylation (tachycardia, increased respiratory rate, labored breathing, profuse sweating, fever, metabolic acidosis), liver effects, and impaired immune function.

In addition to the liver, thyroid, immune, reproductive, and developmental effects, exposure to PCP is also associated with carcinogenic, renal, and neurological effects. The results of several epidemiology studies suggest that PCP may be a human carcinogen.

Monitoring of PCP and other pesticides in drinking and related waters is a difficult and expensive task. Based on the above-presented considerations, it is highly desirable to develop sensitive and convenient technology for the determination of PCP. A wide variety of analytical methods has been developed to detect PCP in contaminated samples, most of them based on gas chromatography (GC) [6.3], [6.4], gas chromatography–mass spectrometry (GC–MS) [6.5], high-performance liquid chromatography (HPLC) [6.6], thin-layer chromatography [6.7], and spectrophotometry [6.8]. Among these, the electrochemical methods have attracted substantial attention because of good simplicity, sensitivity, selectivity,

fast response, and low cost production. Several studies have reported the electrochemical detection of PCP based on carbon paste electrodes and vitreous carbon surfaces [6.9], [6.10].

In our previous work, the results of PCP determination using carbon nanofiber composite electrodes were reported [6.11]. In order to improve the electroanalytical performances for the PCP determination, carbon nanofiber was replaced with multi-wall carbon nanotubes (MWCNTs), taking into account that carbon nanotubes (CNTs) offer exciting possibilities for developing sensitive electrochemical sensors because of their excellent properties, such as high electrical conductivity, good chemical stability, and extreme mechanical strength [6.12]-[6.14].

6.1.2 Experimental

Reagents

Pentachlorophenol (PCP) was purchased from Merck. An aqueous 10 mg/L PCP stock solution was prepared daily by dilution the solid PCP in double distilled water and 0.1 M NaOH. The supporting electrolyte for the characterization and application of electrode material in detection process was 0.1 M Na₂SO₄ solution, which was freshly prepared from Na₂SO₄ of analytical purity (Merck) with double distilled water.

Apparatus and procedures

The electrochemical performance of this electrode was studied by cyclic voltammetry (CV), differential-pulse voltammetry (DPV), square-wave voltammetry (SWV), and multiple-pulsed amperometry (MPA).

Electrochemical measurements were performed in unstirred solutions using a computer controlled Autolab potentiostat/galvanostat PGSTAT 302 (EcoChemie, The Netherlands) with a standard three-electrodes configuration (Figure 6.1.). The three-electrode system consisted of a MWCNT-Epoxy (MWCNT-EP) working electrode with 0.196 cm² geometrical area, a platinum wire as counter electrode, and a saturated calomel reference electrode (SCE). Before each voltammogram, the MWCNT-EP composite electrode was carefully polished with abrasive paper and then on a felt-polishing pad by using 0.3 μm alumina powder (Metrohm, Switzerland). The electrode was then sonicated for 5 min in pure water. All experiments were carried out using standard cell with 50 mL of solution at room temperature (25°C).

6.1. MWCNT-Epoxy composite electrode for pentachlorophenol (PCP) detection- 77

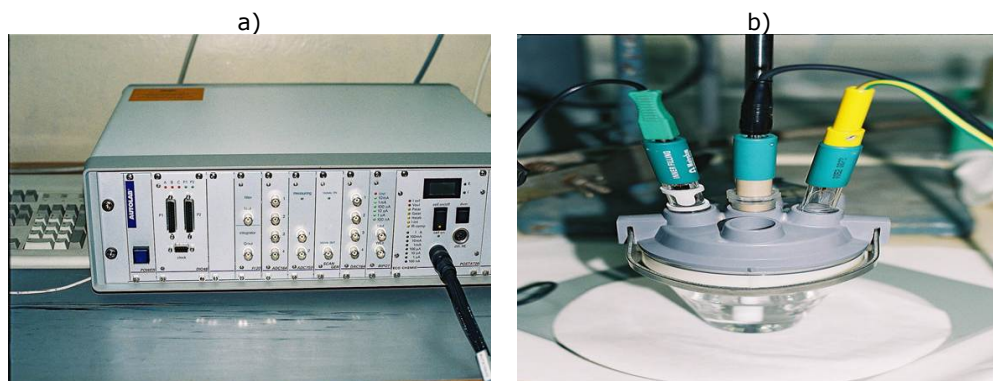


Figure 6.1 (a) Potentiostat/galvanostat PGSTAT 302 (EcoChemie), (b) Metrohm cell with the three electrodes configuration.

6.1.3 Results and discussion

6.1.3.1 Electrochemical characterization of the MWCNT-EP composite electrode using potassium ferricyanide

The ability to obtain kinetic information from voltammetry measurements requires precise knowledge of the oxidation/ reduction current peak positions and area [6.15]-[6.18].

Potassium ferricyanide ($K_3[Fe(CN)_6]$) shows very good performance as an electronic conducting medium. Here, $K_3[Fe(CN)_6]$ is used as a probe to evaluate the conducting property and calculate the electroactive area of the MWCNTs-EP composite electrode. Cyclic voltammetry (CV) of 4 mM $K_3[Fe(CN)_6]$ in 1 M KNO_3 supporting electrolyte at the MWCNTs-EP composite electrode was recorded at different scan rates (Figure 6.2).

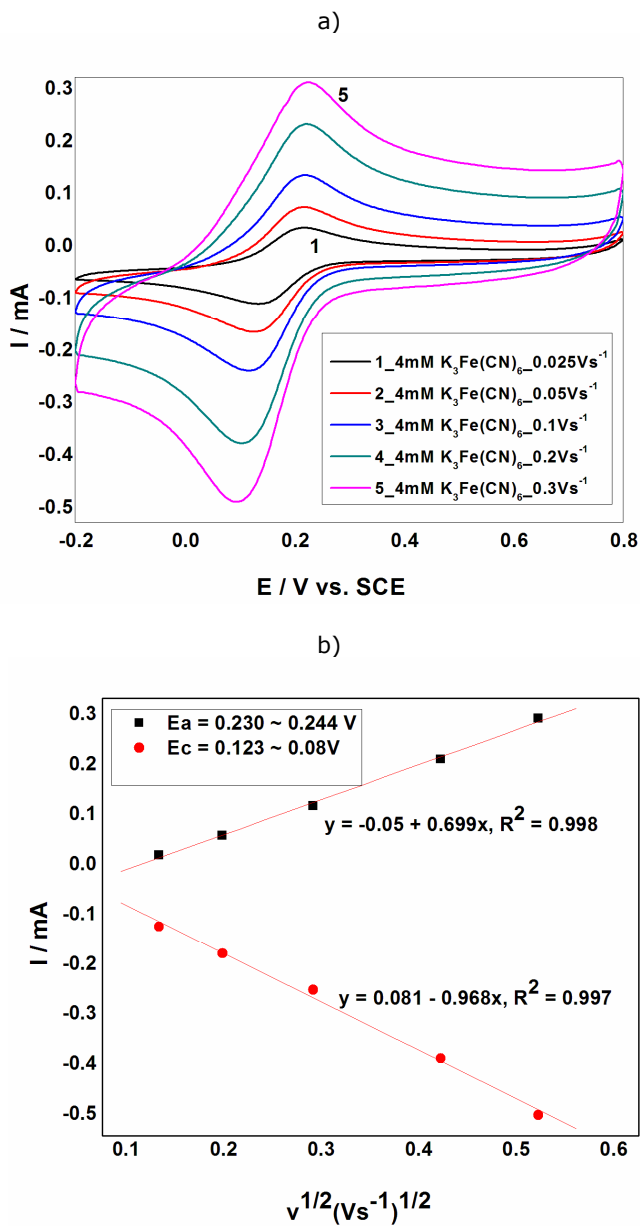


Figure 6.2 (a) CVs of the MWCNT-EP composite electrode in 4 mM $K_3[Fe(CN)_6]$ in 0.1 M KNO_3 supporting electrolyte at different scan rates: 1) 0.025, 2) 0.05, 3) 0.1, 4) 0.2, 5) 0.3 Vs^{-1} . (b) Calibration plots of the oxidative and reductive peak currents vs. square root of scan rate.

6.1. MWCNT-Epoxy composite electrode for pentachlorophenol (PCP) detection- 79

Table 6.2 The electrochemical parameters of the redox system (ferri/ferrocyanide) determined from the anodic branches of CVs.

Scan rate (Vs ⁻¹)	E/ V	I / mA	Δ Ia / mA
0.025	0.230	0.062	0.053
0.05	0.232	0.100	0.284
0.1	0.234	0.160	0.130
0.2	0.240	0.253	0.194
0.3	0.244	0.334	0.247

Table 6.3 The electrochemical parameters of the redox system (ferri/ferrocyanide) determined from the cathodic branches of CVs.

Scan rate (Vs ⁻¹)	E/ V	I / mA	Δ Ic / mA
0.025	0.123	-0.081	-0.072
0.05	0.115	-0.135	-0.118
0.1	0.106	-0.208	-0.175
0.2	0.09	-0.345	-0.279
0.3	0.08	-0.458	-0.361

$$\Delta E = E_a - E_c = 0.236 - 0.08 = 0.156V$$

$$i_a / i_c = 0.181 / 0.245 = 0.738$$

Table 6.4 Apparent diffusion coefficient and the electroactive surface area of MWCNT-Epoxy composite electrode.

Scan rate (Vs ⁻¹)	Diffusion coefficient	Electroactive area	Diffusion coefficient	Total electroactive area	Geometrical area (cm ²)
0.025	3.549 × 10 ⁻⁶	0.143	5.33 × 10 ⁻⁶	0.173	0.196
0.05	4.626 × 10 ⁻⁶	0.158			
0.1	5.225 × 10 ⁻⁶	0.174			
0.2	6.307 × 10 ⁻⁶	0.190			
0.3	6.938 × 10 ⁻⁶	0.200			

6.1.3.2 Cyclic voltammetry measurements

Cyclic voltammetry (CV) is one of the most versatile electrochemical techniques used in the study of electroactive behavior and the characterization of sensors. In order to determine the electroactive surface area of the MWCNTs-EP composite electrode the electrochemical behavior of potassium ferrocyanide K₃[Fe(CN)₆] in 1 M KNO₃ supporting electrolyte was study using cyclic voltammetry recorded at different scan rates.

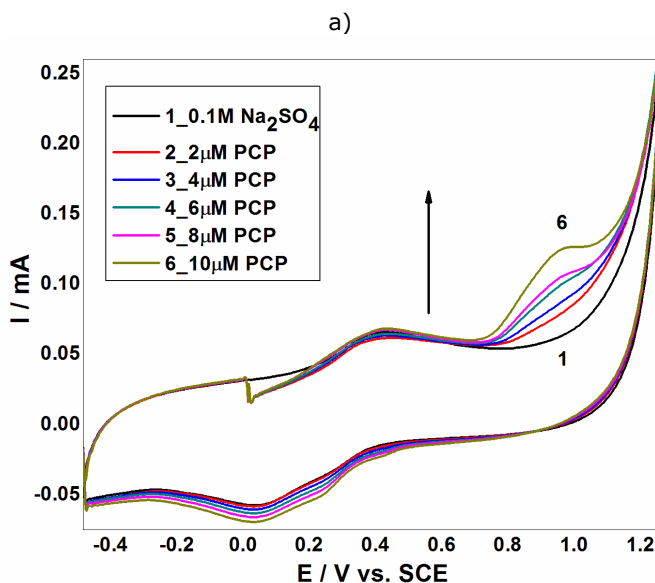
According to the Randles-Sevcik equation (6.1)

$$I_p = 2.69 \times AD^{1/2}n^{3/2}\nu^{1/2}C \quad (6.1)$$

Where A represents the area of the electrode (cm²), n the number of electrons participating in the reaction (and is equal to 1), D the diffusion coefficient of the molecule in solution, C the concentration of the probe molecule in the solution and is 4 mM, and ν is the scan rate (Vs⁻¹). The apparent diffusion coefficient of

$K_3[Fe(CN)_6]$ was determined to be $5.33 \times 10^{-6} \text{ cm}^2 \text{ s}^{-1}$. By comparison with the theoretical diffusion coefficient from the literature value of $6.7 \times 10^{-6} \text{ cm}^2 \text{ s}^{-1}$ [6.19], the value of the active electrode area was determined to be 0.173 cm^2 versus the value of the electrode geometric area of 0.196 cm^2 .

Based on our previous research regarding the electrochemical determination of pentachlorophenol (PCP) on carbon nanofiber-expanded graphite-epoxy composite electrodes [6.11], the electroanalytical peculiarities of this MWCNT-EP composite electrode towards PCP determination were studied. Cyclic voltammograms (CVs) recorded with the MWCNT-EP composite electrode in a $0.1 \text{ M Na}_2\text{SO}_4$ supporting electrolyte and various concentrations of pentachlorophenol (PCP) are shown in Figure 6.3 (a). In the absence of PCP, a first anodic current peak noticed on the CVs around $+0.4 \text{ V vs. SCE}$ with the corresponding cathodic one, owing to MWCNT-EP electrode material. Some interaction between functional groups of the MWCNT-EP surface and PCP are possible, which precede the oxidation process at more positive potential. The oxidation process of PCP on MWCNT-EP composite electrode occurred at the potential value of about $+0.97 \text{ V vs. SCE}$ and one evidenced peak appeared. The current corresponding to the peak oxidation of PCP increased progressively with its concentration. On the following reverse scan from $+1.25$ to -0.5 V vs. SCE , no corresponding reduction peak is observed within the potential range between $+1.25$ and $+0.4 \text{ V vs. SCE}$, revealing that the anodic PCP oxidation on the MWCNT-EP composite electrode is totally irreversible. The anodic peak currents recorded at $+0.97 \text{ V vs. SCE}$ increased linearly with PCP concentrations with a correlation coefficient of 0.990 (Figure 6.3 (b)). In general, a proportional increase of anodic current with concentration gives information about the possibility of a controlled oxidation process by mass transfer [6.20], the desired behavior for the potential amperometric/ voltammetric detection application.



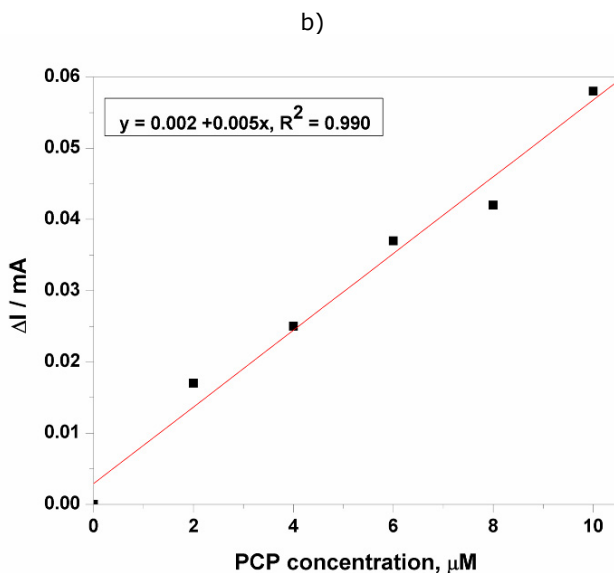
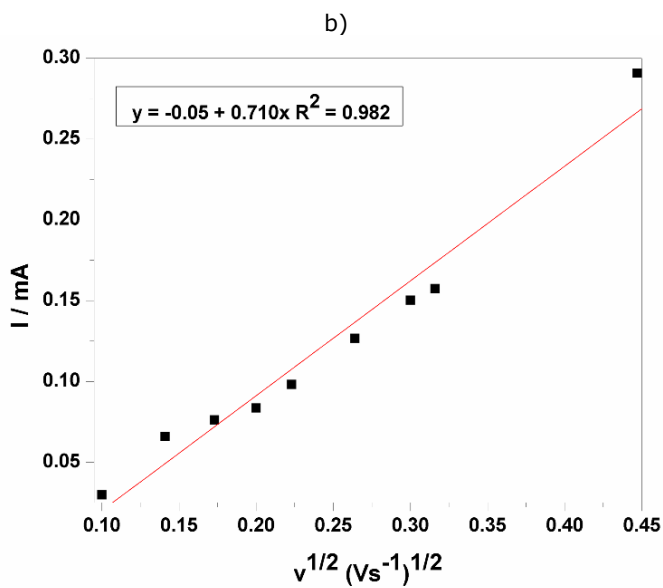
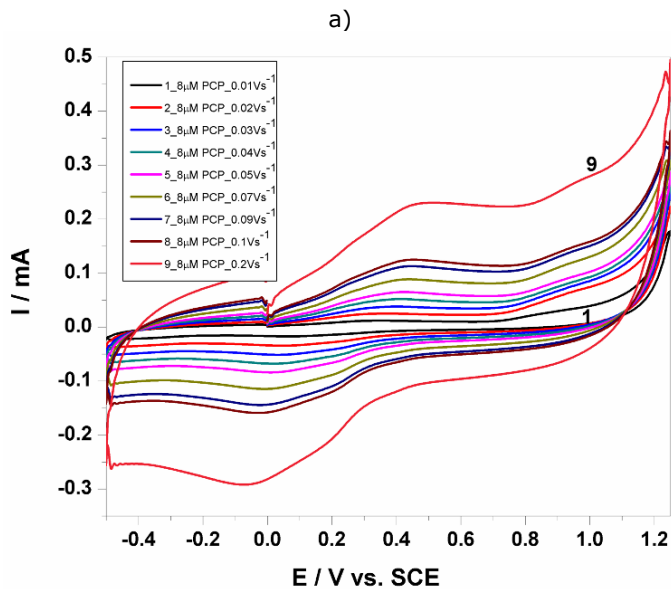


Figure 6.3 (a) CVs of the MWCNT-EP composite electrode recorded at a potential scan rate 0.05 Vs^{-1} and a potential range between -0.5 V and $+1.25 \text{ V/SCE}$ in $0.1 \text{ M Na}_2\text{SO}_4$ supporting electrolyte (curve 1) and in the presence of different PCP concentrations: 2) $2 \mu\text{M}$, 3) $4 \mu\text{M}$, 4) $6 \mu\text{M}$, 5) $8 \mu\text{M}$, 6) $10 \mu\text{M}$. (b) Calibration plot of the anodic currents recorded at $E = +0.97 \text{ V/SCE}$ vs. PCP concentration.

Effect of the scan rate

The oxidation process of phenol derivatives on carbon-based electrodes is a very complex process, involving both the adsorption of the reactant/intermediate or phenol oxidation products and the formation of passive, nonconductive layers of oligomer products of oxidation processes on their surface by electropolymerization [6.21]. The cyclic voltammetry of MWCNT-EP composite electrode at various scan rates ($0.01\text{-}0.2 \text{ Vs}^{-1}$) in the presence of $8 \mu\text{M}$ PCP was studied (Figure 6.4 (a)) to study the mechanistic aspects of the overall oxidation process of PCP on the electrode surface. For the whole range of the scan rates studied, the peak shape that is sensitive to the scan rate shows irreversible characteristics. The anodic current recorded at about $+0.97 \text{ V}$ vs. SCE increased linearly with the square root of the scan rate (Figure 6.4 (b)) suggesting that the reaction is mass-transfer controlled. Moreover, the starting potential of the wave shifted towards positive potential when increasing v indicating that the electrooxidation process of PCP is irreversible (Figure 6.4 (c)).



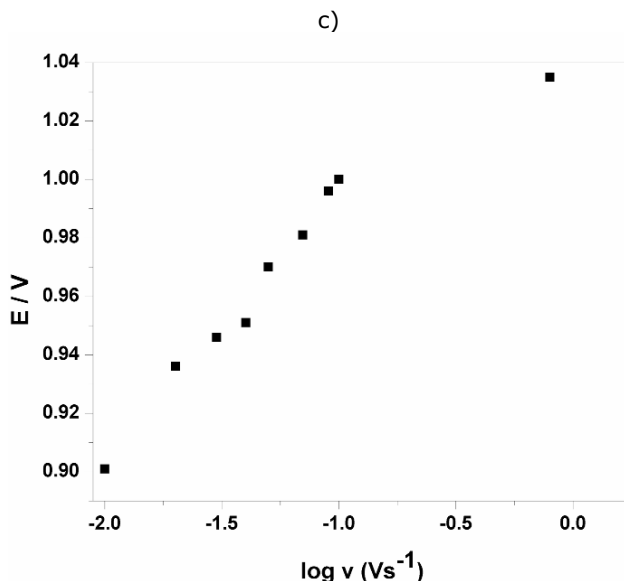


Figure 6.4 (a) CVs of 8 μM PCP at MWCNT-EP composite electrode in 0.1 M Na_2SO_4 supporting electrolyte (1) with different scan rates: 0.01, 0.02, 0.03, 0.04, 0.05, 0.07, 0.09, 0.1, 0.2 Vs^{-1} ; potential range: -0.5 and $+1.2$ V/ SCE. (b) The anodic peak current vs. square root of scan rate; (c) The peak potential E_p vs. $\log(v)$.

6.1.3.3 Pulsed-voltammetric measurements

Differential-pulsed and square-wave voltammetric techniques are widely used to improve the electroanalytical parameters for the voltammetric detection, e.g., the lowest limit of detection and the sensitivities. Also, they can provide information about mechanistic aspects.

Differential-pulsed voltammetry (DPV) has been employed as a technique for the evaluation of the performance of the MWCNT-EP composite electrode for the PCP determination. Modulation amplitude (MA) and step potential (SP) parameters have been considered to optimize the determination method, and the best results were achieved for MA of 0.2 V and SP of 0.02 V. Figure 6.5 (a) shows the DPVs recorded for the PCP concentration ranged between 2 and 12 μM and in the potential range of $+0.5$ to $+1.0$ V/SCE, and the oxidation potential is shifted to the negative direction in comparison with CV results ($+0.80$ V vs. $+0.97$ V/SCE). The useful net current signals corresponding to the oxidation peaks recorded at $+0.80$ V/SCE are linearly dependent on the PCP concentration (Figure 6.5 (b)). The lower detection potential value and a better sensitivity were achieved by using DPV in comparison with CV (see Table 6.5).

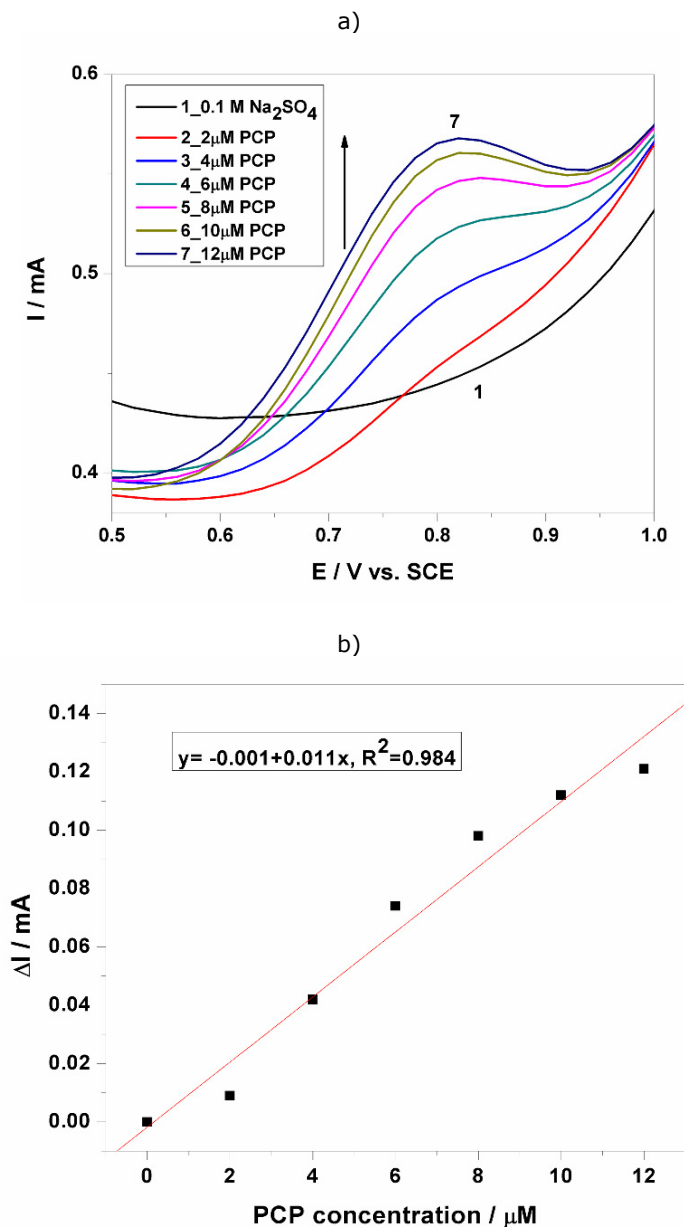
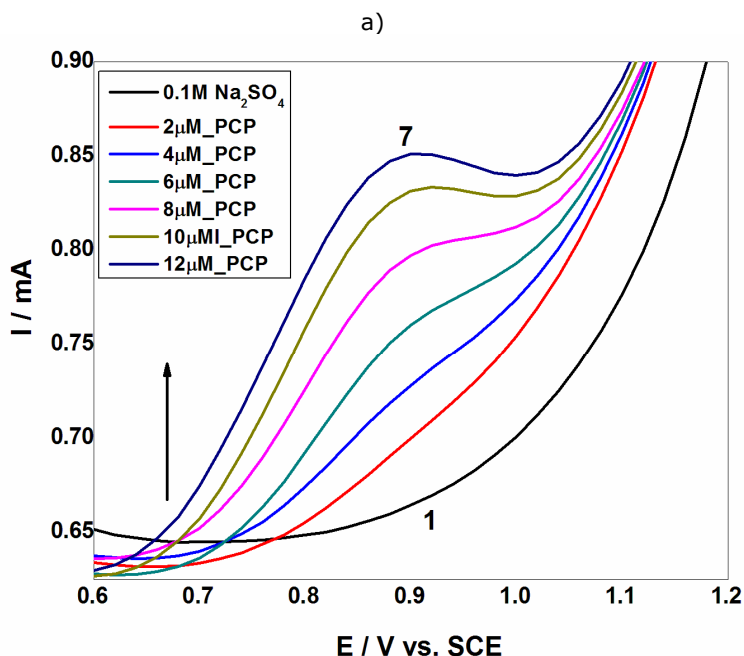


Figure 6.5 (a) DPVs of the MWCNT-EP composite electrode at modulation amplitude 0.2 V, step potential 0.02 V and potential scan rate of 0.05 Vs^{-1} , potential range between +0.5 V and +1.0 V vs. SCE in 0.1 M Na_2SO_4 supporting electrolyte (curve 1) and in the presence of different PCP concentrations: 2) 2 μM , 3) 4 μM , 4) 6 μM , 5) 8 μM , 6) 10 μM , 7) 12 μM . (b) Calibration plot of the anodic currents recorded at $E = +0.80 \text{ V/SCE}$ vs. PCP concentration.

6.1. MWCNT-Epoxy composite electrode for pentachlorophenol (PCP) detection- 85

Figure 6.6 (a) shows SWV responses recorded with the MWCNT-EP composite electrode for various concentrations of PCP under optimized conditions, i.e., frequency (f) of 10 Hz, modulation amplitude (MA) of 0.1 V, and step potential (SP) of 0.01 V. Figure 6.6 (b) corresponds to the calibration curve of the useful current with PCP concentration, which shows the linear dependence for the concentration interval ranged between 2 and 12 μM PCP. Under the conditions of this technique application, the best sensitivity was achieved this result should be attributed to the diminution of the capacitive component and implicit the background current that affects the useful signal of the PCP detection by SWV.

Even if the adsorption property of the carbon-based electrode towards the target analyte is not generally desired because of the electrode fouling generation, this could however be exploited in a positive way, namely to detect PCP at a trace level by applying the preconcentration-voltammetric detection scheme.



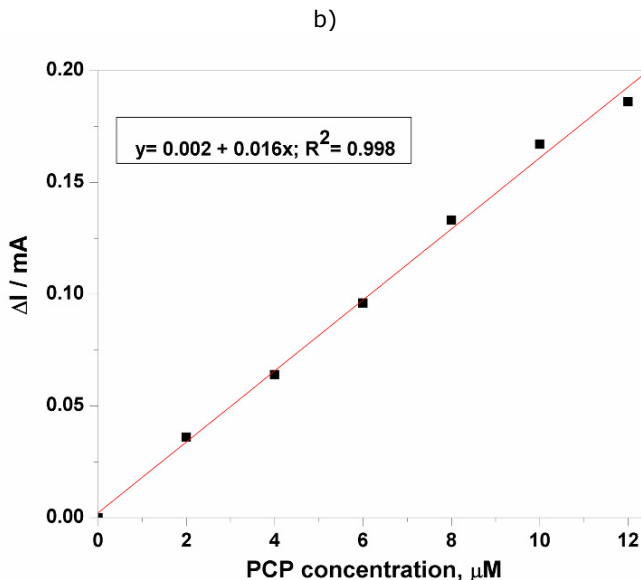


Figure 6.6 (a) SWVs of the MWCNT-EP composite electrode, modulation amplitude 0.1 V, step potential 0.01 V and frequency 10Hz; potential range between +0.6 V and +1.2 V/SCE in 0.1 M Na₂SO₄ supporting electrolyte (curve 1) and in the presence of different PCP concentrations: 2) 2 μM , 3) 4 μM , 4) 6 μM , 5) 8 μM , 6) 10 μM , 7) 12 μM . (b) Calibration plot of the anodic currents recorded at E= +0.90 V/SCE vs. PCP concentration.

In a preconcentration-voltammetric detection scheme, the extent of preconcentration is a function of accumulation time, which determines the degree of adsorption on the electrode surface. The effect of accumulation time on the currents of the differential-pulse anodic peaks recorded at +0.83 V/SCE corresponding to PCP oxidation was investigated. The enhancement factor was determined as the ratio of the peak current recorded at different accumulation times to that recorded without a preconcentration scheme. The useful oxidation peak current and the enhancement factor determined for 8 μM PCP using the preconcentration-voltammetric detection procedure at different accumulation times are shown in Figure 6.7 (a). The oxidation peak currents for this compound increased with accumulation time up to 40 minutes, which was selected as the optimum accumulation time due to a maximum enhancement factor of 11 was reached, because for longer accumulation times the peak currents decreased. The enhancement factor of 11 at the oxidation potential of +0.83 V/SCE revealed an effective concentration effect of the MWCNT-EP composite electrode on PCP regarding the improvement of its oxidation signal. As a consequence, the accumulation time of 40 minutes was chosen as an optimum time for further square-wave voltammetric experiments.

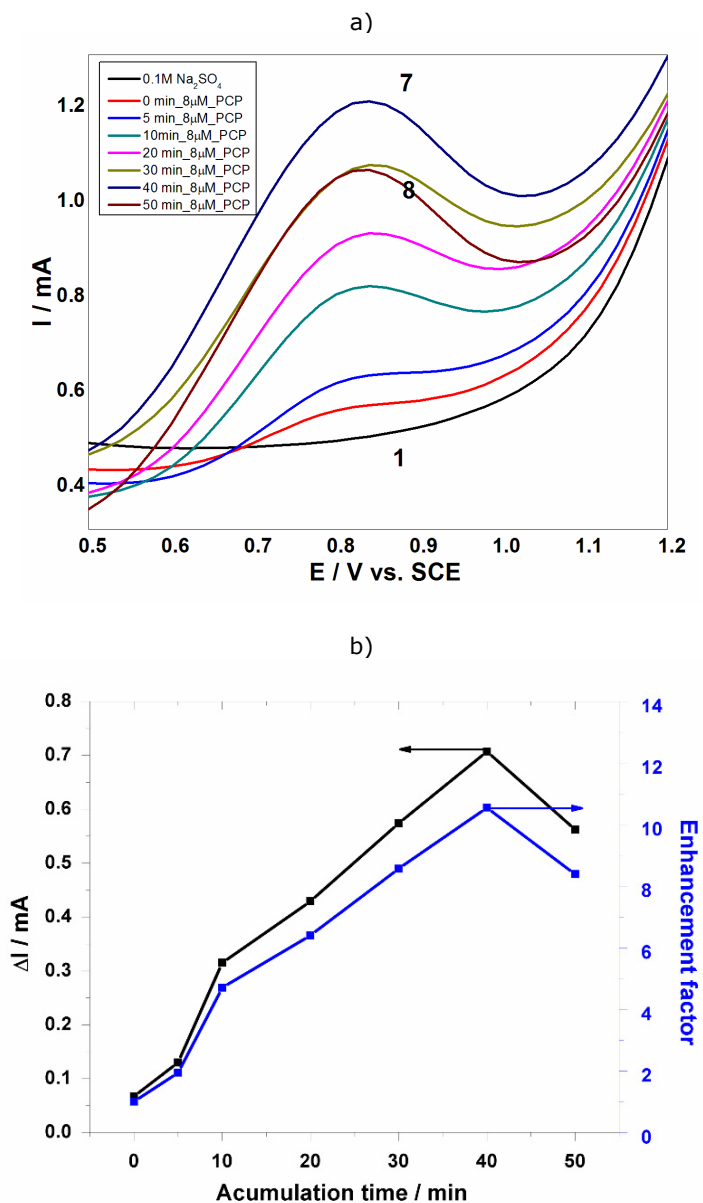
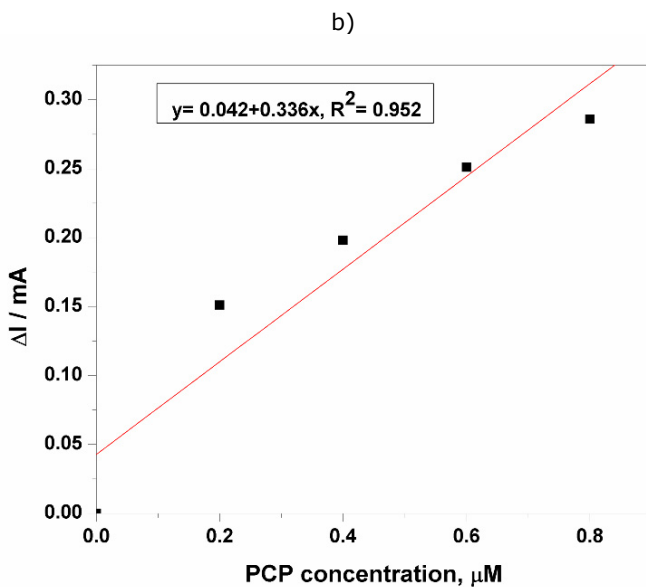
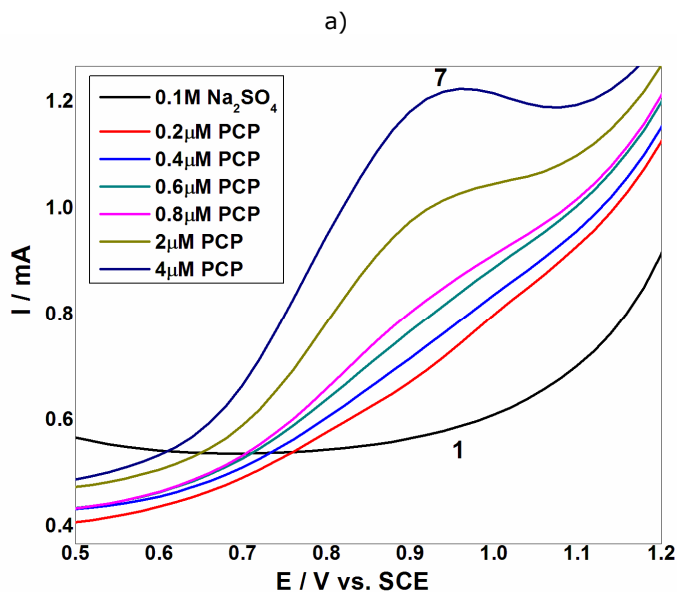


Figure 6.7 (a) DPVs recorded on a MWCNT-EP composite electrode (modulation amplitude 0.2 V, step potential 0.02 V), and a potential scan rate 0.05 Vs^{-1} in the potential range between +0.5 V and +1.2 V vs. SCE in 0.1 M Na_2SO_4 supporting electrolyte (curve 1) and in the presence of $8 \mu\text{M}$ PCP concentration after different accumulation times: 2) 0 min, 3) 5 min, 4) 10 min, 5) 20 min, 6) 30 min, 7) 40 min, 8) 50 min. (b) Peak current responses and enhancement factor for the detection of $8 \mu\text{M}$ PCP at MWCNT-EP composite electrode as a function of the accumulation time recorded at $E = +0.83 \text{ V/SCE}$.

An example of an SWV series recorded under the optimum conditions of the preconcentration scheme that assume the accumulation time of 40 minutes within the PCP concentration range from 0.2 μM to 4 μM is shown in Figure 6.8 (a).



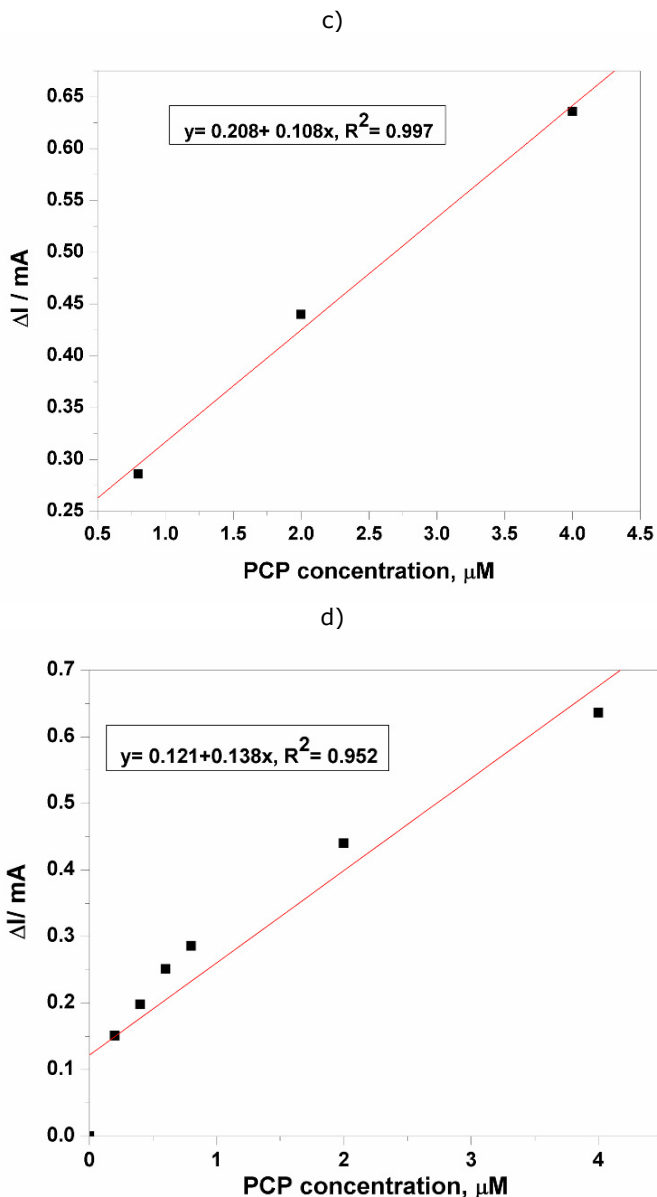
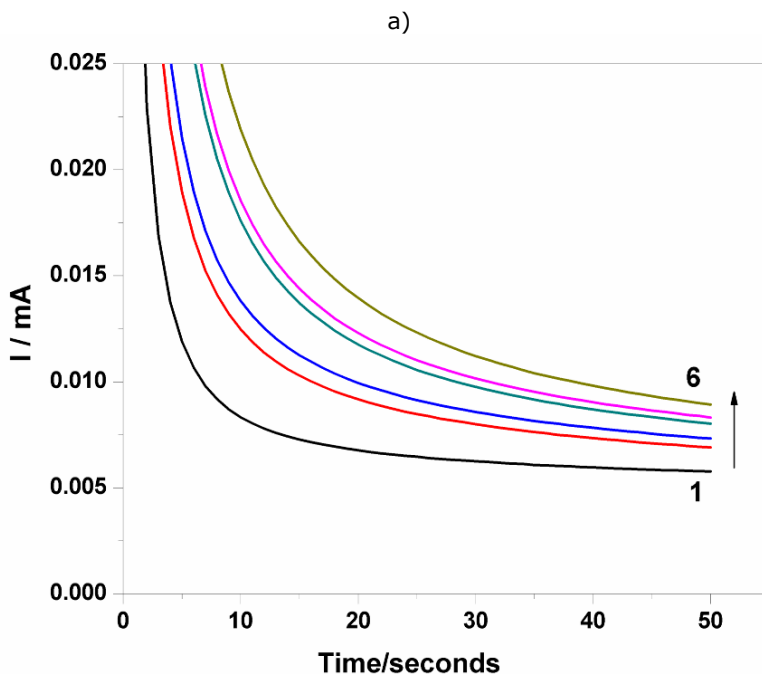


Figure 6.8 (a) SWVs recorded on a MWCNT-EP composite electrode, accumulation time of 40 minutes (modulation amplitude 0.1 V, step potential 0.01 V and frequency 10Hz), potential range +0.5 to +1.2 V vs. SCE in 0.1 M Na₂SO₄ supporting electrolyte (1) and in the presence of different PCP concentrations: 2) 0.2 μM, 3) 0.4 μM, 4) 0.6 μM, 5) 0.8 μM, 6) 2 μM, 7) 4 μM. (b) Calibration plot of the anodic currents recorded at E= +0.95 V/SCE vs. PCP concentrations: 0.2, 0.4, 0.6, 0.8 μM. (c) Calibration plot of the anodic currents recorded at E= +0.95 V/SCE vs. PCP concentrations: 0.8, 2, 4 μM. (d) Calibration plot of the anodic currents recorded at E= +0.95 V/SCE vs. PCP concentrations: 0.2, 0.4, 0.6, 0.8, 2, 4 μM.

Applying the above-proposed preconcentration-voltammetric detection using the SWV technique at modulation amplitude of 0.1 V, a step potential of 0.01 V and a frequency of 10Hz allowed the detection of lower concentrations of PCP. Under these working conditions a significant enhancement of the electroanalytical parameters of PCP detection was achieved, about a 10 times better sensitivity and a 30 times lower the detection limit (see Table 6.5). However, for practical applications the optimum analytical procedure should involve the recording of the chronoamperogram, based on the existing well-established essential point of reference provided by the voltammograms. Thus, a series of chronoamperograms was recorded at the potential value of +0.97 V/SCE within a PCP concentration range between 2 and 10 μM (Figure 6.9 (a)) and the sensitivity obtained was poor compared to CV, probably due to electrode fouling (see Table 6.5).



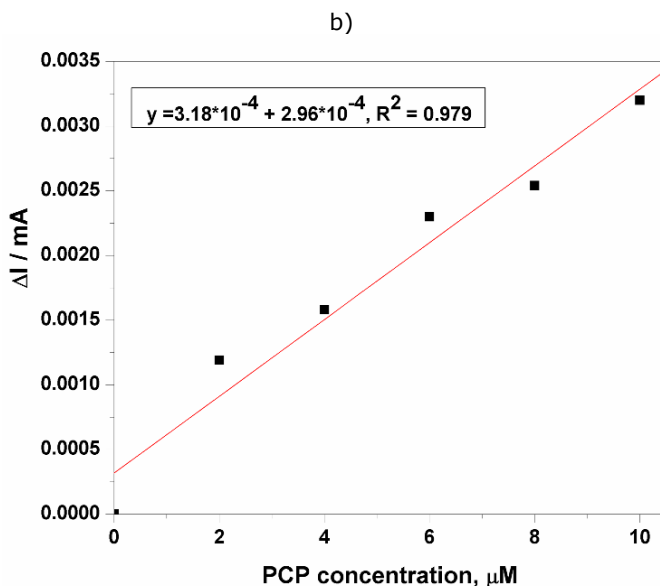


Figure 6.9 (a) CAs recorded on MWCNT-EP composite electrode in 0.1 M Na_2SO_4 supporting electrolyte (curve 1) and in the presence of different PCP concentrations (curves 2-6): 2, 4, 6, 8, and 10 μM recorded at $E=+0.97$ V. (b) Calibration plot of the anodic currents recorded at $E= +0.97$ V vs. PCP concentration.

An alternative to the amperometric detection to improve the electroanalytical parameters and proposed in this work is the use of MPA with three potential pulses, whose values were established based on CV behavior. The pulses were applied continuously using the following scheme:

- 1) +0.97 V/SCE for duration of 50 ms, where PCP is directly oxidized on the electrode surface,
- 2) +1.25 V/SCE for a duration of 50 ms, considered as cleaning potential because O_2 evolution occurred,
- 3) -0.1 V/SCE for a duration of 50 ms, where the reduction process involving the electrode surface occurred.

Figure 6.10 (a) presents the pulsed amperograms recorded at each potential values for PCP detection. As can be seen, for each potential value the corresponding current depended linearly on PCP concentration (Figure 6.10 (b)), but only the anodic ones are taken into consideration. Alternating the advanced oxidation and the reduction processes allows the in-situ regeneration of the electrode surface. Applying the MPA technique improved significantly the detection performance of the electrode for PCP detection. These working conditions for applying MPA led to very good sensitivity that is quite better than one reached by SWV. Also, the best limit of detection (0.006 μM , see Table 6.5) was achieved using this technique, which can be regarded very suitable for the practical application.

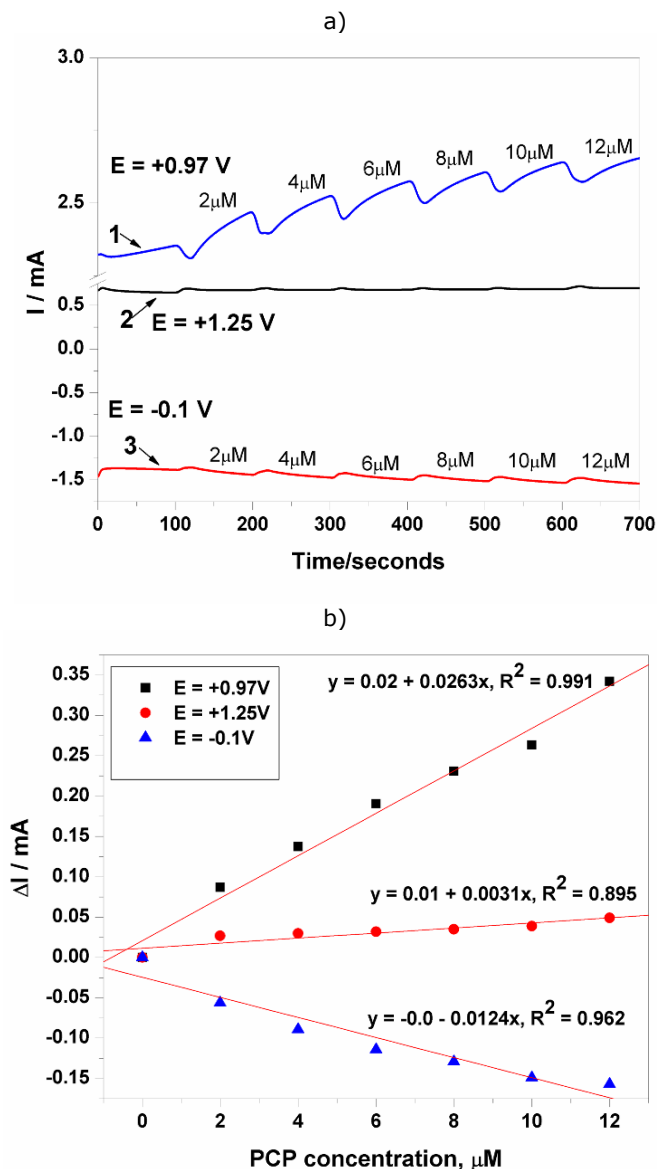


Figure 6.10 (a) MPAs recorded at a MWCNT-EP electrode in 0.1 M Na_2SO_4 supporting electrolyte and in the presence of different PCP concentrations: 2, 4, 6, 8, 10, and 12 μM recorded at 1) $E = +1.25\text{ V}$; 2) $E = +0.97\text{ V}$ and 3) $E = -0.1\text{ V}$ vs. SCE. (b) The calibration plots of the currents recorded at 1) $E = +0.97\text{V}$; 2) $E = +1.25\text{V}$; 3) $E = -0.1\text{ V/ SCE}$ vs. PCP concentration.

The electroanalytical parameters for the concentration ranges where linear dependence was reached at the different potential values in relation with applied

6.1. MWCNT-Epoxy composite electrode for pentachlorophenol (PCP) detection- 93

electrochemical techniques without/ with the preconcentration scheme are gathered in Table 6.5. The limit of detection (LOD) was evaluated based on $3S_B/b$ [6.21], where S_B is the standard deviation of the mean value of three voltammograms/amperegrams of the blank and b is the slope of the straight line in the analytical curve by using each electrochemical technique. The reproducibility of the electrode using the above-mentioned techniques was evaluated for three replicate measurements of PCP detection as relative standard deviation.

Table 6.5 Electroanalytical performance of the MWCNT-Epoxy composite electrode for the detection of PCP in 0.1M Na₂SO₄ supporting electrolyte.

Peak potential	Technique used	Concentration range (μ M)	Sensitivity (μ A/ μ M ⁻¹)	Correlation coefficient (R^2)	LOD (μ M)	LQ (μ M)	RSD [**] (%)
+0.97 V	CV	2-10	5.3	0.990	1.633	5.443	4.284
+0.80 V	DPV	2-12	11	0.984	0.801	2.671	0.572
+0.90 V	SWV	2-12	16	0.998	0.991	3.306	0.786
+0.95 V	Prec./SWV	0-0.8	336	0.952	0.013	0.045	0.224
		0.8-4	108	0.997	0.042	0.142	0.224
		0-4	138	0.952	0.033	0.111	0.224
+0.97 V	MPA	2-12	26.3	0.991	0.006	0.021	1.820
+1.25 V			3.1	0.895	0.055	0.185	5.402
+0.97 V	CA	2-12	0.296	0.979	1.547	5.158	2.476

[**] RSD: relative standard deviation was determined for three replicate

A recovery test was performed by analyzing three parallel tap water samples, which contained 2 μ M PCP. This test was run in 0.1 M Na₂SO₄ as supporting electrolyte and a recovery of 96% with an RSD of 2.8 % was found for PCP determination using MPA applying at three potential values, the first at +0.97 V/SCE for time duration of 50 ms, the second at +1.25 V/SCE for time duration of 50 ms, and the third one at -0.1 V/SCE for time duration of 50 ms. Finally, the results obtained with this method were compared with that obtained by means of a conventional spectrophotometrical method. Based on the results obtained, it can be concluded that the two methods lead to very close results and that the accuracy of the proposed MPA method is good.

6.1.4 Conclusions

MWCNT-EP composite electrode exhibited the electrocatalytic activity towards pentachlorophenol oxidation, which is controlled by diffusion, a desired aspect for electroanalysis. The electrochemical determination of PCP at MWCNT-EP composite electrode was achieved using CV, DPV, SWV, CA, and MPA techniques, which denotes different electroanalytical parameter. Despite the adsorption of PCP on MWCNT is an undesired aspect, this study demonstrated that this property should be exploited in a positive way for PCP determination at the trace level. Under optimized working conditions in relation with the accumulation time and PCP concentration, a significant enhancement of the determination of the electroanalytical parameters was achieved. However, for the practical application, CA as the simplest electrochemical technique did not lead to good electrochemical

detection results, probably because of electrode fouling. MPA applying led to improve the electroanalytical parameters of PCP detection, especially the lowest limit of detection, which makes the composite electrode appropriate for electrochemical determination of a wide range of PCP concentrations in an aqueous solution.

6.2 MWCNT-Epoxy composite electrode for salicylic acid (SA) and acetylsalicylic acid (ASA) detection

6.2.1 Salicylic acid (SA)

Salicylic acid (SA) also known as 2-hydrobenzoic acid, shown in Figure 6.11 is one of an organic micro molecular compound. It is widely distributed in various plants, as an endogenous signalling molecule, playing an important role in the regulation of many physiological processes in plants such as flowering, heat production, seed germination, membrane permeability, and ion adsorption. At the same time, SA is an important chemical and curative raw material which has been widely used in cosmetics [6.22], lotions, and pharmaceuticals industry [6.23] due to its distinct exfoliating and antiseptic, antipyretic, analgesic, and anti-inflammatory properties. SA is also a primary hydrolysate of acetylsalicylic acid (ASA) which is commonly used as anti-inflammatory medicine, and SA determination can be regarded as an indirect determination of ASA. Therefore, the effective and convenient determination of SA represents a very important issue of research.

Many analytical methods for SA determination have been described in literature, such as fluorescence spectrometry [6.24], [6.25], high-performance liquid chromatography [6.26], potentiometry [6.27], amperometry [6.28], voltammetry [6.29], and enzymatic methods [6.30], [6.31]. However, most of the above mentioned methods need a series of sample pretreatments and high cost complicated operation or exhibit poor efficiency.

Recently, the determination of SA with electrochemical methods has received much attention because of sensitivity and simplicity. In the present study, the voltammetric determination of SA and ASA using a MWCNT-EP composite electrode has been investigated.

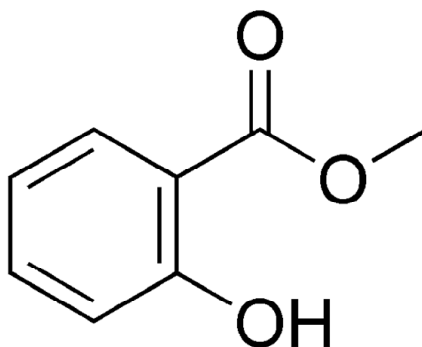


Figure 6.11 Chemical formula of salicylic acid (SA)

6.2.2 Experimental

Reagents

All reagents were of analytical grade and were used as-received without any further purification. A 0.1 M stock solution of SA was prepared daily by dissolving SA in 0.3 M NaOH for testing. All solutions were prepared using double distilled water. The electrochemical measurements were performed in a 0.1 M NaOH supporting electrolyte and a 0.1 M Na₂SO₄ supporting electrolyte, respectively.

Apparatus and procedures

The electrochemical performance of this electrode was studied by cyclic voltammetry (CV), differential-pulse voltammetry (DPV), square-wave voltammetry (SWV), and chronoamperometry (CA).

Electrochemical measurements were performed in unstirred solutions using a computer controlled Autolab potentiostat/galvanostat PGSTAT 302 (EcoChemie, The Netherlands), with a standard three-electrode configuration. The three-electrode system consisted of a MWCNT-EP working electrode with 0.196 cm² geometrical area, a platinum wire as counter electrode, and a saturated calomel reference electrode (SCE). Before each voltammogram, the MWCNT-EP composite electrode was carefully polished with abrasive paper and then on a felt-polishing pad by using 0.3 μm alumina powder (Metrohm, Switzerland). The electrode was then subsequently sonicated for 5 min in pure water. All experiments were carried out with an electrochemical cell of 50 mL at room temperature (25°C).

6.2.3 Results and discussion

Figure 6.12 shows the cyclic voltammograms (CVs) recorded in 0.1 M Na₂SO₄ supporting electrolyte (curve 1) in the presence of 0.6 mM salicylic acid (SA) (curve 2) and 0.1 M NaOH supporting electrolyte (curve 3), and also, in the presence of 0.6 mM salicylic acid (SA) (curve 4). CV shapes show that the MWCNT-EP composite electrode exhibits several differences of the electrochemical behavior in different supporting electrolytes. Thus, as we expected, in 0.1 M NaOH supporting electrolyte the background current corresponding to the capacitive component is higher in comparison with 0.1 M Na₂SO₄ supporting electrolyte, and the oxygen evolution occurred at a lower overpotential (0.68 V in comparison with 0.72 V vs. SCE determined in 0.1 Na₂SO₄ supporting electrolyte). These aspects are not desired for the electroanalysis, but a lower overpotential for SA oxidation is required in 0.1 M NaOH (0.5 V versus 0.6 V/SCE in 0.1 M Na₂SO₄), which provided potential for application in the electroanalysis, regarding interference avoiding and the simultaneous detection in the presence of other analytes.

Based on these results, the further experiments for SA detection have been performed in both the supporting electrolytes, 0.1 M Na₂SO₄ (pH 7) and 0.1 M NaOH (pH 12).

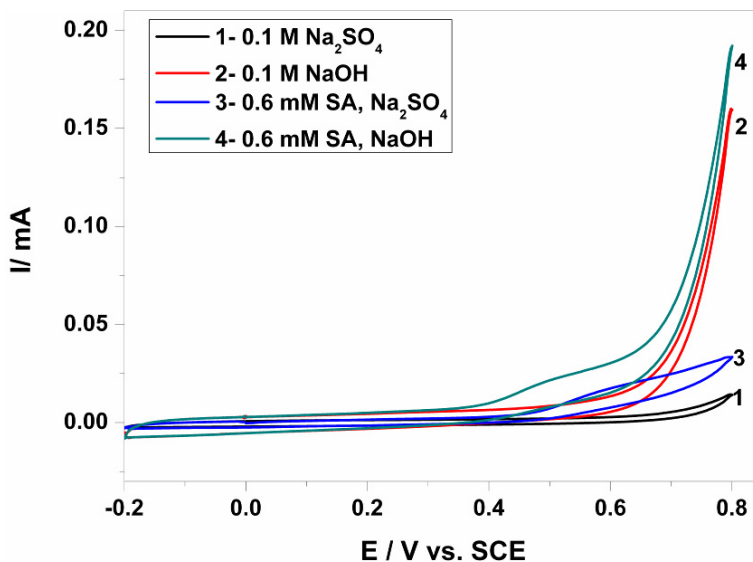
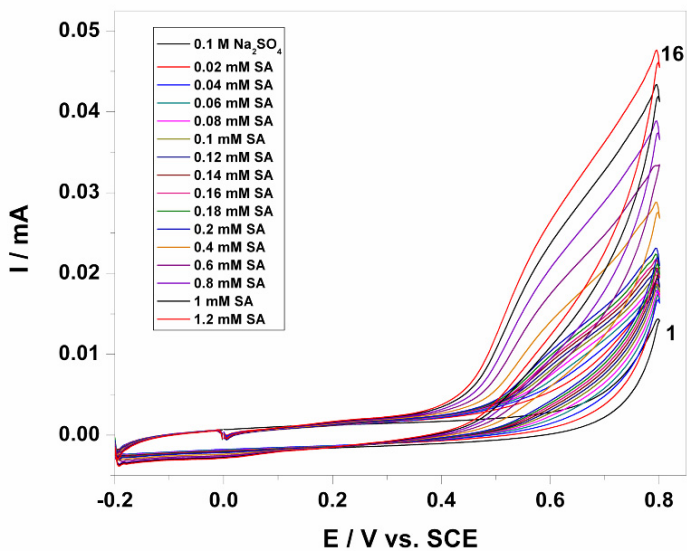


Figure 6.12 CVs of the MWCNT-EP composite electrode in 0.1 M Na_2SO_4 supporting electrolyte (1) and in the presence of 0.6 mM SA (3), and in 0.1 M NaOH supporting electrolyte (2), and in the presence of 0.6 mM SA (4).

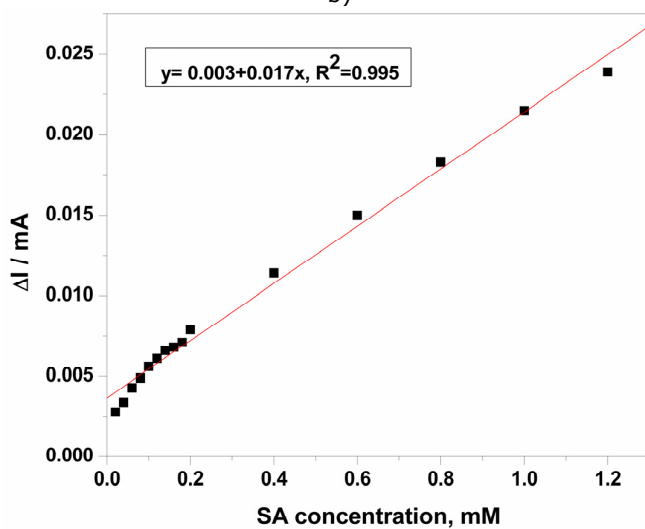
6.2.3.1 Electrochemical detection of salicylic acid in 0.1 M Na_2SO_4 supporting electrolyte

Figure 6.13 (a) depicts a series of CVs obtained for SA standard solution recorded over the concentration range of 0.02 mM–1.2 mM. These results show that the oxidation process of SA occurred at the potential value of +0.6 V vs. SCE and the lack of the corresponding cathodic peak revealed the irreversibility of this oxidation process. The anodic peak increased progressively with SA concentration and the calibration data plot of anodic current peaks versus concentration of SA exhibited good linearity and sensitivity (see Table 6.6 and Figures 6.13 c and d) over two SA concentration ranges because no linear dependence of the anodic current versus SA concentration was achieved for the studied concentration range (see Figure 6.13 (b)). The linear dependence between anodic oxidation current peaks and SA concentrations confirmed the diffusion controlled oxidation process, which is required for the application in voltammetric/amperometric detection.

a)



b)



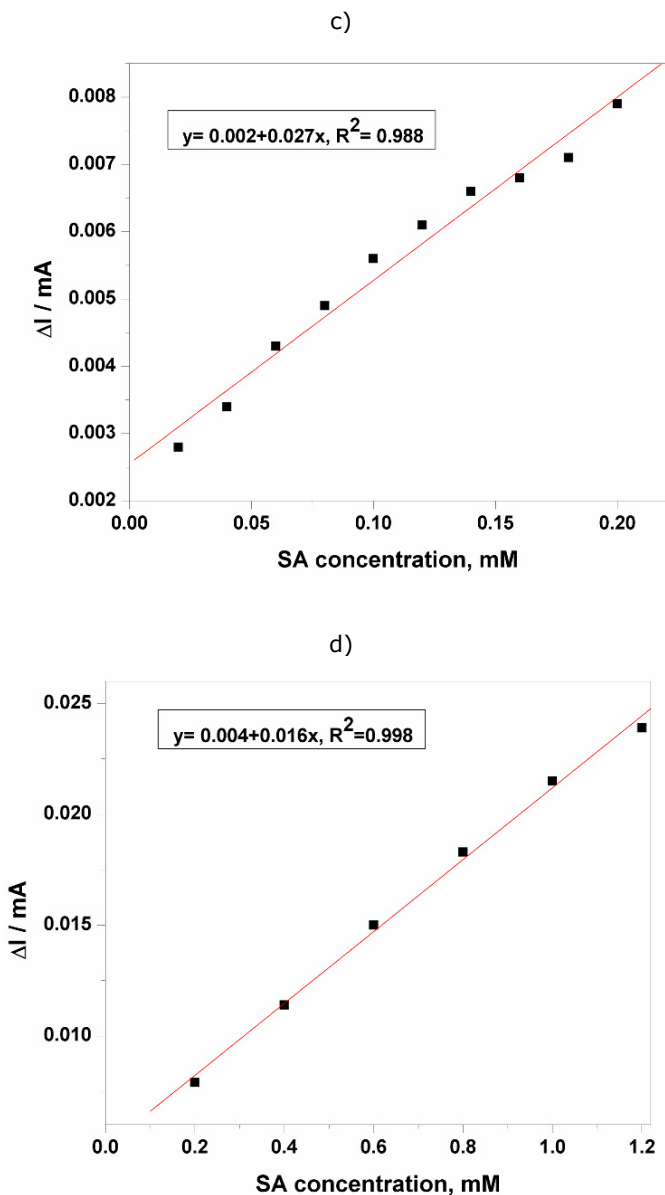


Figure 6.13 (a) CVs of the MWCNT-EP composite electrode in 0.1 M Na_2SO_4 supporting electrolyte (curve 1) and in the presence of: 0.02, 0.04, 0.06, 0.08, 0.1, 0.12, 0.14, 0.16, 0.18, 0.2, 0.4, 0.6, 0.8, 1, 1.2 mM SA; scan rate 0.05 Vs^{-1} . (b) Calibration plots of anodic peak currents recorded at $E = +0.60 \text{ V/SCE}$ vs. SA concentration.

A possible scheme of the oxidation of SA is shown in figure 6.14 [6.32]:

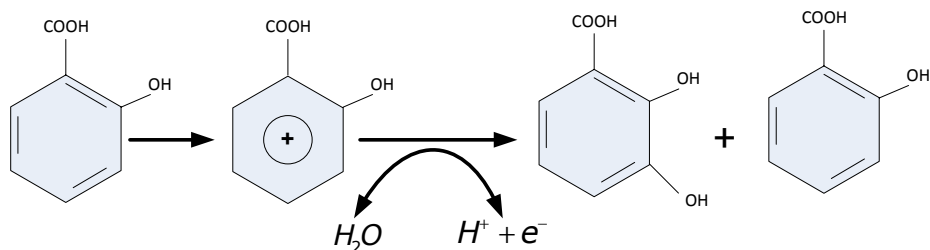
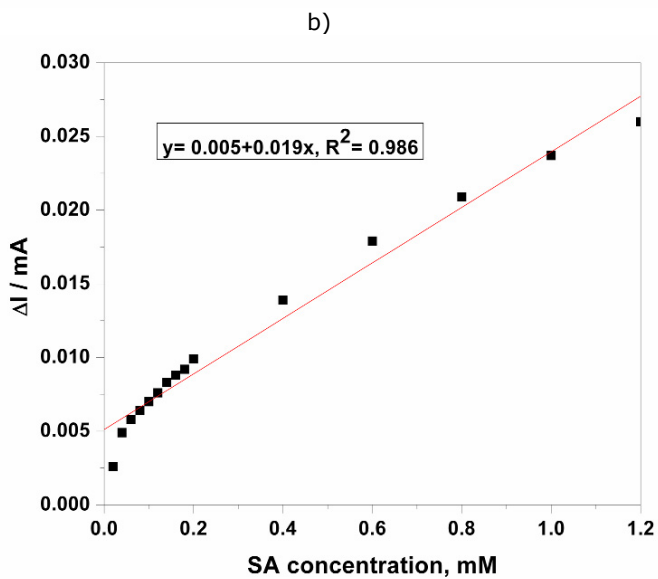
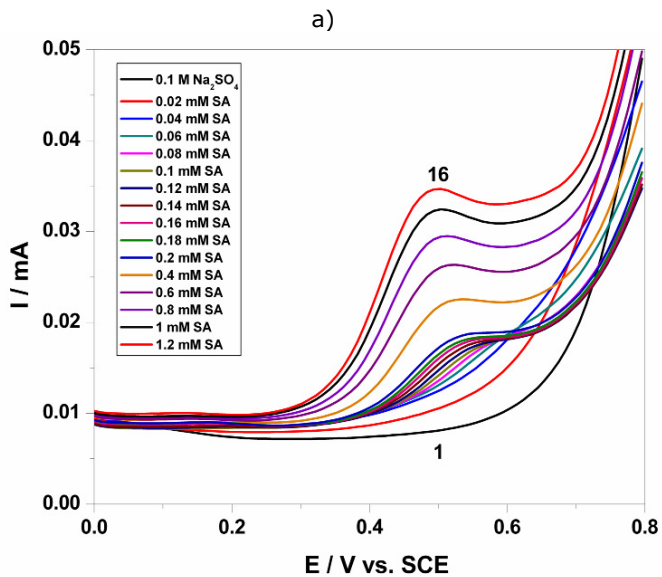


Figure 6.14 The possible scheme of oxidation of SA [6.32]

After this preliminary discussion of cyclic voltammetry data and confirmation of diffusion controlled anodic process, more detailed investigations with electroanalytical application purposes were conducted using two other different techniques, i.e., differential- pulsed voltammetry and square-wave voltammetry.

A series of anodic DPVs presented in Figure 6.15 involving the SA concentration effect at MWCNT-EP composite electrode in 0.1 M Na_2SO_4 supporting electrolyte were recorded over the concentration range of 0.02 mM–1.2 mM SA similar to CV investigation using the SA standard solution. The two SA concentration ranges established based on the linear dependence of the anodic current versus SA concentration were the same as for CV results (see Figure 6.13 c and d). In comparison with CV results, this technique exhibited the advantage of a lower overpotential for SA oxidation (+0.52 V versus +0.6 V/SCE). The calibration plot showed a slightly better sensitivity of $0.035 \text{ mA} \cdot \text{mM}^{-1}$ and a good linearity with a correlation coefficient of 0.970. The LOD value of 0.009 mM is very close to the value obtained when using the CV technique and it was calculated according to the same above-mentioned $3S_B/b$.



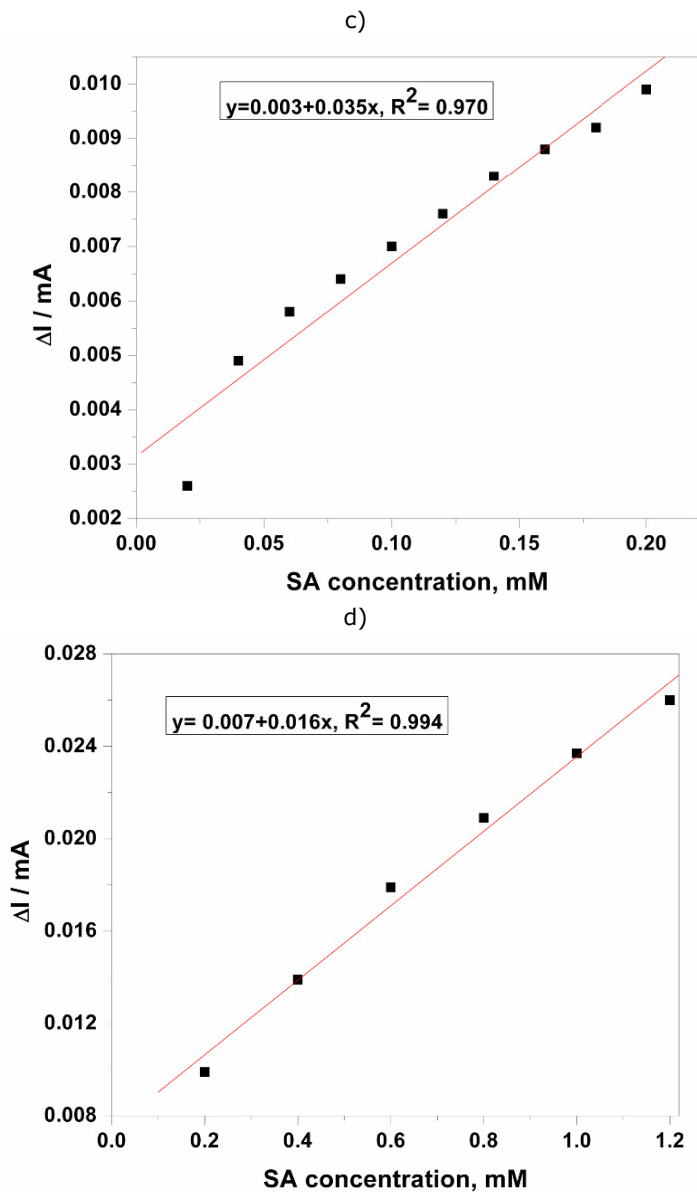
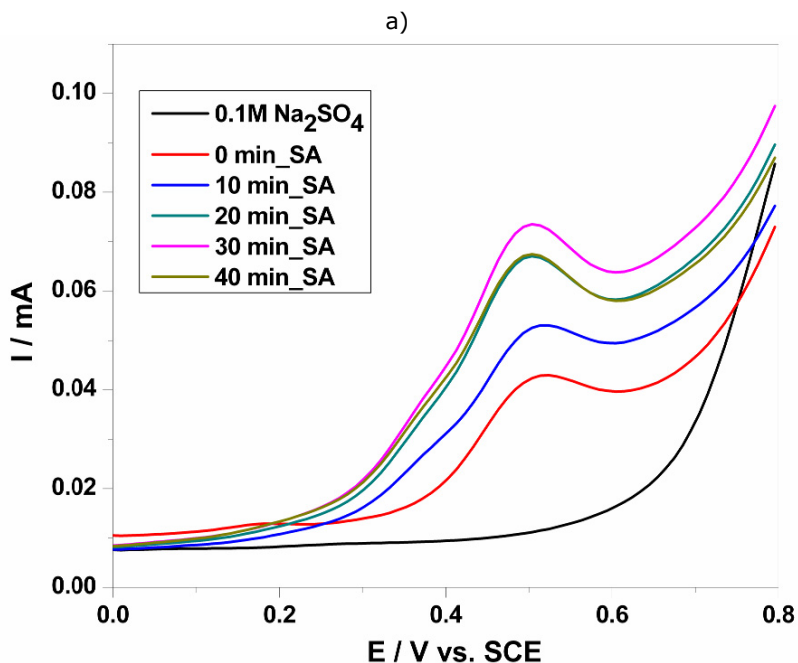


Figure 6.15 (a) DPVs of the MWCNT-EP composite electrode in 0.1M Na_2SO_4 supporting electrolyte (curve 1) (modulation amplitude 0.1 V, step potential 0.01 V), potential scan rate of 0.05 Vs^{-1} in the presence of: 0.02, 0.04, 0.06, 0.08, 0.1, 0.12, 0.14, 0.16, 0.18, 0.2, 0.4, 0.6, 0.8, 1, 1.2 mM SA concentrations. (b) Calibration plots of the anodic currents recorded at $E = +0.52 \text{ V}$ vs. SA concentration in the concentration range: b) 0.02 -1.2 mM SA, c) 0.02-0.2mM SA d) 0.2-1.2 mM SA.

The adsorption capacity of the MWCNT-EP composite electrode towards SA has been investigated envisaging a possible enhancement of the SA detection in relation with the lowest limit of detection and the sensitivity. The adsorption study was carried out by storing the electrode in 0.4 mM SA in 0.1 Na₂SO₄ supporting electrolyte at open-circuit potential at different accumulation times, and subsequently DPVs were recorded. The results are presented in Figure 6.16 and it can be seen that the optimum accumulation is 30 minutes, at which the steady-state is reached. At longer accumulation times, the current corresponding to the SA oxidation decreased, because of a possible over-saturation of the electrode surface with SA, which can also lead to electrode fouling. Under these working conditions an enhancement factor, determined as previously mentioned, of 1.9 was achieved and the further experiment involved a preconcentration step for 30 minutes before DPV applying.



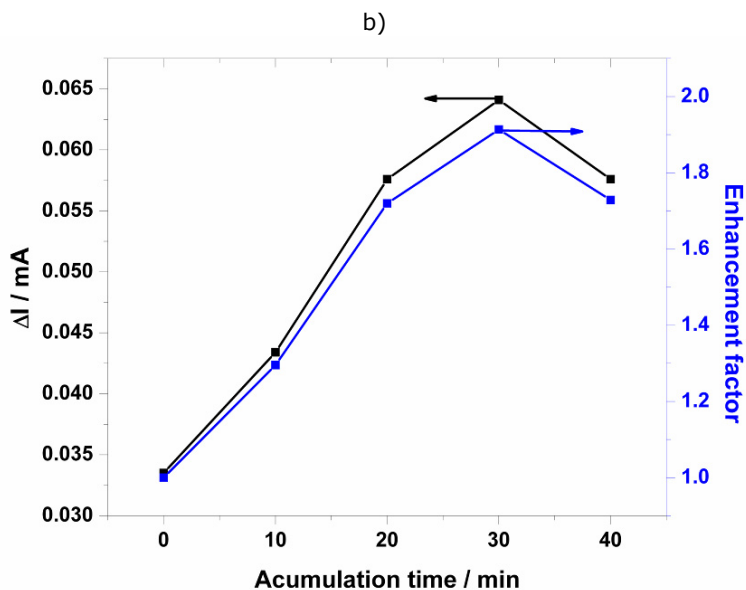


Figure 6.16 DPVs of the MWCNT-EP composite electrode (modulation amplitude 0.1 V, step potential 0.01 V), potential scan rate of 0.05 Vs^{-1} in 0.1M Na_2SO_4 supporting electrolyte and 0.4 mM SA after different accumulation times: 0 min; 10 min; 20 min; 30 min; 40 min. (b) Peak current responses and enhancement factor for the detection of 0.4 mM PCP at MWCNT-EP composite electrode as a function of the accumulation time recorded at $E = +0.46 \text{ V/SCE}$

In Figure 6.17 presents a series of DPVs on the MWCNT-EP composite electrode recorded under the optimum conditions of the preconcentration scheme that assume the accumulation time of 30 minutes within SA concentrations ranging from 0.02 to 0.1 mM SA. A better sensitivity and the lowest limit of detection were achieved (see Table 6.6).

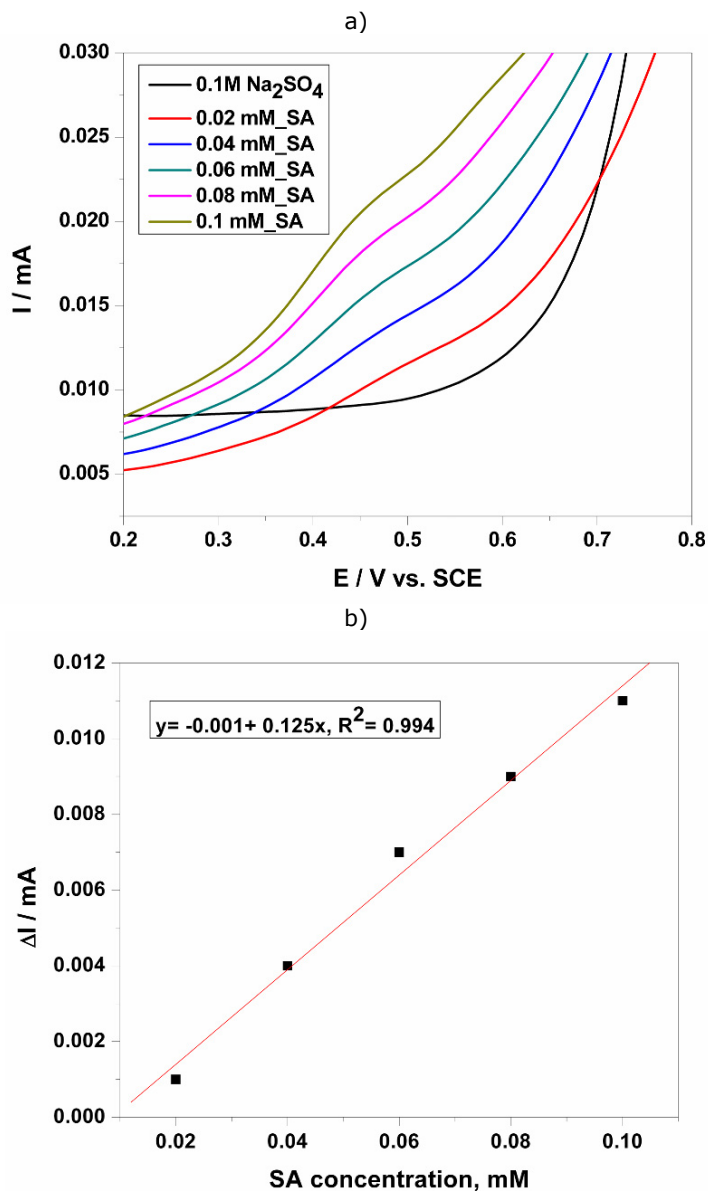
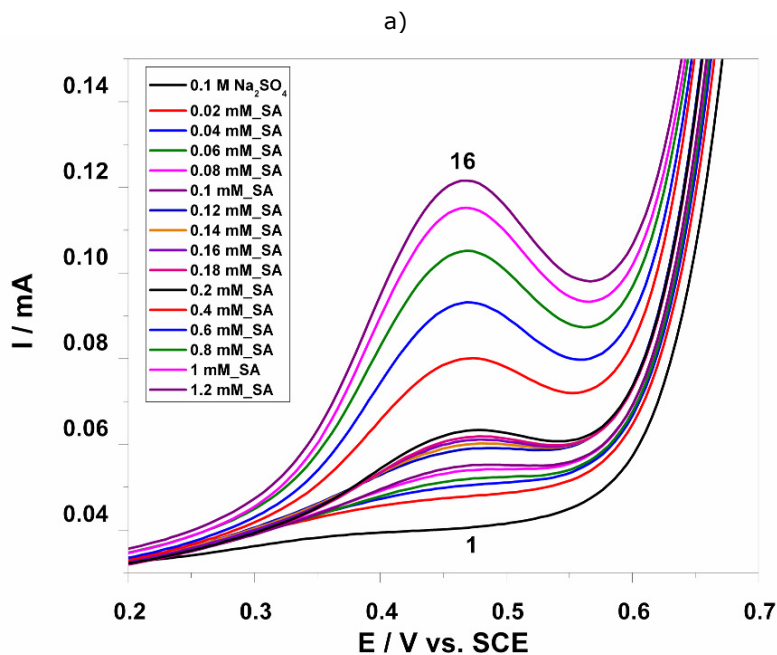


Figure 6.17 (a) DPVs of the MWCNT-EP composite electrode (modulation amplitude 0.1 V, step potential 0.01 V), potential scan rate of 0.05 Vs^{-1} in 0.1M Na_2SO_4 supporting electrolyte and different SA concentrations: 0.02, 0.04, 0.06, 0.08, 0.1 mM SA after 30 min of accumulation time at $E = +0.46 \text{ V/SCE}$. (b) Calibration plot of anodic peak currents recorded at $E = +0.46 \text{ V/SCE}$ vs. SA concentrations.

The other pulsed technique tested to improve the electroanalytical performance for SA detection using the MWCNT-EP composite electrode is square-

wave voltammetry (SWV). Figure 6.18 (a) depicts a series of SWVs recorded using the MWCNT-EP composite electrode over the same SA concentration range (0.02-1.2 mM SA) under optimized conditions, i.e., modulation amplitude 0.05 V, step potential 0.005 V, and frequency of 50 Hz. Figure 6.18 (b) corresponds to the analytical curve, that is, the linear dependence of useful current with SA concentration ranged between 0.02 and 1.2 mM SA. For the SA concentration higher than 1.2 mM a non-linear dependence was noticed because of the saturation electrode surface with SA and/or fouling effect of the electrode surface.



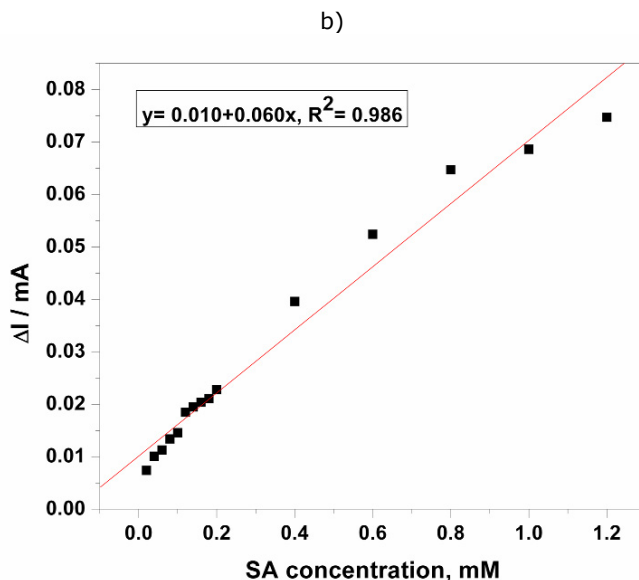


Figure 6.18 (a) SWVs of the MWCNT-EP composite electrode in 0.1M Na₂SO₄ supporting electrolyte (curve 1) (modulation amplitude 0.05 V, step potential 0.005 V, frequency of 50 Hz), and in the presence of: 0.02, 0.04, 0.06, 0.08, 0.1, 0.12, 0.14, 0.16, 0.18, 0.2, 0.4, 0.6, 0.8, 1, 1.2 mM SA concentrations. (b) Calibration plot of the anodic currents recorded at E = +0.46 V vs. SA concentration.

The lowest limit of detection (LOD) and the lowest limit of quantification (LQ) have been calculated according to $3S_b/b$, and respectively, $10S_b/b$ criteria, where S_b was estimated as the standard deviation applied to the voltammetric signal measured for the blank, the slope of the straight line in the analytical curve and RSD ranged between 1 and 3%.

The electroanalytical parameters determined for the voltammetric detection of SA using the MWCNT-EP composite electrode in 0.1 M Na₂SO₄ supporting electrolyte are gathered in Table 6.6.

Table 6.6 The electroanalytical performance of the MWCNT-Epoxy composite electrode for the voltammetric detection of SA in 0.1 M Na₂SO₄ supporting electrolyte.

Peak potential	Technique used	Concentration range (mM)	Sensitivity (mA /mM ⁻¹)	Correlation coefficient (R ²)	LOD (mM)	LQ (mM)	RSD [**] (%)
+0.60 V	CV	0.02-1.2	0.017	0.995	0.012	0.041	2.8
+0.52 V	DPV	0.02-1.2	-	-	-	-	-
		0.02-0.2	0.035	0.970	0.009	0.031	1.315
		0.2-1.2	0.016	0.994	0.015	0.055	1.315
+0.46 V	Prec./DPV	0.02-0.1	0.125	0.994	0.002	0.04	2.90
+0.46 V	SWV	0.02-1.2	0.060	0.986	0.005	0.016	0.250

6.2.3.2 Electrochemical detection of salicylic acid in 0.1M NaOH supporting electrolyte

Figure 6.19 (a) shows a series of CVs obtained for SA standard solution recorded over the concentration range of 0.6 mM–3.6 mM. The anodic peak corresponding to direct oxidation of SA on the electrode surface was noticed at about +0.5 V vs. SCE, which increased progressively with SA concentration. A linear dependence between anodic current and SA concentration was noticed, and a good sensitivity was reached (see Figure 6.19 (b) and Table 6.7). Based on the above-presented results in 0.1 M Na₂SO₄, the similar experiments have been performed to compare and select the best operational conditions for SA and further, for acetylsalicylic acid (ASA) detection.

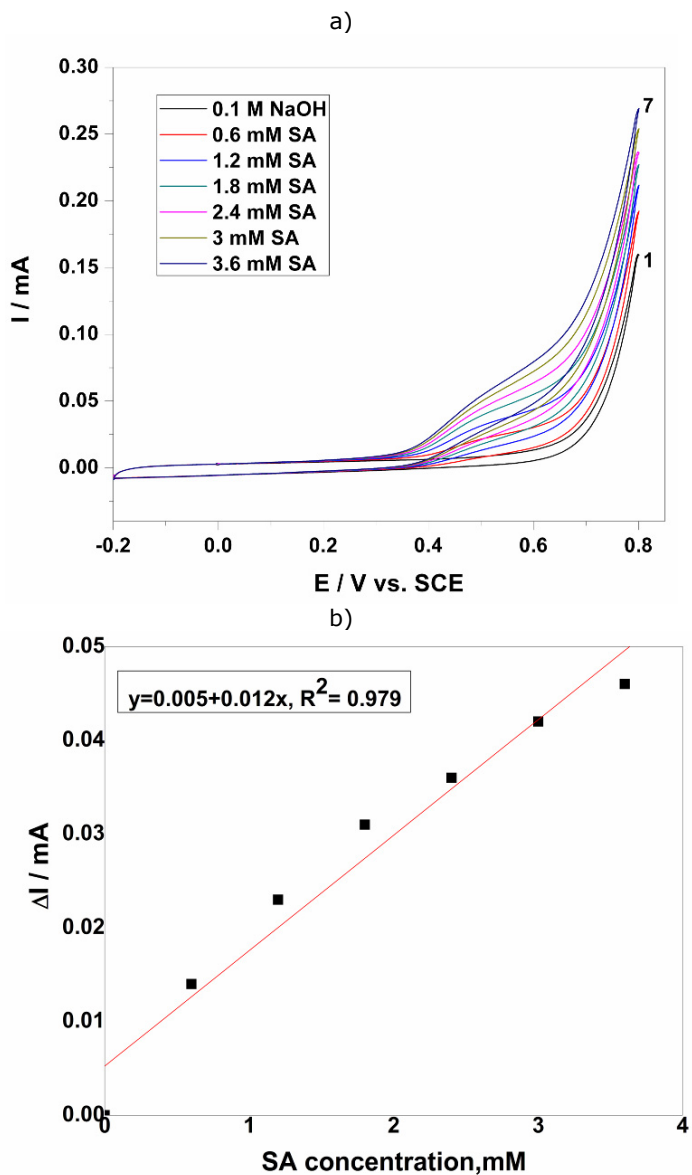
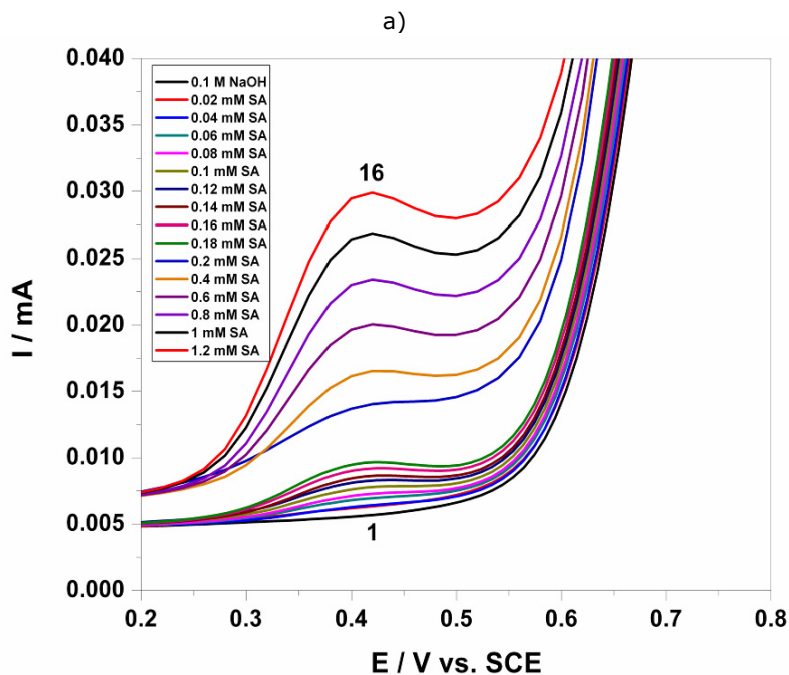


Figure 6.19 (a) CVs of the MWCNTs-EP electrode recorded at a potential scan rate of 0.05 Vs^{-1} , potential range between -0.2 V and $+0.8 \text{ V/SCE}$ in 0.1 M NaOH supporting electrolyte (curve 1) and in the presence of different SA concentrations: 2) 0.6 mM , 3) 1.2 mM , 4) 1.8 mM , 5) 2.4 mM , 6) 3 mM , 7) 3.6 mM . (b) Calibration plot of the anodic currents recorded at $E = +0.50 \text{ V/SCE}$ vs. SA concentration.

Differential-pulsed voltammetry (DPV) has been employed as technique for the evaluation of the performance of the MWCNT-EP composite electrode for the comparative voltammetric SA assessment. Figure 6.20 (a) presents a series of DPVs recorded in the same conditions as 0.1 M Na₂SO₄ supporting electrolyte (previously presented), and can be noticed a more lower overpotential for SA oxidation (+0.41 V/SCE).



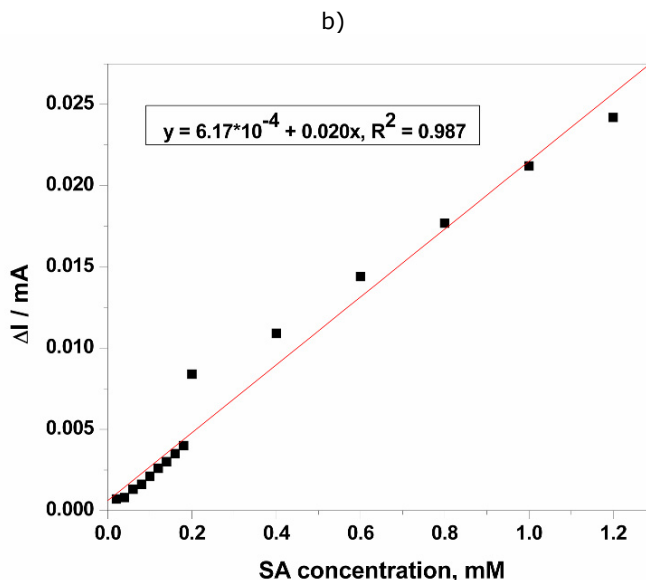


Figure 6.20 (a) DPVs of the MWCNT-EP electrode at (modulation amplitude 0.1 V, step potential 0.01 V), potential scan rate of 0.05 Vs⁻¹ and the potential range between +0.2 V and +0.8 V vs. SCE in 0.1 M NaOH supporting electrolyte (curve 1) and in the presence of different PCP concentrations: 2) 0.02 mM, 3) 0.04 mM, 4) 0.06 mM, 5) 0.08 mM, 6) 0.1 mM, 7) 0.12 mM, 8) 0.14 mM, 9) 0.16 mM, 10) 0.18 mM, 11) 0.2 mM, 12) 0.4 mM, 13) 0.6 mM, 14) 0.8 mM, 15) 1mM, 16) 1.2 mM. (b) Calibration plot of the anodic currents recorded at E= +0.41 V/SCE vs. SA concentration.

Under the working conditions of DPV applying (modulation amplitude of 0.1 V, step potential of 0.01 V), the preconcentration/differential-pulsed voltammetric detection scheme prior established in 0.1 M Na₂SO₄ supporting electrolyte, which assumed 30 minutes accumulation time of SA by maintaining the electrode in a well-known SA concentration under OCP conditions, led also to improve the electroanalytical performance of MWCNT for SA detection. Figure 6.21 (a) depicts a series of DPVs recorded after 30 minutes SA sorption on the electrode surface over the SA concentration range between 0.02 and 0.1 mM SA. Figure 6.21 (b) present the calibration plots data of differential-pulsed anodic current peaks versus concentration of SA exhibited good linearity and better sensitivity (see Table 6.7).

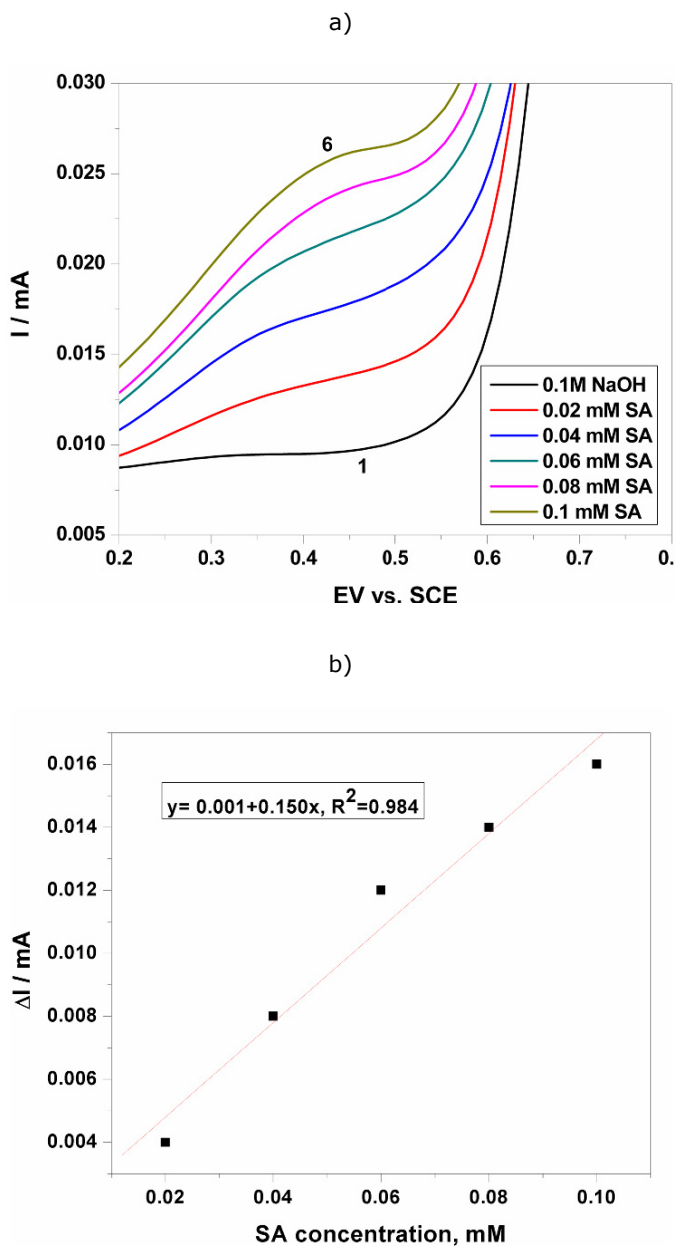
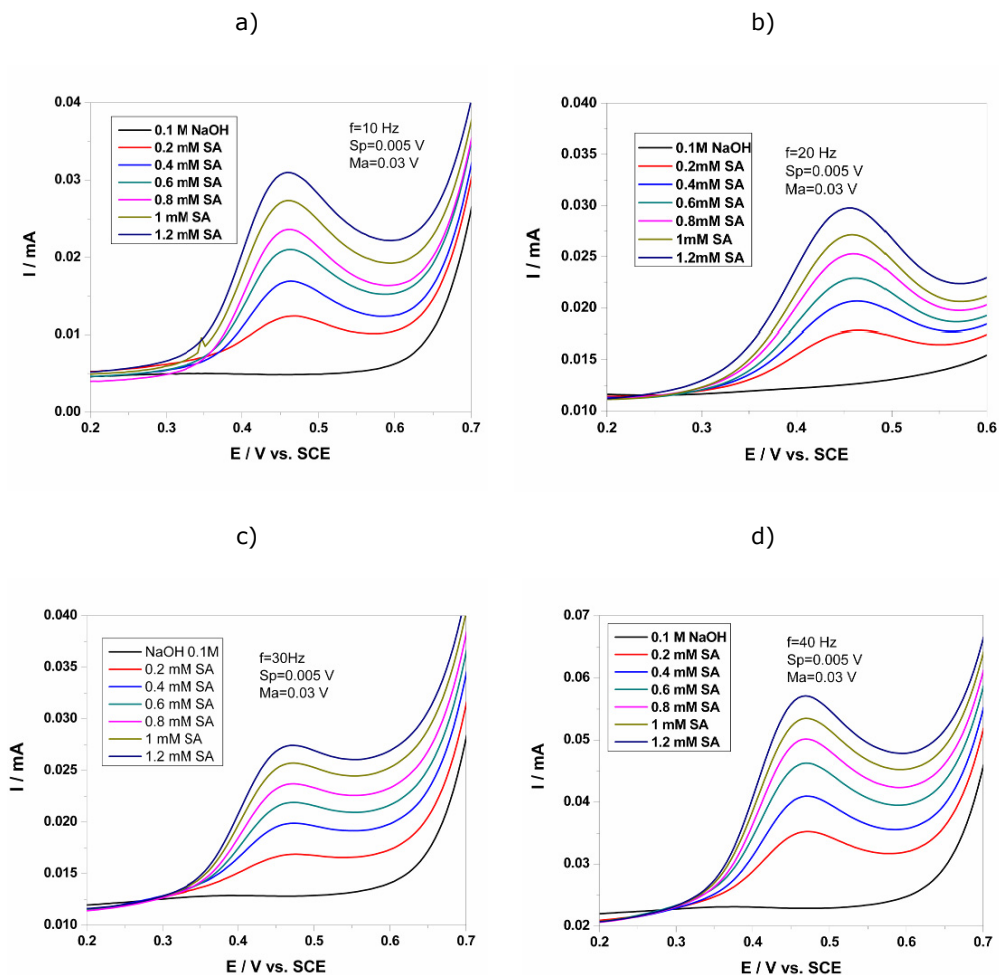


Figure 6.21 (a) DPVs of the MWCNT-EP composite electrode (modulation amplitude 0.1 V, step potential 0.01 V), potential scan rate 0.05 Vs^{-1} in 0.1M NaOH supporting electrolyte and different SA concentrations: 0.02, 0.04, 0.06, 0.08, 0.1 mM SA after 30 min of accumulation time at $E = +0.41 \text{ V/SCE}$. (b) Calibration plot of the anodic currents recorded at $E = +0.41 \text{ V/SCE}$ vs. SA concentration.

Square-wave voltammetry parameters

In order to obtain the optimum conditions for the determination of SA by means of SWV technique, various instrumental parameters such as step potential, modulation amplitude, and frequency were studied over the concentration range 0.2-1.2 mM SA, and the sensitivity and the oxidation potential were determined.

The influence of frequency on the SWV signal expressed as sensitivity was studied for the frequency ranged from 10 to 100 Hz, and Figure 22 (a-f) shows the series of SWVs recorded at the modulation amplitude of 0.03 V, the step potential of 0.005 V and various frequencies, e.g., 10, 20, 30, 40, 50, 100 Hz.



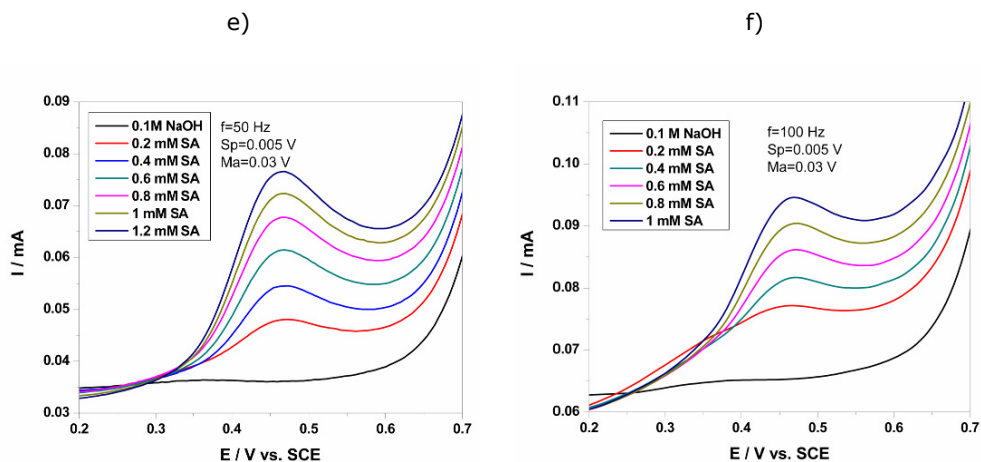
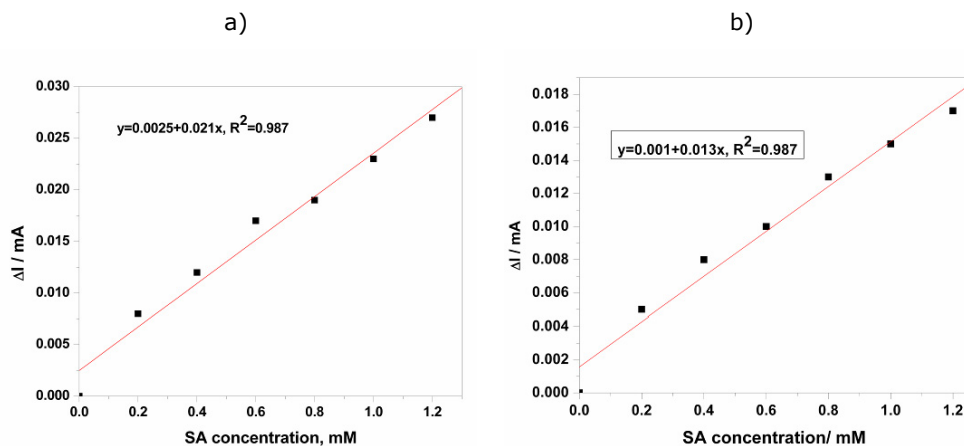


Figure 6.22 SWVs on MWCNT-EP composite electrode (step potential=0.03 V, modulation amplitude=0.005 V), potential range +0.2 to +0.7 V vs. SCE in 0.1 M NaOH and the corresponding signal to SA oxidation in the concentration range 0.2-1.2 mM SA at different frequencies: a) $f=10 \text{ Hz}$, b) $f=20 \text{ Hz}$, c) $f=30 \text{ Hz}$, d) $f=40 \text{ Hz}$, e) $f=50 \text{ Hz}$ and f) $f=100 \text{ Hz}$.

Figure 23 (a-f) shows the calibration plots corresponding to SWVs recorded at the modulation amplitude of 0.03 V, step potential of 0.005 V and various frequencies, e.g., 10, 20, 30, 40, 50, 100 Hz.



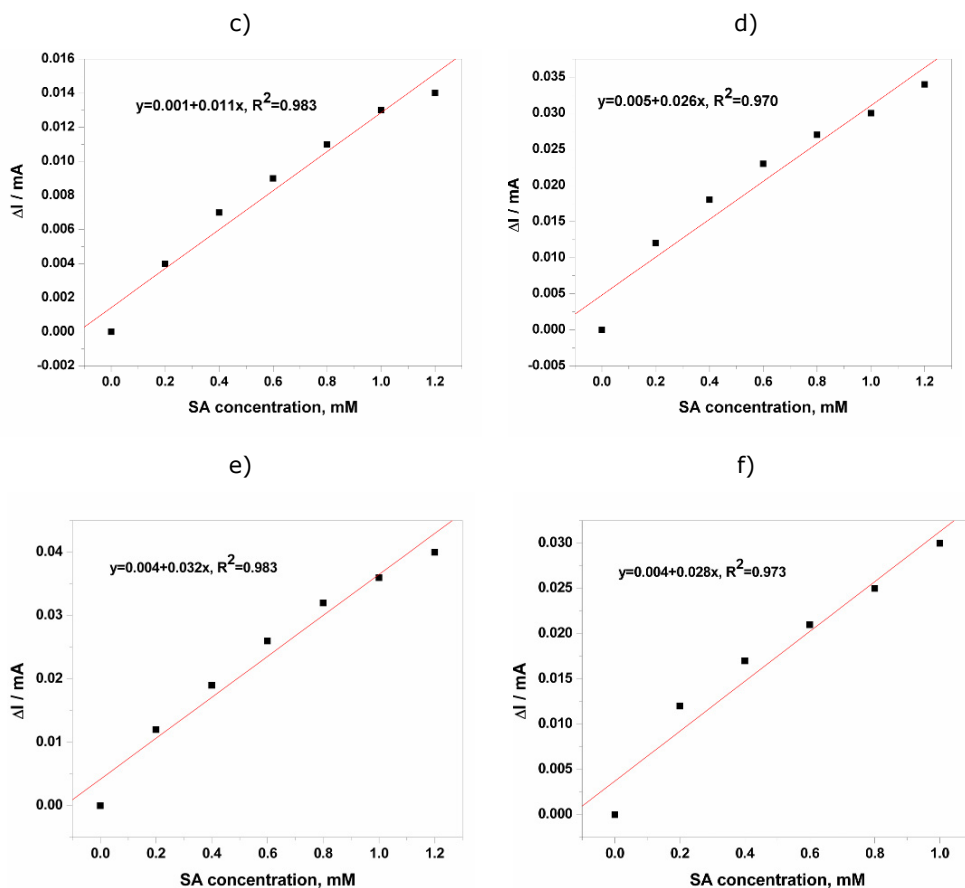


Figure 6.23 Calibration plots of the anodic current recorded at $E=+0.46$ V/SCE vs. SA concentration at different frequencies: a) $f=10$ Hz, b) $f=20$ Hz, c) $f=30$ Hz, d) $f=40$ Hz, e) $f=50$ Hz and f) $f=100$ Hz.

There was no an obvious dependence of the sensitivity with the frequency, but the best sensitivity was reached for frequency of 50 Hz, selected as optimum for the further experiments. Then, for the frequency of 50 Hz, the effect of the step potential was followed. The step potential values of 0.0025 V, 0.005 V and 0.01 V were applied and the series of SWV recorded for the first and second step potential are presented in Figure 6.24 (a and b). Under the conditions of the step potential of 0.01 V, no reproducible responses were achieved, and this step potential value was eliminated (the results are not shown here). It can be noticed that the step potential value of 0.005 V was selected as optimum. Also, the final step of optimization consisted of the study of the modulation amplitude effect on the SWV signals.

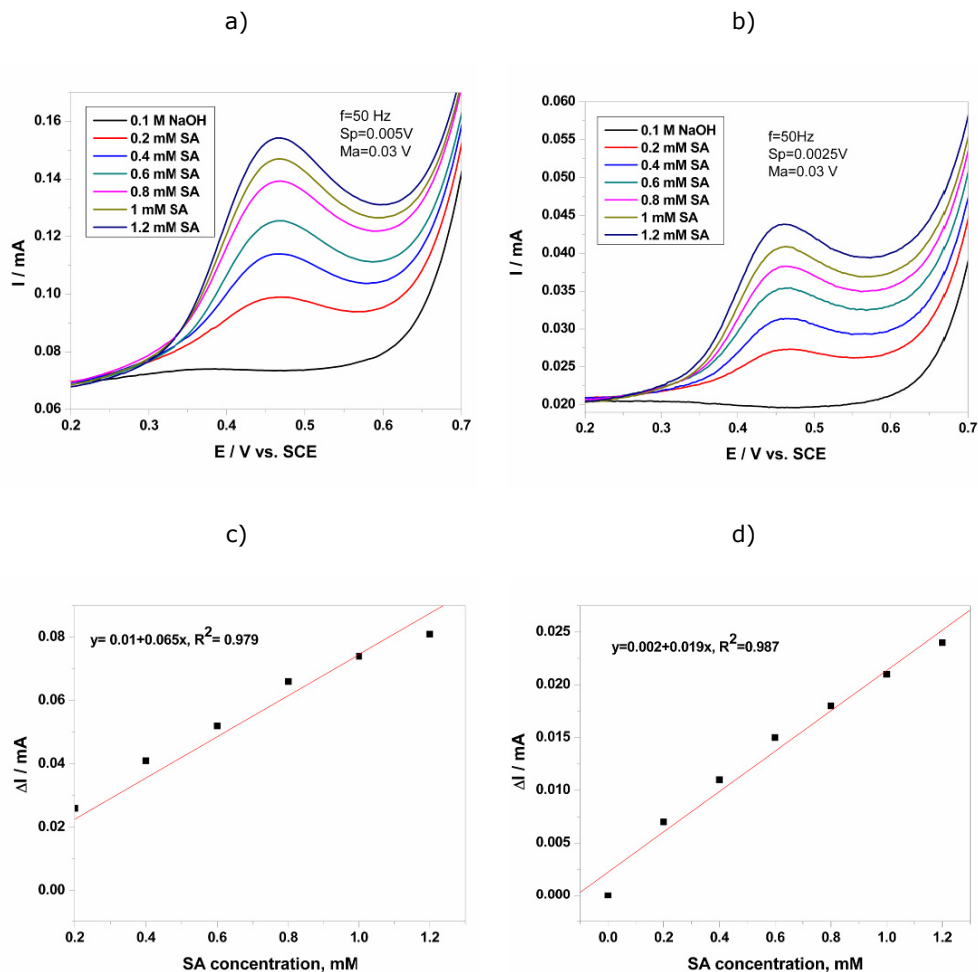


Figure 6.24 SWVs on MWCNT-EP composite electrode (frequency= 50 Hz, modulation amplitude= 0.03 V), potential range +0.2 to +0.7 V vs. SCE in 0.1 M NaOH and in the concentration range 0.2-1.2 mM SA at different step potentials: a) $Sp=0.005$ V and b) $Sp=0.0025$ V. (c and d) Calibration plots of the anodic current recorded at $E = +0.46$ V/SCE vs. SA concentration.

The modulation amplitude values of 0.03 V, 0.05 V and respective, 0.1 V were applied and the corresponding SWV series are presented in Figure 6.25 (a-c). The best response was achieved under 0.05 V modulation amplitude applying.

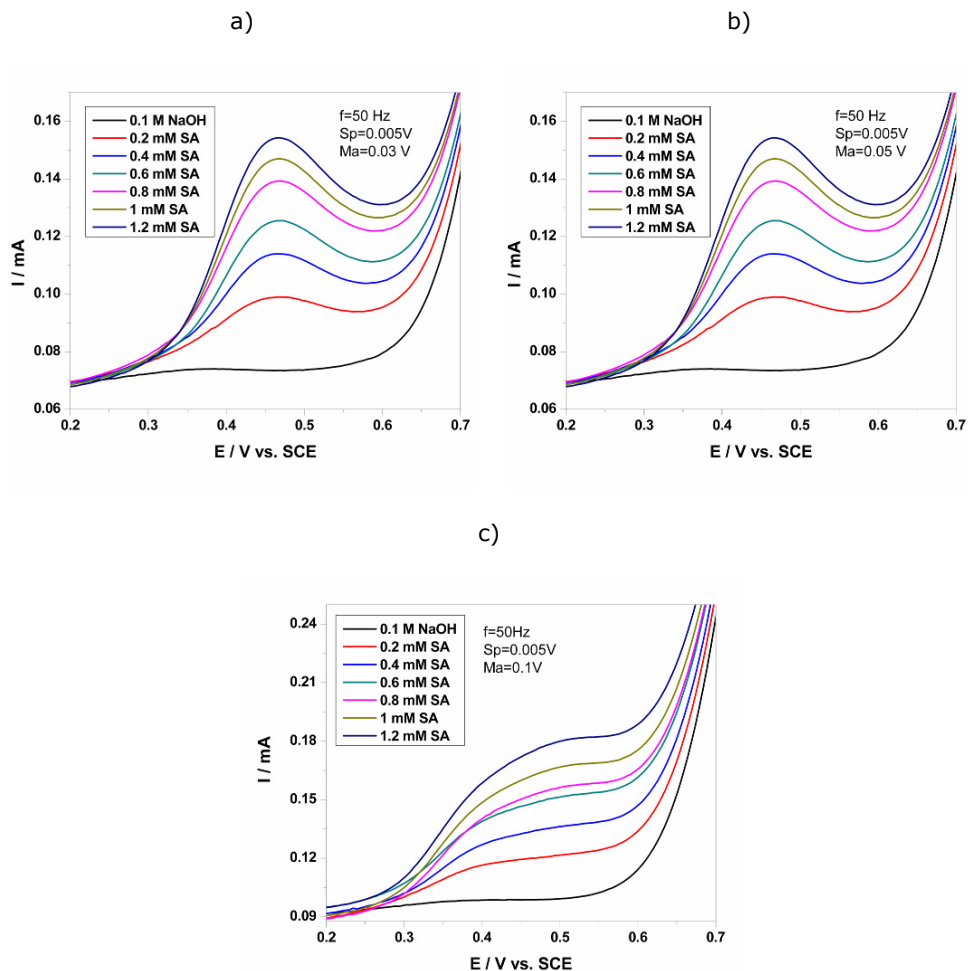


Figure 6.25 SWVs of the MWCNT-EP composite electrode (frequency= 50 Hz, step potential=0.005 V), potential range +0.2 to +0.7 V vs. SCE in 0.1 M NaOH and in the concentration range 0.2-1.2 mM SA at different modulation amplitude: a) $Ma=0.003 \text{ V}$, b) $Ma=0.005 \text{ V}$ and c) $Ma=0.1 \text{ V}$.

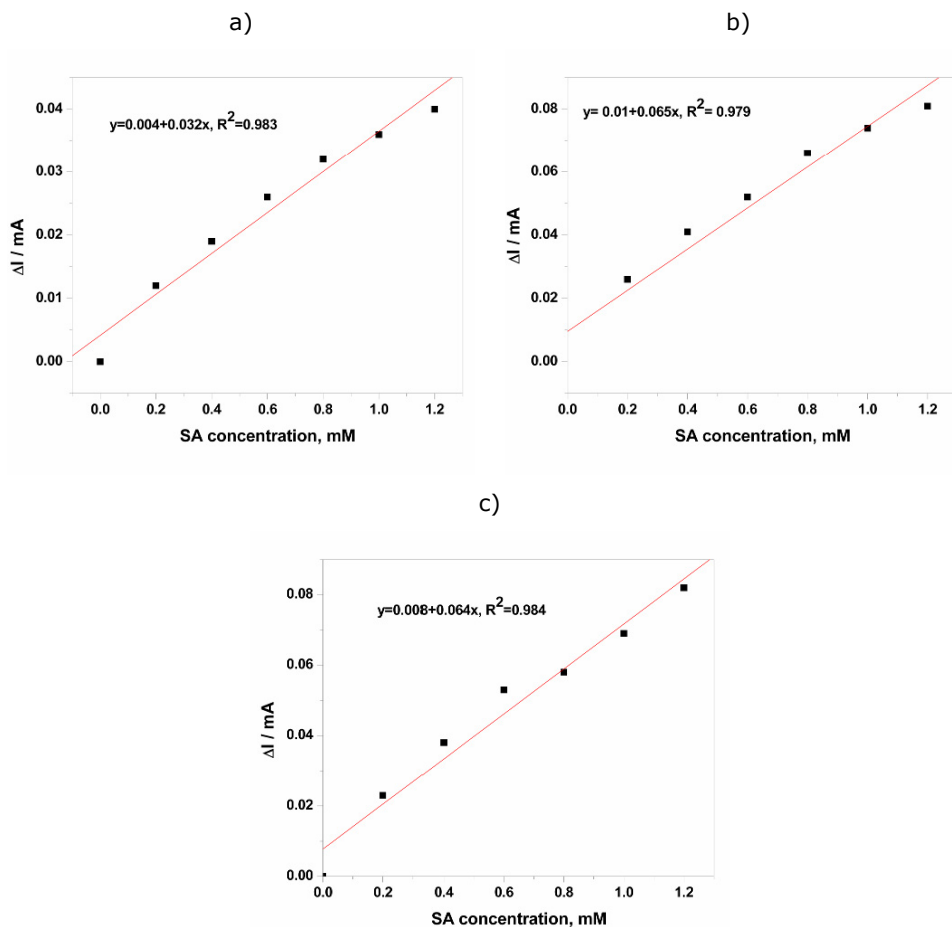


Figure 6.26 Calibration plots of the anodic current recorded at $E=+0.46$ V/SCE vs. SA concentration at different modulation amplitude: a) $Ma= 0.03$ V, b) $Ma= 0.05$ V and c) $Ma=0.1$ V.

A general representation of the optimization scheme is shown in Figure 6.27, and the optimized SWV technique application assumes the step potential of 0.005 V, the modulation amplitude of 0.05 V and the frequency of 50 Hz.

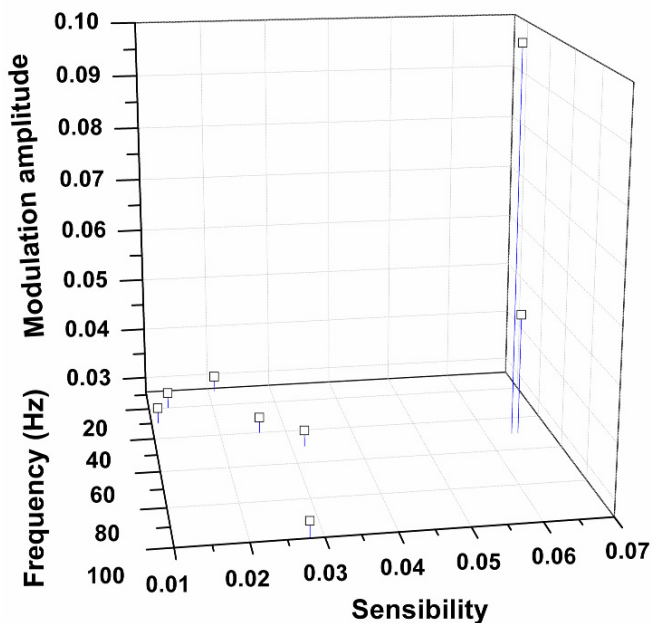


Figure 6.27 3D Optimization SWV parameters

The chronoamperometry was also employed as the easiest detection method in two variants, without and under stirring conditions. Figure 6.28 (a) shows CAs measurements of SA using the MWCNT-EP composite electrode under stationary conditions. This figure represents the current-time profiles obtained by setting the working electrode at +0.5 V vs. SCE for various concentrations of SA. The useful current signals recorded after 50 seconds depended linearly on SA concentration within the explored concentration range between 0.2 mM and 1.2 mM (Figure 6.28 (b)). The sensitivity was almost similar to cyclic voltammetric technique (0.013 vs. 0.012 $\text{mA}\cdot\text{mM}^{-1}$ for CV). No fouling effect occurred within the investigated concentration range below 1.2 mM.

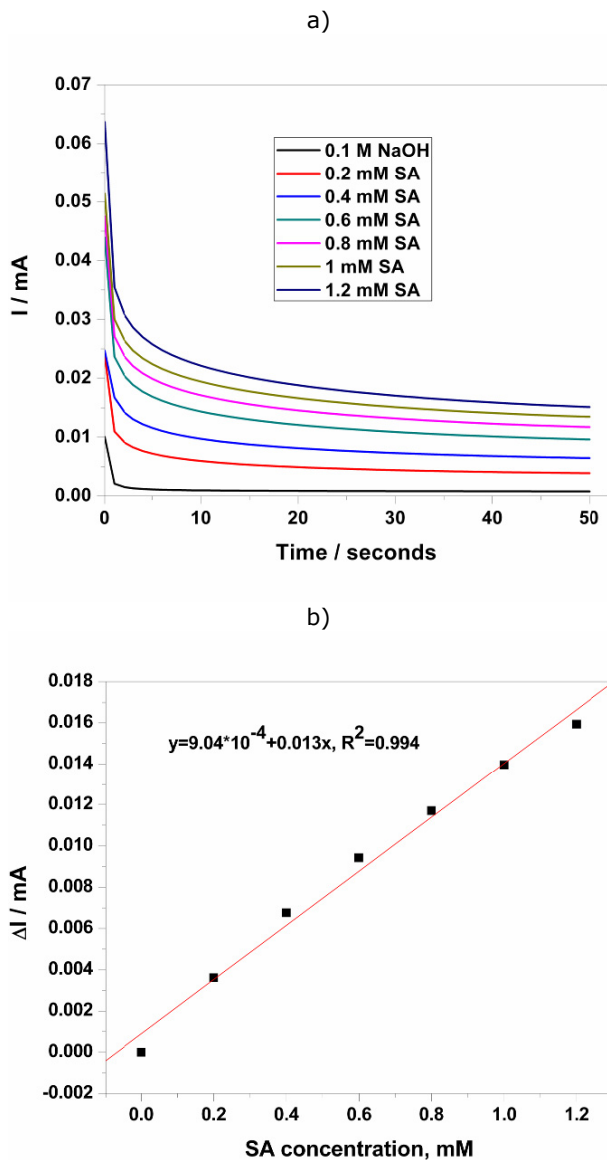
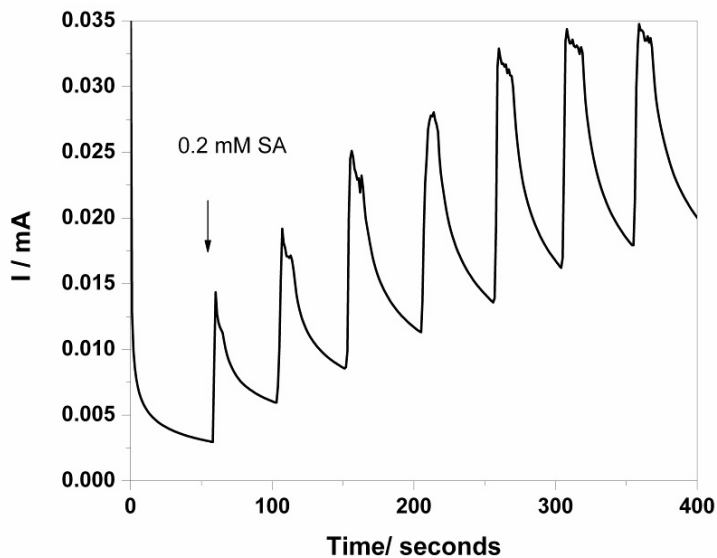


Figure 6.28 a) Chronoamperometric responses of the MWCNT-EP composite electrode recorded at +0.50 V/SCE to successive adding of 0.2 mM SA. b) The calibration plot of useful current vs. SA concentration.

The amperometric response of the MWCNT-EP composite electrode obtained for successive and continuous addition of 0.2 mM SA in a stirring 0.1 M NaOH solution under the conditions of batch system analysis (BSA) at an applied potential of +0.5 V vs. SCE is shown in Figure 6.29 (a). The current response of SA oxidation increased in a straight line within the concentration range of 0.2 mM to 1.2 mM (Figure 6.29 (b)). This technique allowed reaching similar electroanalytical parameters in comparison with the explored amperometric/cyclic voltammetric studies because of the stirring conditions.

a)



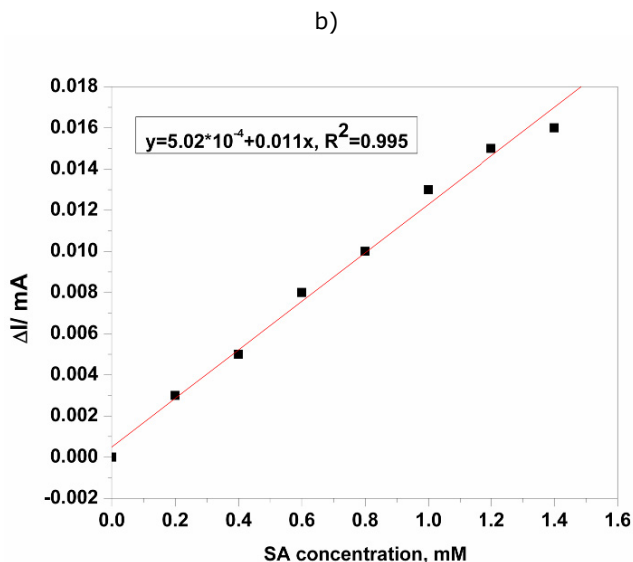


Figure 6.29 (a) Amperometric response (BIA) of the MWCNT-EP composite electrode for the successive and continuous addition of 0.2 mM SA. Applied potential: +0.50 V vs. SCE. (b) The calibration plot of useful signal vs. SA concentration.

The corresponding characteristic electroanalytical parameters, working conditions, and techniques applied in various situations in 0.1 M NaOH supporting electrolyte are gathered in Table 6.7. The reproducibility of the electrode using the above-mentioned technique was evaluated for three replicates measurements of SA detection. The relative standard deviation (RSD) of maximum 3 % showed the good reproducibility of the electrode.

Table 6.7 The electroanalytical performance of the MWCNT-Epoxy composite electrode for the voltammetric detection of SA in 0.1 M NaOH supporting electrolyte.

Peak potential	Technique used	Concentration range (mM)	Sensitivity (mA / mM ⁻¹)	Correlation coefficient (R ²)	LOD (mM)	LQ (mM)	RSD [**] (%)
+ 0.5 V	CV	0.6-3.6	0.012	0.979	0.037	0.125	1.666
+0.41 V	DPV	0.02-1.2	0.020	0.987	0.015	0.050	1.785
+0.41 V	Prec./DPV	0.02-0.1	0.150	0.984	0.002	0.006	1.041
+0.46 V	SWV	0.2-1.2	0.065	0.979	0.006	0.023	0.204
+0.50 V	CA	0.2-1.2	0.013	0.994	2×10^{-5}	9×10^{-5}	0.012
+0.50 V	BIA	0.2-1.2	0.011	0.995	2×10^{-5}	9×10^{-5}	0.012

6.2.3.3 Application of MWCNT-EP composite electrode for salicylic acid detection without supporting electrolyte

Several literature data underline that the carbon based composite electrode can be regarded either ordered (array) or randomized micro/nanoelectrode ensembles [6.33]-[6.35], [6.36]. Under these circumstances, the diffusion flux toward microelectrodes ensembles depend strongly on the experimental timescale. Moreover, the specific micro/nano-dispersed nature of the investigated carbon-based composite electrode suggested a presumptive way to discuss the corresponding electrochemical data considering the typical aspects regarding the behavior of randomized or array structured micro/nano-electrodes systems.

For some carbon-based composite electrode, it has been proved the heterogeneous electroactivity with distinct microzones have a significantly higher electrochemical activity [6.35]. The voltammetric responses of carbon-based composite electrodes are sometimes similarly to that found for „edge effect“, which contribute significantly to the Faradaic current. However, these structured materials, as in our investigated composites, are not rigorously arrays but are truly randomized ensembles, with the size, shape and inter-microelectrode separation distributed over a wide range. The random ensembles of microelectrodes can have array behavior in certain situation [6.35], an important characteristic expected to manifest similarly for our explored electrodes. In the preparation of carbon-based composites with microelectrode array behavior, certain important requirements should be met. The main requirement is that the gaps between individual conductive carbon microzones should be much larger than its radius, when spherical diffusion dominates mass transport. The closely spaced carbon microzones array will behave similar to a macroelectrode (linear diffusion controlled mass transport) because of the diffusion layer overlap [6.36]-[6.44]. Another requirement is subjected to the insulating matrix to prevent current leakage, which resulted in the distortion of the cyclic voltammetry [6.34]. Microelectrode arrays exhibit the advantages of single microelectrodes, e.g., reduced ohmic drop and charging current, the lower detection limit and better sensitivity. In the same time, their use overcomes the disadvantages of single microelectrode subjected to low current output and the high susceptibility to the electrochemical noise [6.39].

Based on the above-presented results regarding the electrochemical behavior of the MWCNT-EP composite electrode characterized by ferri/ferrocyanide classical method, it can be noticed that linear diffusion controlled the mass transport, which is characteristics to the macroelectrode behavior, with a substantial hysteresis. However, another micro/nanoelectrode array peculiarity is given by the ability to deliver the current responses in the absence of any supporting electrolyte, which is an attractive feature when they are compared with the conventional macroelectrodes [6.41]. There are several reason subjected to analytical studies on non-dilute samples in the absence of any supporting electrolyte, i.e., the direct analysis in low ionic strength solutions that make analysis more facile, eliminating the possible interference of the supporting electrolyte and the possibility of extending the upper concentration limit of the analyte under investigation. Based on this aspect, the MWCNT-EP composite electrode was tested to detect SA.

Two different issues have been taken into consideration for testing MWCNT-EP composite electrode for SA detection in tap water and in surface water (Bega River from Timisoara city, Romania). The first issue was the possibility of direct analysis of pharmaceutical compounds in surface water envisaging in-situ determination. The second issue referred to the certification of the

micro/nanoelectrode array behavior of MWCNT-EP composite electrode by SA detection in tap water, without supporting electrolyte.

The responses obtained at MWCNT-EP composite electrode in the absence of supporting electrolyte (Bega River) comparatively with 0.1 M Na_2SO_4 supporting electrolyte are presented in Figure 6.30. It can be seen that a slight higher background current corresponding to more capacitive component of the composite electrode, and also, non considerable ohmic drop increasing was noticed in Bega River, which encourage the further composite electrode testing for SA detection direct in Bega River.

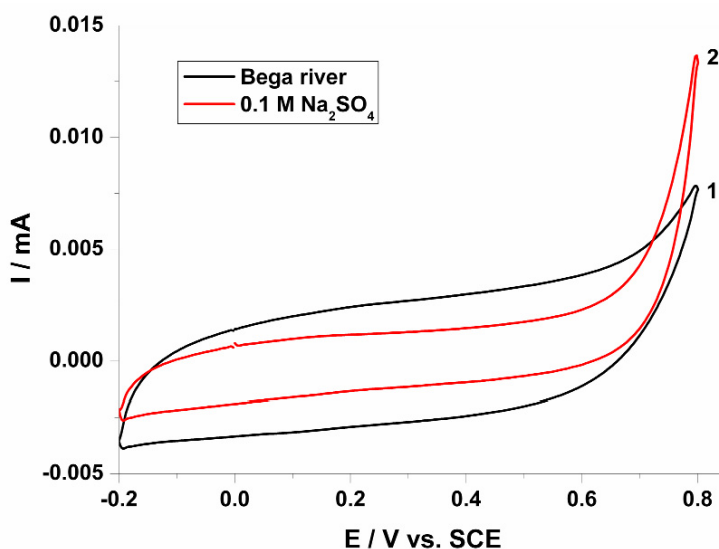


Figure 6.30 CVs recorded at MWCNT-EP composite electrode at a potential scan rate of 0.05 Vs^{-1} and a potential range between -0.2 V and $+0.8 \text{ V/SCE}$ in Bega River, without supporting electrolyte (curve 1) and in $0.1 \text{ M Na}_2\text{SO}_4$ supporting electrolyte (curve 2).

The CVs recorded at MWCNT-EP composite electrode in Bega River in the presence of various SA concentrations range from 0.2 to 1.2 mM SA are shown in Figure 6.31. No shifting the oxidation potential was found and the anodic peak current recorded at $+0.6 \text{ V/SCE}$ (the same as in $0.1 \text{ M Na}_2\text{SO}_4$ supporting electrolyte) increased linearly with SA concentration, with the same sensitivity of $0.017 \text{ mA} \cdot \text{mM}^{-1}$. However, the lowest limit of detection was higher, 0.03 mM vs. 0.012 mM .

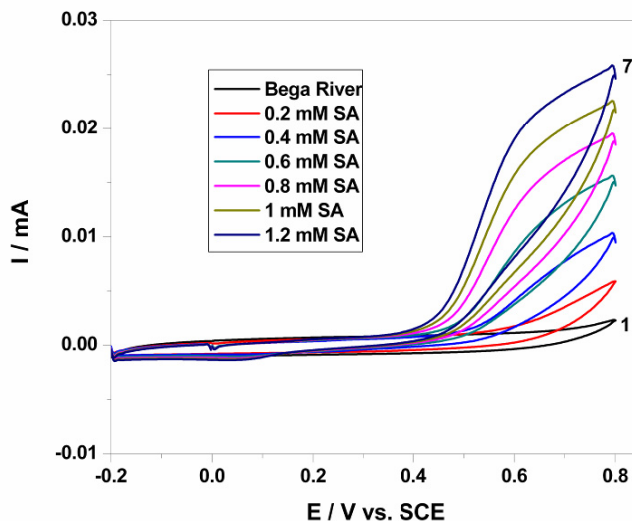


Figure 6.31 (a) CVs of the MWCNTs-EP composite at a potential scan rate 0.05 Vs^{-1} and a potential range between -0.2 V and $+0.8 \text{ V/SCE}$ in Bega River, without supporting electrolyte (curve 1) and in the presence of different SA concentrations: 2) 0.2 mM ; 3) 0.4 mM ; 4) 0.6 mM ; 5) 0.8 mM ; 6) 1 mM ; 7) 1.2 mM .

The potential usefulness of differential-pulsed and square-wave voltammetry methods at the determination of SA content in real surface water samples was verified. A series of anodic DPVs presented in Figure 6.32 involving SA concentration effect at MWCNT-EP composite electrode in Bega River without supporting electrolyte recorded over the concentration range of 0.2 mM – 1.2 mM SA under similar conditions as CV investigation using SA standard solution. The behavior was very similarly as in $0.1 \text{ M Na}_2\text{SO}_4$ supporting electrolyte related to oxidation potential shifting to less positive potential. Also, the oxidation peak potential is shifted to the less positive values with SA concentration increasing, which led also to the appearance of the second oxidation peak at the potential value of $+0.52 \text{ V/SCE}$, probably due to the presence of the oxidation product of SA that can be further oxidized at the electrode surface. No insight study related to this second peak was performed because it is beyond of our study aim. Calibration plot showed a sensitivity of $0.026 \text{ mA} \cdot \text{mM}^{-1}$ that is comparable as reached in $0.1 \text{ M Na}_2\text{SO}_4$ supporting electrolyte, and a good linearity with a correlation coefficient of 0.991 .

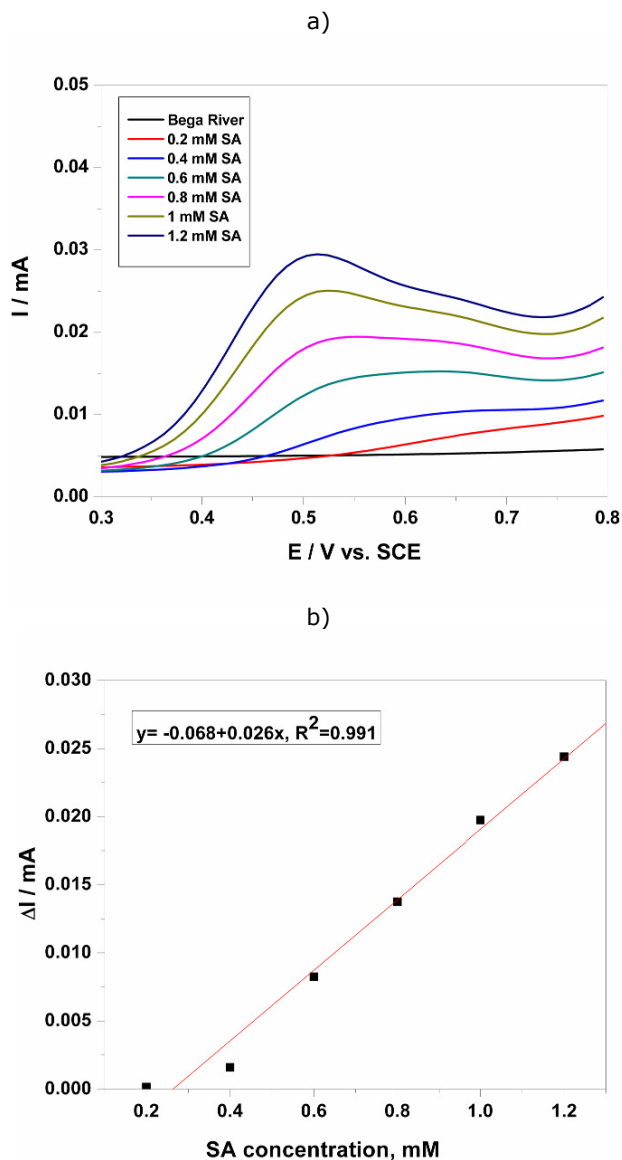
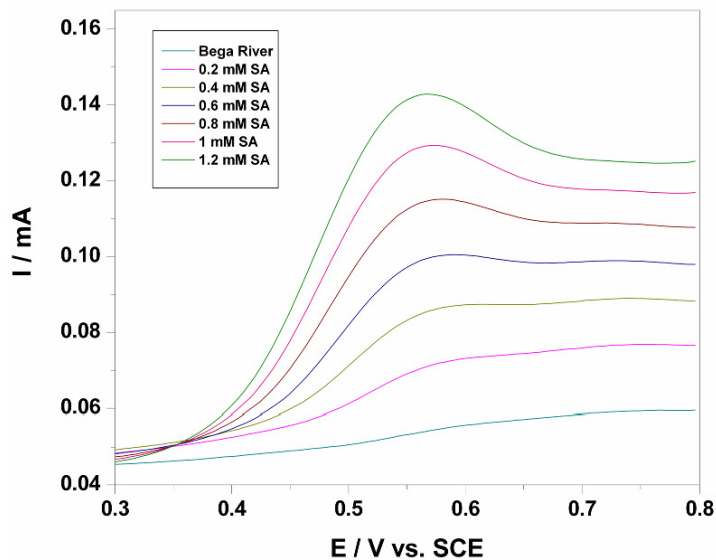


Figure 6.32 (a) DPVs of the MWCNT-Epoxy composite electrode in Bega River without supporting electrolyte (black curve) (modulation amplitude 0.1 V, step potential 0.01 V), potential scan rate of 0.05 Vs^{-1} and in the presence of: 0.2, 0.4, 0.6, 0.8, 0.1, 0.12 mM SA concentrations. (b) Calibration plot of the anodic currents recorded at $E = +0.52 \text{ V}$ vs. SA concentration.

Figure 6.33 (a) presents also a series of SWVs recorded using the MWCNT-EP composite electrode in Bega River under the above-presented optimized conditions of SWV applying in 0.1 M Na_2SO_4 supporting electrolyte. Figure 6.33 (b) shows that the anodic current recorded at the potential value of +0.56 V/SCE depends linearly on the SA concentration in the range 0.2-1.2 mM, with a correlation coefficient better than 0.999 and the sensitivity of $0.073 \text{ mA}\cdot\text{mM}^{-1}$, which is comparable with the sensitivity achieved in 0.1 M Na_2SO_4 supporting electrolyte.

a)



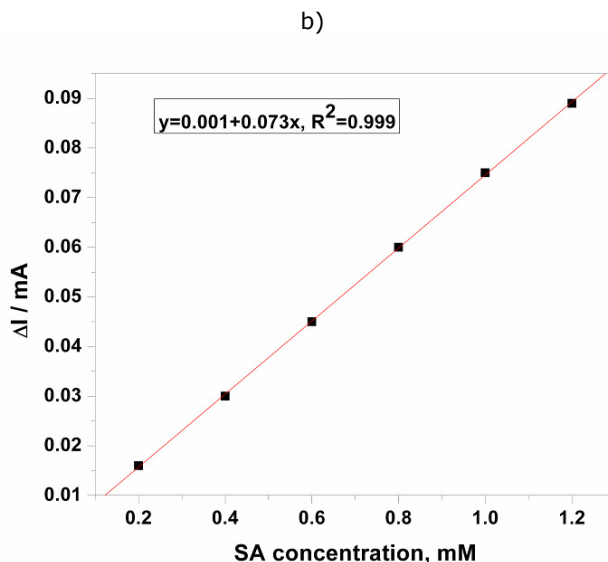


Figure 6.33 (a) SWVs of the MWCNT-EP composite electrode in Bega River without supporting electrolyte (blue curve) (step potential of 0.005 V, the modulation amplitude of 0.05 V and the frequency of 50 Hz), and in the presence of: 0.2, 0.4, 0.6, 0.8, 1, 1.2 mM SA concentrations. (b) Calibration plot of the anodic currents recorded at $E = +0.56$ V vs. SA concentration.

Also, the micro/nanoelectrode array behaviour of MWCNT-EP composite electrode for SA detection in tap water, without supporting electrolyte was checked by DPV and SWV techniques. Under conditions of the applied parameters of differential pulse voltammetry technique (Figure 6.34 (a)), well-defined current peaks corresponding to SA oxidation manifested around +0.65 V/SCE, which is more positive versus 0.1 M Na_2SO_4 supporting electrolyte and Bega River, probably due to the ohmic drop manifestation. Calibration plot (for calibration data, see Table 6.8) of anodic current peak, versus SA concentration showed almost the similar sensitivity of $0.018 \text{ mA} \cdot \text{mM}^{-1}$ and a very good linearity with a determination coefficient of 0.993.

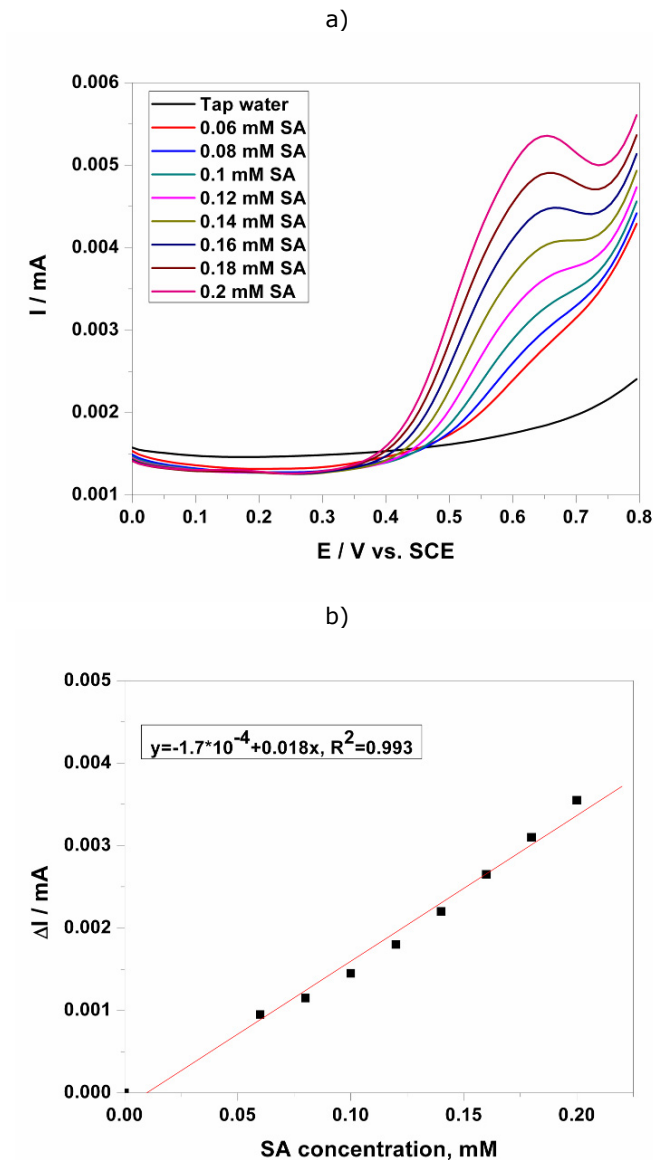


Figure 6.34 (a) DPVs of the MWCNT-EP composite electrode in tap water without supporting electrolyte (black curve) (modulation amplitude 0.1 V, step potential 0.01 V), potential scan rate of 0.05 Vs^{-1} and in the presence of: 0.06, 0.08, 0.1, 0.12, 0.14, 0.16, 0.18, 0.2 mM SA concentrations. (b) Calibration plot of the anodic currents recorded at $E = +0.65 \text{ V}$ vs. SA concentration.

Also, DPV was applied for higher SA concentration ranged from 0.2 mM to 1.2 mM SA, when two oxidation peaks appeared (see Figure 6.35 (a)), the behavior

manifested also, during testing in Bega River by both DPV and SWV techniques, because of high SA concentration that led to sufficient local concentration of the oxidation product of SA detectable at the electrode surface.

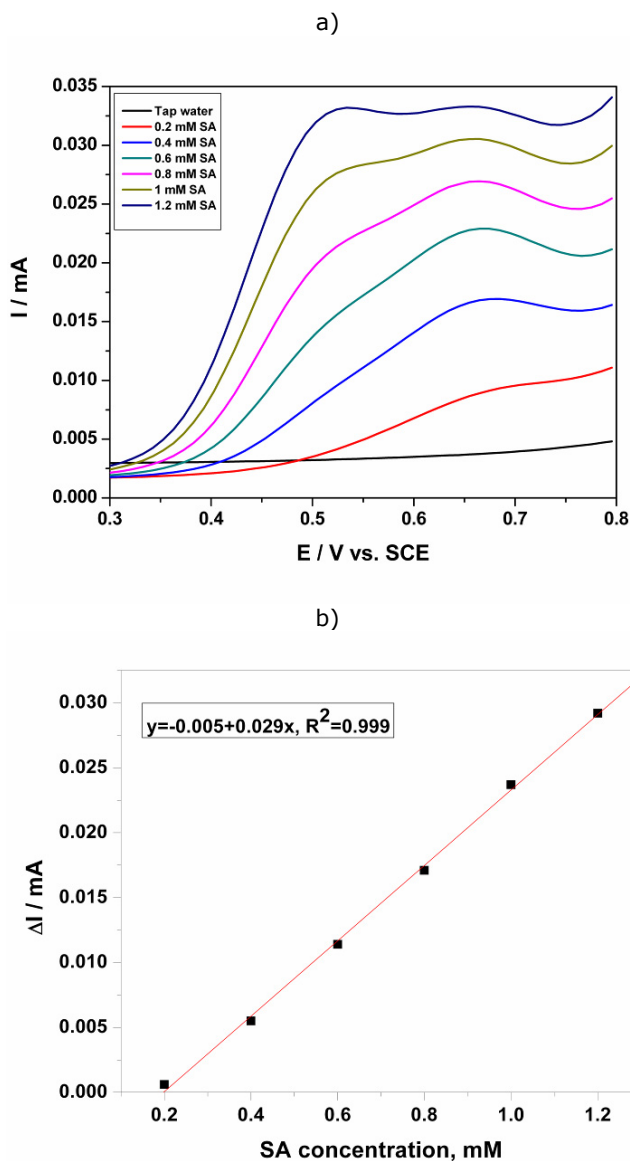


Figure 6.35 (a) DPVs of the MWCNT-EP composite electrode in tap water without supporting electrolyte (curve 1) (modulation amplitude 0.1 V, step potential 0.01 V), and in the presence of: 0.2, 0.4, 0.6, 0.8, 1, 1.2 mM SA concentrations. (b) Calibration plot of the anodic currents recorded at $E = +0.52 \text{ V}$ vs. SA concentration.

The electroanalytical parameters for SA direct detection of the MWCNT-EP composite electrode in Bega River and the tap water are gathered in Table 6.8.

Table 6.8 The electroanalytical parameters for SA direct detection of the MWCNT-Epoxy composite electrode in Bega River and the tap water, without supporting electrolyte.

Aqueous media	Peak potential	Technique used	Concentration range (mM)	Sensitivity (mA/mM ⁻¹)	Correlation coefficient (R ²)	LOD (mM)	LQ (mM)	RSD [**] (%)
Bega River	+0.52V	DPV	0.2-1.2	0.026	0.991	0.005	0.019	0.980
	+0.56V	SWV	0.2-1.2	0.073	0.999	0.004	0.013	0.186
Tap Water	+0.65V	DPV	0.06-0.2	0.018	0.993	0.008	0.028	2.702
	+0.52V		0.2-1.2	0.029	0.999	0.010	0.034	3.030

Based on these above-presented results, it can be concluded that the MWCNT-EP composite electrode manifested the microelectrode array behavior in relation with the direct detection of SA in tap water, without supporting electrolyte. Moreover, the results of the SA detection direct in Bega River, also without the supporting electrolyte adding given to this electrode a real potential for in-situ detection application.

6.2.4 Acetylsalicylic acid (ASA)

Due to the aspirin (acetylsalicylic acid) belongs to the salicylate class, our further study aims to investigate the direct determination of aspirin (ASA) in a pharmaceutical drug. It must be mentioned that the literature data gives the most information about the indirect determination of ASA by direct detection of salicylic acid (SA) as product of ASA hydrolysis [6.32]. The principle of indirect determination of ASA bases on its hydrolysis on SA, which can be easily detected. However, there is information about the direct detection of ASA without hydrolysis at mildly oxidized boron-doped diamond electrode [6.45]

Based on these information's, MWCNT-EP composite electrode was tested for the direct ASA determination both in 0.1 M Na₂SO₄ and in 0.1 M NaOH supporting electrolytes. Figure 6.36 (a) and Figure 6.37 (a) show the series of the CVs recorded at MWCNT-EP composite electrode in 0.1 M Na₂SO₄ supporting electrolyte over two different ASA concentrations ranges, from 0.02 mM to 0.2 mM ASA and from 0.2 mM to 1.2 mM ASA. For both ASA concentration ranges, the linear dependences of the oxidation peak currents recorded at +0.6 V/SCE versus ASA concentrations were found, and very good sensitivities were reached, 0.027 mA·mM⁻¹ and, respectively 0.061 mA·mM⁻¹. In contrast with the literature data related to the lack of a direct oxidation peak on carbon paste electrode, reported by Supalkova [6.32], our results show that MWCNT-EP composite electrode exhibit the electrocatalytic activity towards the direct ASA oxidation at the potential value of +0.6 V/SCE. Also, this electrode exhibited superiority versus boron-doped diamond electrode that oxidized ASA at the potential value of about +0.9 V/SCE [6.45].

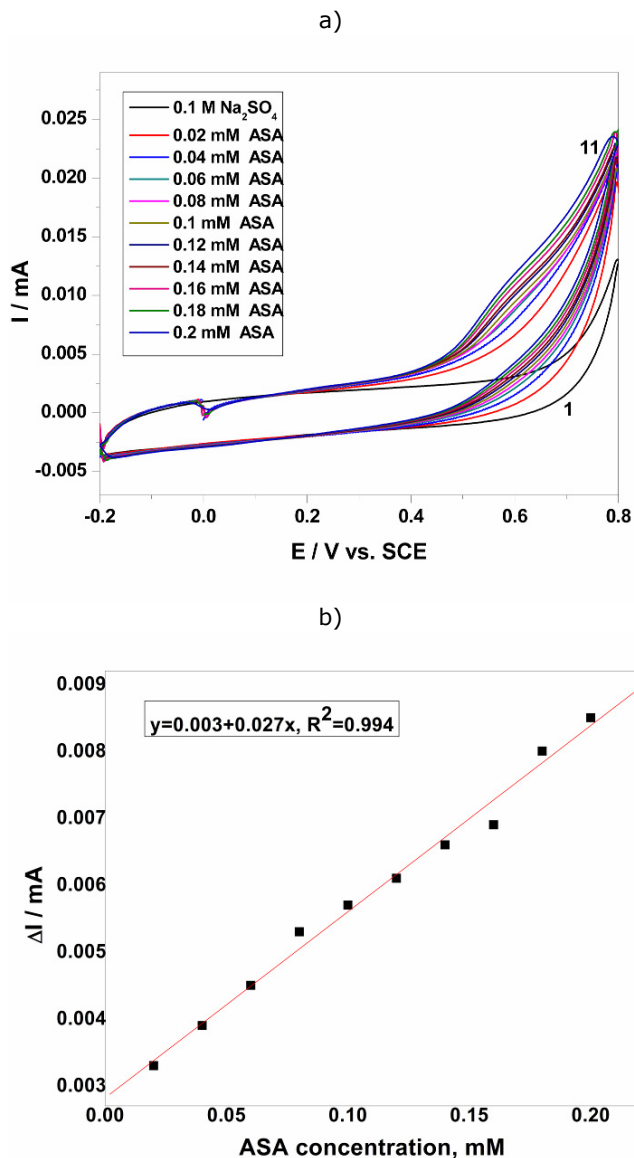


Figure 6.36 (a) CVs of the MWCNT-EP composite electrode in 0.1 M Na_2SO_4 supporting electrolyte (curve 1) and in the presence of: 0.02, 0.04, 0.06, 0.08, 0.1, 0.12, 0.14, 0.16, 0.18, 0.2 mM ASA; scan rate of 0.05 V s^{-1} . (b) Calibration plot of the anodic currents recorded at $E = +0.60 \text{ V/SCE}$ vs. ASA concentration.

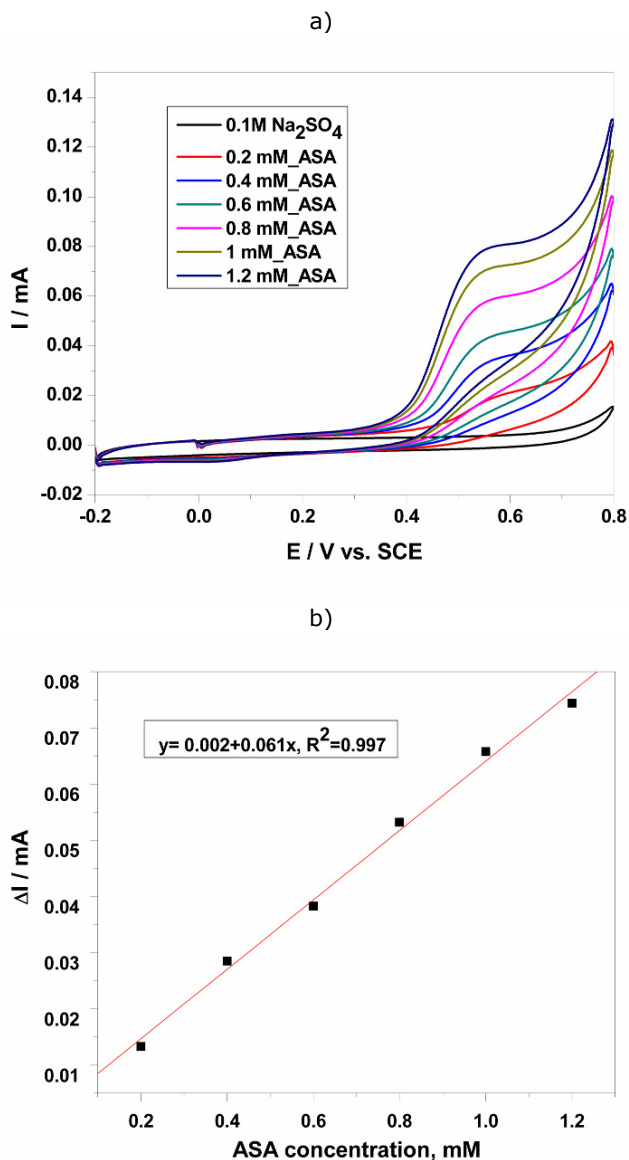
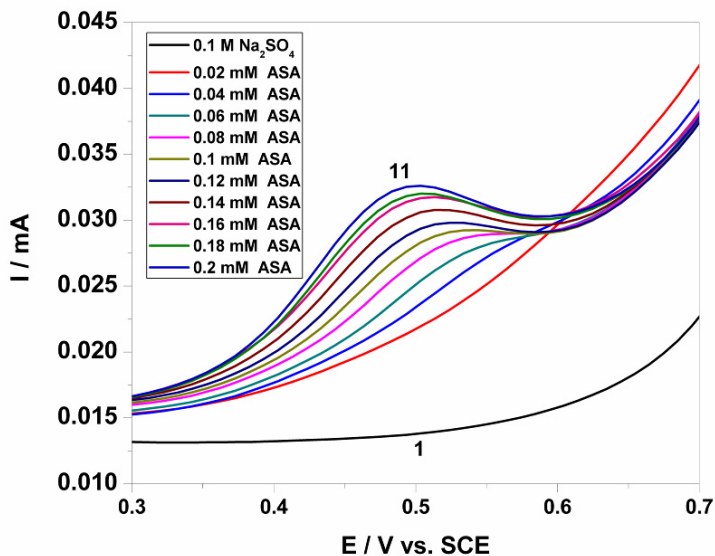


Figure 6.37 (a) CVs of the MWCNT-EP composite electrode in 0.1 M Na_2SO_4 supporting electrolyte (curve 1) and in the presence of: 0.2, 0.4, 0.6, 0.8, 1, 1.2 mM ASA; scan rate of 0.05 V s^{-1} . (b) Calibration plot of the anodic currents recorded at $E = +0.60 \text{ V/SCE}$ vs. ASA concentration.

The potential usefulness of DPV method at the determination of ASA content in real sample solutions was verified using aqueous solutions from tablets of Aspirin OZONE. Figure 6.38 (a) and Figure 6.39 (a) depict two series of DPVs as examples

involving ASA determination in an Aspirin real sample solution. Figures 6.38 (b) and Figure 6.39 (b) showed that the very good sensitivities were achieved, comparable with the ones reached for SA detection using DPV. The exemplified tested real sample was prepared under the conditions mentioned in the experimental part and using a 0.5953 g Aspirin tablet dissolved in 0.3 M NaOH and distilled water. Value of 485 mg ASA/tablet represented the average content determined using anodic DPV technique at MWCNT-EP composite electrode associated with standard addition method. The investigation of 3 Aspirin tablets with an average weight of 0.5946 g led to a value of 485 mg ASA/tablet. According to the general OZONE product specification, each single tablet should contain 500 mg ASA.

a)



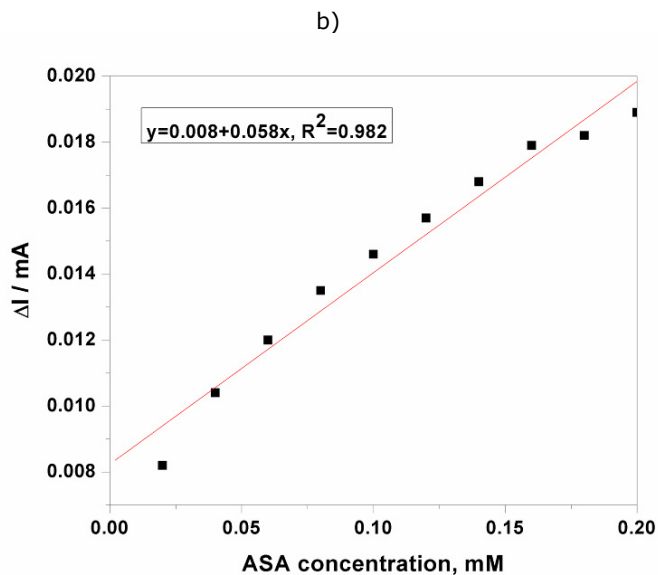
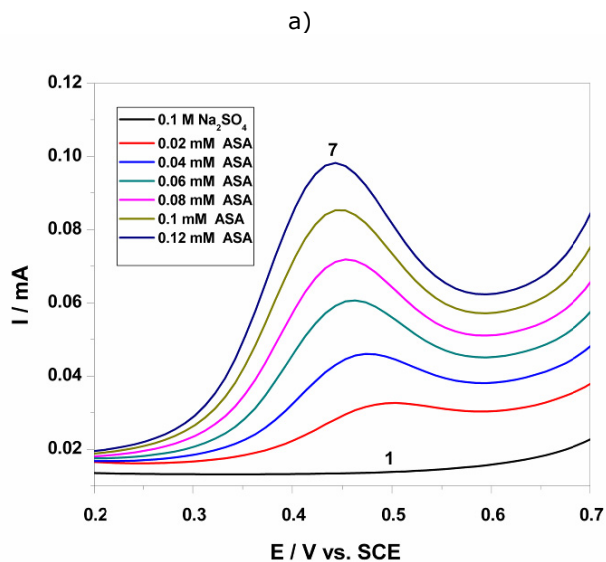


Figure 6.38 (a) DPVs of the MWCNT-EP composite electrode in 0.1 M Na_2SO_4 supporting electrolyte (curve 1) (modulation amplitude 0.1 V, step potential 0.01 V), potential scan rate of 0.05 Vs^{-1} and in the presence of: 0.02, 0.04, 0.06, 0.08, 0.1, 0.12, 0.14, 0.16, 0.18, 0.2 mM ASA concentrations. (b) Calibration plot of the anodic currents recorded at $E = +0.50 \text{ V}$ vs. ASA concentration.



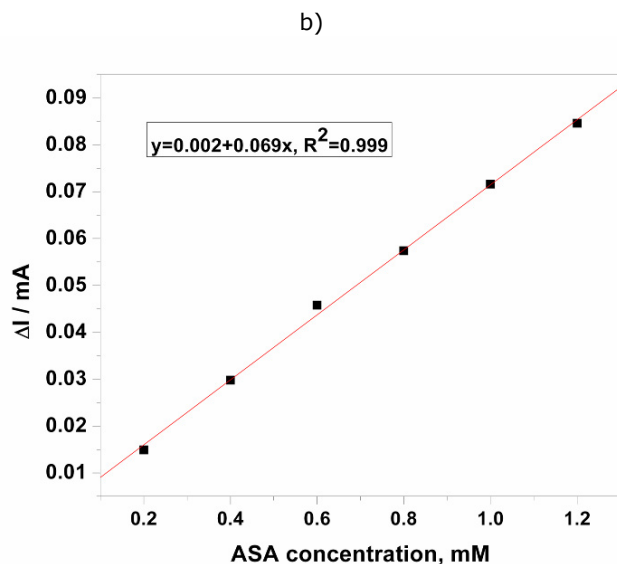


Figure 6.39 (a) DPVs of the MWCNT-EP composite electrode in 0.1 M Na_2SO_4 supporting electrolyte (curve 1) (modulation amplitude 0.1 V, step potential 0.01 V), potential scan rate of 0.05 Vs^{-1} and in the presence of: 0.2, 0.4, 0.6, 0.8, 1, 1.2 mM ASA concentrations. (b) Calibration plot of the anodic currents recorded at $E = +0.50 \text{ V}$ vs. ASA concentration.

The similar detection experiments for ASA determination were performed in 0.1 M NaOH supporting electrolyte and the results are presented in Figure 6.40- Figure 6.42.

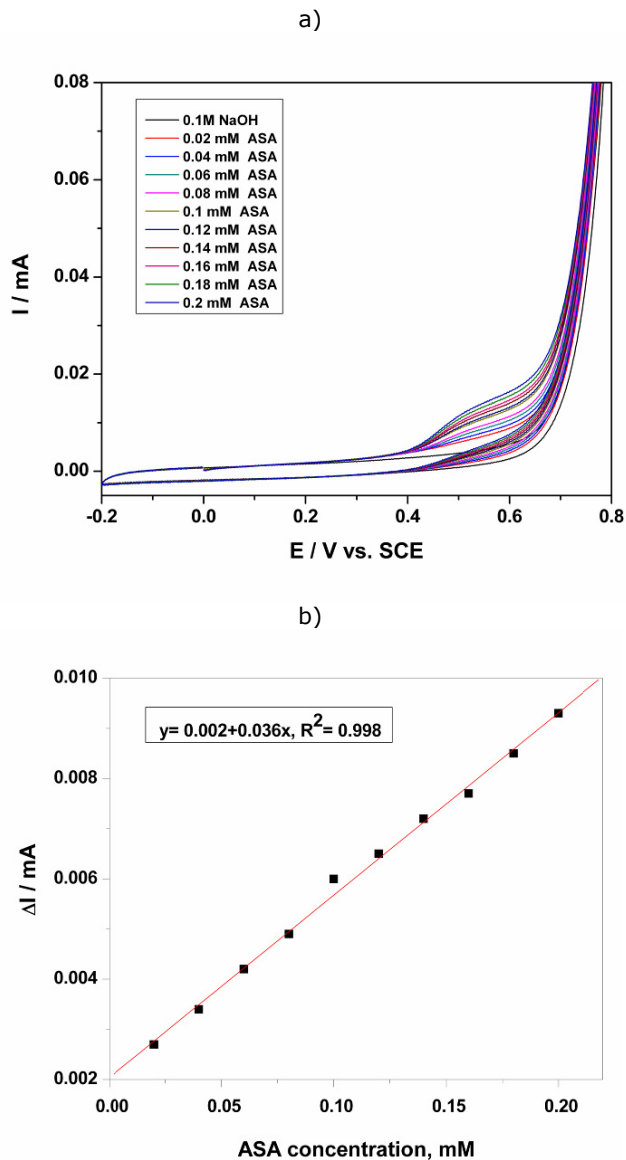


Figure 6.40 (a) Detail of CVs of the MWCNT-EP composite electrode in 0.1 M NaOH supporting electrolyte (black curve) and in the presence of: 0.02, 0.04, 0.06, 0.08, 0.1, 0.12, 0.14, 0.16, 0.18, 0.2 mM ASA concentrations; scan rate of 0.05 Vs⁻¹. (b) Calibration plot of the anodic currents recorded at E= +0.55 V/SCE vs. ASA concentration.

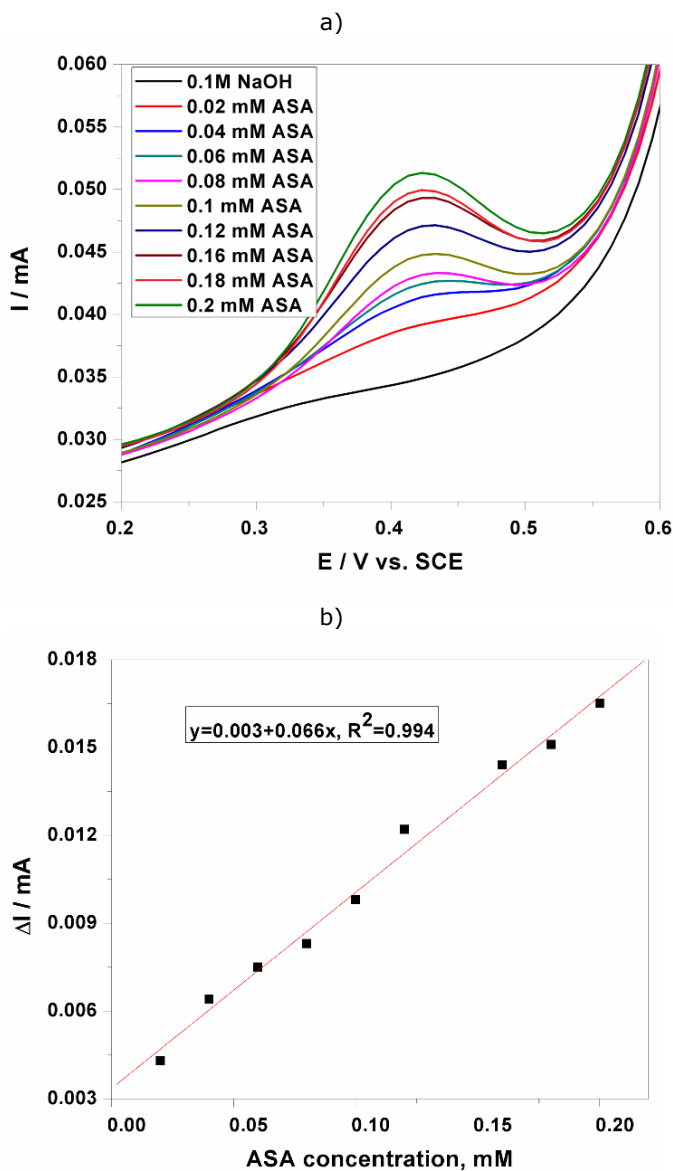


Figure 6.41 (a) DPVs of the MWCNT-EP composite electrode in 0.1 M NaOH supporting electrolyte (curve 1) (modulation amplitude 0.1 V, step potential 0.01 V), and a potential scan rate of 0.05 Vs^{-1} and in the presence of: 0.02, 0.04, 0.06, 0.08, 0.1, 0.12, 0.14, 0.16, 0.18, 0.2 mM ASA concentrations. (b) Calibration plot of the anodic currents recorded at $E = +0.42 \text{ V}$ vs. ASA concentration.

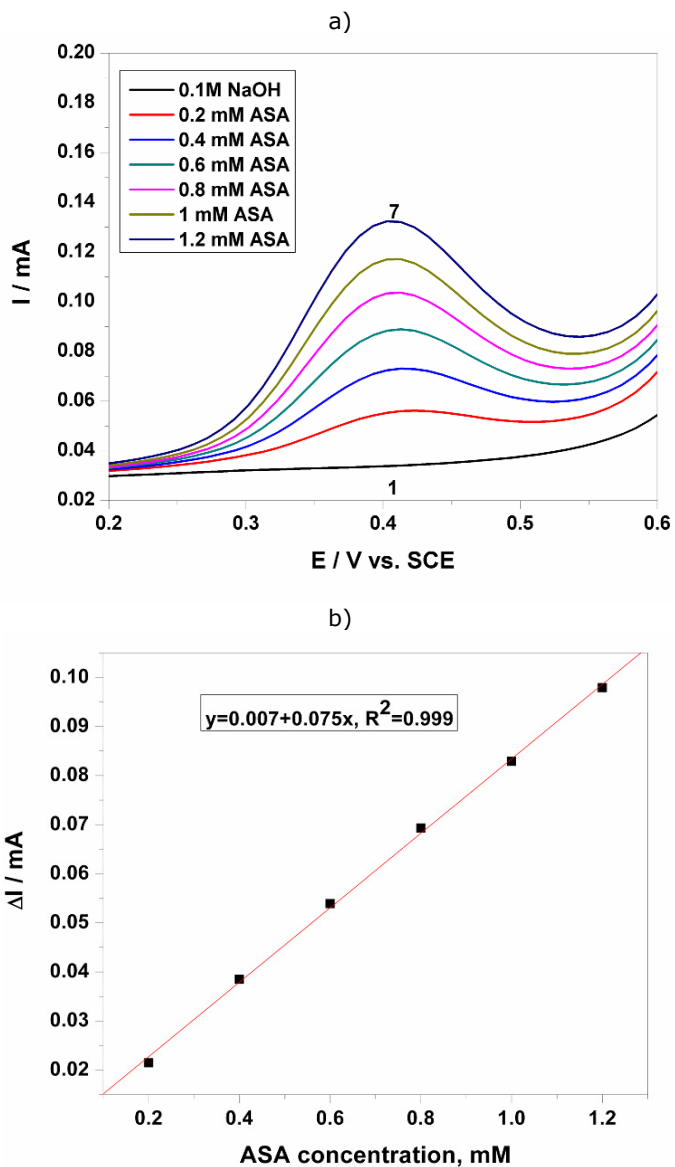


Figure 6.42 (a) DPVs of the MWCNT-EP composite electrode in 0.1 M NaOH supporting electrolyte (curve 1) (modulation amplitude 0.1 V, step potential 0.01 V), potential scan rate of 0.05 Vs^{-1} and in the presence of: 0.02, 0.04, 0.06, 0.08, 0.1, 0.12, 0.14, 0.16, 0.18, 0.2 mM ASA concentrations. (b) Calibration plot of the anodic currents recorded at $E = +0.42 \text{ V}$ vs. ASA concentration.

The electroanalytical parameters for ASA direct detection of the MWCNT-Epoxy composite electrode in 0.1 M Na₂SO₄ and 0.1 M NaOH supporting electrolytes are gathered in Table 6.9.

Table 6.9 The electroanalytical parameters for direct detection of ASA of the MWCNT-Epoxy composite electrode in 0.1 M Na₂SO₄ and 0.1 M NaOH supporting electrolytes.

Supporting electrolyte	Peak potential	Technique used	Concentration range (mM)	Sensitivity (mA / mM ⁻¹)	Correlation coefficient (R ²)	LOD (mM)	LQ (mM)	RSD [**] (%)
0.1M Na ₂ SO ₄	+0.60 V	CV	0.02-0.2	0.027	0.994	0.011	0.037	2.78
			0.2-1.2	0.061	0.997	0.004	0.016	2.78
	+0.50 V	DPV	0.02-0.2	0.058	0.982	0.010	0.034	1.48
			0.2-1.2	0.069	0.999	0.008	0.028	1.48
0.1 M NaOH	+0.55 V	CV	0.02-0.2	0.036	0.998	0.008	0.027	2.22
	+0.42 V	DPV	0.02-0.2	0.066	0.994	0.013	0.045	0.87
			0.2-1.2	0.075	0.999	0.012	0.040	0.87

6.2.5 Conclusions

MWCNT-Epoxy composite electrode exhibited the electro catalytic activity towards salicylic acid (SA) and acetylsalicylic acid (ASA) oxidation, allowing their direct determination. The electrochemical determinations of SA and ASA at MWCNT-EP composite electrode were achieved in both 0.1 M Na₂SO₄ and 0.1 M NaOH supporting electrolytes using CV, DPV and SWV techniques. The alkaline medium did not allow improving the sensitivity for SA and ASA detection but the oxidation potential was shifted to less positive potential in comparison with the neutral medium. A detailed study related to the optimization of working SWV applying was performed, and the best electroanalytical performance for SA determination was achieved under the conditions of simple voltammetric technique applying. Moreover, the preconcentration step involving in the voltammetric detection scheme led to the enhancement of the electroanalytical performance for SA detection, both sensitivity and the lowest limit of detection were improved. SA detection on MWCNT-EP composite electrode was achieved in tap water and in surface water (Bega River from Timisoara city, Romania). SA detection in tap water certified the micro/nanoelectrode array behavior of MWCNT-EP composite electrode without supporting electrolyte. Also, MWCNT-EP composite electrode gives the possibility of direct analysis of salicylic acid in surface water and no supporting electrolyte was needed, envisaging in-situ determination.

Because ASA exhibited the same electrochemical behavior on MWCNT-EP composite electrode as SA, a simultaneous detection of both compounds is possible as cumulative effect but not a selective detection of one compound in the presence of the other can be performed.

6.3 MWCNT-HKUST-Epoxy composite electrode for glucose detection

6.3.1 Glucose

The determination of glucose concentration is extremely important clinically in the diagnosis and treatment of diabetes but also is important in areas such as biotechnology and food industry [6.46]. Since the first enzyme electrode was reported by pioneering work of Clark and Lyons in 1962 [6.47], researchers have generated much interest to the develop of glucose sensor and a variety of improvements regarding the optimization of glucose sensor, the immobilization of enzyme, and design of redox system have been reported [6.48]-[6.50]. The most known amperometric glucose sensors are based on the immobilization of enzymes, such as glucose oxidase (GOx), which catalyzes the oxidation of glucose in the presence of oxygen to hydrogen peroxide, or they are based on the use of redox mediators [6.51], [6.52].

Electrochemical detection of glucose using GOx exhibits a low detection limit, high sensitivity and selectivity, but due to the intrinsic nature of enzymes, such enzyme-based sensors suffer from the stability problem [6.53]-[6.55]. The activity of GOx can be easily affected by temperature, humidity and toxic chemicals. Also, there are several disadvantages of the enzyme-modified electrodes, i.e., high cost of enzyme; a complicated procedure is required for the immobilization of the enzyme on solid electrode, a critical operating situation, which may decrease the activity of GOx [6.56]-[6.58]. Therefore, considerable attention has been paid to develop non-enzymatic electrodes to solve these problems. This can be achieved by using inert metals, metal alloy and metal-dispersed in carbon nanotubes, in which the inert metal or metal alloy are mixed with CNTs to form nanocomposite [6.59]-[6.63].

The aim of this study is to synthesis a MWCNT based composite with the good stability and the long lifetime for the non-enzymatic detection of the glucose in the aqueous solution. Nano-structured copper benzene tricarboxylate (Cu-BTC), which was one of the first reported metal organic frameworks (MOFs) in 1999 and named HKUST-1, was selected to modify the MWCNT based composite electrode for two main reasons. The main reason was the multiple application potential of this material, especial in sensing and the other reason is based on copper presence in its structure, which is well-known as a good electrocatalyst for the glucose oxidation.

First, the electrochemical behavior of glucose was investigated in aqueous solution at MWCNT-Epoxy composite electrode, and no signal appeared, which means that no glucose oxidation occurred on this electrode.

6.3.2 Experimental

Reagents

Standard stock solution of 0.1 M glucose was prepared daily from analytical grade Merck reagents using distilled double water. The supporting electrolyte for the characterization and application of electrode material in detection process was

0.1 M NaOH solution, which was freshly prepared from NaOH of analytical purity (Merck) with double distilled water.

Electrochemical measurements

The electrochemical performance of this electrode was studied by cyclic voltammetry (CV), linear scan voltammetry (LSV), chronoamperometry (CA), and differential-pulsed voltammetry (DPV). Electrochemical measurements were performed in unstirred solutions using a computer controlled Autolab potentiostat/galvanostat PGSTAT 302 (EcoChemie, The Netherlands), with a standard three electrodes configuration. The three-electrode system consisted of a MWCNT-HKUST-Epoxy working electrode, with 0.196 cm² geometrical area, a platinum wire as counter electrode and a saturated calomel reference electrode (SCE). Before each voltammogram, the MWCNT-HKUST-Epoxy composite electrode was carefully polished with abrasive paper and then on a felt-polishing pad by using 0.3 μm alumina powder (Metrohm, Switzerland). The electrode was then sonicated for 5 min in pure water. All experiments were carried out with a typical cell of 50 mL at room temperature (25°C).

6.3.3 Results and discussion

6.3.3.1 Electrochemical characterization of the MWCNT-HKUST-Epoxy electrode using potassium ferricyanide

The electroactive surface area of the MWCNT-HKUST-Epoxy composite electrode was determined based on the classical method involving potassium ferrocyanide $K_3[Fe(CN)_6]$ in 1 M KNO_3 supporting electrolyte using cyclic voltammetry recorded at different scan rates (Figure 6.43 (a)) in according to the Randles-Sevcik equation (1) above-presented.

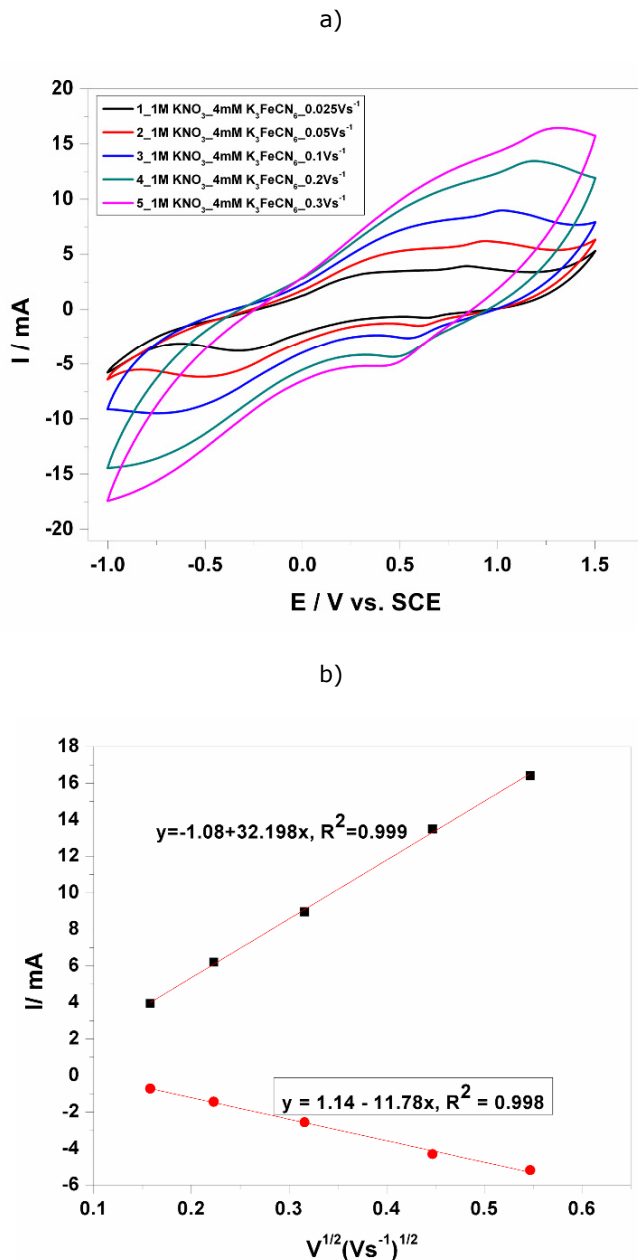


Figure 6.43 (a) CVs of the MWCNT-HKUST-Epoxy composite electrode in 4 mM $K_3[Fe(CN)_6]$ in 0.1 M KNO_3 supporting electrolyte at different scan rates: 1) 0.025, 2) 0.05, 3) 0.1, 4) 0.2, 5) 0.3 Vs^{-1} . (b) Calibration plots of the oxidative and reductive peak currents vs. the square root of the scan rate.

6.3. MWCNT-Epoxy composite electrode for glucose detection - 143

Table 6.10 The electrochemical parameters of the redox system (ferri/ferrocyanide) determined from the anodic branches of CVs

Scan rate/ Vs ⁻¹	E/V	Ia/mA	ΔIa/mA
0.025	0.853	3.93	0.334
0.05	0.963	6.2	0.873
0.1	1.031	8.96	1.438
0.2	1.184	13.49	2.59
0.3	1.378	16.42	3.05

Table 6.11 The electrochemical parameters of the redox system (ferri/ferrocyanide) determined from the cathodic branches of CVs

Scan rate/Vs ⁻¹	E/V	Ic/mA	ΔIc/mA
0.025	-0.0307	-0.716	-0.3024
0.05	-0.118	-1.44	-0.6895
0.1	-0.136	-2.56	-1.10
0.2	-0.223	-4.30	-1.751
0.3	-0.182	-5.18	-1.841

Table 6.12 Apparent diffusion coefficient and the electroactive surface area of MWCNT-HKUST-Epoxy composite electrode.

Scan rate/ Vs ⁻¹	Diffusion coefficient	Electroactive area, cm ²	Total diffusion coefficient	Total electroactive area, cm ²	Geom. area cm ²	Theoretical diffusion coefficient
0.025	0.912×10^{-4}	0.725	3.415×10^{-4}	1.357	0.196	6.7×10^{-6}
0.05	2.749×10^{-4}	1.269				
0.1	3.626×10^{-4}	1.446				
0.2	5.305×10^{-4}	1.749				
0.3	4.483×10^{-4}	1.608				

6.3.3.2 Cyclic voltammetry measurements

Cyclic voltammograms (CVs) recorded on the MWCNT-HKUST-Epoxy composite electrode in 0.1 M NaOH supporting electrolyte and various concentrations of glucose are shown in Fig. 6.44 (a).

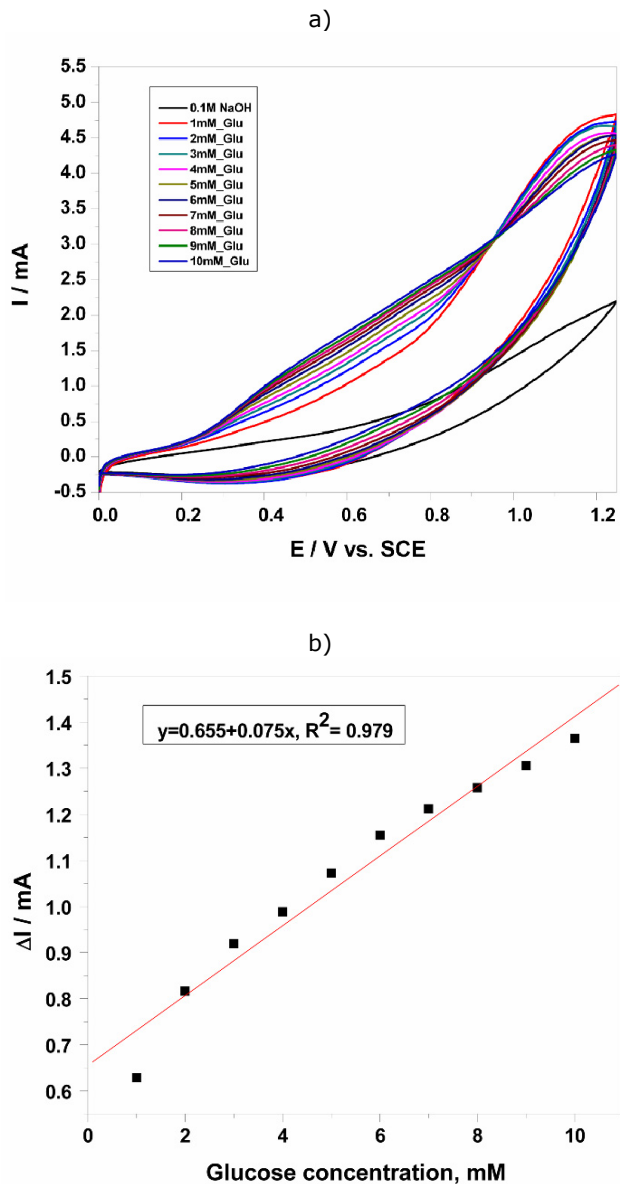
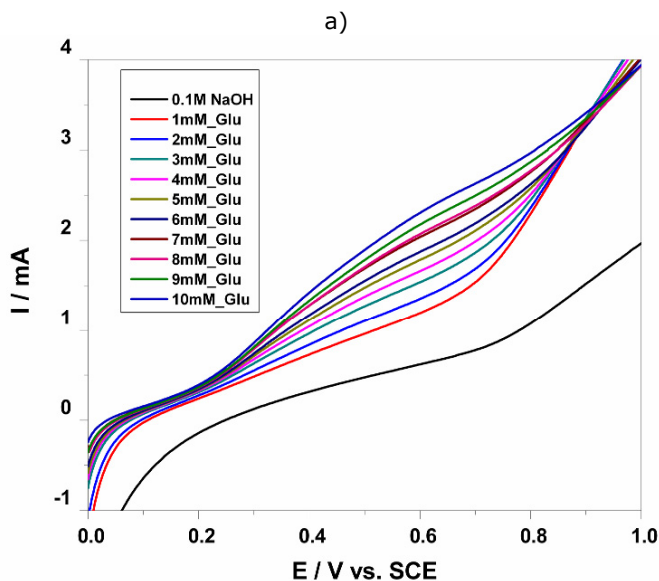


Figure 6.44 (a) CVs of the MWCNT-HKUST-Epoxy composite electrode recorded at a potential scan rate of 0.05 Vs^{-1} and a potential range between 0 V and + 1.2 V/SCE in 0.1 M NaOH supporting electrolyte (black curve) and in the presence of different glucose concentrations: 1-10 mM (curves 2-11). (b) The calibration plot of the anodic currents recorded at $E = +0.60 \text{ V/SCE}$ vs. glucose concentration.

In the absence of glucose, MWCNT-HKUST-Epoxy composite electrode exhibited a large capacitive current and no oxidation peaks characteristics to copper oxidation are evidenced, probably due to the large background that overlaid the peaks. Also, no reduction peaks corresponding to Cu (II) and Cu (I) species. However, in the presence of glucose, the shape of glucose was changed, the oxidation process of glucose on MWCNT-HKUST-Epoxy composite electrode started at the potential value of +0.2 V/SCE, which should assume Cu (I) and Cu (II) species involving in according with the literature data [6.64], [6.65]. The current corresponding to the oxidation potential value of +0.6 V/SCE increased linearly with glucose concentration, with a good correlation coefficient (Figure 6.44 (b))

Based on these encouraging preliminary results, the electrochemical performance of MWCNT-HKUST-Epoxy composite electrode to detect glucose has been assessed by linear-scan voltammetry (LSV), differential-pulsed voltammetry (DPV) and chronoamperometry (CA).

Figure 6.45 (a) shows a series of LSVs recorded at MWCNT-HKUST-Epoxy composite electrode within the glucose concentration range similar as CV running. Also, the linear dependence of the anodic current recorded at +0.6 V/SCE versus glucose concentration was achieved, with a better sensitivity, 0.12 versus 0.075 $\text{mA} \cdot \text{mM}^{-1}$ (see Figure 6.45 (b)).



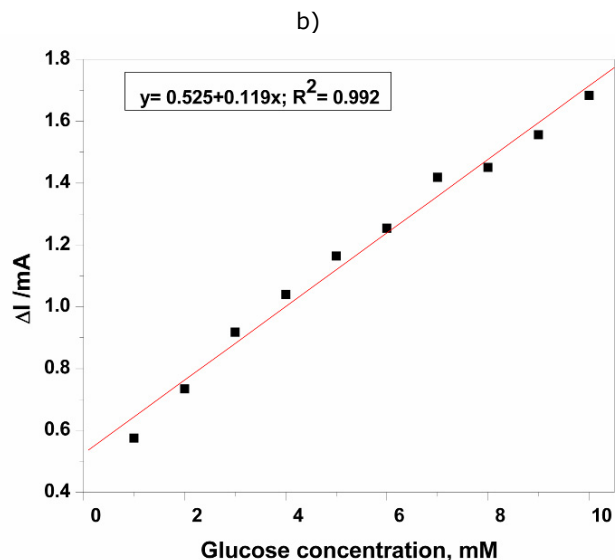


Figure 6.45 (a) LSVs of the MWCNT-HKUST-Epoxy composite electrode recorded at a potential scan rate of 0.05 Vs^{-1} and a potential range between 0 V and + 1.0 V/SCE in 0.1 M NaOH supporting electrolyte (curve 1) and in the presence of different glucose concentrations: 1-10 mM (curves 2-11). (b) The calibration plot of the anodic currents recorded at $E = + 0.60 \text{ V/SCE}$ vs. glucose concentration.

Taking into consideration the adsorption property of MOF, this study aimed to explore the adsorption capacity of HKUST and implicit, of MWCNT-HKUST-Epoxy composite electrode for glucose to improve the electroanalytical performance of this electrode for non-enzymatic detection of the glucose.

To propose a preconcentration/voltammetric detection scheme for glucose determination at MWCNT-HKUST-Epoxy composite electrode, the accumulation time represents an important parameter, because it could influence the degree of adsorption on the electrode surface. An important role that may be played by MOF is its availability to concentrate species within its nano-porous structure. To determine the enhancement factor as the ratio of peak current after and before sorption process, the effect of accumulation time on anodic peak current were investigated by LSV. Figure 6.46 (a) shows the LSVs recorded at MWCNT-HKUST-Epoxy composite electrode after different accumulation time, which represents the time for maintaining the electrode at OCP to concentrate glucose at the electrode surface. The useful oxidation peak current and the enhancement factor determined for 1 mM glucose using preconcentration/voltammetric detection procedure at different accumulation time are shown in Figure 6.46 (b). The oxidation peak currents for this compound increased with accumulation time up to 30 minutes, which was selected as the optimum accumulation time due to a maximum enhancement factor of 2.5 was reached, and at longer accumulation time the peak currents remain constant, and a plateau was reached. The enhancement factor of about 2.5 at the oxidation potential of +0.6 V/SCE revealed an effective concentration effect of the MWCNT-HKUST-Epoxy composite electrode on glucose regarding the improvement of its oxidation signal. As a consequence, the accumulation time of 30 minutes was

chosen as an optimum time for further preconcentration/linear-scan voltammetric detection experiments.

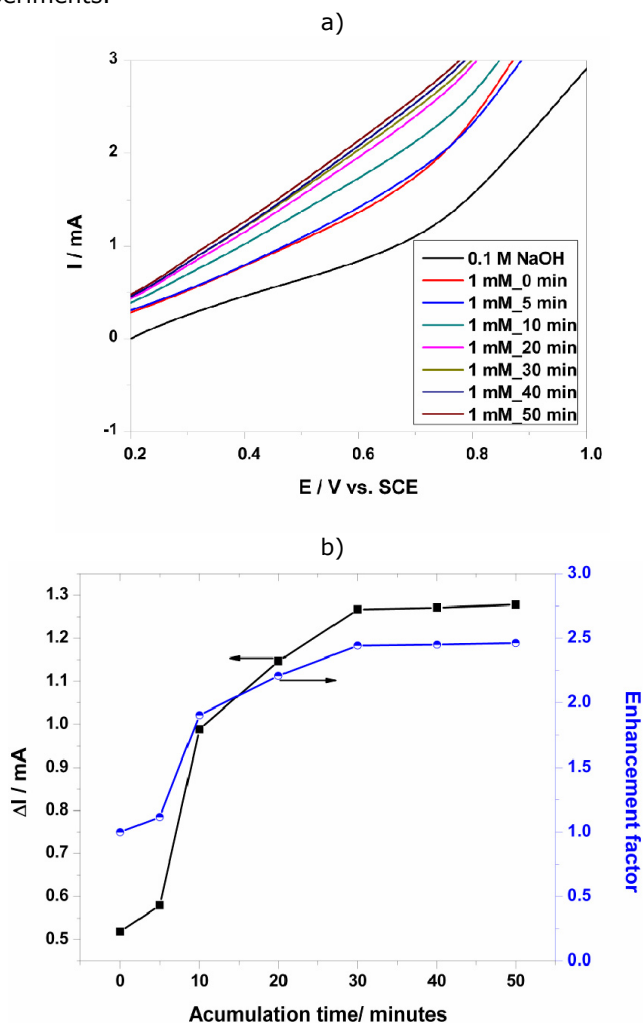


Figure 6.46 (a) LSVs recorded on MWCNT-HKUST-Epoxy composite electrode at a potential scan rate of 0.05 Vs^{-1} in potential range between $+0.2 \text{ V}$ and $+1.0 \text{ V}$ vs. SCE in 0.1 M NaOH supporting electrolyte (curve 1) and in the presence of 1 mM glucose concentration after different accumulation times: 2) 0 min , 3) 5 min , 4) 10 min , 5) 20 min , 6) 30 min , 7) 40 min , 8) 50 min . (b) Peak current responses and enhancement factors for the detection of 1 mM glucose at MWCNT-HKUST-Epoxy composite electrode as a function of the accumulation time recorded at $E = +0.60 \text{ V/SCE}$.

An example of LSV series recorded under the optimum conditions of the preconcentration scheme that assume the accumulation time of 30 minutes within glucose concentration ranged from 0.2 mM to 1 mM is shown in Figure 6.47 (a). Under these working conditions, a significant enhancement of the electroanalytical parameters of glucose detection was achieved, about 5 times better sensitivity and also, 5 times lower the detection limit (see Table 6.13).

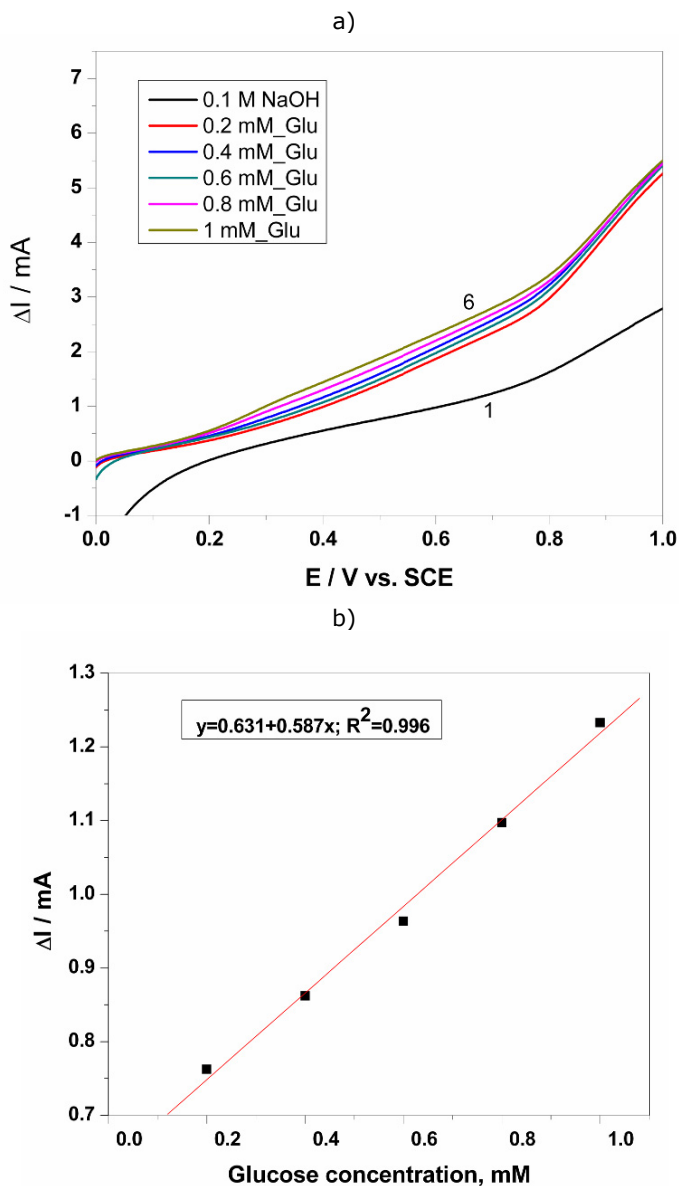
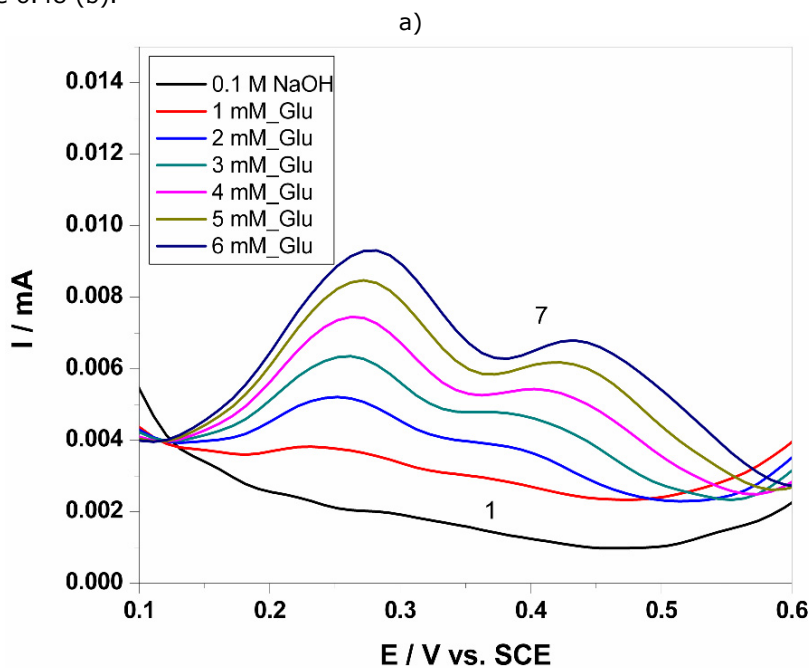


Figure 6.47 (a) LSVs of the MWCNT-HKUST-Epoxy composite electrode, accumulation time of 30 minutes, potential range 0 to + 1.0 V vs. SCE in 0.1 M NaOH supporting electrolyte (1) and in the presence of different glucose concentrations: 2) 0.2 mM, 3) 0.4 mM, 4) 0.6 mM, 5) 0.8 mM, 6) 1mM. (b) Calibration plot of the anodic currents recorded at $E = +0.60 \text{ V/SCE}$ vs. glucose concentration.

Differential-pulsed voltammetry (DPV) has been employed as a technique for the evaluation of the performance of the MWCNT-HKUST-Epoxy composite electrode for the glucose determination. Figure 6.48 (a) shows the differential-pulsed voltammograms recorded for the glucose concentration ranged between 1 and 6 mM and in the potential range of +0.1 V to +0.6 V vs. SCE. The shape of the differential-pulsed voltammogram is very different in comparison with CV and LSV, at the potential values of +0.27 V/SCE and +0.44 V/SCE two very clear oxidation peaks appeared, and their heights increased progressively with glucose concentration. Because in the electroanalysis the lowest potential is desired for analyte detection, the potential value of +0.27 V/SCE was selected for the calibration. The useful net current signals corresponding to the oxidation peak recorded at +0.27 V/SCE are linearly dependent on the glucose concentration (Figure 6.48 (b)).



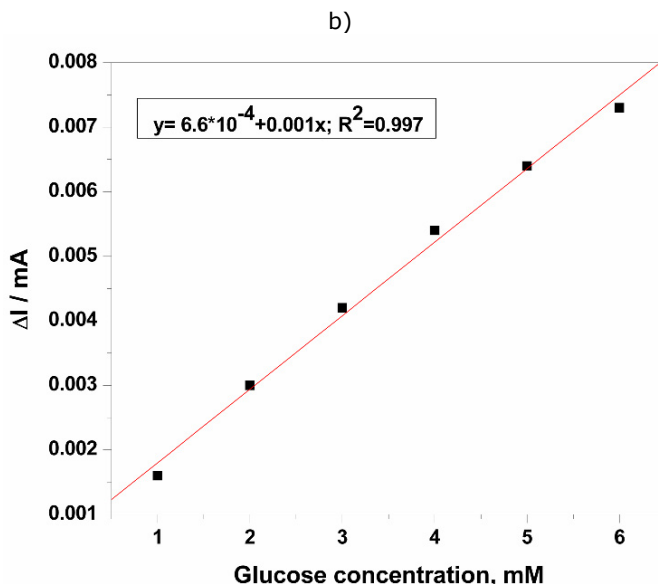


Figure 6.48 (a) Detail of the DPVs of the MWCNT-HKUST-Epoxy composite electrode (modulation amplitude 0.002 V, step potential 0.01 V), potential scan rate of 0.05 Vs⁻¹, potential range between +0.1 V to + 0.6 V vs. SCE in 0.1 M NaOH supporting electrolyte (curve 1) and in the presence of different glucose concentrations: 2) 1 mM, 3) 2 mM, 4) 3 mM, 5) 4 mM, 6) 5 mM, 7) 6 mM. (b) Calibration plot of the anodic currents recorded at E= +0.27 V/SCE vs. glucose concentration.

Also, for practical working applications the optimum analytical procedure should involve the recording of the chronoamperogram as the easiest electrochemical technique, based on the existing well-established essential point of reference provided by the voltammograms. The amperometric response of the MWCNT-HKUST-Epoxy composite electrode obtained for successive and continuous addition of 1 mM glucose in a stirring 0.1 M NaOH solution under the conditions of batch system analysis (BSA) at an applied potential of +0.6 V vs. SCE is shown in Figure 6.49 (a). The current response of glucose oxidation increased linearly within the concentration range of 1 mM to 8 mM (Figure 6.49 b). This technique allowed reaching electroanalytical parameters similar as the explored cyclic voltammetric studies (see Table 6.13) because of the stirring conditions, and no electrode fouling occurred.

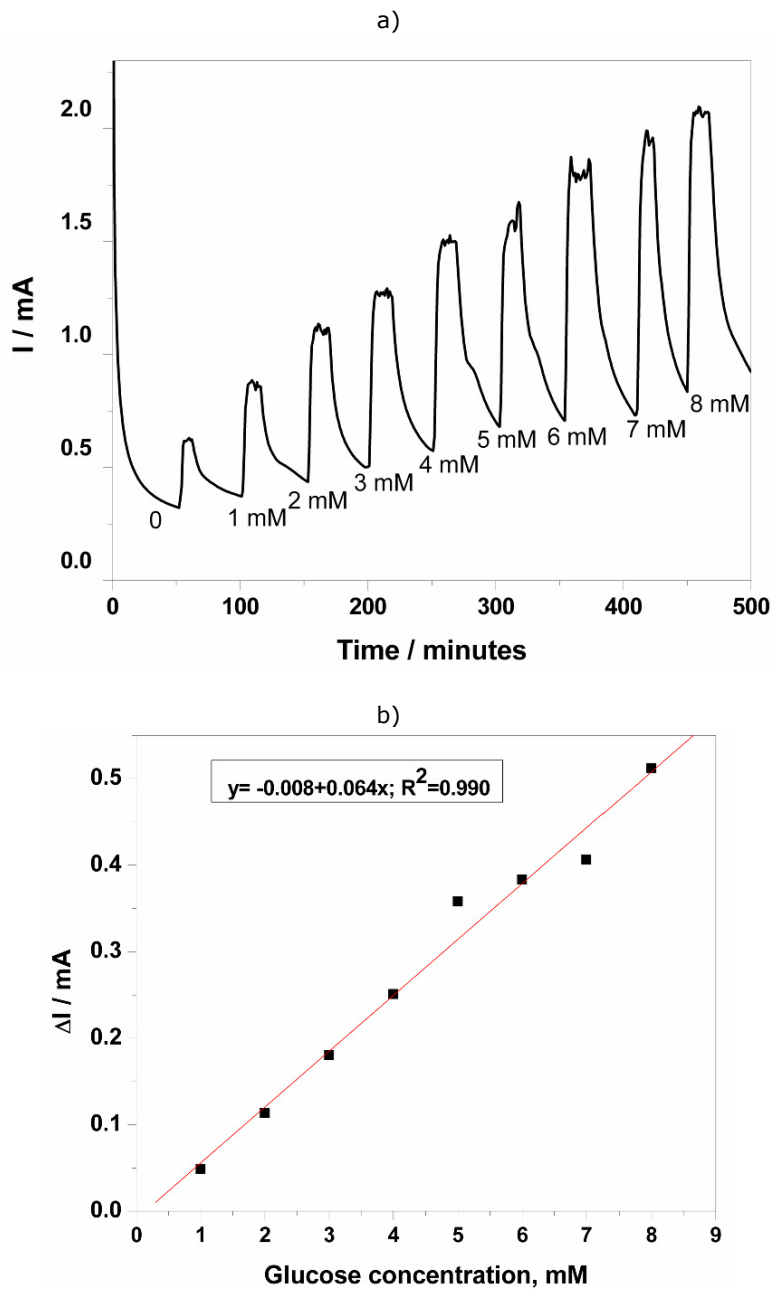


Figure 6.49 (a) Amperometric response (BIA) of the MWCNT-HKUST-Epoxy composite electrode for the successive and continuous addition of 1 mM glucose. Applied potential: +0.60 V vs. SCE. b) The calibration plot of useful signal vs. glucose concentration.

The electroanalytical parameters for non-enzymatic direct detection of glucose of the MWCNT-Cu-BTC-Epoxy composite electrode in 0.1 M NaOH supporting electrolyte are gathered in Table 6.13.

Table 6.13 The electroanalytical parameters for glucose direct detection of the MWCNT-HKUST-Epoxy composite electrode in 0.1 M NaOH supporting electrolyte.

Peak potential	Technique used	Concentration range (mM)	Sensitivity (mA / mM ⁻¹)	Correlation coefficient (R ²)	LOD (mM)	LQ (mM)	RSD [**] (%)
+0.60 V	CV	1-10	0.075	0.979	0.200	0.666	0.683
+0.60 V	LSV	1-10	0.119	0.992	0.655	2.184	4.031
+0.60 V	Prec./LSV	0.2-1	0.587	0.996	0.107	0.357	2.450
+0.27 V	DPV	1-6	0.001	0.997	0.300	1.000	5.000
+0.60 V	CA	1-8	0.064	0.990	0.250	1.037	3.140

The potential usefulness of DPV method at the determination of glucose content in real sample solutions was verified using aqueous solutions from fisiologic serum of glucose containing 25 g glucose/500 ml serum. Figure 6.50 depicts a series of DPVs as an example involving glucose determination in a glucose real serum sample solution. 20 mL glucose serum solution was diluted to 100 mL volume in 0.1 M NaOH supporting electrolyte used as stock glucose solution, and very small volumes of stock solution of glucose were then added. Value of 24.5 g glucose/serum represented the average content determined using anodic DPV technique at MWCNT-HKUST-Epoxy composite electrode associated with standard addition method.

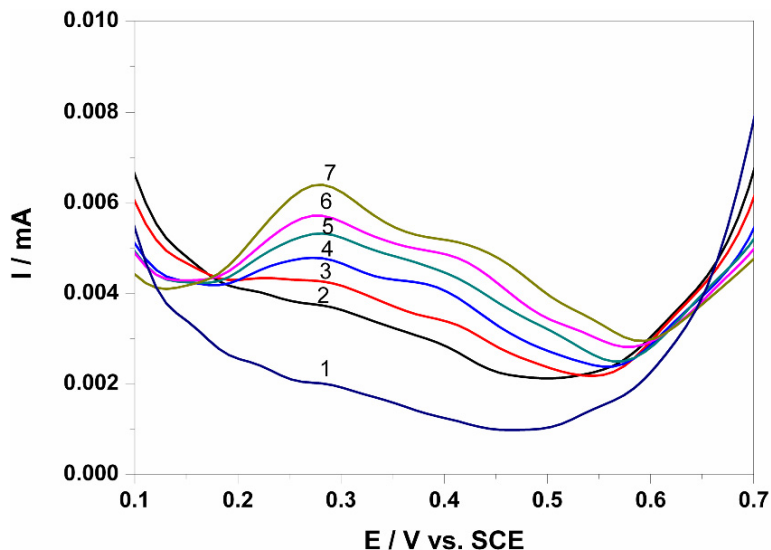


Figure 6.50 DPVs on MWCNT-HKUST-Epoxy composite electrode in (1) supporting electrolyte (0.1 M NaOH), (2) 0.1/50 dilution of *glucose serum stock* solution in supporting electrolyte, (3) 0.2/50 dilution of *glucose serum stock* solution in supporting electrolyte, (4) 0.3/50 dilution of *glucose serum stock* solution in supporting electrolyte, (5) 0.4/50 dilution of *glucose serum stock* solution in supporting electrolyte, (6) 0.5/50 dilution of *glucose serum stock* solution in supporting electrolyte, (7) 0.6/50 dilution of *glucose serum stock* solution in supporting electrolyte.

6.3.4 Conclusions

The non-enzymatic direct detection and determination of glucose using MWCNT-HKUST-Epoxy composite electrode by cyclic voltammetry, linear-scan voltammetry, differential-pulsed voltammetry and chronoamperometry and an easily accessible, simple unbuffered sodium hydroxide solution as supporting electrolyte has been achieved.

Very good linearities of the calibration plots of anodic current versus glucose concentrations resulted from all electrochemical techniques tested. Adjacent analytical data regarding RSD, LOD, and sensitivities were obtained.

The adsorption properties of HKUST and implicit, of MWCNT-HKUST-Epoxy composite electrode for glucose was exploited for the enhancement the electroanalytical performance for the glucose detection by the elaboration of the preconcentration/voltammetric detection scheme, which allowed to improve by 5 times the electroanalytical parameters, i.e., the sensitivity and the lowest limit of detection. By comparison with our previous reported data [6.66], [6.67], this electrode exhibited the superiority in relation with its performance for the glucose detection due to its better electrocatalytic performance for glucose oxidation

The association of differential-pulsed voltammetric method with standard addition method has been successfully used for a fast analytical evaluation of pharmaceutical formulations which contain glucose (serum). The average content of

glucose in serum, explored as real samples, was measured in good accordance with those indicated by the suppliers.

MWCNT-HKUST-Epoxy composite features in relation with the good electrochemical and electrocatalytic properties, good stability, reproducibility, long lifetime claim it very appropriate for the real application for the glucose detection, and for further exploitation in the construction of new electrochemical sensors.

6.4 References

- [6.1] Y. Lin, C.A. Timchalk, D.W. Matson, H. Wu, K.D. Thrall, *Biomedical Microdevices*. 4 (2001) 331.
- [6.2] WHO (1987) Pentachlorophenol. Geneva, World Health Organization, International Programme on Chemical Safety (Environmental Health Criteria 71).
- [6.3] Y.G. Leblance, R. Gilbert, J. Hubert, *Anal. Chem.* 71 (1999) 78.
- [6.4] A. Meyer, W. Kleibohmer, *J. Chromatogr. A*, 718 (1995) 131.
- [6.5] E. Gremaud, R.J. Turesky, *J. Agric. Food Chem.* 45 (1997) 1229.
- [6.6] C. Mardones, J. Palma, C. Sepulveda, A. Berg, D. Von Baer, *J. Sep. Sci.* 26 (2003) 923.
- [6.7] W. Fischer, O. Bund, H.E. Hauck, *Fresenius J. Anal. Chem.* 354 (1996) 889.
- [6.8] A. Mufeed Awawdeh, H.J. Harmon, *Biosens. Bioelectron.* 20 (2005) 1595.
- [6.9] M.A. Ruiz Barrio, J.M. Pingarrón Carrazón, *Fresenius Journal of Analytical Chemistry*. 344 (1992) 34.
- [6.10] E.C. Guijarro, P. Yañez-Sedeño, J.M. Pingarrón Carrazón, L.M. Polo Diez, *Analyst*. 113 (1988) 625.
- [6.11] A. Baciú, F. Manea, A. Remes, S. Motoc, G. Burtica, R. Pode, *Environmental Engineering and Management Journal*. 9 (2010) 1555.
- [6.12] R.R. Moore, C.E. Banks, R.G. Compton, *Anal. Chem.* 76 (2004) 2677.
- [6.13] C.E. Banks, R.R. Moore, T.J. Davies, R.G. Compton, *Chem. Commun.* 16 (2004) 1804.
- [6.14] H. Luo, Z. Shi, N. Li, Z. Gu, Q. Zhuang, *Anal. Chem.* 73 (2001) 915.
- [6.15] J. Yu, J.G. Shapter, M.R. Johnston, J.S. Quinton, J.J. Gooding, *Electrochim. Acta* 52 (2007) 6206.
- [6.16] J. Yu, J.G. Shapter, J.S. Quinton, M.R. Johnston, D.A. Beattie, *Phys. Chem. Chem. Phys.* 9 (2007) 510.
- [6.17] K.M. Roth, A.A. Yasserli, Z. Liu, R.B. Dabke, V. Malinovskii, K.H. Schweikart, L. Yu, H. Tiznado, F. Zaera, J.S. Lindsey, W.G. Kuhr, D. Bocian, *J. Am. Chem. Soc.* 125 (2002) 505.
- [6.18] E. Laviron, *J. Electroanal. Chem. Interfacial Electrochem.* 101 (1979) 19.
- [6.19] S.J. Konopka, B. McDuffie, *Anal. Chem.* 42 (1970) 1741.
- [6.20] M.O. Azzam, M. Al-Tarazi, Y. Tahboub, *Journal of Hazardous Materials B*. 75 (2000) 99.
- [6.21] A. Bebeselea, F. Manea, G. Burtica, L. Nagy, G. Nagy, *Talanta*. 80 (2010) 1068.
- [6.22] B.S. Yu, L.H. Nie, S.Z. Yao, *J High Resol Chromatogr* 20 (1997) 227.
- [6.23] M. Ehrendorfer, G. Sontag, F. Pittner, *Fresenius' J Anal Chem.* 356 (1996) 75.
- [6.24] A.M. de la Peña, F. Salinas, I.D. Meras, *Anal Chem* 60 (1988) 2493.
- [6.25] A. Villari, M. Micali, M. Fresta, G. Puglisi, *Analyst* 119 (1994) 1561.
- [6.26] F. Kees, D. Jehnich, H. Grobecker, *J Chromatogr B* 677 (1996) 172.
- [6.27] L.T. Kubota, J.C.B. Fernandes, L. Rover, G.D. Neto, *Talanta* 50 (1999) 661.
- [6.28] M. Newmayr, O. Friedrich, G. Sontag, F. Pittner, *Anal. Chim. Acta*. 273 (1993) 469.
- [6.29] Y.S. Fung, S.F. Luk, *Analyst* 114 (1989) 943.
- [6.30] L. Campanella, E. Gregori, M. Tomassetti, *J Pharm Biomed. Anal.* 42 (2006) 94.
- [6.31] P. Bouvrette, J.H.T. Loung, *Anal. Chim. Acta*. 335 (1996) 169.
- [6.32] V. Supalkova, J. Petrek, L. Havel, S. Krizkova, J. Petrlova, V. Adam, D. Potesil, P. Babula, M. Beklova, A. Horna, R. Kizek, *Sensors* 6 (2006) 1483.
- [6.33] J. Wang, In *Analytical Electrochemistry*; VCH Publishers: New York, 2000; Chapter 4, p.100-139.

- [6.34] B. Ballarin, M.M. Cordero-Rando, E. Blanco, J.L. Hidalgo-Hidalgo De Cisneros, R. Seeber, D. Tonelli, *Collect. Czech. Chem. Commun.* 68 (2003) 1420.
- [6.35] S. Ramirez-Garcia, S. Alegret, F. Cespedes, R.J. Forster, *Analyst* 127 (2002) 1512.
- [6.36] K. Stulik, C. Amatore, K. Holub, V. Marecek, W. Kutner, *Pure Appl. Chem.* 72 (2000) 1483.
- [6.37] A.O. Simm, C.E. Banks, S. Ward-Jones, T.J. Davies, N.S. Lawrence, T.G.J. Jones, L. Jiang, R.G. Compton, *Analyst* 130 (2005) 1303.
- [6.38] T.J. Davies, R.G. Compton, *J. Electroanal. Chem.* 585 (2005) 63.
- [6.39] A. Cięciwa, R. Wuthrich, C. Comminellis, *Electrochem. Commun.* 8 (2006) 375.
- [6.40] K.L. Soh, W.P. Kang, J.L. Davidson, S. Basu, Y.M. Wong, D.E. Cliffel, A.B. Bonds, G.M. Swain, *Diam. Relat. Mater.* 13 (2004) 2009.
- [6.41] R. Feeney, S.P. Kounaves, *Electroanalysis* 12 (2000) 677.
- [6.42] S. Fletcher, M.D. Horne, *Electrochem. Commun.* 1 (1999) 502.
- [6.43] N.S. Lawrence, M. Pagels, A. Meredith, T.G.J. Jones, C.E. Hall, C.S.J. Pickles, H.P. Godfried, C.E. Banks, R.G. Compton, L. Jiang, *Talanta* 69 (2006) 829.
- [6.44] H.J. Lee, C. Beriet, R. Ferrigno, H. Girault, *J. Electroanal. Chem.* 502 (2001) 138.
- [6.45] C. Cofan, C. Radovan, *Internat. J. of Electrochemistry* (2011), 9 pages.
- [6.46] T. Koschinsky, L. Heinemann, *Aspects. Diabetes Metab. Res. Rev.* 113 (2001) 17.
- [6.47] L.C. Clark, C. Lyons, *N.Y. Ann. Acad. Sci.* 102 (2006) 29.
- [6.48] M. Pasta, F. La Mantia, Y.Cui, *Electrochim. Acta.* 55 (2010) 5561.
- [6.49] V.G. Gavalas, S.A. Law, C.J. Ball, R. Andrews, L.G. Bachasa, *Anal. Biochem.* 329 (2004) 247.
- [6.50] M.H. Yang, Y.H. Yang, Y.L. Liu, G.L. Shen, R.Q. Yu, *Biosens. Bioelectron.* 21 (2005) 1125.
- [6.51] S. Cherevko, C.H. Ghung, *Talanta* 80 (2010) 1371.
- [6.52] R.Q. Rong, C. Yang, Q.Y. Qian, X.H. Xia, *Talanta* 72 (2007) 819.
- [6.53] M.M. Gvozdenovic, B.Z. Jugovic, D.I. Bezbradica, M.G. Antov, Z.D. Knezevic- Jugovic, B.N. Grgur, *Food. Chem.* 134 (2011) 396.
- [6.54] Y.P. Sun, H. Buck, T.E. Mallouk, *Anal. Chem.* 73 (2001) 1599.
- [6.55] W. Shoji, M.S. Freud, *J. Am. Chem. Soc.* 123 (1992), 3383.
- [6.56] R. Wilson, A.P.F. Turner, *Biosens. Bioelectron.* 7 (1992) 165.
- [6.57] M. Yang, Y. Yang, H. Yang, G. Shen, R. Yu, *Biomaterial.* 27 (2006) 246.
- [6.58] M. Yang, Y. Yang, Y. Liu, G. Shen, R. Yu, *Biosens. Bioelectron.* 21 (2006) 1125.
- [6.59] C.H. Chou, J.C. Chen, C.C. tai, I.W. Sun, J.M. Zen, *Electroanal.* 20 (2008) 771.
- [6.60] F. Kurniawan, V. Tsakova, V.M. Mirsky, *Electroanal.* 18 (2006) 1937.
- [6.61] M. Tominaga, M. Nagashima, I. Taniguchi, *Electrochem Commun.* 9 (2007) 1892.
- [6.62] M.M. Maye, L. Han, N.N. Kariuki, N.K. Ly, W.B. Chan, J. Lou, C.J. Zhong, *Anal. Chim. Acta.* 496 (2003) 17.
- [6.63] H. Zhu, X. Lu, M. Li, Y. Shao, Z. Zhu, *Talanta* 79 (2009) 1446.
- [6.64] D. Sun, L. Zhu, G. Zhu, *Anal. Chim. Acta.* 564 (2006) 243.
- [6.65] J. M. Marioli, T. Kuwana. *Electrochim. Acta.* 37 (1992) 1187.
- [6.66] A. Pop, Elaboration, characterization and application of some zeolite-modified electrodes for the evaluation and quantitative analysis of electrochemical active species from aqueous solutions, Ed. Politehnica, Timisoara, Romania, 2008.
- [6.67] F. Manea, Elaboration, characterization and application of some amperometric systems for direct detection of organic load from wastewaters, Timisoara, Romania, 2004.

CHAPTER 7

GENERAL CONCLUSIONS AND FUTURE PERSPECTIVES

"I learned very early the difference between knowing the name of something and knowing something". (Richard P. Feynman)

Summary

The main conclusions of this thesis are highlighted in this chapter. It is demonstrated how the research presented in this Phd. thesis contributes to the research carried out in the field of carbon nanotube/polymer composites. An outlook for future research is subsequently suggested.

7.1 General conclusions

The original research described in this Phd. thesis consists of both the manufacturing and design conditions of composite electrodes based on metal-organic framework (MOF)-modified/unmodified multi-wall carbon nanotubes (MWCNTs) within an epoxy matrix and their multiple applications in environmental life, and health quality control. The new composite electrode synthesized in this study allowed an easy detection way, fast response, high sensitivity, appropriate for real samples, small volume, avoiding chemical reagents adding for the simultaneous / selective assessment of analytes. The microelectrode array behavior of these composite electrodes under certain working conditions provided the possibility of in-situ detection, without requiring the supporting electrolyte addition. Thus, innovation degree is given by the easy method of synthesis of new composite electrodes with improved electrocatalytic properties for the detection of pethachlorophenol, salicylic acid, and acetylsalicylic acid. Moreover, modifying the composite electrode with a certain MOF, namely copper benzene tricarboxylate (HKUST), selectivity for the non-enzymatic detection of glucose was achieved.

Degree of originality and complexity consisted of:

- Elaboration of some new and advanced composite electrode materials based on multi-walled carbon nanotubes and modified with metal-organic framework(MOF) for the quantitative evaluation of selected organic compounds,
- Composition optimization of the composite materials,
- Obtaining of new electrodes based on the selected composites,
- Comparative electrochemical characterization of electrode materials in different supporting electrolytes and in the presence of target analyte by cyclic voltammetry (CV),
- Identification and selection of optimal conditions for composite electrode material types with microelectrode array behavior,

- Achievement of individual amperometric / voltametric detection experiments by using cyclic voltammetry (CV), differential pulse voltammetry (DPV), square wave voltammetry (SWV), chronoamperometry (CA), and multiple-pulsed amperometry (MPA),
- Preconcentration / detection scheme development based on the sorption property of the composite electrode to improve the electroanalytical performance,
- Multiple- pulse amperometry characteristics exploitation to enhance also the detection electroanalytical performances,
- Exploitation of the microelectrodes array advantage for analyte detection in the absence of supporting electrolyte,
- Assessment of the selective and / or simultaneous detection for certain analytes. Establishing of the detection electroanalytical performances,
- The evaluation of the retrieval for each optimal detection method proposed by real samples. Accuracy assessment for each proposed detection method by comparison with the conventional methods,
- Testing of obtained sensors for non-invasive quantitative evaluation of some compounds of interest in medicine and pharmaceutical products.
- Two types of composite electrodes, i.e., multi-wall carbon nanotubes-epoxy composite electrodes with an optimum multi-wall carbon nanotubes loading (MWCNTs-Epoxy) and Copper benzene tricarboxylate (metal-organic framework-MOF)-modified-multi-wall carbon nanotubes-epoxy (MWCNT-HKUST-Epoxy) composite electrode were synthesized successfully by a two-roll mill method and characterized envisaging their use for detection of the several analytes: pentachlorophenol (PCP), salicylic acid (SA), acetylsalicylic acid (ASA) and glucose in aqueous medium.
- The technique based on pre-dispersion of MWCNTs in a solvent, followed by mixing with epoxy resin, has been proven to be the easiest, least laborious, and very effective way to achieve relatively uniform MWCNTs dispersion in composites, and has proven its efficiency.
- Based on the Dynamic Light Scattering results regarding the length and diameter distributions of MWCNTs by sonication in different types of solvents, tetrahydrofuran (THF) solvent was selected as optimum in comparison with DMF, toluene, acetone, ethanol and chloroform.
- The Raman Spectroscopy results indicated that no significant increase of defects or breakage in nanotubes structure was caused by the sonication process.
- The electrical properties of the composite materials strongly depended on the MWCNT loading and the homogeneity of MWCNTs distribution within the epoxy matrix. The optimum MWCNT loading into the composite material was selected as 25 %, wt. based on the electrical percolation threshold results and taken into consideration the further electrochemical application quite without the supporting electrolyte adding.
- The MOF (HKUST) loading within the composite material was chosen to reach a MWCNT/MOF ratio of 1.
- For both composite electrodes, SEM micrographs showed that the MWCNTs and MOF distribution was quite homogeneous within the epoxy matrix.
- MWCNT-Epoxy composite electrode exhibited the electrocatalytic activity towards pentachlorophenol (PCP) oxidation, which is controlled by diffusion, a desired aspect for electroanalysis. The linear dependence of current versus PCP concentrations was reached in a wide concentration range from 0.2 to 12 μM PCP and the electrochemical determination of PCP at MWCNT-Epoxy composite electrode was achieved using cyclic voltammetry (CV), differential-pulsed voltammetry (DPV),

square-wave voltammetry (SWV), chronoamperometry (CA), and multiple-pulsed amperometry (MPA) procedures. Despite the adsorption of PCP on MWCNT is an undesired aspect, this study demonstrated that this property should be exploited in a positive way for PCP determination at the trace level. Under optimized working conditions in relation with the accumulation time and PCP concentration a significant enhancement of the electroanalytical parameters was achieved. However, for the practical application, CA as the simplest electrochemical technique did not allow to obtain good electrochemical detection results, probably because of electrode fouling. MPA applying led to improve the electroanalytical parameters of PCP detection, especially the lowest limit of detection, which makes this composite electrode appropriate for electrochemical determination of a wide range of PCP concentrations in the aqueous solution.

➤ MWCNT-Epoxy composite electrode exhibited electrocatalytic activity towards salicylic acid (SA) and acetylsalicylic acid (ASA) oxidation, allowing their direct determination. The electrochemical determinations of SA and ASA using the MWCNT-Epoxy composite electrode was achieved in both 0.1 M Na₂SO₄ and 0.1 M NaOH supporting electrolytes using CV, DPV and SWV techniques. The alkaline medium did not allow improving the sensitivity for SA and ASA detection but the oxidation potential was shifted to a less positive potential in comparison with the neutral medium. A detailed study related to the optimization of SWV applying was performed and the best electroanalytical performance for SA determination was achieved under the conditions of simple the voltammetric technique applying. Moreover, the preconcentration step involved in the voltammetric detection scheme led to the enhancement of the electroanalytical performance for SA detection, both sensitivity and the lowest limit of detection were improved. SA detection on the MWCNT-Epoxy composite electrode was achieved in tap water and in surface water (Bega River from Timisoara city, Romania). SA detection in tap water certified the micro/nanoelectrode array behavior of the MWCNT-Epoxy composite electrode without supporting electrolyte. Also, the MWCNT-Epoxy composite electrode gives the possibility of direct in-situ analysis of salicylic acid in surface water and no supporting electrolyte was needed.

➤ The association of the electrochemical techniques with standard addition method has been successfully used for a fast analytical evaluation of pharmaceutical formulations which contain acetylsalicylic acid (aspirin/tablet supplied by OZONE). The average content of aspirin/tablet, explored as real samples, was measured in good accordance with those indicated by the suppliers.

➤ Because ASA exhibited the same electrochemical behavior with the MWCNT-Epoxy composite electrode as SA, a simultaneous detection of both compounds assuming their presence in surface water, for example, is possible only as a cumulative effect but not a selective detection of one compound in the presence of the other can be performed.

➤ The ease of preparation, high sensitivity, stability of this composite electrode corroborated with its electrocatalytic properties towards various analytes oxidation should open novel avenues and applications for fabricating robust sensors for many important and various species.

➤ The non-enzymatic direct determination of glucose using multiwall-carbon nanotube-copper benzene tricarboxylate (HKUST)-epoxy (MWCNT-HKUST-Epoxy) composite electrode by cyclic voltammetry, linear-scan voltammetry, differential-pulsed voltammetry, and chronoamperometry and an easily accessible, simple unbuffered sodium hydroxide solution as supporting electrolyte has been achieved. Very good linearities of the calibration plots of anodic currents versus glucose

concentrations resulted from all electrochemical techniques tested. Adjacent analytical data regarding RSD, LOD, and sensitivities were obtained. The adsorption properties of HKUST and implicit of MWCNT-HKUST-Epoxy composite electrode for glucose was exploited for the enhancement the electroanalytical performance for the glucose detection by the elaboration of the preconcentration/voltammetric detection scheme, which allowed to improve by 5 times the electroanalytical parameters, i.e., the sensitivity and the lowest limit of detection. By comparison with our previous reported data, this electrode exhibited the superiority in relation with its performance for the glucose detection due to its better electrocatalytic performance for glucose oxidation. The association of differential-pulsed voltammetric method with standard addition method has been successfully used for a fast analytical evaluation of pharmaceutical formulations which contain glucose (serum). The average content of glucose in serum, explored as real samples, was measured in good accordance with those indicated by the suppliers. MWCNT-HKUST-Epoxy composite features in relation with the good electrochemical and electrocatalytic properties, good stability, reproducibility, long lifetime claim it very appropriate for the real application for the glucose detection, and for further exploitation in the construction of new electrochemical sensors.

- Due to the great complexity of objective proposed for this study, this research was conceived and tackled as a necessary and obligatory stage that to precede the effective implementation of detectors for specific practical applications in relation with the environment, life, and health quality control.

- The basic study for electrode elaboration, characterization and use for sensing under various conditions is a stage that conditions fundamental and hard criteria of „know-how“ for concrete application.

- The fast exploitation, high sensitivity, stability, and the easy maintenance of the amperometric/voltammetric detectors, including fast regeneration of fouled should constitute an advantage versus the classical analysis methods of organics.

- Due to these sensors can be used for many applications, e.g., environmental protection, process control, clinical diagnosis, food etc, the sensor composition, shape and dimension is a function of its application. In general, regarding sensing stage, these sensors can be used under certain conditions, which are not appropriate for other detection variants, a specific electrode material associated with well-established electrochemical technique based detection procedure are required.

7.2 Future perspectives

These obtained results may constitute a basis for the future research:

- Possibilities of electrode miniaturization in order to obtain an ordered nano-electrode array,

- Modifying the electrode composition to achieve the selectivity for specific analyte detection,

- Electrochemical technique selection and optimization in relation with the electrochemical behavior of the electrode material to enhance the electroanalytical performance for the analysis method,

- Non-invasive monitoring of environment and other clinical analysis, pharmaceutical and food products analysis reference compounds, water quality and pollution control, timely measuring and in-situ analysis, measurements accuracy, diminishing prior pretreatment of samples, avoiding further addition of chemical reagents.

List of publications and conference presentations

Articles published in International ISI Journals

1. F. Manea, M. Ihos, **A. Remes**, G. Burtica and J. Schoonman, "Electrochemical determination of diclofenac sodium in aqueous solution on Cu-doped zeolite expanded graphite-epoxy electrode", *Electroanalysis*, vol. 22 (17-18), pp. 2058-2063, September 2010.
2. F. Manea, **A. Remes**, C. Radovan, R. Pode, S. Picken and J. Schoonman, "Simultaneous electrochemical determination of nitrate and nitrite in aqueous solution using Ag-doped zeolite- expanded graphite-epoxy electrode", *Talanta*, vol. 83 (1) , pp. 66-71, November 2010.
3. A. Baciú, F. Manea, **A. Remes**, S. Motoc, G. Burtica and R. Pode, "Anodic determination of pentachlorophenol from water using carbon fiber based composite electrode", *Environmental Engineering and Management Journal*, vol. 9 (11), pp. 1555-1562, November 2010.
4. M. Ihos, **A. Remes** and F. Manea, "Electrochemical determination of diclofenac in water using boron-doped diamond electrode", *Journal of Environmental Protection and Ecology* (in press).

Articles published at International Conferences (ISI Proceedings)

1. C. Bandas, C. Lazau, P. Sfirloaga, **A. Remes**, V. Tiponut, I. Grozescu and F. Manea, "TiO₂ modified-zeolite for a novel multiwalled carbon nanotube based composite electrode", *Proceedings of the International Semiconductor Conference, CAS*, 17-19 October, 2011, vol 2, pp. 225-228.
2. A. Pop, F. Manea, **A. Remes**, A. Baciú, C. Orha, N. Vaszilcsin, Stephen J. Picken and Joop Schoonman, " Silver-functionalized multi-wall carbon nanotubes composite electrode for non-enzymatic detection of glycerol", *Proceedings of IEEE Sensors*, 28-31 October, Limerick, Ireland, 2011, pp. 581-584.

Articles presented and published at International Conferences

1. **A. Remes**, F. Manea, G. Burtica, C. Ratiu, S.J. Picken and J. Schoonman, "Amperometric detection of nitrite from water using zeolite based composite electrode", *Proceedings of the 16th Symposium on Analytical and Environmental Problems, SZAB, Szeged*, pp. 152-155, September, 2009.
2. M. Ihos, **A. Remes**, D. Botau and F. Manea, "Removal of pharmaceuticals from wastewaters by electrooxidation", *Proceedings of The 17th Symposium on Analytical and Environmental Problems, SZAB, Szeged, Hungary*, pp. 335-338, September, 2011.
3. **A. Remes**, F. Manea, G. Burtica and R. Pode, "Environmental friendly electrochemical determination of aspirin from alkaline aqueous solution", *Proceedings of The 17th Symposium on Analytical and Environmental Problems, SZAB, Szeged, Hungary*, pp. 384-387, September, 2011.
4. A. Baciú, A. Pop, **A. Remes**, F. Manea and G. Burtica, "Non-enzymatic electrochemical determination of glucose on silver-doped zeolite CNT-composite electrode", *Advanced Science Engineering and Medicine (Journal of Scientific Conference Proceedings)*, vol. 3 (13-19), 2011.

Articles presented and published at International Conferences in Romania (BDI)

1. **A. Remes**, F. Manea, D. Sonea, G. Burtica, S.J. Picken and J. Schoonman, "Electrochemical determination of nitrate from water sample using Ag-doped zeolite modified expanded graphite composite electrode", Ovidius University Annals of Chemistry, vol. 20(1), pp. 61-65, 2009.

Articles in preparation

1. **A. Remes**, A. Pop, F. Manea, A. Baci, S.J.Picken and J. Schoonman, "Electrochemical determination of pentachlorophenol from water on multiwalled carbon nanotube- epoxy composite electrode", in preparation.

2. **A. Remes**, F. Manea, A. Pop, N.K.K. Kowgi, S.J. Picken and J. Schoonman, "MWCNT- epoxy composite electrodes for environmentally friendly detection of pharmaceuticals compounds", in preparation.

3. **A. Remes**, F. Manea, A. Baci, A.M. Joaristi, J. Gascon and J. Schoonman, "Multi-walled Carbon Nanotube-HKUST-Epoxy composite sensor for non-enzymatic electrochemical determination of glucose", in preparation.

Conference presentations

21-25/11/2011 Trends in Nanotechnology, Tenerife, Spain (poster presentation)

12-15/09/2011 EUROMAT, Montpellier, France (poster presentation)

4-8/07/2011 Journées d'Electrochimie, Grenoble, France (poster presentation)

26/06-02/07/2011 European Polymer Congress, Granada, Spain (poster presentation)

8-11/05/2011 9th Spring Meeting of the International Society of Electrochemistry, Turku, Finland (oral presentation)

27-29/04/2011 2nd Nanomaterials and Nanotechnology Meeting, Ostrava, Czech Republic (oral presentation)

4-5/11/2010 2nd Nanostructured Multifunctional Materials, Iasi, Romania (oral presentation)

9-13/12/2009 Modern Electroanalytical Methods, Prague, Czech Republic (oral presentation)

13-16/05/2009 CHIMIA- New Trends in Applied Chemistry, Constanta, Romania (poster presentation)

All Databases

Results Author=(Remes Adriana*)
 Timespan=2010-2012.
 Search language=English Lemmatization=On

Scientific WebPlus^{WEB} View Web Results >>

Results: 3 Page 1 of 1 Go Sort by: Publication Date -- newest to oldest

Hide Refine

Refine Results

Search within results for

Search

Databases

General Categories Refine

SCIENCE TECHNOLOGY

Subject Areas Refine

CHEMISTRY

ELECTROCHEMISTRY

ENVIRONMENTAL SCIENCES

ECOLOGY

more options / values...

Document Types

Authors

Authors - Chinese

Group/Corporate Authors

Editors

Funding Agencies

Funding Agencies - Chinese

Source Titles

Source Titles - Chinese

Conference/Meeting Titles

Publication Years

Languages

Countries/Territories

Countries/Territories - Chinese

+ (0) Save to: EndNote Web
 EndNote ResearcherID more options Create Citation Report

1. Title: **Simultaneous electrochemical determination of nitrate and nitrite in aqueous solution using Ag-doped zeolite-expanded graphite-epoxy electrode**

Author(s): Manea Florica; Remes Adriana; Radovan Ciprian; et al.
 Source: TALANTA Volume: 83 Issue: 1 Pages: 66-71 DOI: 10.1016/j.talanta.2010.08.042 Published: NOV 15 2010
 Times Cited: 1 (from All Databases)

Full Text View abstract

2. Title: **ANODIC DETERMINATION OF PENTACHLOROPHENOL FROM WATER USING CARBON NANOFIBER-BASED COMPOSITE ELECTRODE**

Author(s): Baciu Anamaria; Manea Florica; Remes Adriana; et al.
 Source: ENVIRONMENTAL ENGINEERING AND MANAGEMENT JOURNAL Volume: 9 Issue: 11 Pages: 1555-1562 Published: NOV 2010
 Times Cited: 0 (from All Databases)

View abstract

3. Title: **Electrochemical Determination of Diclofenac Sodium in Aqueous Solution on Cu-Doped Zeolite-Expanded Graphite-Epoxy Electrode**

Author(s): Manea Florica; Ilios Monica; Remes Adriana; et al.
 Conference: International Conference on Modern Electroanalytical Methods Location: Sci Charles Univ Prague, Czech Chem Soc, Inst Phys Chem Acad Sci Czech Rep, Prague, CZECH REPUBLIC Date: DEC 09-13, 2009
 Sponsor(s): European Soc Electroanalytical Chem; Int Soc Electrochem Source: ELECTROANALYSIS Volume: 22 Issue: 17-18 Pages: 2058-2063 DOI: 10.1002/elan.201000074 Published: SEP 2010
 Times Cited: 1 (from All Databases)

Full Text View abstract

Results: 3 Show 10 per page Page 1 of 1 Go Sort by: Publication Date -- newest to oldest

Output Records

Step 1:

- Selected Records on page
- All records on page
- Records to

Step 2:

- Authors, Title, Source
- plus Abstract

Step 3: [How do I export to bibliographic management software?]

Save to: EndNote Web EndNote
 ResearcherID
 Save to other Reference Software Save
 + (0)

Curriculum Vitae

Adriana Ileana Remes was born on the 10th of December 1983, in Zalau, Salaj. After finishing secondary school in 1998 ('Simion Barnutiu' Highschool, Simleu-Silvaniei, Salaj, Romania), she studied Biology and Geology at Babes-Bolyai University in Cluj-Napoca, Romania.

In October 2008, she started her Ph.D. study in the department of CAICAM at Politehnica University of Timisoara, Romania, under the supervision of Prof.dr.eng. Gerogeta Burtica and Associate Prof.dr.eng. Florica Manea. The second year of the PhD study was performed within the NanoStructured Materials (NSM) group, Chemical Engineering Department at Delft University of Technology, The Netherlands, under the supervision of Prof. dr.dr.h.c. Joop Schoonman and Prof.dr. Stephen J. Picken.

The main results of her Ph.D. research are described in this thesis.

Titluri recent publicate în colecția „TEZE DE DOCTORAT” seria 4: Inginerie Chimică

BUPT

1. **Svetlana Capig** – *Posibilitatea utilizării extractelor vegetale ca ingrediente naturali pentru medicamente, cosmetice și alimente*, ISBN: 978-973-625-428-4, (2007);
2. **Narcis Mihai Duțeanu** – *Studii asupra performanțelor pilelor de combustie metanol/aer (oxigen) și borohidruură/aer (oxigen) echipate cu electrolit polimer solid*, ISBN: 978-973-625-437-6, (2007);
.....
.....
52. **Valentina-Liliana Udrescu** - *Optimizarea metodelor spectrometrice de masă prin chip-electrospray pentru studiul biomoleculilor*, ISBN:978-606-554-367-6, (2011);
53. **Ilie PISOI** - *Contribuții privind rețehnologizarea fluxului de potabilizare a apei de suprafață caracterizată prin turbiditate mică*, ISBN:978-606-554-377-5, (2011);
54. **Iulia Andreea Pînzaru** - *Flavonoide și bioconjugați cu activitate biologică: obținere, analiză și biodisponibilizare prin încapsulare moleculară*, ISBN:978-606-554-398-0, (2011);
55. **Mihai-Cosmin Pascariu** - *Surfactanți derivați din zaharide*, ISBN:978-606-554-413-0, (2011);
56. **Livia Nicoleta Corîci** - *Utilizarea alcalazei imobilizate în sinteza peptidelor*, ISBN:978-606-554-419-2, (2011);
57. **Anamaria Dabici** - *Materiale oxidice cu activitate fotocatalitică utilizate la mineralizarea coloranților din apele reziduale*, ISBN:978-606-554-420-8, (2011);
58. **Adriana Ileana Remeș** - *Multi-wall carbon nanotubes-based composite electrodes for electroanalysis applications*, ISBN: 978.606-554-437-6, (2012).



EDITURA POLITEHNICA

Lista completă a tezelor publicate sub sigla Editurii Politehnica poate fi consultată
la adresa: <http://www.editurapolitehnica.upt.ro>

